

Aus der Abteilung Genvektoren
Helmholtz Zentrum München
Vorstand: Prof. Dr. Wolfgang Hammerschmidt



***The Role of Raf-1 and B-Raf in B cell activation, differentiation,
and tumorigenesis in mice***

Dissertation
zum Erwerb des Doktorgrades der Naturwissenschaften
an der Medizinischen Fakultät der
Ludwig-Maximilians-Universität München

vorgelegt von
Laura Scheffler
aus
Hamm

Jahr
2023

Mit Genehmigung der Medizinischen Fakultät
der Universität München

Betreuerin: PD Dr. Ursula Zimmer-Strobl

Zweitgutachter: Prof. Dr. Vigo Heissmeyer

Dekan: Prof. Dr. Thomas Gudermann

Tag der mündlichen Prüfung: 11.10.2023

Table of Contents

ABSTRACT	7
ZUSAMMENFASSUNG	8
LIST OF FIGURES	10
LIST OF TABLES	11
LIST OF ABBREVIATIONS	12
1. INTRODUCTION	16
1.1 The immune system	16
1.2 B cells	16
1.2.1 B cell development.....	17
1.2.1.1 Bone marrow B cell development.....	17
1.2.1.2 Peripheral B cell maturation and cell fate decision.....	19
1.2.2 B cell differentiation.....	20
1.2.2.1 Cellular processes of B cell differentiation.....	20
1.2.2.2 Marker expression during plasma cell differentiation.....	21
1.2.3 Signaling during B cell activation.....	22
1.2.3.1 B cell receptor signaling.....	22
1.2.3.2 CD40 receptor signaling.....	25
1.2.3.3 Toll-like receptor 4 signaling.....	26
1.3 Raf-kinases	27
1.3.1 Raf-kinase family.....	27
1.3.2 The Ras-Raf-MEK-ERK signaling pathway.....	28
1.3.3 Raf mutations.....	30
1.3.4 Raf mediated functions in B cells.....	31
1.4 Model systems	32
1.4.1 The Raf-1 ^{fl/fl} //B-Raf ^{fl/fl} //mb1-Cre ^{+/-} (DKO) transgenic mouse model.....	32
1.4.2 The Raf-1 ^{fl/fl} //B-Raf ^{fl/fl} //LMP1/CD40 ^{f^{STOP}+/-} //CD19-Cre ^{+/-} (RafDKO/LC40) transgenic mouse model.....	33
2. AIM	34
3. RESULTS	36
3.1 The role of B-Raf and Raf-1 in B cell receptor signaling	36
3.1.1 Increased basal and BCR mediated ERK phosphorylation in DKO B cells.....	36
3.1.2 Unaltered BCR downstream signaling in DKO B cells.....	39
3.1.3 Increased ERK phosphorylation upon pan-Raf inhibitor treatment.....	40
3.1.4 BCR induced SYK, PI3K and RAC/Pak dependent ERK phosphorylation in mature B cells.....	43
3.2 The role of B-Raf and Raf-1 in PC differentiation	46
3.2.1 Impaired TI immune response in DKO mice.....	46

3.2.2	Impaired LPS mediated PC differentiation in DKO B cells <i>in vitro</i>	47
3.2.3	Increased LPS mediated ERK phosphorylation in DKO B cells	50
3.2.4	A sharp increase of pERK as a prerequisite for PB differentiation <i>in vitro</i>	54
3.3	The effects of B-Raf//Raf-1 inactivation on CD40 induced B cell activation.....	57
3.3.1	Negative regulatory function of B-Raf and Raf-1 on CD40 mediated ERK phosphorylation	57
3.3.2	PI3K dependency of long-term CD40 mediated pERK in control and DKO B cells	58
3.3.3	Enhanced ERK phosphorylation in RafDKO/LC40 B cells	59
3.4	Attenuated LC40 mediated phenotype upon B-Raf//Raf-1 inactivation	60
3.4.1	Diminished B cell expansion in RafDKO/LC40 mice	60
3.4.2	Diminished pathological splenomegaly in old RafDKO/LC40 mice.....	62
3.4.3	Diminished LC40 mediated outgrowth of the aberrant CD21 ^{low} CD23 ^{low} CD43 ⁺ B cell population by inactivation of B-Raf and Raf-1	66
3.4.4	Alteration of the LC40 mediated B cell activation upon B-Raf//Raf-1 inactivation.....	68
3.4.5	Detection of Raf proficient B cells in old RafDKO/LC40 mice	69
3.5	Alteration of the LC40 induced gene expression pattern by B-Raf//Raf-1 inactivation.....	70
3.5.1	B-Raf//Raf-1 inactivation reduced the expression of genes with a tumor promoting function in LC40 B cells	71
3.5.2	Alterations of biological processes upon B-Raf//Raf-1 inactivation.....	75
3.5.3	Increased MZ B cell differentiation in LC40 mice is reverted in the absence of B-Raf and Raf-1 75	75
3.5.4	Reduced Notch2 and non-canonical NFκB mediated gene expression in RafDKO/LC40 mice.	76
3.5.5	Requirement of B-Raf and Raf-1 for LC40 induced activation of the Notch2 and non-canonical NFκB signaling pathways	79
4.	DISCUSSION	82
4.1	Negative regulation of BCR mediated pERK levels by Raf-kinases in mature B cells	82
4.2	Impaired PC differentiation upon B-Raf//Raf-1 inactivation	84
4.3	Negative regulation of CD40 mediated pERK by Raf-kinases.....	85
4.4	Diminished LC40 phenotype upon B-Raf//Raf-1 inactivation	86
4.4.1	Reduced cell expansion in young RafDKO/LC40 mice	86
4.4.2	Reduced LC40 mediated aberrant B cell expansion in old RafDKO/LC40 mice	87
4.4.3	Altered LC40 mediated B cell activation in RafDKO/LC40 mice	88
4.4.4	Detection of Raf proficient B cells in old RafDKO/LC40 mice	89
4.5	Changed LC40 mediated gene expression pattern upon B-Raf//Raf-1 inactivation	90
4.5.1	Diminished expression of tumor associated genes in RafDKO/LC40 B cells	91
4.5.2	Changed expression of genes involved in immune responses and cell adhesion in RafDKO/LC40 B cells	92
4.5.3	Contribution of B-Raf and Raf-1 to the LC40 induced MZ B cell expansion	93
4.5.4	Reduced LC40 mediated Notch2 and non-canonical NFκB signaling in RafDKO/LC40 mice	94
4.6	Raf-kinases: more than a kinase towards MEK/ERK.....	95

5. MATERIAL	97
5.1 Mouse strains	97
5.1.1 C57BL/6	97
5.1.2 mb1-Cre	97
5.1.3 RafDKO//mb1-Cre (DKO)	97
5.1.4 CD19-Cre	98
5.1.5 LMP1/CD40//CD19-Cre (LC40)	98
5.1.6 RafDKO//LMP1/CD40//CD19-Cre (RafDKO/LC40)	98
5.2 Antibodies	99
5.3 Chemicals, enzymes, commercial kits and consumable material	100
5.4 Inhibitors	102
5.5 Stimuli	102
5.6 Buffer and media composition	103
5.7 Software	103
6. METHODS	104
6.1 Mouse genotyping	104
6.1.1 Isolation of genomic DNA	104
6.1.2 Polymerase chain reaction and gel electrophoreses	104
6.2 Mouse immunization	106
6.3 Organ preparation	106
6.4 Single cell suspensions	107
6.5 B cell enrichment with MACS purification	107
6.6 B cell culture, stimulation, and inhibitor treatment	107
6.6.1 Short-term stimulation	107
6.6.2 Long-term stimulation with LPS	108
6.7 Protein analysis	108
6.7.1 Protein extraction of whole cell lysates	108
6.7.2 Nuclear cytoplasmic fractionation	109
6.7.3 Protein quantification	109
6.7.4 SDS-PAGE and Western blot	110
6.7.5 Western blot quantification	111
6.7.6 Protein Simple WES	112
6.8 Flow Cytometry (FACS)	113
6.9 ELISA	114
6.10 ELISpot Assay	115
6.11 RNA-Sequencing	116
6.12 Statistics	118

REFERENCES.....	119
SUPPLEMENTARY DATA	141
DANKSAGUNG	152
AFFIDAVIT	153

Publication based on the results of this dissertation and copyright statement:

Scheffler L, Feicht S, Babushku T, Kuhn LB, Ehrenberg S, Frankenberger S, et al. ERK phosphorylation is RAF independent in naïve and activated B cells but RAF dependent in plasma cell differentiation. *Sci Signal*. 2021 May 11;14(682).
doi:10.1126/scisignal.abc1648 (Scheffler et al. 2021)

In part, components of figures are shared between this thesis and the above publication. All used figures were created by Laura Scheffler.

Abstract

B cells are part of the adaptive immune system and, as plasma cells, fight various pathogens by producing antibodies. The development, homeostasis, and self-tolerance of B cells are regulated by several key cellular processes. These cellular key functions, as proliferation, differentiation, but also apoptosis and cell cycle arrest are controlled by different signaling pathways. One major regulator of these processes is the extracellular signal-regulated kinase (ERK), which is mainly activated by the mitogen-activated protein kinase (MAPK) pathway Ras-Raf-MEK-ERK. In B cells, the contribution of the Ras-Raf-MEK-ERK signaling pathway to B cell development, activation, differentiation, and transformation was described by the analyses of the components Ras and ERK in different cell lines.

To investigate the role of the Raf-kinases on these processes specifically in primary murine B cells, Raf-1^{fl/fl}//B-Raf^{fl/fl}//mb1-Cre^{+/-} (DKO) mice were generated leading to the B cell specific deletion of the two kinases from the early B cell development onwards. This mouse model was used within this thesis to analyze Raf mediated functions during B cell development, activation, and differentiation. Within this dissertation, important roles of B-Raf and Raf-1 in the following processes was revealed: (I) B-Raf and Raf-1 were not required to mediate ERK phosphorylation in BCR, LPS and CD40 stimulated B cells but rather acted as negative regulators of PI3K or Rac/PAK mediated ERK phosphorylation in resting and activated mature B cells. (II) Inactivation of B-Raf and Raf-1 in DKO mice resulted in an impaired T independent immune response. (III) B-Raf//Raf-1 inactivation caused a block in plasma cell differentiation at the transition of activated B cells to pre-plasmablasts and in their further differentiation into plasmablasts. We found that at this stages B-Raf and Raf-1 mediate a strong increase in ERK phosphorylation, which seemed to be essential for plasma cell differentiation.

Furthermore, Raf-1^{fl/fl}//B-Raf^{fl/fl}//LMP1/CD40^{flSTOP+/-}//CD19-Cre^{+/-} (RafDKO/LC40) mice were compared with LMP1/CD40^{flSTOP+/-}//CD19-Cre^{+/-} (LC40) and control mice to examine the effect of the genetic inactivation of B-Raf and Raf-1 on B cells with a constitutively active CD40 signal and the resulting LC40 driven B cell transformation. Inactivation of B-Raf and Raf-1 in RafDKO/LC40 mice decreased the LC40 mediated phenotype of B and T cell expansion and B cell transformation. As revealed by an RNA-Seq analysis, this appeared to be predominantly caused by decreased LC40 mediated *Myc* expression, and reduced Notch2 and non-canonical NFκB activation. These data, suggest that Raf-kinases modulate the activation of these two signaling pathways downstream of CD40.

Zusammenfassung

B-Zellen sind Teil des adaptiven Immunsystems und bekämpfen als Plasmazellen durch Antikörperproduktion verschiedene Krankheitserreger. Die Entwicklung, Homöostase und Selbsttoleranz von B-Zellen werden durch mehrere zelluläre Schlüsselprozesse reguliert. Diese umfassen Proliferation, Differenzierung, aber auch Apoptose und Zellzyklusarrest und werden durch verschiedene Signalwege gesteuert. Ein wichtiger Regulator dieser Prozesse ist die extrazelluläre signalregulierte Kinase (ERK), die hauptsächlich durch den Mitogen-aktivierten Proteinkinase (MAPK)-Signalweg Ras-Raf-MEK-ERK aktiviert wird. In B-Zellen wurde der Beitrag des Ras-Raf-MEK-ERK-Signalwegs zur Entwicklung, Aktivierung, Differenzierung und Transformation von B-Zellen durch die Analyse der Komponenten Ras und ERK in verschiedenen Zelllinien beschrieben.

Um die Rolle der Raf-Kinasen auf diese Prozesse speziell in primären murinen B-Zellen zu untersuchen, wurden Raf-1^{fl/fl}//B-Raf^{fl/fl}//mb1-Cre^{+/-} (DKO)-Mäuse erzeugt. Diese weisen eine B-Zell-spezifischen Deletion der beiden Kinasen ab der frühen B-Zell-Entwicklung auf. Dieses Mausmodell wurde in dieser Arbeit verwendet, um die Raf-vermittelten Funktionen während der B-Zellentwicklung, -aktivierung und -differenzierung zu analysieren. Im Rahmen dieser Dissertation wurden wichtige Rollen von B-Raf und Raf-1 in den folgenden Prozessen aufgedeckt: (I) B-Raf und Raf-1 waren nicht erforderlich, um die ERK-Phosphorylierung in BCR-, LPS- und CD40-stimulierten B-Zellen zu vermitteln, sondern fungierten vielmehr als negative Regulatoren der PI3K- oder Rac/PAK-vermittelten ERK-Phosphorylierung in ruhenden und aktivierten reifen B-Zellen. (II) Die Inaktivierung von B-Raf und Raf-1 in DKO-Mäusen führte zu einer beeinträchtigten T-Zell unabhängigen Immunantwort. (III) Die B-Raf//Raf-1-Defizienz verursachte eine Blockade der Plasmazell-Differenzierung beim Übergang von aktivierten B-Zellen zu Prä-Plasmablasten und bei ihrer weiteren Differenzierung zu Plasmablasten. Wir fanden heraus, dass B-Raf und Raf-1 in diesen Stadien einen starken Anstieg der ERK-Phosphorylierung bewirken, der für die Plasmazell-Differenzierung wesentlich zu sein scheint.

Darüber hinaus wurden Raf-1^{fl/fl}//B-Raf^{fl/fl}//LMP1/CD40^{flSTOP+/-}//CD19-Cre^{+/-} (RafDKO/LC40)-Mäuse mit LMP1/CD40^{flSTOP+/-}//CD19-Cre^{+/-} (LC40)- und Kontrollmäusen verglichen, um die Auswirkungen einer genetischen Inaktivierung von B-Raf und Raf-1 auf B-Zellen mit einem konstitutiv aktiven CD40-Signal und die daraus resultierende LC40-getriebene B-Zelltransformation zu untersuchen. Die Inaktivierung von B-Raf und Raf-1 in RafDKO/LC40-Mäusen verringerte den LC40-vermittelten Phänotyp der B- und T-Zell-Expansion sowie der B-Zelltransformation. Wie eine RNA-Seq-Analyse ergab, scheint dies in erster Linie auf eine verringerte LC40-vermittelte Myc-Expression und eine reduzierte Notch2- und nichtkanonische NFκB-Aktivierung zurückzuführen zu

sein. Diese Daten deuten darauf hin, dass Raf-Kinasen die Aktivierung dieser beiden Signalwege stromabwärts von CD40 modulieren.

List of Figures

Figure 1: Schematic illustration of the B cell development in the BM.	18
Figure 2: Scheme of the B220, PAX5, IRF4, CD138, and BLIMP1 regulation during PB formation.	22
Figure 3: Schematic illustration of B cell receptor (BCR) signaling in mature B cells.	24
Figure 4: Schematic illustration of the main events of signal transduction upon CD40 signaling.	26
Figure 5: Simplified schematic illustration of the main events of signal transduction upon TLR4/LPS signaling.	27
Figure 6: Scheme of the protein structure of Raf-kinases.	28
Figure 7: Scheme of the Raf-1 ^{fl/fl} //B-Raf ^{fl/fl} //mb1-Cre ^{+/-} (DKO) transgenic mouse model.	32
Figure 8: Scheme of the Raf-1 ^{fl/fl} //B-Raf ^{fl/fl} //LMP1/CD40 ^{flSTOP+/-} //CD19-Cre ^{+/-} (RafDKO/LC40) transgenic mouse model.	33
Figure 9: DKO B cells exhibited increased pERK levels, which could be further induced upon anti-IgM stimulation.	37
Figure 10: B-Raf//Raf-1 inactivation resulted in elevated basal pERK levels.	37
Figure 11: B-Raf//Raf-1 inactivation increased the pERK levels in recirculating B cells.	38
Figure 12: DKO B cells displayed unaltered BCR signaling with respect to pSYK, pJNK, pp38, pIkB α , and pAKT.	39
Figure 13: Similar A-Raf expression in mature control and DKO B cells.	40
Figure 14: Titration of pan-Raf inhibitors on control B cells.	41
Figure 15: The chemical or genetic inactivation of Raf-kinases led to increased pERK levels.	42
Figure 16: SYK inhibition reduced basal and anti-IgM mediated pERK levels of control and DKO B cells.	43
Figure 17: Basal and anti-IgM mediated pERK levels of control and DKO B cells was PI3K dependent.	44
Figure 18: The RAC/PAK signaling contributed to the basal and anti-IgM mediated pERK levels of control and DKO B cells.	45
Figure 19: Basal and anti-IgM mediated pERK levels of control and DKO B cells were independent of the canonical NF κ B signaling pathway.	46
Figure 20: DKO mice displayed a diminished TI immune response.	47
Figure 21: DKO B cells failed to adopt the PB state upon LPS stimulation <i>in vitro</i> .	48
Figure 22: DKO B cells exhibited normal IRF4 but impaired BLIMP1 upregulation.	48
Figure 23: LPS stimulated DKO B cells displayed a block in the transition into pre-PB and PB.	49
Figure 24: Both control and DKO B cells upregulated pERK upon LPS stimulation.	51
Figure 25: DKO B cells exhibited increased ERK phosphorylation, which could be further upregulated upon <i>in vitro</i> stimulation.	51
Figure 26: LPS induced pERK levels of control and DKO B cells is partially PI3K dependent.	52
Figure 27: DKO B cells featured a prolonged ERK phosphorylation in the nucleus.	53
Figure 28: Gating strategy of the different B cell differentiation stages upon LPS stimulation <i>in vitro</i> .	55
Figure 29: A sharp increase of pERK levels in pre-PBs as a prerequisite for PB formation.	56
Figure 30: DKO B cells displayed increased pERK levels upon CD40 stimulation.	57
Figure 31: Long-term CD40 stimulation induced a PI3K dependent ERK phosphorylation.	58
Figure 32: RafDKO/LC40 B cells exhibited higher ERK phosphorylation than LC40 B cells.	60
Figure 33: B-Raf//Raf-1 inactivation weakened the LC40 induced B and T cell expansion.	61

Figure 34: B-Raf//Raf-1 inactivation weakened the LC40 induced expansion of Fo B and MZ B cells.	62
Figure 35: B-Raf//Raf-1 inactivation diminished the LC40 mediated pathological splenomegaly.	63
Figure 36: B-Raf//Raf-1 inactivation reduced the LC40 mediated outgrowth of the aberrant B cell population.	67
Figure 37: The expression pattern of the different B cell activation markers in control, LC40 and RafDKO/LC40 mice.	68
Figure 38: In old RafDKO/LC40 mice Raf proficient B cells are detectable.	69
Figure 39: The B-Raf//Raf-1 inactivation changed the gene expression pattern in LC40 expressing B cells.	71
Figure 40: B-Raf//Raf-1 inactivation increased Ahnak and decreased Myc and Odc1 RNA expression in LC40 expressing B cells.	72
Figure 41: LC40 B cells exhibit predominantly a MZ B cell gene signature, which is abrogated in RafDKO/LC40 B cells.	76
Figure 42: The Notch2 induced gene signature of LC40 expressing B cells was diminished in RafDKO/LC40 B cells.	77
Figure 43: The non-canonical NFκB induced gene signature of LC40 expressing B cells was diminished in RafDKO/LC40 B cells.	78
Figure 44: B-Raf//Raf-1 inactivation decreased HES1, CD21 and NFκB2 RNA expression in LC40 expressing B cells.	79
Figure 45: RafDKO/LC40 B cells displayed significantly reduced HES1 and p52 protein expression.	81

List of Tables

Table 1: Splenic cell composition of old control, LC40 and RafDKO/LC40 mice.	65
Table 2: Splenic B cell composition of old control, LC40 and RafDKO/LC40 mice.	66
Table 3: Genes within the Top 25 significant differentially expressed protein coding genes with a higher expression in LC40 than in RafDKO/LC40 B cells.	73
Table 4: Genes within the Top 25 significant differentially expressed protein coding genes with a lower expression in LC40 than in RafDKO/LC40 B cells.	74
Table 5: Antibodies used in FACS with its corresponding conjugates, clones, the company and its used dilution.	99
Table 6: Antibodies used in ELISpot with its corresponding clones, the company, and its used dilution.	99
Table 7: Antibodies used in ELISA with its corresponding clones, the company, and its used dilution.	99
Table 8: Antibodies used in protein analyses (Western blot and WES) with its corresponding clones, the company, and its used dilution.	100
Table 9: Material/Chemicals/Enzymes/Commercial kits and the company the products were obtained from.	100
Table 10: Inhibitors with its corresponding target, the company, and its used concentration.	102
Table 11: Stimuli with its corresponding company, its used concentration, and the incubation time points. Mostly used timepoints are marked with bolt type.	102
Table 12: Formula of media and uncommercial buffers	103
Table 13: Specific PCRs needed to be performed for the indicated mouse strains	105

Table 14: Primer and primer sequences used in the different PCRs	105
Table 15: PCR mixtures specific for each PCR	105
Table 16: PCR programs of the thermal cycler specific for each PCR	106
Table 17: Sizes of the different PCR products of the specific PCRs	106

List of Abbreviations

aCD40	anti-CD40
ADAM	A Disintegrin And Metalloproteinase
APS	Ammonium persulfate
ASC	antibody secreting cell
BAFF(-R)	B cell activating factor (receptor)
BCM	B cell medium
BCR	B cell receptor
BLIMP1	B lymphocyte induced maturation protein 1
BLK	B Lymphoid Tyrosine Kinase
BM	bone marrow
bp	base pair(s)
BSA	bovine serum albumine
BTK	Burton's tyrosine kinase
C	C-terminal
Cam	calmodulin
CamK	Calmodulin kinase
CD	Cluster of differentiation
cDNA	copy-DNA
CFSE	Carboxy-Fluoreszein Diacetat Succinimidyl-Ester
CGG	Chicken Gamma Globulin
CLP	common lymphoid progenitor
CR	conserved region
CRD	cysteine-rich domain
Cre	recombinase derived from the P1 bacteriophage (causes recombination)
CSR	class-switch recombination
ctrl	control
Dab	Dabrafenib
DAG	diacylglycerol
DKO	B-Raf//Raf-1 double knockout (Raf-1 ^{fl/fl} //B-Raf ^{fl/fl} //mb1-Cre ^{+/-})
DLL-1	delta-like canonical Notch ligand 1
DMSO	dimethyl sulfoxide
DNA	deoxyribonucleic acid
dNTP	deoxynucleotide triphosphates
DPBS	Dulbecco's Phosphate Buffered Saline
DTT	Dithiothreitol
DUSP	Dual-specificity phosphatase
EBV	Epstein-Barr virus
EDTA	Ethylenediaminetetraacetic acid

ELISA	Enzyme-linked Immunosorbent Assay
ELISpot	Enzyme Linked Immuno Spot Assay
ERK	extracellular-signal regulated kinase
FACS	Fluorescence Activated Cell Sorting
FCS	fetal calf serum
FDR q-val	false discovery rate
Fo B	Follicular B cell
GAPDH	glyceraldehyde phosphate dehydrogenase
GC	germinal center
GEF	Guanin exchange factor
HES1	hairy and enhancer of split-1
HRP	horseradish peroxidase
HSC	hematopoietic stem cell
ICAM	Intercellular adhesion molecule
ICOS-L	Inducible T-cell Co-stimulator Ligand
Ig	immunoglobulin
Igα/Igβ	immunoglobulin-associated protein α/β
IκB	nuclear factor of kappa light polypeptide gene enhancer in B-cells inhibitor
IKK	I κ B kinase
IL	interleukin
IP3	inositol triphosphate
IRF4	Interferon Regulatory Factor 4
ITAM	immunoreceptor tyrosine-based activation motif
JAK	Janus kinase
JNK	c-Jun-N-terminal kinase
kDa	kilodalton
KO	knockout (deleted gene)
LC40	LMP1/CD40 fusion Protein
LMP1	latent membrane protein 1
loxP	locus of crossing, x
LPS	lipopolysaccharide
LY29	LY294002
LY30	LY3009120
MACS	magnetic cell sorting
MAPK	Mitogen-activated protein kinase
MEK	mitogen-activated protein kinase/ERK kinase
MEKK	MAPK/ERK Kinase Kinase
MFI	median fluorescence intensity
MHC	major histocompatibility complexes
mRNA	messenger RNA
MyD88	myeloid differentiation primary response gene 88
MZ B	Marginal zone B cell
N	N-terminal
n.i.	not immunized
NES	normalized enrichment score
NFκB	nuclear factor kappa-light-chain-enhancer of activated B cells

NOM p-val	nominal p-value
Notch2IC	Notch2 intracellular domain
NP	nitrophenyl acetyl
OD	optical density
Odc1	Ornithine decarboxylase 1
PAK	p21-aktivierte Kinase
PAMP	pathogen-associated molecular pattern
PAX5	Paired box protein 5
PB	plasmablast
PBS	Phosphate buffered saline
PC	plasma cell
PCR	polymerase chain reaction
PFA	paraformaldehyde
PI3K	phosphatidyl inositol-3 kinase
PIP2	phosphoinositide-3,4-bisphosphate
PKA	protein kinase A
PKC	protein kinase C
PLCγ	phospholipase C gamma
pre-PB	pre-plasmablast
PTK	protein tyrosine kinase
Rac	Ras-related C3 botulinum toxin substrate
Raf	rapidly growing fibrosarcoma
RafDKO/LC40	Raf-1 ^{fl/fl} //B-Raf ^{fl/fl} //LMP1/CD40 ^{flSTOP+/-} //CD19-Cre ^{+/-}
RAG	recombination-activating genes
Ras	rat sarcoma
RBC	red blood cell
RBD	Ras-binding domain
RBPJ	Recombination Signal Binding Protein For Immunoglobulin Kappa J Region
RIP1	receptor-interacting protein 1
RKIP	Raf kinase inhibitory protein
RNA	ribonucleic acid
RNA-Seq	RNA sequencing
rpm	revolutions per minute
rRNA	ribosomal RNA
SA	Streptavidin
SD	standard deviation
SDS	sodium dodecyl sulfate
SH2	Src Homology 2
SHM	somatic hypermutation
SLC	surrogate light chain
Sor	Sorafenib
SP	spleen
STAT	signal transducer and activators of transcription
SYK	Spleen tyrosine kinase
TAE	Tris-acetate-EDTA
TBS	Tris-buffered saline

TBST	Tris-buffered saline with Tween20
TCR	T cell receptor
TD	T cell dependent
TE	Tris-EDTA
TEMED	N,N,N',N'-Tetramethylethylenediamine
TF	transcription factor
TI	T cell independent
TIR	Toll/IL-1 receptor
TLR	Toll-like receptor
TNF	tumor necrosis factor
TNFR	TNF receptor
TPL2	Tumor progression locus 2
TRAF	TNF receptor associated factors
TRIF	TIR domain-containing adaptor inducing IFN- β
Tris	Trishydroxymethylaminomethane
v/v	volume per volume
w/o	without
w/v	weight per volume
μ	heavy chain of the immunoglobulin

1. Introduction

1.1 The immune system

In mammals the innate and adaptive immune system exist to eradicate pathological microbes (1). Cells of the innate immunity originate from the myeloid lineage and are the first line of the immune response. They immediately fight the infection and bridge the time until the adaptive immune system responds with a time delay of about 4 to 7 days. (1–3). The adaptive immune system acts through the humoral B cell and the cellular T cell response (2). B and T cells both originate from the lymphoid lineage and are characterized by antigen specificity. Each B or T cell expresses exactly one of the antigen specific B or T cell receptors (BCR and TCR), respectively (1–3). The entire B and T cell population covers a large repertoire of receptors against the majority of pathogens (1).

Activation of naïve T cells by antigen presenting cells within the secondary lymphoid organs leads to differentiation into either CD8⁺ cytotoxic T cells fighting infected cells or CD4⁺ T helper cells. CD4⁺ T cell activation provoke the T cell dependent (TD) immune response. Hereby, the native antigens are trapped by the BCR leading to BCR signaling in the B cell. Furthermore, the BCR bound antigen is internalized, processed and antigen peptides are presented by MHC class II molecules on the B cell surface. These complexes are recognized by specific CD4⁺ T cells inducing costimulatory signals in the B cell. This complete B cell activation results in affinity maturation, class switching and final differentiation to antibody secreting plasma cells (PC) or memory B cells (1–5).

In addition to the TD immune response, B cells could differentiate in a T cell independent (TI) manner (2,5,6). Two different types are distinguished, which are categorized according to their antigens. TI type I antigens, such as lipopolysaccharide (LPS), trigger B cell activation through Toll-like receptors (TLRs). In contrast, repetitive polysaccharides initiate a TI type II immune response through BCR crosslinking (6). The latter needs the support of T and natural killer cells by cytokine production (7). No adjustment of antibody affinity occurs in the TI immune response resulting in a very rapid production of low-affinity IgM antibodies (2,5,6).

1.2 B cells

The mature B cell population can be categorized in B1 and B2 cells. B1 cells predominantly home to the body cavities, such as the peritoneal cavity. They respond rapidly to pathogens by producing natural IgM antibodies and are considered to have the property

of self-renewal (8,9). Furthermore, B1 cells are subdivided in B1a and B1b cells by a CD5^{high} and CD5^{low} expression, respectively (8–10).

In the murine spleen, the two mature B2 cell populations, CD23^{high}CD21⁺IgD^{high}IgM^{low} follicular B (Fo B) cells and CD23^{low}CD21^{high}IgD^{low}IgM^{high} marginal zone B (MZ B) cells are distinguished (8,11,12). Thereby, a major part of splenic B cells is made up by Fo B cells (11). Fo B cells migrate highly throughout the lymphatic system and reside in the follicular structures of the secondary lymphoid organs near to the T cell boarder. They predominantly respond in a TD immune response (8,11,13). MZ B cells are stationary located in the marginal zone at the border of white to red pulp in the murine spleen. Here, they are in direct contact with blood and can therefore rapidly respond to blood-borne pathogens. They predominantly react T cell independently (13,14). However, MZ B cells are not completely sessile, as shuttling of MZ B cells into the follicle has been described. This plays a key role in the transport of blood-borne pathogen antigens to follicular dendritic cells (FDCs) of the follicles (8,13,15).

1.2.1 B cell development

1.2.1.1 Bone marrow B cell development

The B1 B cell subset is hypothesized to develop during fetal hematopoiesis in the liver (10). The more prominent B2 B cell subset derive from common lymphoid progenitor (CLP) cells of the lymphoid lineage. The B cell development of adult mammals takes place in the bone marrow (BM) (1–3) (Figure 1).

An important process occurring during B cell development is the generation of the various BCRs, which are repeatedly tested for functionality and self-tolerance (16). The BCR is composed of immunoglobulins, consisting of 2 heavy and 2 light chains, complexed with the transmembrane signaling heterodimer of the immunoglobulin-associated proteins Ig α (CD79a, mb1) and Ig β (CD79b) (17). The heavy and light chains are encoded by multiple variable (V), diverse (D), and joining (J) gene segments (1,17). Both immunoglobulin chains are formed by recombination during B cell development. The heavy chains consist of one of each of the different V_H, D and J_H gene segments, while the light chain is formed by V_LJ_L rearrangement (2,18). The high diversity is not only based on the random combination of the different segments but is increased by imprecise splicing and the insertion of nucleotides by the deoxyribonucleotidyltransferase (1,16).

Rearrangement of the immunoglobulin heavy chain takes place in the pro-B cell (18,19). The pro-B cells arise from the CLP and express the pro-BCR consisting of calnexin and the signaling heterodimer of Ig α and Ig β (16). At the transition of pro-B cells to early large pre-B cells the pre-BCR is expressed on the cell surface. This surface expression is only possible, if a functional heavy chain V_HDJ_H (μ) could associate with a surrogate light

chain (SLC). The resulting immunoglobulin is associated with the signaling heterodimer $Ig\alpha/Ig\beta$. Signaling of the pre-BCR mediates intense proliferation resulting in a positive selection of cells, which successfully rearranged their heavy chain (16,18,20). Subsequently, the recombined heavy chain is protected from renewed rearrangement by allelic exclusion (20–23). During the transition of early large pre-B cells to small pre-B cells V_LJ_L recombination of the immunoglobulin light chain is induced (23,24). After passing the checkpoint for successful rearrangement of the light chain, a functional BCR containing 2 rearranged heavy and light chains and the signaling domains $Ig\alpha$ and $Ig\beta$ is formed (16). The expression of the BCR on the surface of the B cell reflects the transition of the small pre-B cell to the immature B cell. The different stages of B cell development can be distinguished by the marker expression of CD25, CD43 and B220 (Figure 1).

The immature B cells are checked for self-reactivity to ensure self-tolerance (2,25). While strong BCR signaling upon binding of self-antigens seems to lead to apoptosis, moderate BCR binding of self-antigens initiate receptor editing of the light chain. If this is not successful, apoptosis or anergy is induced in immature B cells (16,18,25). Anergic B cells can still migrate out of the BM but cannot be activated and are not able to differentiate into antibody producing PCs (19). However, immature B cells passing the negative selection migrate as transitional B cells to the periphery, predominantly in the spleen, where they finally mature into Fo B or MZ B cells (2,16,25).

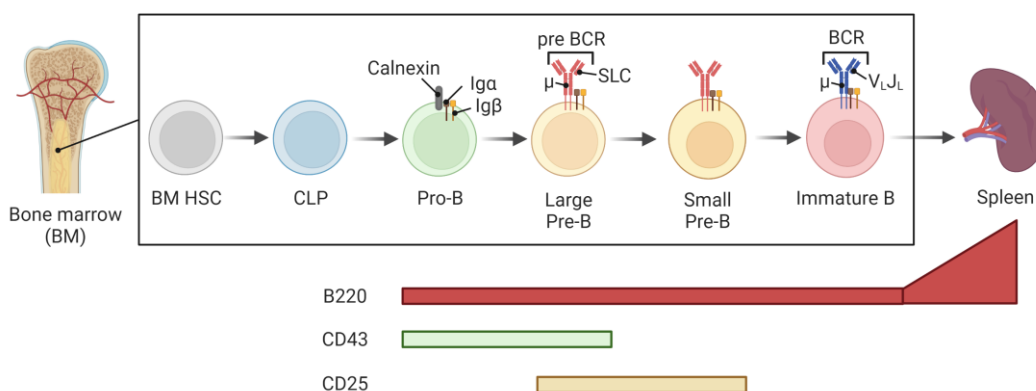


Figure 1: Schematic illustration of the B cell development in the BM. Based on Meffre et al. 2000 and Hardy et al. 2001 (16,18). BM hematopoietic stem cells (BM HSC) differentiate into common lymphoid progenitors (CLP) and further to pro-B cells (pro-B) expressing the pro-BCR (calnexin, $Ig\alpha$ and $Ig\beta$). In pro-B cells VDJ recombination of the heavy chains takes place. Expression of the pre-BCR [rearranged immunoglobulin heavy chain μ and the surrogate light chain (SLC)] occurs in large pre-B cells (large pre-B). In the small pre-B cells the light chains are recombined. In immature B cells, the mature BCR [rearranged heavy (μ) and light (V_LJ_L) chain] is expressed and checked for self-tolerance by negative selection. Immature B cells passing this checkpoint emigrate into the periphery and differentiate into mature B cells in the spleen. The surface ex-pression of B220, CD43 and CD25 in BM B cells is depicted. This figure was designed using BioRender Basic, biorender.com.

1.2.1.2 Peripheral B cell maturation and cell fate decision

The negative selection of B cells expressing a self-reactive BCR does not stop with emigrating from the BM. A relevance of negative selection of autoreactive transitional B cells *in vivo* is discussed because transitional B cells do not proliferate upon BCR crosslinking, but feature BCR induced apoptosis *in vitro* (26,27). Transitional B cells are categorized in three stages T1, T2, and T3 (26,28). T1 cells that have successfully migrated into the follicular structures of the spleen immediately become T2 cells (29). Allman et al. could show in 2001, that transitional B cells featured a linear progression from the T1 to the T2 and further to the T3 stage (26). However, the mature Fo B and MZ B cells were described to originate from the T2 stage (14). In contrast, the T3 B cell population does not give rise to mature B cells but appears to be composed of autoreactive B cells, which are consequently forced into an anergic state (30,31).

The cell fate decision of the T2 B cell to become Fo B or MZ B cells depends on various signaling pathways and further their strength (11). It has been suggested that strong BCR signaling in transitional B cells favors the transition to Fo B cells, while weak BCR signals leads to the development of MZ B cells (11,29).

In addition, Notch2 signaling drives T2 maturation into the MZ B cell phenotype. This was demonstrated by experiments inactivating Notch2 resulting in a reduced MZ B cell population (32) and by experiments with constitutively active Notch2 leading to increased amounts of MZ B cells (33). Notch2 is a transmembrane receptor binding its membrane bound ligand DLL-1 expressed by another cell. Receptor engagement induces Notch2 cleavage by an ADAM protein. Subsequent cleavage by the γ -secretase releases the intracellular domain of Notch2 (Notch2IC) from the plasma membrane into the cytoplasm. After translocation of Notch2IC into the nucleus, it binds together with the DNA-binding protein RBPJ to the DNA causing changes in the gene expression pattern (34). Furthermore, NF κ B signaling influences the survival, differentiation, and cell fate decision of maturing B cells (11). NF κ B signaling is predominantly induced by the BCR and some receptors of the tumor necrosis factor (TNF) family like CD40 and the B cell activating factor receptor (BAFF-R) (35,36). In mammals, the five NF κ B transcription factors p50, p52, RelA (p65), RelB and c-Rel are known to bind as homo- and heterodimers to κ B enhancers of the DNA and thus influence the expression of target genes (35–37). The NF κ B transcription factors pre-exist in inactivated states in the cell (38). This inactivation is mediated by I κ B proteins (inhibitor of the nuclear factor of kappa light polypeptide gene enhancer in B-cells), which on the one hand masks the nuclear localization sequence of the NF κ B, and on the other hand favors a cytoplasmic localization of I κ B and its complexed proteins by the nuclear export sequence of I κ B (35,38,39). Ligand binding of different receptors result in activation of the I κ B kinase (IKK) complex, which

mediates phosphorylation of the I κ B. The resulting ubiquitination and proteasomal degradation of the I κ B proteins release the NF κ B transcription factors. Furthermore, the IKK complex phosphorylates the precursor proteins p100 (NF κ B2) and p105 (NF κ B1), which leads to a partial degradation to p52 and p50, respectively. Then NF κ B dimers translocate to the nucleus and induce changes in the gene expression pattern of the cell (35,36,40). In addition to the canonical (classical) pathway, the non-canonical (alternative) NF κ B signaling pathway was identified in 2001 (41). These two NF κ B signaling pathways not only differ in the components used but are also activated by different receptors. BCR signaling mainly leads to the activation of the canonical NF κ B pathway (42,43). It is based on p105 processing to the p50 protein, which dimerizes primarily with RelA and c-Rel (44,45). BAFF-R mediated signaling mainly favors the non-canonical NF κ B signaling by activation of the IKK α (41,44,46–48). After phosphorylation of p100 and subsequent proteasomal processing to p52, the latter dimerizes predominantly with RelB (44,49,50). CD40 signaling activates both the canonical and the non-canonical NF κ B signaling pathway (51). Finally, it should be mentioned that the beneficial effect of NF κ B signaling on most of the peripheral B2 cells was described but seems to play a more prominent role regarding MZ B cell expansion (52,53).

So far, a most widely linear development of mature B cells was described. But several authors also mentioned the possibility of plasticity between Fo B and MZ B cells (11,13,14). In 2021, this was proven in mice by Lechner et al. They observed the Notch2 driven generation of MZ B cells from Fo B cells (54).

1.2.2 B cell differentiation

1.2.2.1 Cellular processes of B cell differentiation

Antigen contact of naïve B cells leads to the generation of PCs. Depending on the type of antigen (TD or TI), and which B cell subtype (Fo B, MZ B or B1 cell) encounters the antigen, either extra-follicular short-lived or long-lived germinal center (GC) derived PCs are generated (55). MZ B cells and B1 cells usually differentiate very rapidly after antigen exposure in a TI immune response to short-lived PCs. This takes place in extra-follicular foci. Thus, no affinity maturation and only little immunoglobulin isotype switching takes place. Furthermore, these short-lived PCs remain in the secondary lymphoid organs and do not exhibit migratory properties towards the BM (8,56,57).

Fo B cells respond primarily to TD antigens, and the intensity of BCR stimulation by the antigen determines the mode of PC differentiation. Strong BCR-antigen binding allows Fo B cells to rapidly differentiate in extra-follicular foci into short-lived PCs (55,58). Fo B cells with rather weak to intermediate antigen mediated BCR signaling migrate to

the B-T cell border. Those activated Fo B cells receive co-stimulatory signals from activated T cells (59,60). Additionally, the B-T cell interactions lead to class-switch recombination (CSR) of the constant regions of the immunoglobulins, which results in an isotype switch from IgM/IgD to IgG, IgA or IgE. The different isotypes of immunoglobulins have different effector functions (61–63). Co-stimulated Fo B cells reenter the follicle and induce the GC reaction (59,60). While early GC are characterized by a strong proliferation of B cells, mature GC are divided into two areas (55,60,64). The proliferating centroblasts are located in the dark zone and perform somatic hypermutation (SHM), which leads to affinity maturation by the introduction of point mutations in the variable regions of the rearranged gene loci of the immunoglobulins. By migrating into the light zone, the cells stop proliferating and are then designated as centrocytes. Here, the BCR affinity of centrocytes is checked (65,66). While low BCR affinity leads to reentry into the dark zone and renewed SHM, B cells with high-affinity BCRs receive strong signals. These lead to differentiation of centrocytes into PCs. GC derived PCs egress through the dark zone, feature a long lifespan, high antibody affinity, represent different immunoglobulin isotype classes and home predominantly to the BM. Memory B cells are more likely to arise from centrocytes through survival signals and displayed most likely low BCR affinity (55,67,68). They leave the GC through the light zone and reside in the marginal zone of the spleen (69,70).

In any case, contact with an adequate stimulus initially leads to intensive proliferation of activated B cells. Some of these B cells then differentiate into plasmablasts (PB), which, while still proliferating, already secrete antibodies. Cells that stop proliferation and exclusively secrete antibodies are then referred to as mature PCs (55). Antibodies bind the antigens and can either have a neutralizing function or lead to phagocytosis of the pathogens or infected cells by activating the innate immune system or the complement system (1,2).

1.2.2.2 Marker expression during plasma cell differentiation

In all the processes of terminal differentiation to PCs described so far, the transcription factors PAX5 (Paired box protein 5), IRF4 (Interferon Regulatory Factor 4) and BLIMP1 (B lymphocyte induced maturation protein 1) play a crucial role (55). PAX5 induces B cell identity already from the pro-B cell stage during B cell development (71). PAX5 represses genes important for PC differentiation, such as *Xbp1* (72). Thus, PAX5 downregulation is a prerequisite for PC differentiation (55,73), which already occurs at the pre-plasmablast (pre-PB) stage (74). Beyond the plasmablast (PB) stage, PAX5 expression is no longer detectable (55).

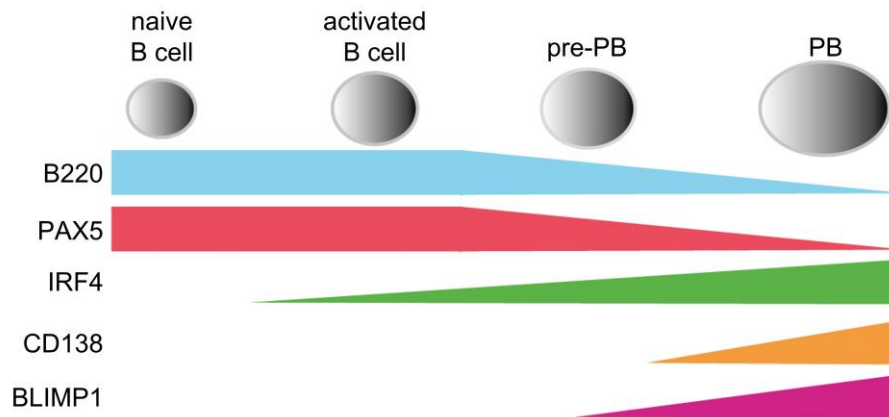


Figure 2: Scheme of the B220, PAX5, IRF4, CD138, and BLIMP1 regulation during PB formation. From the pre-PB state onwards, B220 and PAX5 get downregulated, while BLIMP1 and CD138 are upregulated. IRF4 is already expressed in activated B cells and is further upregulated during PC differentiation. The same illustration adapted from Oracki et al. 2010 (55) can be found in Scheffler et al. 2021.

In addition, PC differentiation is driven by the expression of the transcription factors IRF4 and BLIMP1. On the one hand, this leads to further inhibition of *PAX5* and other genes that stabilize the identity of the mature B cells (55,75). On the other hand, PC genes, such as *Xbp1* and *CXCR4*, are expressed (76,77). Moreover, a certain dose dependence is described for IRF4. While moderate IRF4 expression induces CSR, high IRF4 levels mediate BLIMP1 expression (78). Whereas IRF4 is already steadily upregulated in activated B cells up to the PB stage, BLIMP1 expression has a delayed onset. It is upregulated in PBs and continues to increase further during differentiation into PC. At the transition from pre-PB to the PB stage, the B cell marker B220 is downregulated. At the same time, the PC marker CD138 (syndecan) is expressed. The downregulation of B220 and the upregulation of CD138 continue to increase as PBs differentiate into PCs (55). This marker expression pattern of the different PC differentiation stages from naïve B cells into PBs is important for some flow cytometric analyses used in this work (Figure 2).

1.2.3 Signaling during B cell activation

1.2.3.1 B cell receptor signaling

Due to the high complexity of BCR signaling in the different B cell stages, the focus will be on the main antigen induced signaling pathways in mature B cells (Figure 3). As mentioned above, the BCR consists of 2 rearranged heavy and light chains and the signaling domains Ig α and Ig β (16). Both Ig α and Ig β contain an immunoreceptor tyrosine-based activation motif (ITAM) in their intracellular domains (79). Upon BCR stimulation by antigen crosslinking and recruitment to lipid rafts in the plasma membrane, the ITAMs of Ig α

and Ig β are phosphorylated by the protein tyrosine kinases (PTK) of the Src-family (LYN, BLK, and FYN) (80). The double phosphorylated ITAMs provide a docking site for the PTK SYK, which binds to it via its 2 Src Homology 2 (SH2) domains. Consequently, SYK is phosphorylated and activated either by Src-PTKs or by autophosphorylation (80,81). Activated SYK mediates phosphorylation of the adaptor protein Src homology [SH2] domain-containing leukocyte protein of 65 kD (SLP-65, also known as BLNK), which links the BCR mediated activation of PTKs with the different downstream signaling pathways (80,82,83). SLP-65 is constitutively associated with the guanine nucleotide exchange factor Vav and the Grb2-Sos complex (82,83). Recruitment of SLP-65 with its associated proteins to the plasma membrane in the proximity to BCR activated PTKs allows activation of Vav and Grb2-Sos (83), resulting in activation of the three different Mitogen-activated protein kinase (MAPK) pathways. Vav is hypothesized to activate the Rac-MEKK-JNK/p38 pathway, while Grb2/Sos is described to induce the Ras-Raf-MEK-ERK signaling cascade (83–85). The different MAP kinases p38, JNK (c-Jun-N-terminal kinase), and ERK (extracellular-signal regulated kinase) phosphorylate diverse cytoplasmic and nuclear targets. These include transcription factors (TF), which in turn achieve changes in the gene expression. For example, nuclear ERK phosphorylates and activates the transcription factors Elk-1 and Ets (86,87). JNK phosphorylates Jun, which then together with Fos, forms the transcription factor AP-1 (2,80,86). While p38 and JNK are described to integrate inflammatory signals, ERK plays a crucial role inducing proliferation and differentiation of the cells (80). The Ras-Raf-MEK-ERK signaling pathway will be described below in more detail (see 1.3.2).

In addition to MAPK activation, phosphorylated SLP-65 acts as a scaffold for the interaction of SYK, the Burton's tyrosine kinase (BTK) and the phospholipase C gamma (PLC γ). SYK and BTK mediated activation of PLC γ leads to the hydrolysis of phosphoinositide-3,4-bisphosphate (PIP₂) to diacylglycerol (DAG) and inositol triphosphate (IP₃) (80,88). The latter mediates an increase of cytoplasmic Ca²⁺, which leads to the calmodulin (Cam) mediated activation of Cam kinases (CamK) or calcineurin. The Cam kinase II (CamK2) can translocate to the nucleus and for instance modulates the transcription factor Ets-1. Additionally, activated Calcineurin dephosphorylates NFAT, which then translocates to the nucleus and acts as transcription factor. DAG activates the protein kinase C (PKC), which can contribute to the activation of the Ras-Raf-MEK-ERK pathway (80,88–91). Additionally, PKC can activate NF κ B signaling by indirectly activating the IKK complex, which leads to the release and translocation of NF κ B dimers (92).

BCR signaling is influenced by the CD19-CD21-CD81 coreceptor complex, as its activation lowers the threshold of signal strength required for BCR activation. CD21, also known as complement receptor 2 (CR2), directly interacts with CD19 and binds the C3

component of the complement system, integrating information from the innate immune system into the adaptive immune response (93). A pathogen covered by components of the complement system concurrently binds to the BCR by its antigen itself and to CD21 by the C3 component attached to the pathogen. This simultaneous binding brings the BCR and the CD19-CD21-CD81 coreceptor complexes into close proximity. Thus, the Src-family kinases activated by the BCR-antigen interaction can also lead to phosphorylation of the CD19 receptor (2). Upon activation CD19 interacts, for example, with the phosphatidylinositol-3 kinase (PI3K), leading to phosphorylation and activation of AKT (93). Phospho-AKT mediates survival signals by the inhibition of Foxo1 (Forkhead family of transcription factors 1) and the activation of the mTOR (mammalian target of rapamycin) signaling pathway (94).

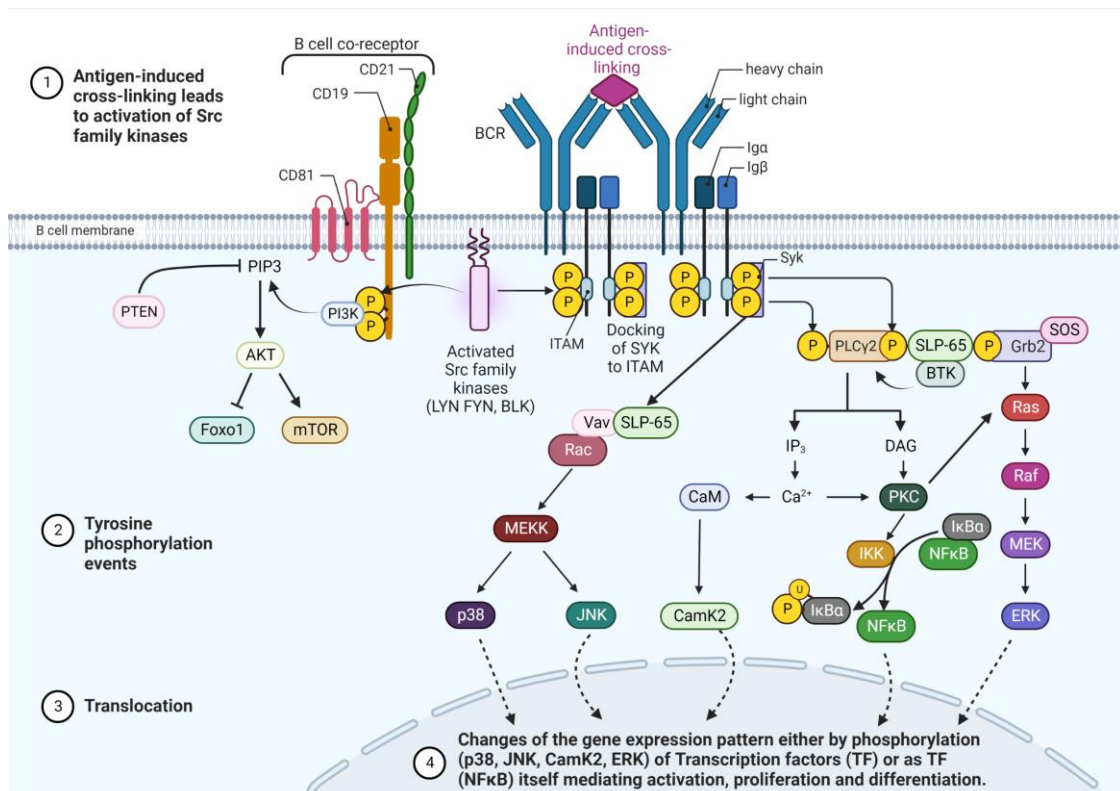


Figure 3: Schematic illustration of B cell receptor (BCR) signaling in mature B cells. Based on Kurosaki 1999 and Dal Porto et al. 2004 (80,85). The BCR consists of a membrane bound immunoglobulin (2 heavy chains, 2 light chains) associated with the signaling hetero dimer Igα/Igβ each containing an ITAM (immunoreceptor tyrosine-based activation motif). The BCR is associated with the B cell coreceptor complex CD21-CD19-CD81, which mediates PI3K/AKT signaling upon Src mediated phosphorylation occurring upon antigen stimulation of the BCR. AKT itself leads to mTOR activation and Foxo1 repression. After antigen-crosslinking the BCR mediates recruitment and activation of the Src kinases (LYN, FYN, BLK), which in turn phosphorylate the ITAMs of Igα and Igβ. SYK is recruited to the phosphorylated ITAMs and itself recruits the adaptor protein SLP-65 to the membrane, thereby activating PLCγ and MAPK downstream signaling events. MAPK signaling results in the activation of p38, JNK and ERK. PLCγ activation induces calcium signaling and in turn NFκB signaling. After nuclear translocation of the effector proteins, gene expression is changed either by phosphorylation of target proteins by p38, JNK, CamK2 or

ERK, or as transcription factors (TF) itself (NFκB). This figure was created using BioRender Basic, biorender.com.

1.2.3.2 CD40 receptor signaling

The CD40 receptor, mainly expressed on B cells, belongs to the tumor necrosis factor (TNF) family integrating costimulatory signals (40,95). CD40 stimulation of B cells *in vitro* results in upregulation of the activation markers (ICAM-1 and CD95), proliferation, improved survival, and differentiation (95–97). *In vivo* experiments with CD40 deficient mice suggest an essential role of CD40 in TD immunoglobulin class switching and germinal center formation, but not for TD IgM responses and TI antibody responses (98).

The interaction of the CD40 ligand (CD40L, CD154) expressed on CD4⁺ T_H cells with CD40 expressed on B cells leads to trimerization of CD40 and association with TNF receptor associated factors (TRAF), which transduce the CD40 signal to different signaling pathways (99). The TRAF family consists of 6 members, of which TRAF1, TRAF2, TRAF3, TRAF5 and TRAF6 interact with CD40 (100). TRAFs themselves do not exhibit enzyme activity, but function as adaptor proteins (101). Thereby, different TRAFs cooperatively mediate different signaling pathways.

CD40 interaction with either TRAF6 or a TRAF2/3 complex activates PI3K and PLCγ in a LYN dependent manner (100–103). The phosphorylation and activation of ERK might be induced either Ras independently by a TRAF6 mediated PI3K/AKT dependent pathway or by a TRAF2/3 induced LYN/SYK activation leading to Ras-Raf-MEK-ERK signaling (103–107). The TRAF1/TRAF2 complex induces exclusively the canonical NFκB signaling pathway, while TRAF3/TRAF5 interaction with the CD40 receptor activates both the canonical and the non-canonical NFκB signaling pathway (100). The activation of non-canonical NFκB activation upon CD40 crosslinking further depends on the TRAF2 dependent degradation of TRAF2 and TRAF3, which results in the release and stabilization of the NFκB inducing kinase (NIK). The latter is required for the p100 processing to p52 (40,100,101). TRAF2 not only mediates degradation, but further activates MEKK1 and thereby JNK and p38 (100,108). In contrast to the TRAF dependent CD40 mediated signaling pathways, JAK binds directly to the activated CD40 receptor without the participation of any TRAFs and results in the activation of STAT transcription factors (100,109). In summary (Figure 4), the interaction of CD40 with its ligand mediates the activation of the MAP kinases ERK, JNK and p38, of the canonical and non-canonical NFκB pathway, as well as of PI3K, PLCγ and JAK/STAT signaling (97,100,101).

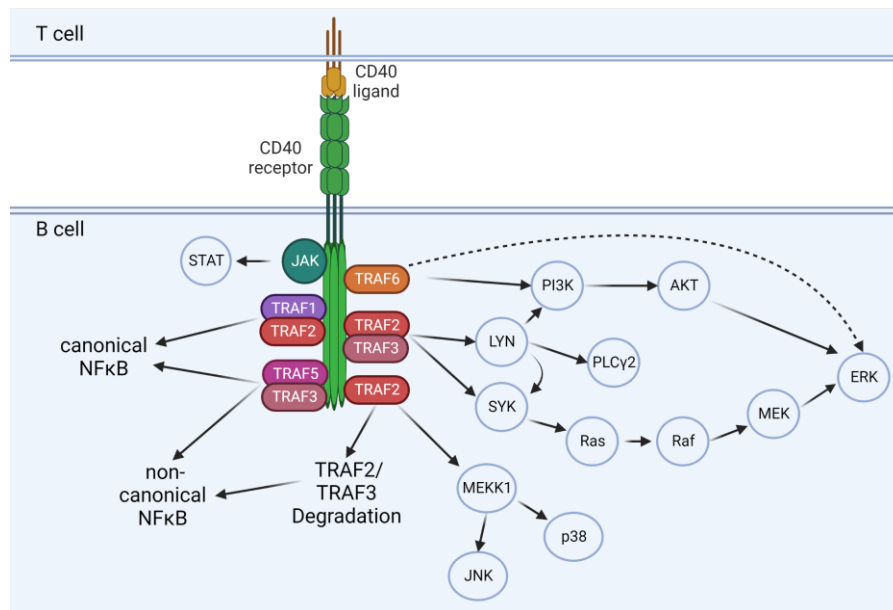


Figure 4: Schematic illustration of the main events of signal transduction upon CD40 signaling. Based on Kashiwada et al. 1998, Elgueta et al. 2009, Vidalain et al. 2000, Ren et al. 1994, Nair et al. 2020 and Bishop 2004 (100,102–105,110). Upon crosslinking of the CD40 receptor on B cells with its CD40 ligand on T cells clustering takes place, followed by association with different TRAF adaptor proteins or JAK leading to the activation of the MAP kinases ERK, JNK and p38, of the canonical and non-canonical NFκB pathway, as well as of PI3K, PLCγ2 and JAK/STAT signaling. This figure was created using BioRender Basic, biorender.com.

1.2.3.3 Toll-like receptor 4 signaling

Besides BCR and TNF receptors, B cells also respond to pathogens via Toll-like receptor (TLR) signaling. TLRs belong to the germline-encoded pattern-recognition receptors, which recognize specific pathogen-associated molecular patterns (PAMPs) (111–113). The different TLRs recognize specific PAMPs. For example, TLR9 is activated by hypomethylated CpG motifs of viral DNA, while TLR3 recognizes double-stranded RNA, which is usually found only in pathogens. TLR4 binds LPS of the outer membrane of gram-negative bacteria and is present in the plasma membrane of B cells (112–114). TLR4 stimulation of B cells induces a T1 immune response resulting in proliferation and PC differentiation (113,114). Ligand binding is mediated by the ectodomain containing leucine-rich repeats. The downstream signaling (Figure 5) is transduced by the Toll/IL-1 receptor (TIR) domain (115). TLR4 engagement with LPS leads to oligomerization of the receptor resulting in its interaction of the TIR domain with MyD88 (myeloid differentiation primary response gene 88). MyD88 signaling induces endocytosis of the TLR4 followed by TRIF (TIR domain-containing adaptor inducing IFN-β) mediated signaling (112–117). MyD88 dependent signaling indirectly activates TRAF6, which on the one hand leads to the activation of IKKs and thereby induces NFκB signaling, and on the other hand to the induction of various MAP kinases. Like MyD88/TRAF6, the adapter protein TRIF activates IKKs and MAP kinases by the recruitment of RIP1 (receptor-interacting protein 1) (112,116). Many mechanisms of these signaling pathways have been explored using

macrophages and cell lines. In B cells, a participation of the BCR/SYK axis in TLR4 mediated ERK phosphorylation and cross talks between the TLR4 and the BCR are described but needed to be further validated (114,118). Furthermore, an involvement of TPL2 in ERK activation is assumed (119).

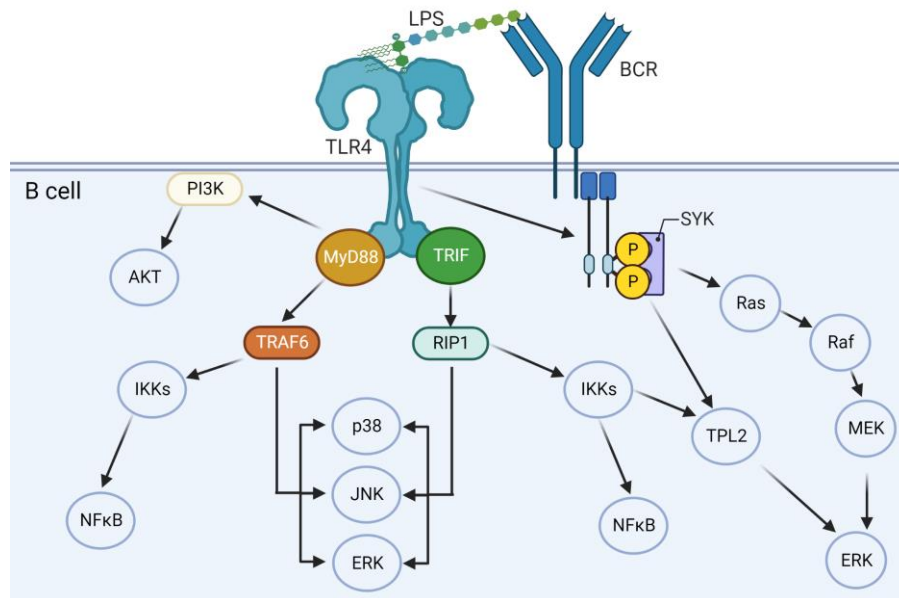


Figure 5: Simplified schematic illustration of the main events of signal transduction upon TLR4/LPS signaling. Based on Ciesielska et al. 2020, Lu et al. 2008, Schweighoffer et al. 2017, Kuriakose et al. 2014 (112,114,117,119). Upon LPS binding TLR4 oligomerize leading to the association with either MyD88 or TRIF. These interactions indirectly result in the activation of the MAP kinases ERK, JNK and p38, or the NFκB pathway, as well as PI3K signaling. ERK phosphorylation is further mediated in a BCR/SYK dependent manner. This figure was created using BioRenderBasic, biorender.com.

1.3 Raf-kinases

1.3.1 Raf-kinase family

The serine/threonine kinases of the Raf (rapidly growing fibrosarcoma) family are important intermediates in the signal transduction. In mammals, 3 isoforms exist A-Raf (68 kDa), B-Raf (70-100 kDa) and Raf-1 (C-Raf; 72-74 kDa) (120). First Raf-1 was identified as a transforming oncogene in mouse and chicken in 1983. It attracted even more attention, when Raf-1 was proven as a direct Ras target protein mediating ERK phosphorylation (121,122). Then the transforming effect of B-Raf mutations in cancer were discovered (123–125). Although tissue-specific expression of the various Raf isoforms was previously reported, most recently an almost ubiquitous expression of A-Raf, B-Raf, and Raf-1 has been assumed (120,126).

The structure of all three Raf isoforms (Figure 6) is divided into a regulatory N-terminal and a C-terminal kinase domain. The regulatory N-terminal domain is composed of the

conserved regions CR1 and CR2, with CR1 including the Ras-binding domain (RBD) and a cysteine-rich domain (CRD) (120,127). While RBD binds Ras, CRD can bind both Ras and membrane lipids. Upon binding, both domains induce conformational changes leading to the removal of autoinhibition and the membrane recruitment of Raf (see section 1.3.2) (128,129). CR2 contains serine and threonine residues, which upon phosphorylation have an inhibitory influence on the Raf activation by the interaction with the 14-3-3 protein (130,131). The conserved C-terminal CR3 region contains the kinase domain and regulatory amino acids that must be phosphorylated for Raf activation (132). The Raf isoforms exist in the cytoplasm of quiescent cells, due to the absence of a distinct subcellular localization sequence (133).

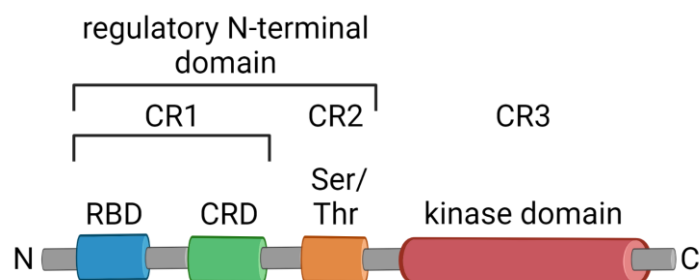


Figure 6: Scheme of the protein structure of Raf-kinases. Raf-kinases contain a regulatory N-terminal domain consisting of the 2 conserved regions CR1 and CR2. The CR1 contains the Ras-binding domain (RBD) and the cysteine-rich domain (CRD). The CR2 consists of a Ser/Thr-rich domain. The C-terminal domain is formed by a third conserved region CR3, which contains the kinase domain. This figure based on Lavoie et al. 2015 (134) and was created using BioRender Basic, biorender.com.

1.3.2 The Ras-Raf-MEK-ERK signaling pathway

Raf activity is tightly controlled and in unstimulated cells Raf-kinases are maintained in an inactive state mediated by autoinhibition, inhibitory phosphorylation and binding to repressors, such as RKIP. Autoinhibition is achieved by an inactive conformation (129). This inactive conformation is stabilized by the binding of the 14-3-3 protein dimer to one phosphorylated serine in the CR2 domain and to one in the C-terminal domain (131). Furthermore, the interaction between 14-3-3 and CR2 masks the CRD and thus prevents Raf activation (135).

The exact mechanism of Raf regulation has not yet been fully elucidated. The key assumptions of the Raf activation/inactivation cycle are as followed: Cell stimulation leads to receptor mediated recruitment of the Grb2-Sos complex. The guanine nucleotide exchange factor Sos causes the GDP-GTP exchange of Ras (129,136). Active Ras-GTP recruits cytosolic Raf-kinases to the plasma membrane through RBD binding (121,129).

This allows binding of the CRD domain of Raf either to Ras-GTP or to phosphatidyl serine in the plasma membrane (129,137,138). The subsequent dissociation of the 14-3-3 protein from the CR2 domain of the Raf-kinases allows the protein phosphatases PP1 and PP2a to dephosphorylate inhibitory phosphate residues (129,135,139,140). Subsequently, in Raf-1 and A-Raf, tyrosine residues in the kinase domain are phosphorylated by Src kinases, which themselves have been activated by stimulation. Next, phosphorylation of serine residues in the same region by different kinases, for instance PKA, takes place (129,141,142). The resulting negatively charged region in the kinase domain of Raf abolishes autoinhibition (128,129,143). In B-Raf, this region is already negatively charged by aspartate residues and a constitutive phosphorylation of serine-445 (S445) (129,141). After abrogation of autoinhibition, homo- and heterodimerization of the Raf-kinases occur. Dimerization leads to an additional conformational change that activates the kinase activity of Raf (129). Preferentially, B-Raf/Raf-1 heterodimers are formed, which exhibit the highest kinase activity (129,144–146).

To date, MEK1 and MEK 2 (mitogen-activated protein kinase/ERK kinase) are the only accepted substrates of activated Raf-kinases (120,127). Several other proteins, such as Rb, MYPT, BAD, or ASK1 are discussed as Raf substrates, influencing cell cycle progression, cell motility as well as apoptosis (127). Although all Raf isoforms activate MEK by phosphorylation at two serine residues in the activation loop (S117 and S221) (136,141,147), B-Raf exhibits the highest kinase activity with respect to MEK, followed by Raf-1. A-Raf exhibits only a low capacity of MEK phosphorylation (148). Activated MEK in turn leads to ERK activation through phosphorylation of the Thr-Xxx-Tyr motif in the activating segment (120,149). As activated serine/threonine kinase phospho-ERK (pERK) regulates many different cytoplasmic (RSK, MLCK) but also nuclear (Elk-1, c-Fos, c-Myc) target proteins (150,151). Thereby, pERK influences various cellular processes, such as differentiation, proliferation, survival, but also apoptosis (120,127). The outcome of the Ras-Raf-MEK-ERK signaling pathway seems to depend on the intensity and temporal dynamics of ERK activation as well as on the cell type (120,152,153). Although the Ras-Raf-MEK-ERK signaling pathway is the conventional pathway for ERK phosphorylation, Ras/Raf independent pathways of ERK phosphorylation through PI3K, PAK, MEKK1, or TPL2 has also been described in various cell types (107,150,154–157). To regulate and terminate the Ras-Raf-MEK-ERK signaling, Raf-kinases are inactivated by various processes. Protein phosphatase PP5 dephosphorylates activating phosphate groups of Raf (158). In addition, Raf-kinases are inactivated via an ERK-mediated feedback loop. Thus, ERK phosphorylates regions in the CR2 domain of Raf, abolishing the Ras-Raf interaction but also Raf dimerization (127,129,159). Subsequently, the inactivated Raf monomers are recycled back to the inactive conformation (129).

1.3.3 Raf mutations

Knockout experiments of Raf revealed some non-redundant functions of the different mammalian Raf isoforms A-Raf, B-Raf and Raf-1. Conventional A-Raf knockout mice survived in utero but died 7 to 21 days after birth, suffering from neuronal and intestinal malformations (160). Mice with a conventional knockout of B-Raf or Raf-1 were both embryonic lethal (161,162). The B-Raf deficiency led to neuronal defects, but the probable cause of death was vascular malformations resulting in massive hemorrhage (161). B-Raf is also the main activator of MEK and ERK in the placenta, which is essential for its development (163). Embryonic lethality in Raf-1 knockout mice likely results from high apoptosis in the liver. However, these mice also show defects in the placenta and the hematopoietic system. In addition, Raf-1 appears to contribute to ERK activation during embryonic development (164,165). These results support the high importance of Raf-kinases in very multifaceted cellular processes.

Additionally, the Ras-Raf-MEK-ERK pathway is often hyperactivated by mutations in various human cancers (120,125,166,167). These mutations predominantly affect B-Raf while rare mutations have been detected in Raf-1 and A-Raf (120,168). The best known B-Raf mutation V600E is predominantly found in melanomas but could also be detected in 4 % of multiple myelomas (168–170). In the V600E mutation, a valine at position 600 is replaced by glutamic acid, which constitutively activates B-Raf (120,171). In 2004, Wan et al. were able to demonstrate that of 22 B-Raf mutants tested, 81.8 % had increased B-Raf kinase activity (170). The analyses of the Raf mutations occurring in human cancer support the important role of Raf mediating ERK hyperactivation in tumor development and progression.

Therefore, Raf inhibitors have been developed for the treatment of Ras and Raf driven cancers. Dabrafenib was developed to treat melanoma featuring the hyperactive V600E B-Raf mutation (171), but in high concentrations Dabrafenib could inhibit all three Raf isoforms (172). Sorafenib is a multi-targeted tyrosine kinase inhibitor, also inhibiting all three Raf-kinases (173). Dabrafenib and Sorafenib act by interaction with the ATP-binding site of a Raf monomer thereby inhibiting its kinase activity (174,175).

This mechanism is effectively working at high inhibitor concentrations saturating all Raf molecules. But at non-saturating concentrations, the so-called paradoxical ERK activation may occur (172,176). It is assumed that at low inhibitor concentrations not all Raf monomers are bound and inhibited by the inhibitors. The Raf monomer bound to the inhibitor got inactivated and favors dimerization with an unbound non-inhibited Raf monomer. This dimerization leads to conformational changes of the uninhibited Raf followed by its hyperactivation, causing the so-called paradoxical ERK phosphorylation

(172,174,176,177). Therefore, the newer pan-Raf inhibitor LY3009120 (LY30) was developed. It was described to have a comparable inhibitory effect on all three Raf isoforms and the paradoxical ERK activation, that has been described in cells treated with sorafenib and dabrafenib, is barely detectable with LY3009120 (172,173,176).

1.3.4 Raf mediated functions in B cells

Although Raf-kinases have been the subject of research for nearly 30 years, little is known about their role in B cell development and activation. Raf mediated ERK phosphorylation in B cells upon BCR stimulation was demonstrated by Brummer et al. in 2002 through induced B-Raf//Raf-1 deficiency in the chicken B cell line DT40 (178). The block in B cell development caused by a dominant-negative mutant of Ras could be rescued by constitutively active Raf-1 (179). Moreover, constitutively active Raf-1 promoted B cell maturation and expansion (180). Rowland et al. showed in 2010, that reduced BCR surface expression in immature B cells led to impaired differentiation of immature B cells into transitional and mature B cells. Introduction of a constitutive active N-Ras increases ERK phosphorylation and enables immature B cells, with a low BCR expression to differentiate into transitional and mature B cells. Although this study did not consider the individual Raf isoforms, these results suggest that the Ras-Raf-MEK-ERK pathway, activated by tonic BCR signaling, affects the differentiation of immature B cells (181). Furthermore, the importance of MEK/ERK phosphorylation in the activation of mature B cells was demonstrated by MEK inhibition, which inhibits BCR mediated proliferation (182). In 2015, Lionetti et al. analyzed Ras and Raf mutations in patients with plasma cell dyscrasia. In about 21.7% of these samples, mutations in Ras or Raf were detected. This supports the assumption that Raf-kinases may play an important role in plasma cell differentiation (183).

In our group, the influence of B-Raf and Raf-1 inactivation was investigated in murine B cells with and without constitutively active CD40 signaling (see section 1.4). The project was started by Samantha Feicht during her PhD thesis. Mice harboring a B cell specific deletion of either Raf-1, B-Raf or both, revealed a block in the B cell development at the transition from pro- to pre-B cells, but also from large pre-B to small pre-B cells (184). Initially, we assumed that this phenotype was due to a reduced ERK phosphorylation, as Yasuda et al. in 2008 demonstrated an ERK dependence in maturation from pro- to pre-B cells (185). Furthermore, B cell specific inactivation of B-Raf and/or Raf-1 revealed a redundant role of these two Raf-kinases in the generation and maturation of transitional B cells, which resulted in reduced splenic B cell numbers. Thereby, Fo B cells were more affected than MZ B cells. Although ERK phosphorylation was still inducible in B-Raf//Raf-

1 single or double deficient B cells, the TD immune response was slightly impaired in B-Raf//Raf-1 deficient B cells resulting in reduced GC B cells and antibody titers (184).

1.4 Model systems

1.4.1 The Raf-1^{fl/fl}//B-Raf^{fl/fl}//mb1-Cre^{+/-} (DKO) transgenic mouse model

To investigate the contribution of the Raf isoforms B-Raf and Raf-1 in B cell development and activation, our group analyzed mice with B cell specific inactivation of *B-Raf* and *Raf-1* or both in C57BL/6 mice. Here, the previously published mouse strains Raf-1^{fl/fl} (186) and B-Raf^{fl/fl} (187) were used. In the Raf-1^{fl/fl} mouse strain, exon 3, encoding for the RBD, and in B-Raf^{fl/fl} mice, exon 12, encoding for parts of the kinase domain, are biallelically flanked with loxP sites (locus of crossing, x) (186,187). By crossbreeding of homozygous Raf-1^{fl/fl}//B-Raf^{fl/fl} mice with heterozygous mb1-Cre^{+/-} mice, the loxP-flanked exons of *B-Raf* and *Raf-1* were deleted in B cells (Figure 7). In mb1-Cre^{+/-} mice, the Cre-recombinase is expressed under the control of one *Igα* locus from the early pro-B cell stage onwards (188). Here, only heterozygous mb1-Cre^{+/-} mice were used, since mb1-Cre^{+/+} mice exhibit severely reduced B cell numbers due to a biallelic deletion of the *Igα* locus resulting in a loss of BCR surface expression (189).

Thus, in the crossbred Raf-1^{fl/fl}//B-Raf^{fl/fl}//mb1-Cre^{+/-} (DKO) mice, a B cell specific deletion of exon3 of *Raf-1* and exon 12 of *B-Raf* is already achieved in pro-B cells. Deletion of the exons leads to frameshifts and consequently to a knockout of *Raf-1* and *B-Raf*.

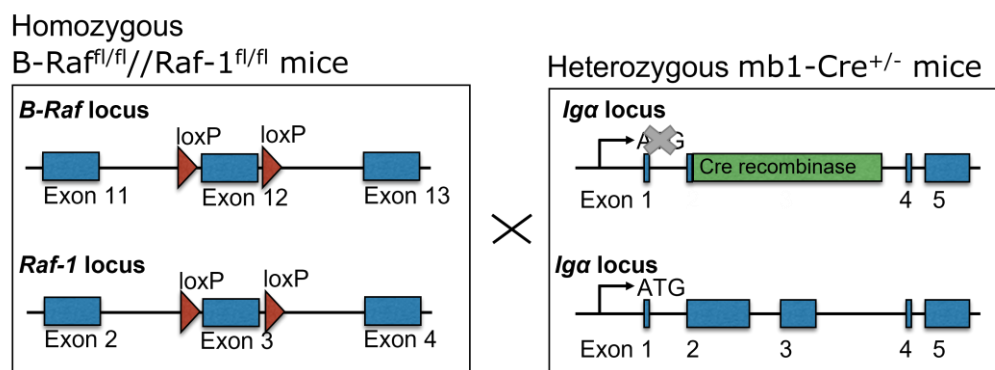


Figure 7: Scheme of the Raf-1^{fl/fl}//B-Raf^{fl/fl}//mb1-Cre^{+/-} (DKO) transgenic mouse model. This mouse model was created by crossing homozygous B-Raf^{fl/fl}//Raf-1^{fl/fl} mice (left panel) with heterozygous mb1-Cre^{+/-} mice (right panel). In homozygous B-Raf^{fl/fl}//Raf-1^{fl/fl} mice, the exon 12 of both *B-Raf* alleles, encoding for parts of the kinase domain (187), and the Ras-binding domain (exon 3) of both *Raf-1* alleles (186) were flanked by loxP sites (red arrows). In heterozygous mb1-Cre^{+/-} mice a humanized *Cre-recombinase* (green) was integrated into the exon 2 and 3 of one allele of the *Igα* gene (188). B cell specific expression of the Cre-recombinase leads to the deletion of the loxP flanked exons of *B-Raf* (exon 12) and *Raf-1* (exon 3) from the early pro-B cell stage onwards. Deletion of the exons leads to a knockout of Raf-1 and B-Raf.

1.4.2 The *Raf-1^{fl/fl}//B-Raf^{fl/fl}//LMP1/CD40^{flSTOP+/-}//CD19-Cre^{+/-}* (RafDKO/LC40) transgenic mouse model

Additionally, the role of B-Raf and Raf-1 in B cell activation, expansion, and transformation upon constitutive CD40 signaling was examined. Constitutive CD40 signaling in B cells is induced by the B cell specific expression of the LMP1/CD40 fusion protein. The latter contains the transmembrane domain of the *LMP1* gene of the Epstein-Barr virus (EBV) fused to the intracellular signaling domain of CD40. To prevent ubiquitous expression of LMP1/CD40 in all tissues, a loxP flanked STOP cassette was inserted prior to the *LMP1/CD40* transgene. This whole *Stop-flox/LMP1/CD40* gene cassette (*LMP1/CD40^{flSTOP}*) was integrated into the *rosa26* locus, which is ubiquitously active. The B cell specific expression of the fusion protein LMP1/CD40 was achieved by crossbreeding to *CD19-Cre^{+/-}* mice, where the *Cre-recombinase* was heterozygously inserted into the exon 2 of one *CD19* gene (190). Therefore, the Stop cassette of the *LMP1/CD40^{flSTOP}* gene is specifically deleted in B cells under the control of the CD19 promoter (52). To analyze the role of B-Raf and Raf-1 in the LMP1/CD40 induced phenotype, the above mentioned mouse strains *Raf-1^{fl/fl}* (186) and *B-Raf^{fl/fl}* (187) were homozygously crossed to the *LMP1/CD40^{flSTOP+/-}//CD19-Cre^{+/-}* (LC40) mice (52). The resulting *Raf-1^{fl/fl}//B-Raf^{fl/fl}//LMP1/CD40^{flSTOP+/-}//CD19-Cre^{+/-}* (RafDKO/LC40) mice exhibit a knockout of both *Raf-1* and *B-Raf* genes with a concomitant expression of the fusion protein LMP1/CD40 in B cells (Figure 8).

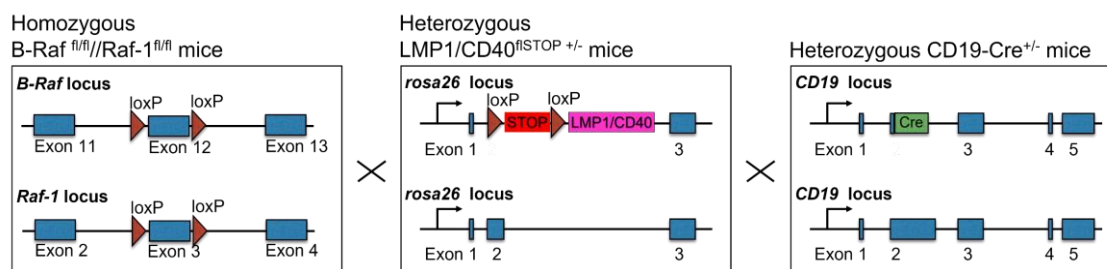


Figure 8: Scheme of the *Raf-1^{fl/fl}//B-Raf^{fl/fl}//LMP1/CD40^{flSTOP+/-}//CD19-Cre^{+/-}* (RafDKO/LC40) transgenic mouse model. This mouse model exhibits a homozygous *B-Raf^{fl/fl}//Raf-1^{fl/fl}* (left panel), a heterozygous *LMP1/CD40^{flSTOP+/-}* (middle panel), and a heterozygous *CD19-Cre^{+/-}* (right panel) genotype. In homozygous *B-Raf^{fl/fl}//Raf-1^{fl/fl}* mice, the exon 12 of both *B-Raf* alleles, (188) and exon 3 of both *Raf-1* genes (186) were flanked by loxP sites (red arrows). In heterozygote *LMP1/CD40^{flSTOP+/-}* mice, the transgene for the fusion protein LMP1/CD40 (pink) was linked to a loxP flanked STOP cassette (red). This *LMP1/CD40^{flSTOP}* transgene was inserted into the exon 2 of one allele of the *rosa26* locus (52). In heterozygous *CD19-Cre^{+/-}* mice the *Cre-recombinase* gene (green) was integrated into the exon 2 of one allele of the *CD19* gene (190). B cell specific expression of the Cre-recombinase occurs already during B cell development and leads to the deletion of the loxP flanked regions. CD19-Cre mediated deletion of the loxP flanked exons of the Raf-kinases results in a knockout of Raf-1 and B-Raf and LMP1/CD40 expression under the control of the constitutive active *rosa26* promoter in B cells.

2. Aim

The Ras-Raf-MEK-ERK signaling pathway plays an important role in the transduction of extracellular stimuli in many different cell types, leading to changes in cellular processes such as proliferation, differentiation, but also cell cycle arrest or apoptosis. In B cell but also in lymphoma development an essential involvement of Ras and ERK has been described. The contribution of the intermediate Raf-kinases of this signaling pathway has rarely been analyzed. To date, little is known about the functions of Raf in mammalian B cell development, activation, differentiation, and lymphoma generation. To fill this knowledge gap, a model system was developed in which Raf-1 and B-Raf were conditionally deleted in murine B cells from the pro-B cell stage onwards. Since in previous experiments, B-Raf and Raf-1 showed a largely redundant function in mature B cells, only Raf-1^{fl/fl}//B-Raf^{fl/fl}//mb1-Cre^{+/-} (DKO) mice with a B cell specific double knockout of B-Raf and Raf-1 should be analyzed in this work. Furthermore, the contribution of B-Raf and Raf-1 to constitutive B cell activation and lymphoma generation should be investigated by studying mice with an inactivation of Raf-1 and B-Raf in B cells expressing a constitutive active CD40 receptor. In detail, the aims of this doctoral thesis were:

1) The investigation of the role of B-Raf and Raf-1 in mature B cells

Against the expectations Samantha Feicht could observe during her thesis that in DKO B cells the BCR mediated ERK phosphorylation was not reduced (191). First, I should confirm the reproducibility of these unexpected results. Furthermore, the mechanisms leading to BCR mediated ERK phosphorylation in the absence of B-Raf and Raf-1 should be uncovered. Therefore, *in vitro* anti-IgM stimulation of isolated control and DKO B cells in the absence or presence of different inhibitors were performed.

Furthermore, Samantha Feicht could show that DKO mice displayed an impaired TD immune response (184,191). In addition to this, I should investigate whether Raf-kinases also play a role in the TI B cell response. Therefore, control and DKO B cells were immunized with NP-Ficoll. Furthermore, plasma cell differentiation of isolated LPS stimulated control and DKO B cells was analyzed *in vitro*. Additionally, the ERK phosphorylation during this LPS induced plasma cell differentiation of control and DKO B cells was examined *in vitro*.

2) The analysis of the role of B-Raf and Raf-1 on CD40 signaling in B cells:

Next to BCR and LPS signaling, CD40 is an important B cell receptor important for the integration of costimulatory signals (40,95). To complete the investigation of the role of Raf-kinases in the main signaling events in mammalian B cells, the contribution of B-Raf

and Raf-1 to CD40 mediated ERK phosphorylation should be elucidated by *in vitro* stimulation of isolated control and DKO B cells with anti-CD40.

Constitutive CD40 signaling by LC40 expression in B cells leads to B cell expansion, activation, and lymphoma generation (52). The participation of hyperactivated ERK to the LC40 mediated phenotype was already described (107). To investigate the contribution of B-Raf and Raf-1 to the LC40 induced phenotype, those two Raf-kinases were conditionally inactivated in B cells of LC40 mice. Young and aged RafDKO/LC40 mice were compared to aged-matched LC40 and control mice regarding the pERK level, the B and T cell composition, the B cell activation, and the outgrowth of an aberrant CD21^{low}CD23^{low}CD43⁺CD5^{low} B cell population. Furthermore, RNA-Seq analyses of isolated B cells of young LC40 and RafDKO/LC40 mice were performed to investigate the effects of the B-Raf//Raf-1 deficiency on the gene expression in general.

3. Results

3.1 The role of B-Raf and Raf-1 in B cell receptor signaling

The Ras-Raf-MEK-ERK signaling pathway has already been described in detail in the literature. B-Raf and Raf-1 mainly function as a kinase towards MEK leading to the activation of ERK and its downstream targets. However, many of these data were generated using cell lines. Moreover, a dependence of the consequences of Raf signaling on the cell type and on the respective activation or differentiation stage of the cell was described (192). Thus, only little is known about the role of Raf-kinases in B cells. This knowledge gap will be addressed below by analyzing the role of Raf-kinases specifically during the activation and differentiation of primary mouse splenic B cells.

To shed light on this, mice were generated with a B cell specific knockout of B-Raf and Raf-1. For this purpose, homozygous B-Raf^{fl/fl}//Raf-1^{fl/fl} mice (186,187) were crossed with heterozygous mb1-Cre^{+/-} mice (188). In the resulting B-Raf^{fl/fl}//Raf-1^{fl/fl}//mb1-Cre^{+/-} (hereafter referred to as DKO) mice, Cre-recombinase is expressed B cell specifically under the control of the *Iga locus* very early during B cell development. This results in the deletion of the Ras-binding domain (exon 3) of Raf-1 and one part of the kinase domain (exon 12) of B-Raf from the early pro-B cell stage onwards. These deletions lead to a double knockout of the B-Raf and Raf-1 proteins. Because of the wildtype like phenotype of heterozygous mb1-Cre^{+/-} mice, both mb1-Cre^{+/-} mice and C57BL/6 wildtype mice were used as controls and summarized under the term controls (abbreviated ctrl).

3.1.1 Increased basal and BCR mediated ERK phosphorylation in DKO B cells

To get a deeper insight into the role of B-Raf and Raf-1 in BCR signaling, short-time stimulation experiments were performed. Thereby, isolated B cells of DKO and control mice were either kept unstimulated or were treated with an agonistic anti-IgM antibody, to induce BCR signaling. The total and phosphorylated protein levels of the Raf downstream targets MEK, ERK1, and ERK2 were analyzed by Western blot.

While the total MEK, ERK1, and ERK2 level were similar in control and DKO B cells regardless of the stimulation, differences could be observed with respect to the phosphorylation state of MEK, ERK1, and ERK2. In both genotypes, anti-IgM stimulation led to a significant increase of MEK, ERK1, and ERK2 phosphorylation compared to the unstimulated condition. Strikingly, unstimulated and anti-IgM stimulated DKO B cells exhibited significantly increased pERK1 and pERK2 levels compared to controls. MEK

phosphorylation was also elevated in DKO B cells, but the increase did only reach significance upon anti-IgM treatment (Figure 9). These data indicated a regulatory role of B-Raf and Raf-1 towards the MEK and ERK phosphorylation in mature B cells.

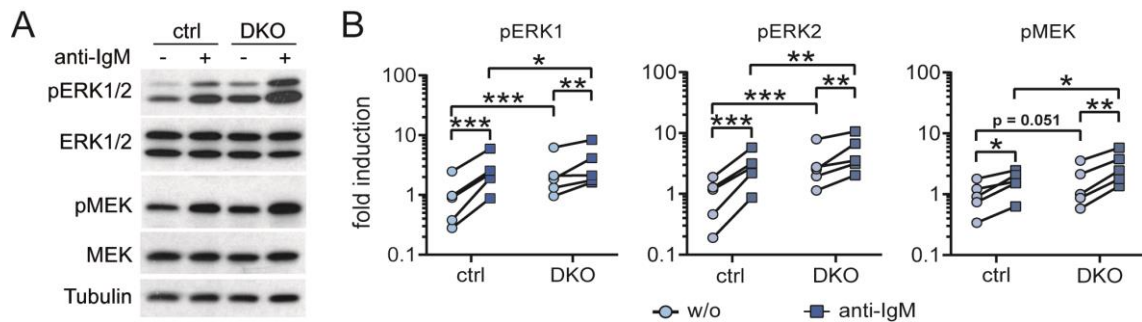


Figure 9: DKO B cells exhibited increased pERK levels, which could be further induced upon anti-IgM stimulation. Pooled splenic B cells from 2 to 3 mice per genotype (ctrl or DKO) were either kept unstimulated or were treated with anti-IgM for 2.5 min *in vitro*. (A) A representative Western blot for total and phosphorylated MEK and ERK1/2 for the two genotypes with and without anti-IgM stimulation is shown. Tubulin served as loading control. (B) The graph summarizes the fold induction of pERK1, pERK2 and pMEK in comparison to unstimulated controls. The calculation of the fold induction is described in section 6.7.5. Each dot represents one of $n = 5$ independent experiments. Lines connect the corresponding values of the different time points of one genotype per Western blot. Due to the lognormal distribution the data sets were logarithmical transformed and statistically analyzed by the Two-way ANOVA with Tukey's multiple comparisons test. * $p < 0.05$; ** $p < 0.01$; *** $p < 0.001$; **** $p < 0.0001$. These illustrations can also be found in Scheffler et al. 2021.

The *in vitro* stimulation experiments described above were performed on B cells isolated using CD43-MACS depletion. To exclude an influence of the performed B cell isolation on pERK, pERK levels were determined in B cells *ex vivo* using flow cytometry. Thereby, splenic B cells were subdivided into Follicular (Fo B; CD23^{high}CD21⁺) and Marginal zone (MZ B; CD23⁻CD21^{high}) B cells (Figure 10A).

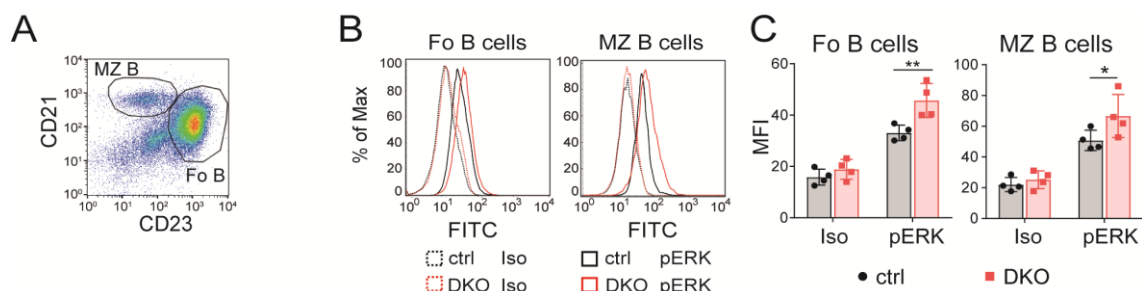


Figure 10: B-Raf//Raf-1 inactivation resulted in elevated basal pERK levels. The p-ERK level in Fo B (CD23^{high}CD21⁺) and MZ B (CD23⁻CD21^{high}) cells was analyzed in $n = 4$ control (ctrl) and $n = 4$ DKO mice. (A) The gating strategy for Fo B and MZ B cells pre-gated on B220⁺ B cells is shown. (B) A representative histogram overlay for pERK and its isotype control (Iso) of the gated Fo B and MZ B cells of ctrl and DKO mice. (C) The Median Fluorescent Intensity (MFI) of pERK and its isotype control (Iso) are illustrated for Fo B and MZ B cells of ctrl and DKO mice. The dots correspond to individual mice. The bars and error bars represent the mean \pm standard deviation. The data were normally distributed. Two-way ANOVA with Sidak's multiple comparisons test was performed. * $p < 0.05$; ** $p < 0.01$. Similar illustrations are included in Scheffler et al. 2021.

B-Raf//Raf-1 inactivation in DKO B cells caused a slight but significant elevation of the basal ERK phosphorylation in both Fo B and MZ B cells compared to their controls. Within one genotype, ERK phosphorylation was approximately 1.5-fold higher in MZ B cells than in Fo B cells (Figure 10B-C).

As described earlier, DKO mice displayed a defect in the B cell development in the BM (184). Therefore, not only splenic but also BM B cells of control and DKO mice were examined with respect to their ERK phosphorylation. Mature recirculating (recirc) B cells were identified as B220^{high}CD43^{low}. The additional marker CD25 in combination with B220 and CD43 allowed the distinction of pro (B220^{low}CD43^{high}CD25⁻), early large pre (B220^{low}CD43^{high}CD25⁺), pre (B220^{low}CD43^{low}CD25⁺) and immature (B220^{low}CD43^{low}CD25⁻) B cells (Figure 11A). Like mature splenic B cells, the pERK levels of mature recirculating B cells were higher in the DKO compared to controls (Figure 11B-C). Detailed examination of the pERK levels of each subset of developing B cells (pro, early large pre, pre, and immature) showed that in both genotypes all developing B cells exhibited lower ERK phosphorylation than mature recirculating B cells. In addition, no differences between genotypes in the pERK signals of developing B cells could be detected (Figure 11C).

These results implied the independence of ERK phosphorylation from B-Raf and Raf-1 in unstimulated and short-term anti-IgM stimulated mature B cells. Furthermore, these results suggested an inhibitory function of the Raf-kinases B-Raf and Raf-1 on the pERK levels in mature B cells.

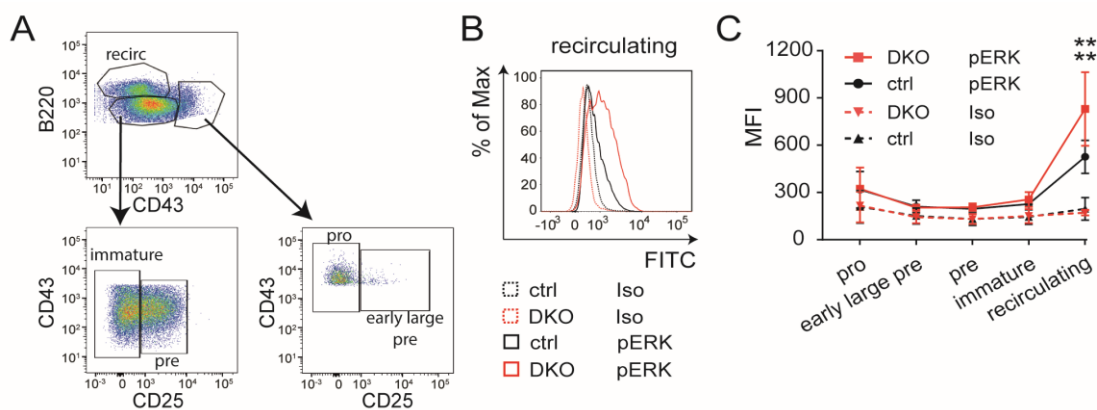


Figure 11: B-Raf//Raf-1 inactivation increased the pERK levels in recirculating B cells. The pERK levels in different subsets of *ex vivo* BM B cells of $n = 4$ control (ctrl) and $n = 4$ DKO mice were analyzed by flow cytometry. In (A) the gating strategy for the different subsets of B cells in the BM are shown. B cells are pre-gated on B220⁺ cells and are subdivided in pro (B220^{low}CD43^{high}CD25⁻), early large pre (B220^{low}CD43^{high}CD25⁺), pre (B220^{low}CD43^{low}CD25⁺), immature (B220^{low}CD43^{low}CD25⁻), and recirculating (recirc; B220^{high}CD43^{low}) B cells. (B) Representative histogram overlay of pERK and its isotype control (Iso) in recirculating B cells in the BM of control and DKO mice. (C) The Median Fluorescent Intensity (MFI) of pERK or its isotype control (Iso) of control and DKO BM B cell subsets gated as indicated in (A). The dots and error bars represent the mean \pm standard deviation. The data were normally distributed. Two-way ANOVA with Tukey's multiple comparisons test was applied in (F). **** $p < 0.0001$. Similar illustrations are included in Scheffler et al. 2021.

3.1.2 Unaltered BCR downstream signaling in DKO B cells

Since many cross talks and feedback loops exist between different signaling pathways, the question arose whether the inactivation of B-Raf and Raf-1 also influences other BCR mediated signaling pathways. Therefore, BCR mediated activation of different signaling molecules was investigated by Western blot on unstimulated and anti-IgM stimulated splenic B cells of control and DKO mice.

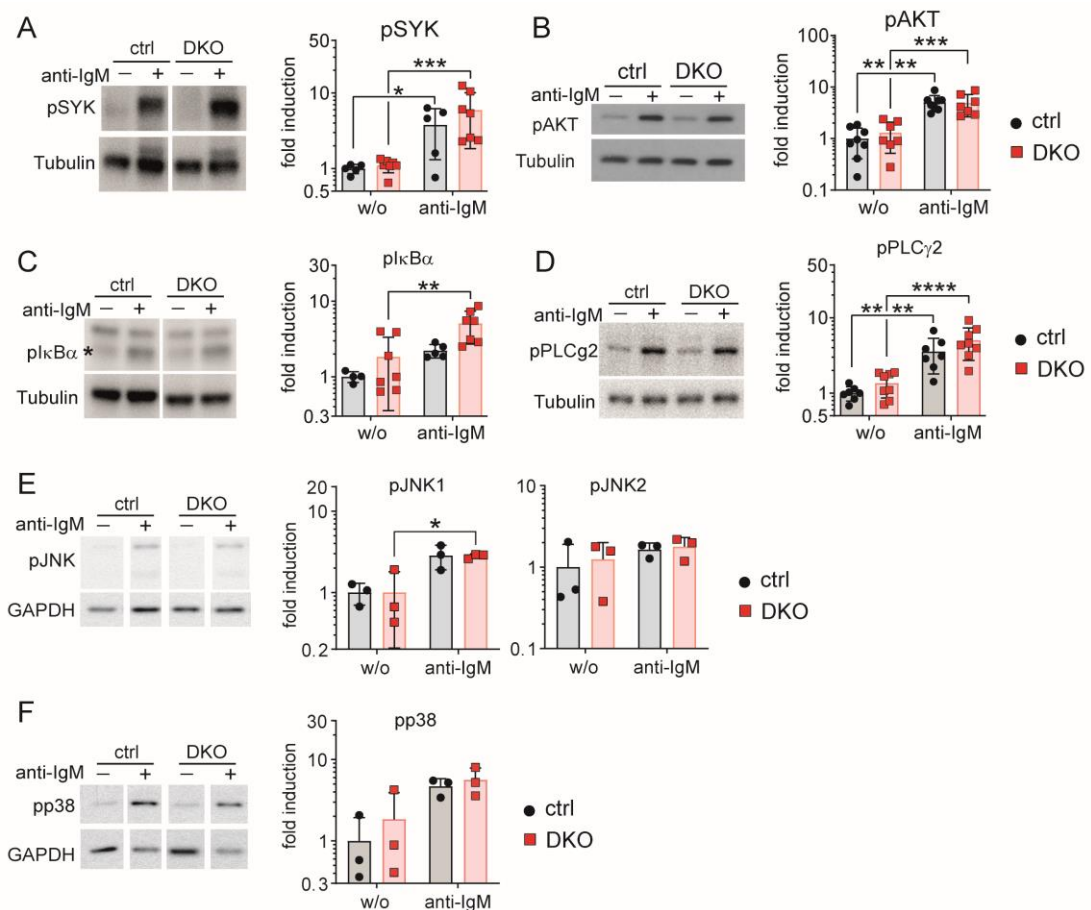


Figure 12: DKO B cells displayed unaltered BCR signaling with respect to pSYK, pJNK, pp38, plkBα, and pAKT. Isolated splenic B cells of control (ctrl; n = 3 to 8) and DKO (n = 3 to 8) mice were either left untreated or were stimulated with anti-IgM for 2.5 min *in vitro*. (A-F) A representative Western blot for pSYK (A), pAKT (B), plkBα (C), pPLCγ2 (D), pJNK1/2 (E), and pp38 (F) and their indicated loading control (Tubulin or GAPDH) is shown for the two genotypes with and without anti-IgM stimulation. The graphs summarize the indicated fold induction in comparison to unstimulated controls. The calculation of the fold induction is described in section 6.7.5. Each dot represents an individual mouse. The bars and error bars represent the mean ± standard deviation. Due to the lognormal distribution the data sets were logarithmical transformed and statistically analyzed by the two-way ANOVA with Tukey's multiple comparisons test. *p < 0.05; **p < 0.01; ***p < 0.001; ****p < 0.0001. Similar graphs are included in Scheffler et al. 2021.

First, the activation of SYK, a main signaling molecule directly interacting with the BCR (81,193), was examined. Additionally, we analyzed the activity of the PI3K/AKT signaling pathway by determining pAKT levels (194) and of the NFκB pathway by investigating the phosphorylation of the inhibitory protein IκBα, which leads to NFκB activation (195,196).

Furthermore, the activities of the MAPK JNK and p38 were explored, which are phosphorylated upon BCR stimulation (91). Phosphorylated PLC γ 2 was described as an activator of the PKC, which could mediate MAPK activation (197). Therefore, we studied the phosphorylation of PLC- γ 2.

Under both conditions, unstimulated and anti-IgM stimulated, control and DKO B cells displayed comparable levels of pSYK, pAKT, pI κ B α , pPLC γ 2, pJNK1/2, and pp38. Thereby, in both genotypes, anti-IgM stimulation resulted in an induction of SYK, AKT, I κ B α , PLC γ 2, JNK1, and p38 phosphorylation (Figure 12). Thus, the activities of all analyzed signaling molecules were similar between DKO and control B cells. These results led to the assumption that the previously described inhibitory function of B-Raf and Raf-1 is restricted to ERK phosphorylation and that B-Raf//Raf-1 inactivation did not affect NF κ B, PI3K/AKT, and PLC γ 2/JNK/p38 MAPK signaling upon BCR stimulation. Next, we analyzed how ERK phosphorylation was mediated in mature B cells of DKO mice.

3.1.3 Increased ERK phosphorylation upon pan-Raf inhibitor treatment

First, we investigated whether in DKO B cells, ERK phosphorylation is mediated by the third Raf-kinase family member A-Raf. A-Raf is considered to have only a low kinase activity with respect to MEK (148,153), which is why previous analyses focused on B-Raf and Raf-1. To investigate whether A-Raf is expressed in mature murine B cells, Western blots were performed on unstimulated and anti-IgM stimulated splenic B cells of control and DKO mice.

The Western blots and the corresponding quantified fold induction revealed comparable A-Raf level in unstimulated and anti-IgM stimulated mature B cells of control and DKO mice (Figure 13). Thus, A-Raf is expressed in B cells and B-Raf//Raf-1 inactivation in DKO B cells did not appear to lead to a compensatory change in the A-Raf expression.

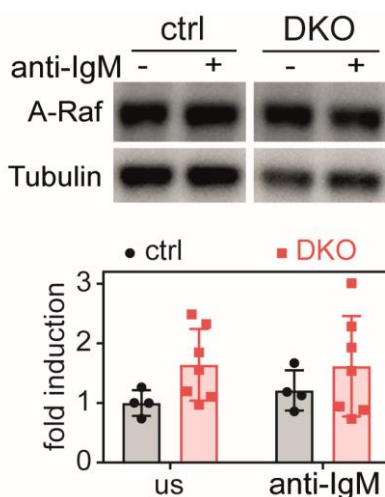


Figure 13: Similar A-Raf expression in mature control and DKO B cells. The A-Raf expression of unstimulated or anti-IgM stimulated splenic B cells of $n = 4$ control (ctrl) and $n = 7$ DKO mice was measured by Western blot. A representative Western blot for A-Raf and the loading control Tubulin is shown for the two genotypes with and without anti-IgM stimulation. The graph summarizes the fold induction of A-Raf in comparison to unstimulated controls. The calculation of the fold induction is described in section 6.7.5. Each dot represents an individual mouse. The bars and error bars represent the mean \pm standard deviation. The data followed a normal distribution. For statistical analysis the Two-way ANOVA with Tukey's multiple comparisons test was performed. A similar illustration of the data is shown in Scheffler et al. 2021.

To test whether A-Raf mediates the ERK phosphorylation in the absence of B-Raf and Raf-1, inhibition experiments were performed with the different pan-Raf inhibitors Dabrafenib, Sorafenib and LY3009120 (LY30). As already described in section 1.3.3, Dabrafenib and Sorafenib could inhibit all 3 Raf-kinases, but they could also lead to paradoxical ERK activation under non-saturating concentrations (172,173,176). Additionally, the paradox-breaking inhibitor LY3009120 was used, which was described to comparably inhibit all three Raf-kinases and barely induce paradoxical ERK activation (172). According to the literature paradoxical ERK activation should only occur with low but not with high concentrations (10 μ M) of the pan-Raf-inhibitors (172).

Therefore, first titration experiments of the three inhibitors Sorafenib, Dabrafenib, and LY3009120 were performed on unstimulated and anti-IgM stimulated control B cells. Treatment with each inhibitor resulted in an increased ERK phosphorylation at each concentration tested compared with the corresponding solvent control DMSO. Moreover, pERK levels continued to increase with rising concentrations for all three inhibitors, arguing against paradoxical ERK activation (Figure 14).

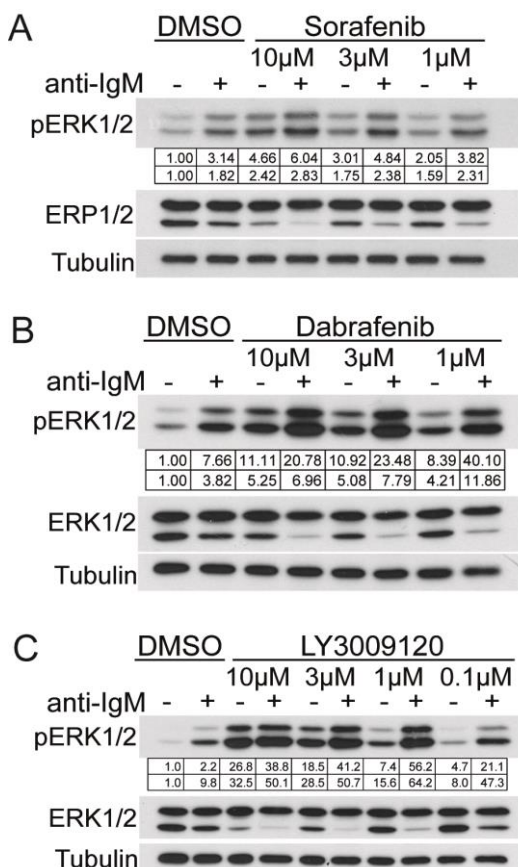


Figure 14: Titration of pan-Raf inhibitors on control B cells.

Pooled isolated splenic B cells of 2 control mice were pre-treated with the different pan-Raf inhibitors Sorafenib (A), Dabrafenib (B) or LY3009120 (C) for 1.5 h using the indicated concentrations or its solvent control DMSO. Unstimulated or anti-IgM stimulated samples were analyzed for total and phosphorylated ERK using Western blot analyses. Tubulin served as loading control. Representative Western blots and the fold induction of the pERK1 and pERK2 signals in comparison to the unstimulated DMSO treated controls are shown. The calculation of the fold induction is described in section 6.7.5. Each titration of the different inhibitors Sorafenib (A), Dabrafenib (B), and LY3009120 (LY30) (C) was performed in $n = 2$ independent experiments. A similar illustration of the data is shown in Scheffler et al. 2021.

Next, the effect of pan-Raf inhibitor treatment on the ERK phosphorylation was analyzed in DKO B cells. For all three pan-Raf inhibitors, induction of ERK phosphorylation was detected in both unstimulated and stimulated DKO B cells compared with the DMSO treated DKO B cells. In particular, the DMSO samples and the samples treated with lower

pan-Raf inhibitor concentrations again showed higher pERK levels in DKO samples compared to the corresponding samples of control B cells (Figure 15A-C).

Due to the high similarity of the behavior of the control and DKO B cells with respect to the different pan-Raf inhibitors, we focused on the LY3009120 treated samples and the corresponding controls for quantification. Thereby, the significant elevated pERK levels of DKO B cells compared to controls could be confirmed. Furthermore, LY3009120 treatment of B cells of both genotypes led to significantly increased pERK levels (Figure 15D). Because high concentrations of pan-Raf inhibitors and the inhibitor LY3009120, which exhibits little paradoxical ERK activation, had a pERK inducing effect, it can be almost excluded that the increased ERK phosphorylation was caused by paradoxical ERK activation. The experiments suggested that inhibition of the Raf-kinases induced the ERK phosphorylation similar to the genetic knockout of B-Raf and Raf-1.

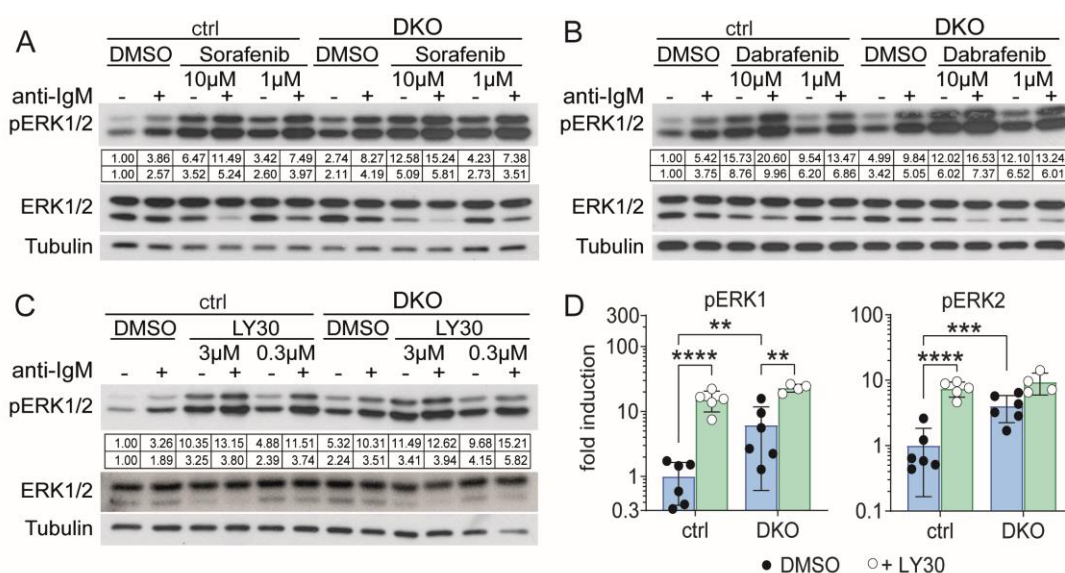


Figure 15: The chemical or genetic inactivation of Raf-kinases led to increased pERK levels. (A-C) Pooled isolated splenic B cells of 2 to 3 mice per genotype (control [ctrl] or DKO) were pre-treated with the different pan-Raf inhibitors Sorafenib (A), Dabrafenib (B), or LY3009120 [(LY30); (C)] for 1.5 h using the indicated concentrations or its solvent control DMSO. Unstimulated or anti-IgM stimulated samples were analyzed for total and phosphorylated ERK using Western blot analyses. Tubulin served as loading control. Representative Western blots and the fold induction of the pERK1 and pERK2 signals in comparison to the unstimulated DMSO treated controls are shown. These analyses were performed for Sorafenib (A) with $n = 2$, for Dabrafenib (B) with $n = 1$; and for LY3009120 (C) with $n = 2$ independent experiments. (D) The graphs summarize the fold induction of pERK1 and pERK2 of DMSO or LY3009120 (3 µM) treated (1.5 h) control and DKO B cell samples in comparison to the mean of DMSO treated control B cell samples measured by Western blot analyses similar to (C). The calculation of the fold induction is described in section 6.7.5. Each dot represents one of $n = 4-6$ independent experiments. Bars and error bars indicate the mean \pm standard deviation. Due to lognormal distribution the data sets were logarithmically transformed and statistically analyzed by the Two-way ANOVA with Sidak's multiple comparisons test. ** $p < 0.01$; *** $p < 0.001$; **** $p < 0.0001$. (A-D) The calculation of the fold induction is described in section 6.7.5. The same illustrations can be found in Scheffler et al. 2021.

3.1.4 BCR induced SYK, PI3K and RAC/Pak dependent ERK phosphorylation in mature B cells

In the following section, the mechanism of pERK induction in control and DKO B cells was investigated. For this purpose, isolated mature B cells of control and DKO mice were preincubated with different inhibitors for SYK (p505-15; iSYK), PI3K (LY294002; LY29), AKT (Akt8; iAKT), PAK (PF-3758309; iPAK) and IKK2 (IKK2-inhibitor 8; ilkk2). Subsequently, the samples were either left unstimulated or were stimulated with anti-IgM. The ERK phosphorylation was examined by Western blot.

SYK is phosphorylated after BCR crosslinking and activates a broad spectrum of different signaling pathways (81,193). Phospho-AKT was reduced upon iSYK treatment, reflecting the inhibitory effect of iSYK (194). Additionally, the iSYK treated control and DKO B cells showed decreased pERK levels compared to the corresponding solvent control samples treated with DMSO. This was true for both basal and anti-IgM induced pERK. Furthermore, iSYK treatment strongly reduced the elevated pERK levels of unstimulated DKO B cells to the level of DMSO treated unstimulated controls (Figure 16).

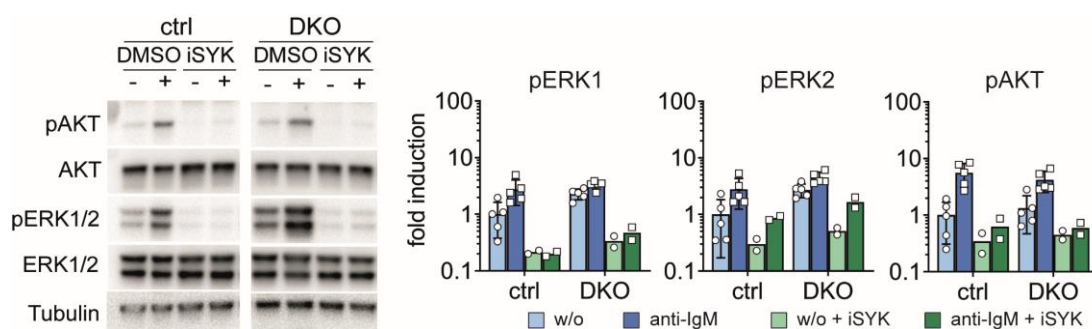
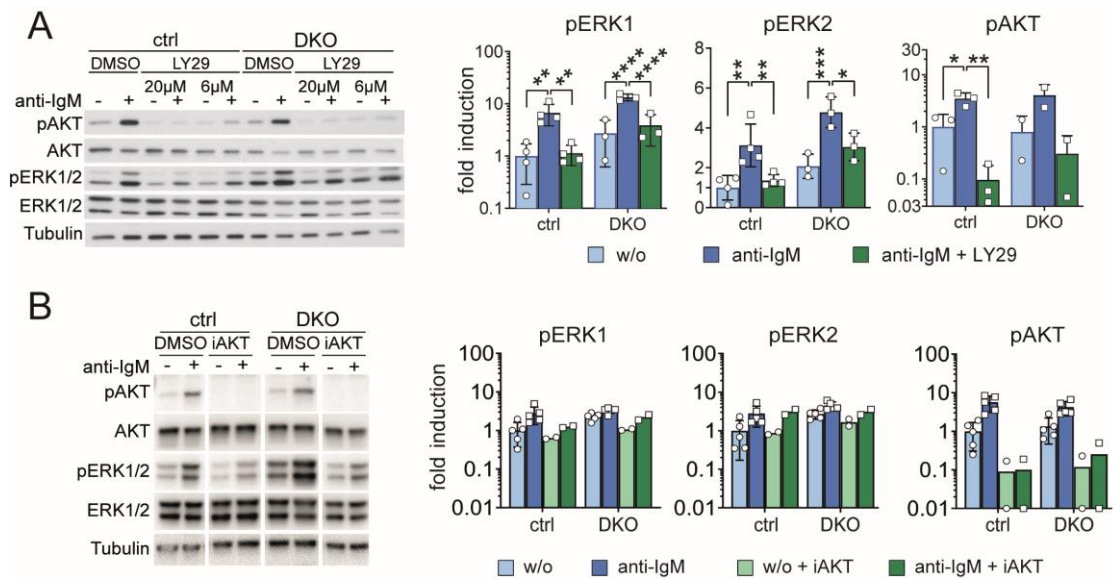


Figure 16: SYK inhibition reduced basal and anti-IgM mediated pERK levels of control and DKO B cells. Isolated splenic B cells of 4 mice were pooled per genotype. Control (ctrl) and DKO B cell samples were pre-treated for 1.5 h with 0.5 μ M of the SYK inhibitor p505-15 (iSYK) or its solvent control DMSO. Subsequently, the samples were left unstimulated (w/o) or were stimulated with anti-IgM for 2.5 min. The expression and phosphorylation of AKT and ERK were analyzed by Western blot. Tubulin served as loading control. One representative Western blot and the fold induction of pAKT, pERK1, and pERK2 in comparison to unstimulated controls is illustrated. The calculation of the fold induction is described in section 6.7.5. Since this experiment was only performed in $n = 2$ independent experiments, the statistical evaluation is not indicated. These illustrations are published in Scheffler et al. 2021.

Because mature B cells with a constitutive active CD40 signal display a CD19/PI3K dependent ERK phosphorylation (107), the pERK levels were analyzed in the presence of a PI3K or an AKT inhibitor. In both genotypes, the PI3K and AKT inhibitors resulted in reduced pAKT levels in unstimulated and anti-IgM stimulated B cells, confirming the efficacy of the inhibitors. While the AKT inhibitor did not show any inhibitory effect on the pERK levels, the PI3K inhibitor LY294002 reduced the ERK phosphorylation in a dose-dependent manner in unstimulated and anti-IgM stimulated B cells of both genotypes (Figure 17).



RAC/PAK mediated ERK phosphorylation has been described in human neutrophils (154). Therefore, the possibility of a RAC/PAK dependent ERK, MEK, and AKT phosphorylation was investigated in unstimulated and anti-IgM stimulated B cells of control and DKO mice by iPAK treatment. In both genotypes iPAK treated samples displayed consistently lower pERK levels than in the corresponding DMSO treated controls. Thereby, ERK2 phosphorylation was less sensitive to iPAK treatment than pERK1. Already the use of 5 μM iPAK on unstimulated DKO B cells reduced the basal pERK levels almost to DMSO treated control levels. Additionally, unstimulated, and anti-IgM stimulated control and DKO B cells showed a similar dose-dependent inhibition of pMEK upon iPAK treatment. The inhibitory effect of iPAK on pAKT was similar in DKO and control B

cells. Thereby, the basal pAKT level were more sensitive to iPAK treatment than the AKT phosphorylation of anti-IgM stimulated samples (Figure 18).

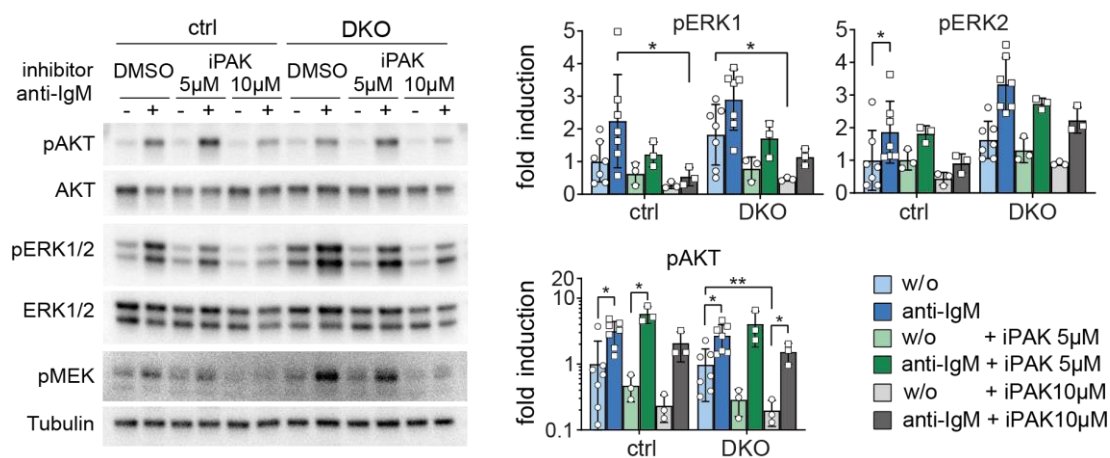


Figure 18: The RAC/PAK signaling contributed to the basal and anti-IgM mediated pERK levels of control and DKO B cells. Isolated splenic B cells of 2 to 4 mice were pooled to generate B cell samples of control (ctrl) and DKO mice. They were pre-treated for 1.5 h with 5 or 10 μM of the PAK inhibitor PF-3758309 (iPAK) or its solvent control DMSO. For both genotypes, unstimulated (w/o) samples were compared to anti-IgM stimulated (2.5 min) ones. One representative Western blot for pAKT, AKT, pERK1/2, ERK1/2, pMEK and Tubulin is shown. The fold induction of pAKT, pERK1, and pERK2 are illustrated in comparison to unstimulated DMSO treated controls. The calculation of the fold induction is described in section 6.7.5. Each dot represents an individual B cell sample analyzed in $n = 3$ independent experiments. Bars and error bars indicate the mean \pm standard deviation. The data set was lognormal distributed. After logarithmic transformation the data were statistically analyzed by the Two-way ANOVA with Sidak's multiple comparisons test. * $p < 0.05$, ** $p < 0.01$. The same data are published in Scheffler et al. 2021.

To investigate if the IKK dependent TPL2/ERK signaling pathway, which was previously described in innate immune cells (155,156), contribute to the ERK phosphorylation in DKO B cells, unstimulated and anti-IgM stimulated control and DKO B cells were pre-incubated either with the iIKK2 or its solvent control DMSO. Hereby, the iIKK2 mediated inhibition of the I κ B α phosphorylation determined to proof the efficacy, which could nicely be detected in both genotypes. Neither ERK nor AKT exhibited an iIKK2 dependent reduction of phosphorylation in unstimulated and anti-IgM stimulated B cells of both genotypes (Figure 19).

In summary, the described inhibitor experiments established that BCR crosslinking led to SYK phosphorylation, which resulted in phosphorylation of ERK via PI3K and RAC/PAK signaling pathways. AKT and IKK2 do not appear to play a significant role in this process. Comparable results have also been observed in DKO B cells, arguing against compensatory activation of other signaling pathways. The fact that SYK, PI3K and RAC/PAK inhibitors lowered the basally elevated pERK level in DKO B cells to control levels indicated that ERK phosphorylation in DKO B cells was mediated by conventional pathways, which seemed to be negatively regulated by Raf-kinases.

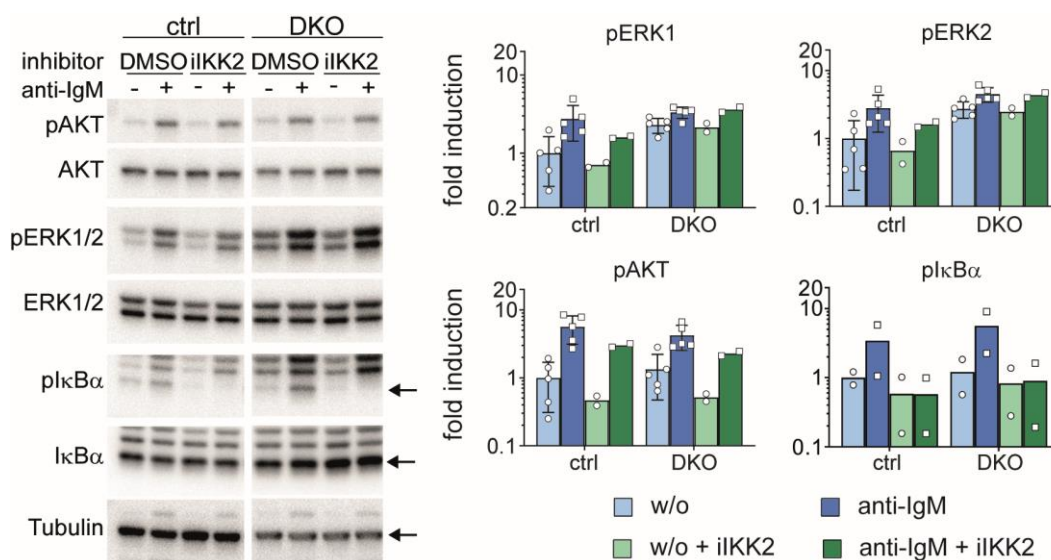


Figure 19: Basal and anti-IgM mediated pERK levels of control and DKO B cells were independent of the canonical NFκB signaling pathway. Control (ctrl) and DKO samples were generated by pooling of isolated splenic B cells of 2 to 4 mice per genotype. After pre-incubation for 1.5 h with 5 μM of the IKK2 inhibitor8 (iIKK2) or its solvent control DMSO, samples of both genotypes were left unstimulated (w/o) or stimulated with anti-IgM (2.5 min). Western blots were performed to analyze total and phosphorylated AKT, ERK1/2, and IκBα. A representative Western blot and the fold induction of pAKT, pERK1, pERK2 and pIκBα in comparison to unstimulated DMSO treated controls are illustrated. The calculation of the fold induction is described in section 6.7.5. Since this experiment was performed in n = 2-5 independent experiments, the statistical evaluation is not indicated. Individual B cell samples are represented by the dots. Bars and error bars indicate the mean ± standard deviation. The data are similarly illustrated in Scheffler et al. 2021.

3.2 The role of B-Raf and Raf-1 in PC differentiation

3.2.1 Impaired TI immune response in DKO mice

The TD immune response was slightly impaired in DKO mice (184). To analyze if a B cell specific B-Raf//Raf-1 inactivation influences the TI immune response, control and DKO mice were immunized intraperitoneally with NP-Ficoll. After 14 days, the amount of NP-specific antibody secreting cells (ASC) was analyzed by ELISpot. The ASCs were discriminated by their isotype-specificity (IgM and IgG3). The immunization of control mice led to a clear generation of NP-specific ASCs compared to its unimmunized (n.i.) counterpart. In contrast, immunized DKO mice displayed significantly reduced amounts of NP-specific IgM and IgG3 ASCs compared to immunized controls (Figure 20A).

In addition, the serum titers of NP-specific IgM and IgG3 antibodies were measured by ELISA. Both antibody titers were elevated in immunized compared to unimmunized controls. NP-specific IgM antibodies were present in immunized DKO mice, but their titers were significantly lower than in immunized controls. The titers of NP-specific IgG3 antibodies were barely detectable in immunized DKO mice (Figure 20B).

In summary, PC differentiation seems to be markedly reduced in DKO mice upon TI immune response. Compared to the previous results of the TD immune response of DKO mice (184), the deficits of DKO mice to react to TI immunization were even stronger.

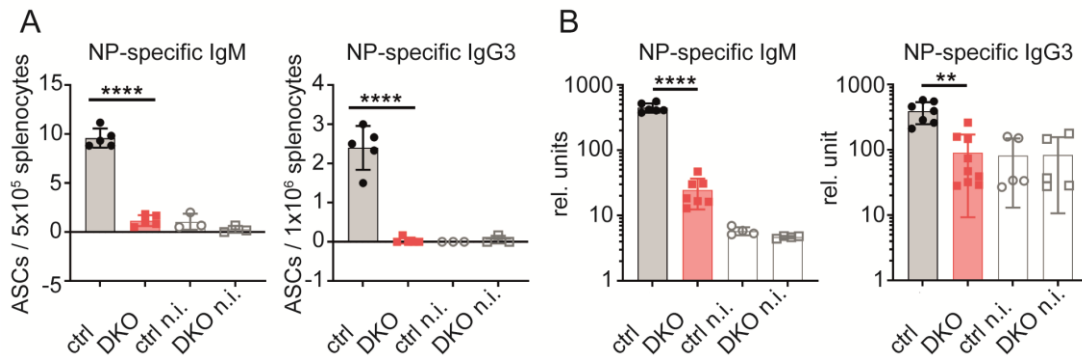


Figure 20: DKO mice displayed a diminished TI immune response. 14 days after intraperitoneal NP-Ficoll immunization of control (n = 5 to 7) and DKO (n = 5 to 9) mice, (A) NP-specific IgM and IgG3 ASCs were measured by ELISpot and (B) relative (rel.) units of NP-specific IgM and IgG3 antibody serum titers were determined by ELISA. Unimmunized (n.i.) control (n = 3 to 5) and DKO (n = 3 to 5) mice served as negative controls. Each data point represents the value of one individual mouse. The bars and error bars signify the mean \pm standard deviation. ELISpot (A) and logarithmized ELISA (B) data sets were normal distributed. Two-way ANOVA with Tukey's multiple comparisons test were performed. **p < 0.01; ****p < 0.0001. A similar presentation of the data can be found in Scheffler et al. 2021.

3.2.2 Impaired LPS mediated PC differentiation in DKO B cells *in vitro*

To demonstrate a direct role of B-Raf and Raf-1 in the PC differentiation, *in vitro* LPS stimulation was performed with isolated splenic B cells of DKO and control mice for 3 days. LPS stimulation is described to induce the TI type I immune response by activating the Toll-like receptor 4 (112) leading to plasmablast (PB) formation *in vitro*. In the following, the expression of the different markers B220, CD138, PAX5, IRF4 and BLIMP1 that are up- or down-regulated during PB differentiation (Figure 2) was investigated by flow cytometry.

First, the percentage of generated PBs (CD138^{high}B220^{low}) after 3 days of LPS stimulation was determined. The formation of PBs was significantly impaired in DKO samples compared to controls. Thus, the controls had about 4.4 times more PBs than the DKO samples (Figure 21). These data suggested an important role of B-Raf and Raf-1 during the formation of PBs.

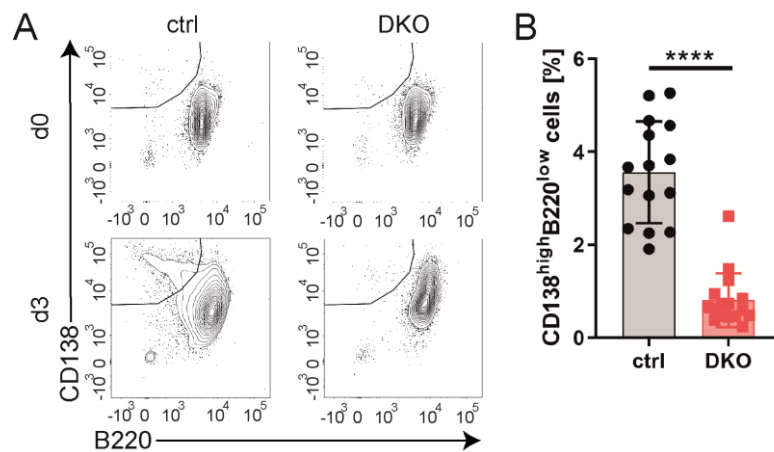


Figure 21: DKO B cells failed to adopt the PB state upon LPS stimulation *in vitro*. Isolated control (ctrl; n = 15) and DKO (n = 15) B cells of the spleen were stimulated with LPS for 3 days *in vitro* and analyzed by FACS. Unstimulated cells of both genotypes (d0) were used as negative controls. All FACS plots were pre-gated on living cells (TOPRO^{neg}). (A) Representative B220/CD138 FACS plots and the gating strategy of PBs (CD138^{high}B220^{low}) are depicted. (B) The amounts of PBs gated as illustrated in (A) from different experiments are compiled in the graph. Values of individual mice are represented by different data points. The bars and error bars signify the mean \pm standard deviation. The data set (B) was normal distributed and statistically analyzed using the Unpaired Student's t-test. ****p < 0.0001. In (B) some data of Samantha Feicht were summarized with own data. The illustration can also be found in Scheffler et al. 2021.

Next, we checked for the expression of the B cell activation marker IRF4 and of the PC differentiation factor BLIMP1. Here, both control and DKO B cells showed comparable IRF4 activation after 3 days of LPS stimulation (Figure 22A), but the proportion of BLIMP1^{pos} cells was approximately 4-fold higher in controls than in DKO samples (Figure 22B). Furthermore, the remaining BLIMP1^{pos} DKO B cells were not capable of generating the CD138^{high}B220^{low} PB population, which could be detected in controls (Figure 22C).

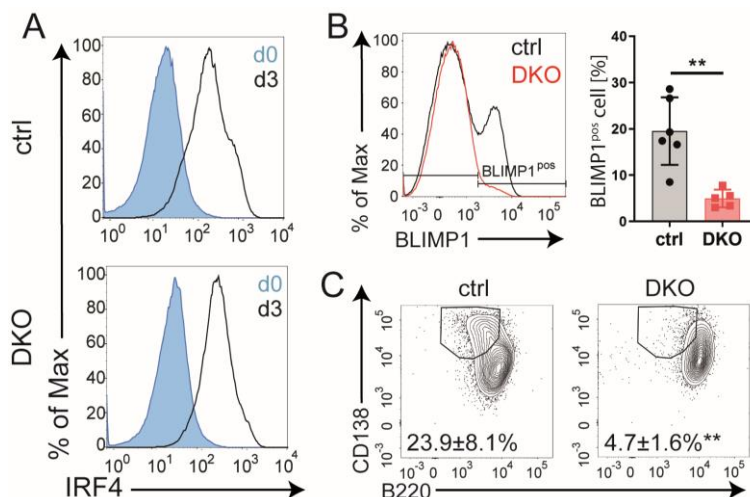


Figure 22: DKO B cells exhibited normal IRF4 but impaired BLIMP1 upregulation. Flow cytometry was performed on unstimulated (day 0; d0) and LPS stimulated (3 days; *in vitro*; d3) isolated splenic B cells of n = 6 control (ctrl) and n = 5 DKO mice. All FACS plots were pre-gated on living cells (Fixable Live/Dead^{neg}). (A) Representative overlays of IRF4 of d0 compared to d3 in control and DKO B cells. (B) Representative overlay of BLIMP1

and a graph compiling the data of BLIMP1^{pos} cells of control and DKO B cells. Each data point represents one mouse. The bars and error bars signify the mean \pm standard deviation. (C) The gating and amounts of PBs (CD138^{high}B220^{low}) within the BLIMP1^{pos} cell population as gated in (B). Numbers represent the mean \pm standard deviation. The data sets in (B) and (C) were lognormal distributed. After logarithmic transformation the unpaired Student's t-test was performed. **p < 0.01. These illustrations can also be found in Scheffler et al. 2021.

To get a deeper insight at which stage of PB differentiation B-Raf and Raf-1 are important, FACS stainings were performed with B220, PAX5, IRF4 and CD138. This FACS staining made it possible to distinguish naïve B cells ($PAX5^{high}IRF4^{low}$) from day zero from activated B cells ($PAX5^{high}IRF4^{+}$), pre-PBs ($PAX5^{low}IRF4^{high}CD138^{+}B220^{high}$) and PBs ($PAX5^{low}IRF4^{high}CD138^{high}B220^{low}$) generated after 3 days of LPS stimulation.

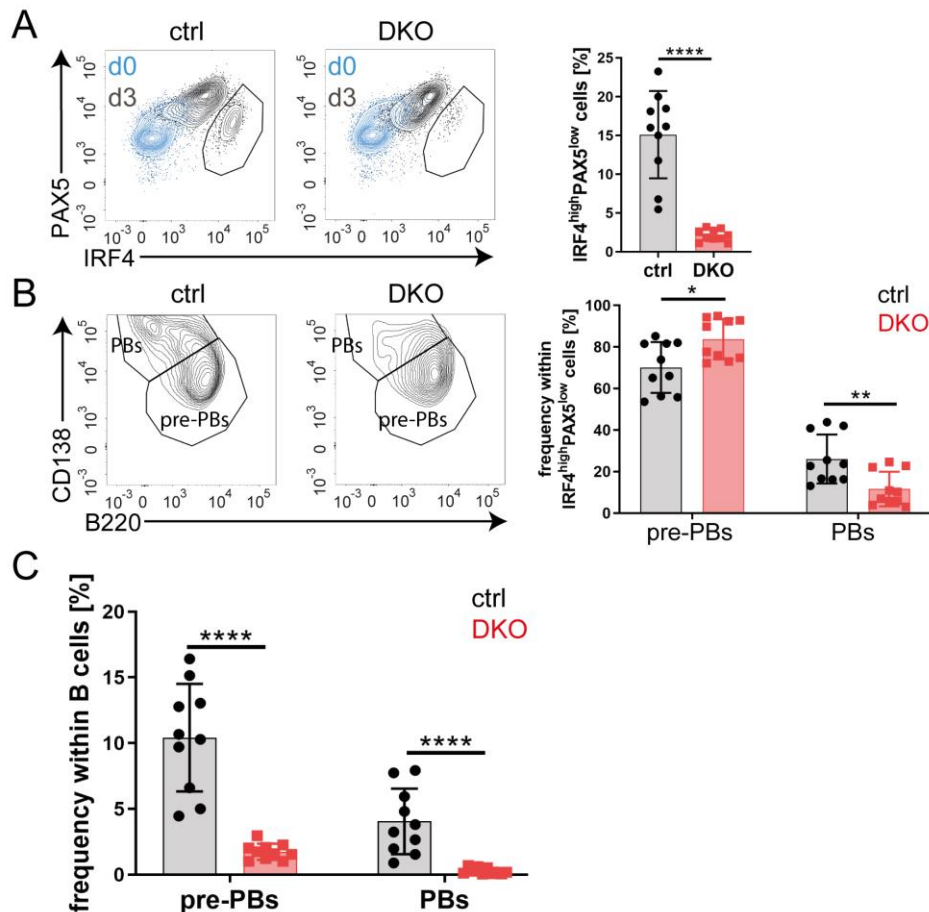


Figure 23: LPS stimulated DKO B cells displayed a block in the transition into pre-PB and PB. (A-C) Flow cytometric analyses of unstimulated (day 0; d0) and LPS stimulated (3 days; *in vitro*; d3) isolated splenic B cells of control (ctrl) and DKO mice (n = 10 for each genotype). Plots were pre-gated on living cells (fixable Live/Dead^{neg}). (A) Representative contour plots for PAX5/IRF4 illustrating the gating of IRF4^{high}PAX5^{low} B cells in control and DKO samples and a graph compiling the amounts of this population. (B) Gating strategy and a graph compiling the data of control and DKO pre-PBs (CD138⁺B220^{high}) and PBs (CD138^{high}B220^{low}) within the PAX5^{low}IRF4^{high} population described in (A). (C) Calculation of the amounts of pre-PBs and PBs gated in (B) within all living B cells. (A-C) Each data point represents one mouse. The bars and error bars indicate the mean \pm standard deviation. The data sets of (A) and (C) were lognormal and the one in (B) was normal distributed. The data sets of (A) and (C) were logarithmically transformed. In (A) the unpaired Student's t-test and in (B) and (C) the Two-way ANOVA with Sidak's multiple comparisons test were performed. *p < 0.05; **p < 0.01; ****p < 0.0001. These illustrations can also be found in Scheffler et al. 2021.

Regardless of the genotype, nearly no naïve B cells could be observed after three days of LPS stimulation. Compared to controls, DKO B cells displayed significantly reduced amounts of IRF4^{high}PAX5^{low} cells (Figure 23A). This population includes both pre-PBs

and PBs. Thus, the IRF4^{high}PAX5^{low} population was further subdivided by the expression of CD138 and B220. Within the IRF4^{high}Pax5^{low} gate, DKO B cells exhibited higher amounts of pre-PBs (CD138⁺B220^{high}) and reduced frequencies of PBs (CD138^{high}B220^{low}) compared to controls (Figure 23B) indicating a differentiation block from pre-PBs to PBs. Calculating the total amounts of pre-PBs and PBs within all B cells demonstrated significantly decreased percentages of both pre-PBs and PBs in DKO samples (Figure 23C). These results suggested that not only the final PB differentiation, but already the differentiation of activated B cells to pre-PBs is impaired in DKO B cells. Taken together, both control and DKO B cells displayed a similar LPS mediated B cell activation. Nonetheless, the DKO B cells were partially blocked at the transition from activated B cells to pre-PB and further to PB, illustrating the important role of B-Raf and Raf-1 during PB differentiation.

3.2.3 Increased LPS mediated ERK phosphorylation in DKO B cells

As just demonstrated, DKO mice displayed a reduced PC differentiation both *in vivo* after NP-Ficoll immunization and *in vitro* upon LPS stimulation. Raf-kinases are postulated to mediate ERK phosphorylation (178). Moreover, a role of pERK in the upregulation of BLIMP1 and the subsequent PC differentiation was previously described (198). Therefore, the ability of DKO B cells to upregulate pERK upon LPS stimulation was examined in the following.

First, isolated mature B cells from DKO and control mice were stimulated with LPS *in vitro* up to three days. Flow cytometry was used to determine the pERK levels in living B cells from day 0 to day 3. As expected, ERK phosphorylation steadily increased in control B cells over time, which reflected the B cell activation upon LPS stimulation. Surprisingly, even in the absence of B-Raf and Raf-1 in DKO B cells, LPS stimulation led to a continuous increase of pERK levels. Similar to the previously described results of unstimulated and anti-IgM stimulated DKO B cells (see 3.1.1), pERK levels were higher in DKO B cells than in the corresponding controls upon LPS stimulation at all time points, reaching significance at day 3 (Figure 24). Thus, ERK phosphorylation was still inducible in DKO B cells by long-term LPS stimulation.

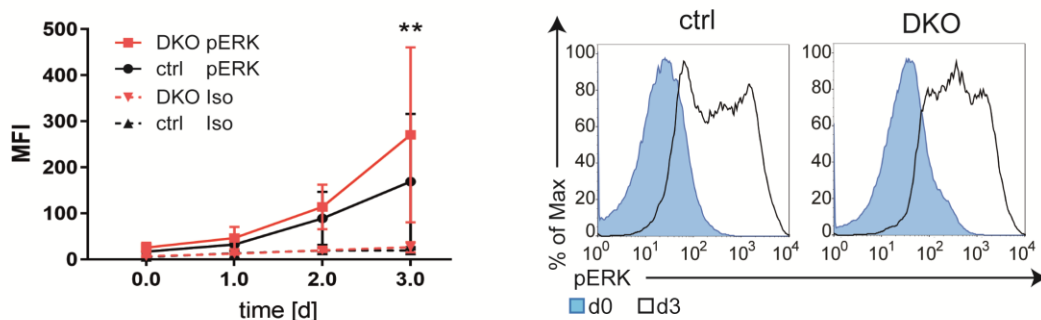


Figure 24: Both control and DKO B cells upregulated pERK upon LPS stimulation. Isolated splenic B cells from two mice per genotype were pooled and stimulated with LPS for up to 3 days. The pERK levels in living B cells (Fixable Live/Dead^{neg}) were determined by FACS, with an isotype control (Iso) included. Unstimulated cells were used for day 0 (d0). Both a representative pERK overlay of d0 and d3 and a graph compiling the median fluorescent intensity (MFI) as mean \pm standard deviation of $n=3$ independent experiments were depicted. The data were normally distributed. Two-way ANOVA with Tukey's multiple comparisons test was performed. $**p < 0.01$. These illustrations can also be found in Scheffler et al. 2021.

To get a deeper insight into the role of B-Raf and Raf-1 during the initial phase of B cell activation, short-term stimulations for 1 or 5 min with LPS were performed on isolated splenic B cells of control and DKO mice. Again, basal ERK phosphorylation was significantly increased in unstimulated DKO B cells compared with the unstimulated control.

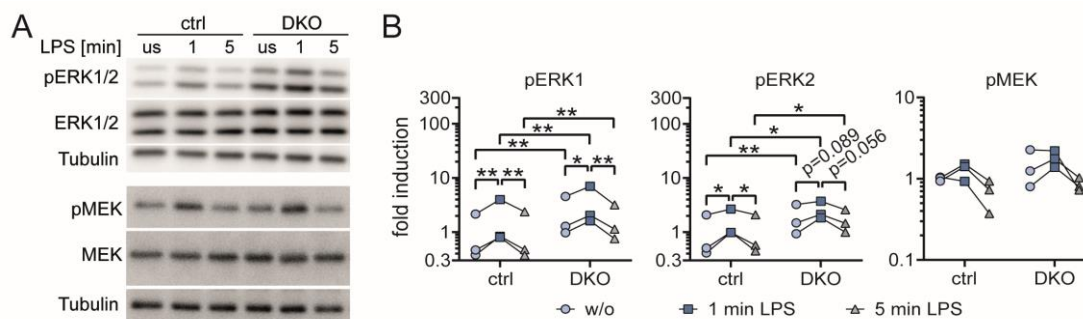


Figure 25: DKO B cells exhibited increased ERK phosphorylation, which could be further upregulated upon *in vitro* stimulation. Isolated splenic B cells from 2 to 3 mice were pooled per genotype. The pooled samples were either kept unstimulated (w/o) or were treated with LPS for 1 or 5 min *in vitro*. (A) A representative Western blot for total and phosphorylated MEK and ERK1/2 for the two genotypes with and without LPS stimulation is shown. Tubulin served as loading control. (B) The graphs summarize the fold induction of pERK1, pERK2 and pMEK in comparison to unstimulated controls. The calculation of the fold induction is described in section 6.7.5. Each dot represents one of $n = 3$ independent experiments. The corresponding values of the different time points of one genotype per Western blot were connected by a line. Due to the lognormal distribution the data sets were logarithmically transformed and statistically analyzed by the Two-way ANOVA with Tukey's multiple comparisons test. $*p < 0.05$; $**p < 0.01$. These illustrations can also be found in Scheffler et al. 2021.

Furthermore, an increased MEK and ERK phosphorylation of DKO B cells compared to controls was also evident upon LPS stimulation. However, the time course of pMEK and pERK was similar between controls and DKO B cells. Here, regardless of the genotype

an upregulation of pMEK and pERK was observed after 1 min of LPS stimulation, which dropped back to the unstimulated level after 5 min (Figure 25). These data underline that B-Raf and Raf-1 do not mediate but rather negatively regulate the initial LPS mediated MEK and ERK phosphorylation in mature B cells.

To investigate the mechanisms of LPS mediated ERK phosphorylation, inhibitor experiments were performed. First, the participation of A-Raf to LPS mediated ERK phosphorylation was analyzed by treating isolated control and DKO B cells with either LY3009120 or its solvent control DMSO and subsequent short-term LPS stimulation. As before, in the DMSO treated control B cells an LPS mediated ERK phosphorylation after 1 min of LPS stimulation was detectable, which was reduced again at the 5 min timepoint. The LY3009120 treatment of the control B cells increased the ERK phosphorylation to such high levels, that an additional effect on the pERK levels by LPS stimulation could not be observed. DKO B cells displayed a high increase in the ERK activation upon LY3009120 treatment compared to the corresponding DMSO treated DKO samples, too (Figure 26A). These results indicated, an inhibitory role of A-Raf on the basal and LPS mediated ERK phosphorylation redundant to B-Raf and Raf-1 in control and DKO B cells.

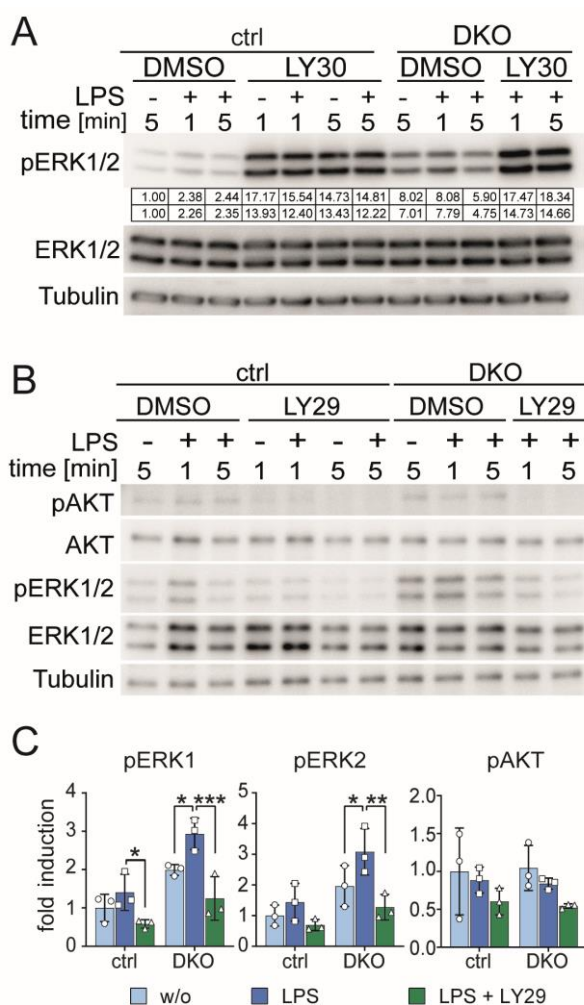


Figure 26: LPS induced pERK levels of control and DKO B cells is partially PI3K dependent. Pooled splenic B cells of 2 to 3 mice per genotype were incubated with 3 μ M LY3009120 [LY30; (A)] or with 20 μ M LY294002 [LY29; (B)], or its solvent control DMSO. Subsequently, the samples were left unstimulated or were stimulated with LPS for 1 or 5 min. (A) One representative Western blot of total and phosphorylated ERK, its loading control Tubulin and the fold induction of pERK1 and pERK2 compared to the unstimulated DMSO control is illustrated. The calculation of the fold induction is described in section 6.7.5. (B) One representative Western blot of total and phosphorylated AKT and ERK and its loading control Tubulin is illustrated. (C) The fold induction of pAKT, pERK1, and pERK2 compared to the unstimulated DMSO controls measured by Western blots similar to (B) is depicted. The calculation of the fold induction is described in section 6.7.5. (A) was performed in $n = 2$ and (B+C) in $n = 3$ independent experiments represented in individual dots (C). Bars and error bars indicate the mean \pm standard deviation. (C) The data sets were normal distributed and statistically analyzed by the Two-way ANOVA with Dunnett's multiple comparisons test. * $p < 0.05$, ** $p < 0.01$; *** $p < 0.001$.

0.001; **** $p < 0.0001$. Similar figures are illustrated in Scheffler et al. 2021.

Furthermore, a PI3K-dependency of the LPS mediated ERK phosphorylation was investigated, by treating isolated control and DKO B cells with the PI3K-inhibitor LY294002 and subsequent short-term LPS stimulation. The PI3K inhibitor LY294002 led to decreased pAKT levels in unstimulated and LPS stimulated B cells of both genotypes, which reflected the efficacy of the inhibitor. In both genotypes the LY294002 treatment reduced the LPS mediated ERK phosphorylation (Figure 26B-C). Thus, to some extent short-term TLR4 signaling mediated ERK phosphorylation in a PI3K dependent manner in control and DKO B cells.

ERK acts as a kinase to phosphorylate many cytoplasmic and nuclear target proteins. The outcome of ERK activation also seems to depend on the subcellular localization of pERK (199). Because a possible role of B-Raf in the nuclear localization of pERK has been described (200), the subcellular pERK levels were investigated in control and DKO B cells upon LPS stimulation. Isolated mature B cells of control and DKO mice were left untreated or were stimulated with LPS for up to 10 min. Afterwards, proteins of the cytoplasmic and nuclear fractions were isolated, and their pERK levels were determined using the protein simple WES system.

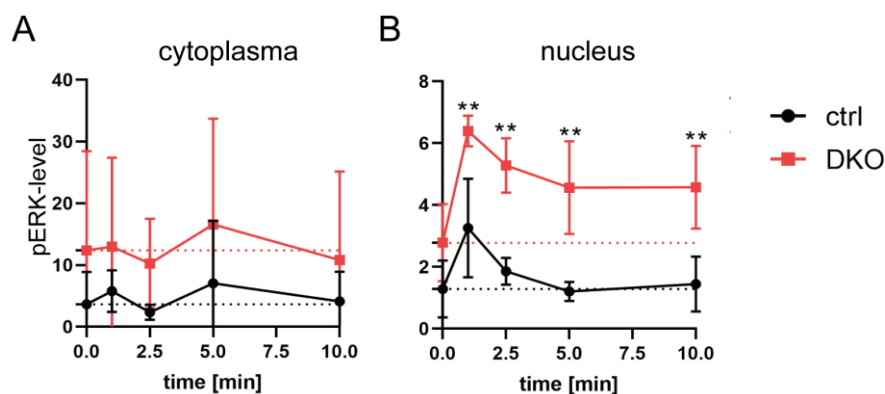


Figure 27: DKO B cells featured a prolonged ERK phosphorylation in the nucleus. Isolated splenic B cells of 3 control (ctrl) and 3 DKO mice were pooled per genotype and subsequently stimulated with LPS *in vitro* for the indicated time points. After nuclear/cytoplasmic fractionation, pERK levels were analyzed in the cytoplasmic (A) and the nuclear (B) fraction by protein simple WES. The dots and error bars represent the mean \pm standard deviation of $n = 3$ independent experiments. The data were normally distributed. Two-way ANOVA with Sidak's multiple comparisons test was performed. ** $p < 0.01$. A similar graph for the nuclear fraction is included in Scheffler et al. 2021.

Regardless of the treatment, in both subcellular compartments ERK phosphorylation was higher in DKO B cells compared to controls. A similar kinetic of the pERK levels could be observed in the cytoplasmic fractions of DKO and control samples (Figure 27A). In

the nuclear fraction, an initial peak of pERK could be monitored after 1 min of LPS stimulation in both genotypes. In the controls, the pERK signal declined after the initial peak and returned to the baseline pERK levels of the unstimulated control after 5 min of LPS treatment. At the 10 min time point, no new increase in pERK could be detected in control B cells (Figure 27B). A decrease in the pERK signal after the initial peak was also observed in DKO B cells, but the pERK level remained at a constantly elevated level compared to the baseline pERK level of unstimulated DKO B cells (Figure 27B). Thus, a prolonged nuclear localization of pERK in DKO B cells compared to controls could be observed upon LPS stimulation *in vitro*. The B-Raf//Raf-1 inactivation did not appear to reduce, but rather to enhance, the nuclear localization of pERK upon short-term LPS stimulation in DKO B cells.

Taken together, TLR4 signaling appears to induce a PI3K dependent ERK phosphorylation, which seems to be negatively regulated by the redundantly acting Raf-kinases A-Raf, B-Raf, and Raf-1. The increased ERK phosphorylation in DKO B cells caused by the B-Raf//Raf-1 inactivation compared with controls was reflected in both the cytoplasm and the nucleus. The nucleus also showed a longer lasting ERK phosphorylation in DKO B cells compared to controls. Thus, contrary to our original hypothesis that the PC defect in DKO B cells could be caused by impaired LPS mediated ERK phosphorylation, no reduced pERK levels were detected in mature DKO B cells compared to controls upon LPS stimulation *in vitro*.

3.2.4 A sharp increase of pERK as a prerequisite for PB differentiation *in vitro*

Up to now only whole populations of mature B cells were analyzed with respect to the ERK phosphorylation. Because of similar defects in the PC differentiation of the previously published ERK1/2 double knockout chicken DT40 B cell line and our murine DKO B cells (178), the pERK levels at the different stages of PC differentiation in LPS stimulated control and DKO B cells were examined.

To determine the total and phosphorylated ERK levels in the different PC differentiation stages, the markers already described in section 3.2.2 were used in flow cytometry. Since LPS stimulation for 3 days caused a general activation of all isolated B cells *in vitro*, naive B cells (PAX5^{high}IRF4⁻) of CD43-depleted control and DKO B cells were examined for their total and phosphorylated ERK levels at day 0. In each sample activated B cells (PAX5^{high}IRF4⁺), pre-PBs (pre-PBs; PAX5^{low}IRF4^{high}CD138⁺B220^{high}) and PBs (PAX5^{low}IRF4^{high}CD138^{high} B220^{low}) were distinguished after 3 days of LPS stimulation (Figure 28).

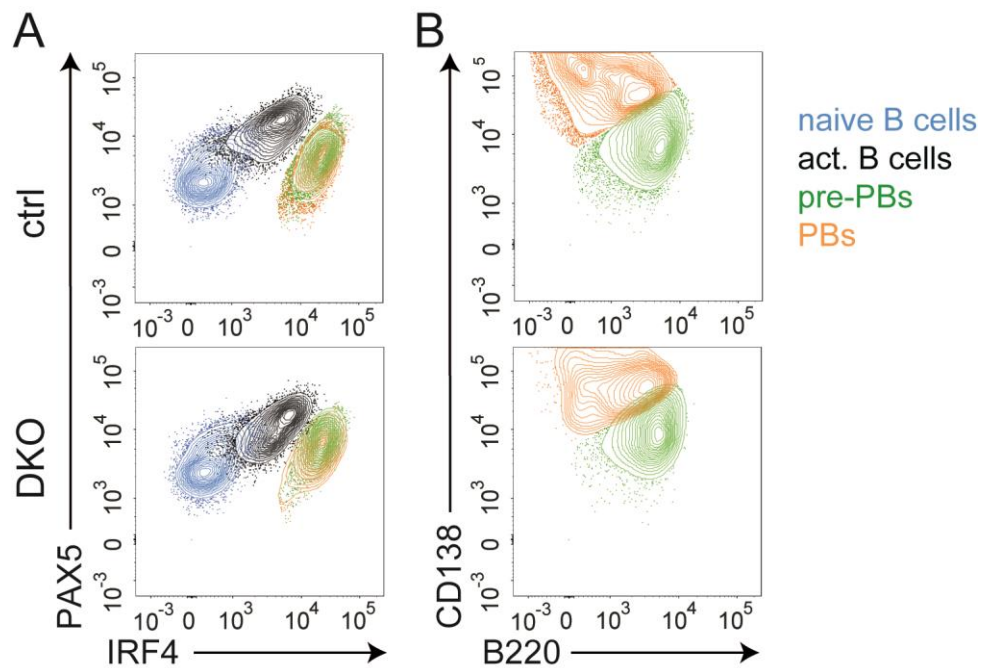


Figure 28: Gating strategy of the different B cell differentiation stages upon LPS stimulation *in vitro*. Isolated splenic B cells of control (ctrl) and DKO mice were either measured at day 0 as unstimulated cells or were stimulated with LPS for 3 days. (A) Representative overlaid contour FACS plots for PAX5/IRF4 of isolated splenic B cells of control and DKO mice of day 0 displaying naïve B cells (PAX5^{high}IRF4⁻) and after 3 days (d3) of LPS stimulation to distinguish activated (act) B cells (PAX5^{high}IRF4⁺) from PAX5^{low}IRF4^{high} B cells. In (B) CD138/B220 contour plots to depict the distribution of pre-PBs (PAX5^{low}IRF4^{high}CD138⁺B220^{high}) and PBs (PAX5^{low}IRF4^{high}CD138^{high}B220^{low}) within the PAX5^{low}IRF4^{high} population described in (A). All samples were pre-gated on living cells (Fixable Live/Dead^{neg}).

An increase in pERK- and ERK-levels could be observed in both genotypes in the transition from naïve to activated B cells, to pre-PBs and further to PBs (Figure 29A-B). In control B cells, a sharp upregulation of pERK levels occurred in the transition from activated B cells into pre-PBs. This increase was significantly attenuated in DKO B cells. Similar results could be observed by analyzing pERK levels in pre-PBs in comparison to PBs (Figure 29A). Since ERK expression also appeared to increase during PC differentiation and plateaued in the last differentiation step from pre-PB to PB (Figure 29B), the ratio pERK/ERK was calculated in addition. Already in naïve B cells, a tendency of elevated ERK phosphorylation in DKO compared to control B cells could be detected. The pERK/ERK ratio approximated each other in activated B cells of control and DKO mice. Then, the amount of phosphorylated ERK sharply increased during subsequent differentiation to pre-PBs and PB in controls. In contrast, the pERK/ERK ratios in DKO B cells increased only slightly upon differentiation to pre-PBs and PBs (Figure 29C).

In summary, in addition to the inhibitory regulatory function of the B-Raf and Raf-1 in naïve and activated B cells, a B-Raf//Raf-1 dependent ERK phosphorylation during PC differentiation could be demonstrated. Here, B-Raf and Raf-1 appear to mediate a strong

boost in the ERK phosphorylation in the progression from activated B cells to pre-PB and further to PB and might therefore play a crucial role in this differentiation process.

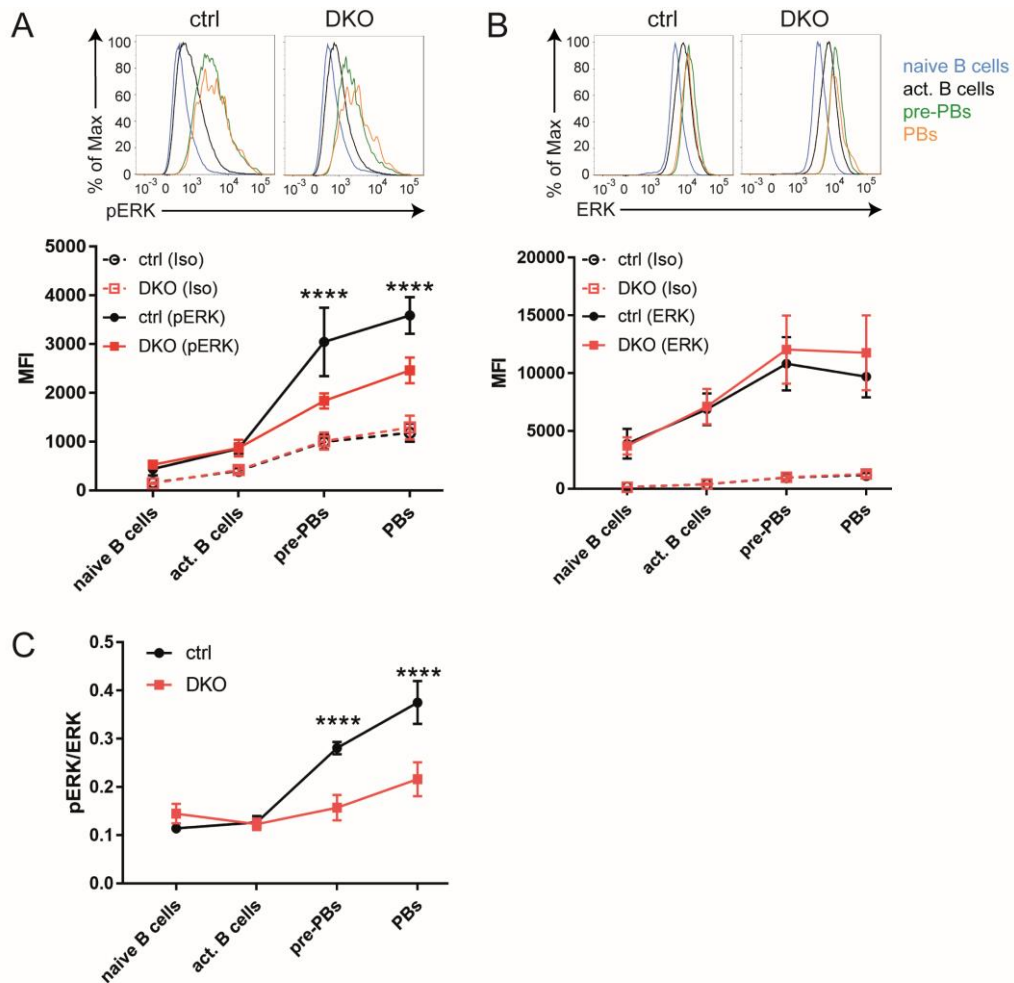


Figure 29: A sharp increase of pERK levels in pre-PBs as a prerequisite for PB formation.

Isolated splenic B cells of control (ctrl; $n = 4$) and DKO ($n = 5$) mice were either measured at day 0 as unstimulated cells or were stimulated with LPS for 3 days. The gating strategy presented in Figure 28 was used for the determination of naïve B cells ($PAX5^{high}IRF4^{-}$) at day 0 and activated (act) B cells ($PAX5^{high}IRF4^{+}$), pre-PBs ($PAX5^{low}IRF4^{high}CD138^{+}B220^{high}$) and PBs ($PAX5^{low}IRF4^{high}CD138^{high}B220^{low}$) after 3 days (d3) of LPS stimulation. (A-B) Representative histogram overlays and graphs summarizing the Median fluorescent intensity (MFI) of pERK (A) and total ERK (B) levels of the distinct differentiation states (naïve B cells, activated B cells, pre-PBs, and PBs) are depicted. Isotype controls (Iso) were included in the FACS stainings. (C) The ratio of the MFIs of pERK (A) to ERK (B) was calculated for each differentiation stage of control and DKO B cells. (A-C) All data sets were normal distributed. Two-way ANOVA with Tukey's multiple comparisons test was used. **** $p < 0.0001$. Similar illustrations can be found in Scheffler et al. 2021.

3.3 The effects of B-Raf//Raf-1 inactivation on CD40 induced B cell activation

3.3.1 Negative regulatory function of B-Raf and Raf-1 on CD40 mediated ERK phosphorylation

The role of B-Raf and Raf-1 in CD40 mediated ERK phosphorylation in splenic B cells of control and DKO mice was investigated by stimulation with an agonistic anti-CD40 antibody for different time points. In both genotypes, CD40 stimulation led to a peak of pERK levels after 10 min, which declined to unstimulated levels after 30 min. After 2 h, the ERK phosphorylation increased again in both genotypes. These results suggested that pERK was increased in DKO B cells with and without stimulation, however B-Raf//Raf-1 inactivation did not influence the pERK kinetic upon CD40 stimulation (Figure 30A-B).

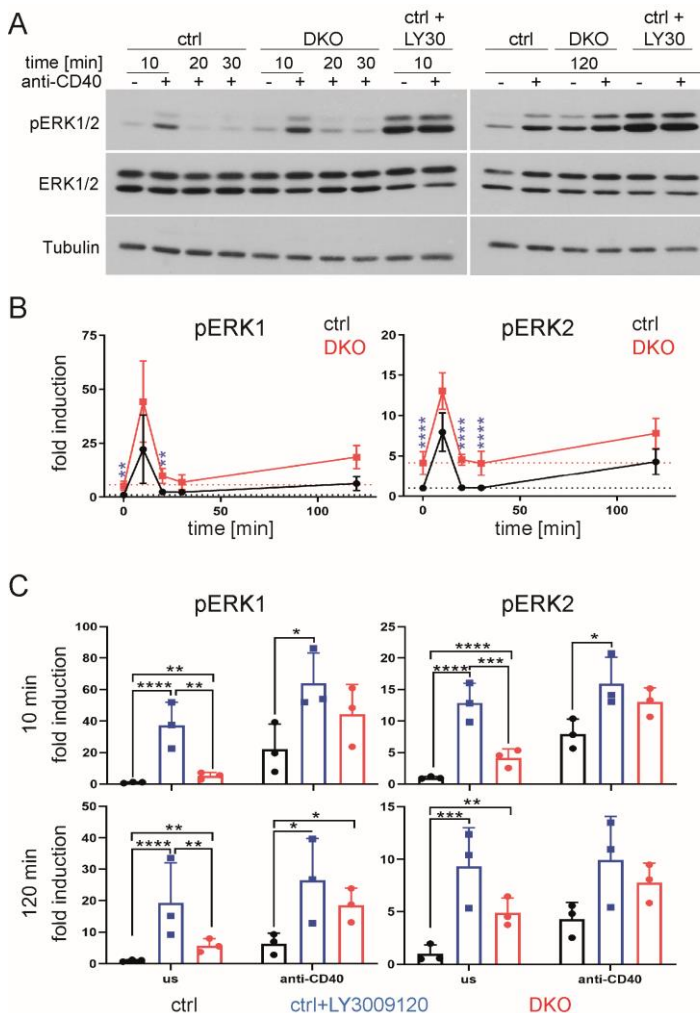


Figure 30: DKO B cells displayed increased pERK levels upon CD40 stimulation.

Isolated splenic B cells of 2 to 3 control (ctrl; black) and DKO (red) mice were pooled per genotype. Control B cell samples were either left untreated or pre-incubated with 3 μ M LY3009120 (LY30; blue) for 1.5 h. The different B cell samples were either left unstimulated or were stimulated with anti-CD40 for different time points (10, 20, 30, or 120 min). Total and phosphorylated ERK was analyzed by Western blot. Tubulin served as loading control. (A) Representative Western blot of the described control and DKO B cell samples treated as indicated. (B) Fold induction of pERK1 and pERK2 at different time points of anti-CD40 stimulation of the control and DKO B cell samples without LY30 pre-incubation. Dots and error bars represent the mean \pm standard deviation of $n = 3$ independent experiments. (C) Quantification of unstimulated or anti-CD40 stimulated (10 min or 120 min) control, DKO, and LY30 pre-treated control B cell samples constituted as fold induction of pERK1 and

pERK2. Bars and error bars represent the mean \pm standard deviation of $n = 3$ independent experiments indicated as dots. (B+C) The calculation of the fold induction is described in section 6.7.5. The data sets were lognormal distributed, logarithmically transformed and statistically analyzed by the Two-way ANOVA with either Sidak's (B) or Tukey's (C) multiple comparisons test. * $p < 0.05$, ** $p < 0.01$, *** $p < 0.001$, **** $p < 0.0001$.

To exclude a compensatory role of A-Raf in our experimental setup, control B cells were additionally treated with the pan-Raf inhibitor LY3009120 (172). In unstimulated and CD40 stimulated control B cells treatment with LY3009120 led even to higher pERK levels than the genetic inactivation of B-Raf and Raf-1 alone (Figure 30A+C). Taken together, the results of the genetic and the chemical (LY3009120) inactivation of Raf-kinases indicated that CD40 mediated ERK phosphorylation is Raf independent and confirmed an inhibitory function of Raf-kinases in mature and activated B cells towards pERK.

3.3.2 PI3K dependency of long-term CD40 mediated pERK in control and DKO B cells

Previous data (107,184) hinted to a CD19/PI3K dependency of the ERK phosphorylation in mature B cells. To test this upon CD40 stimulation control and DKO B cells were treated with the PI3K inhibitor LY294002 or its solvent control DMSO in the presence or absence of CD40 stimulation.

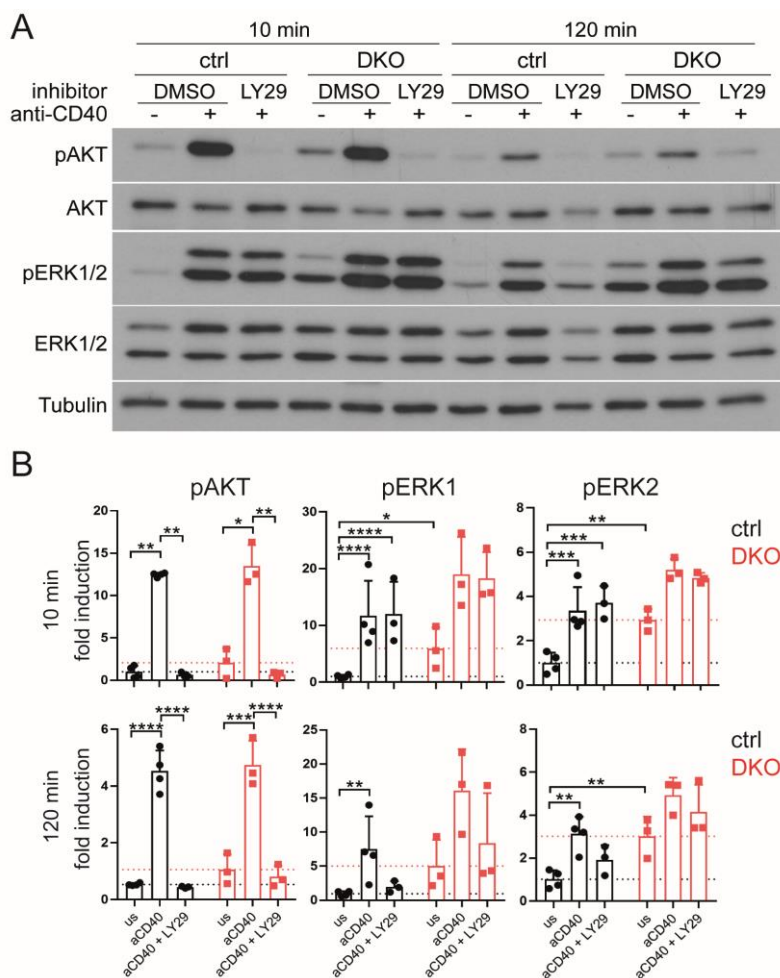


Figure 31: Long-term CD40 stimulation induced a PI3K dependent ERK phosphorylation. Splenic B cells of 2 to 3 control (ctrl) and DKO mice were pooled and either pre-incubated with DMSO or with 20 μ M LY294002 (LY29) for 1.5 h. Afterwards cells were either left unstimulated (us) or were stimulated with anti-CD40 for 10 min or 120 min. The total and phosphorylated AKT and ERK1/2 were analyzed by Western blot. Tubulin served as loading control. (A) Representative Western blot of the described control and DKO B cell samples treated as indicated. (B) The graphs show the fold induction of pAKT, pERK1, and pERK2 in comparison to unstimulated DMSO treated controls. The calculation of the fold induction is described in section 6.7.5. Each data point represents one B cell sample.

The bars and error bars represent the mean \pm standard deviation of $n = 3$ independent experiments. Due to lognormal distribution the data were logarithmically transformed. Two-way ANOVA with Tukey's multiple comparisons test. * $p < 0.05$; ** $p < 0.01$; *** $p < 0.001$; **** $p < 0.0001$.

At both time points LY294002 treatment led to a strong reduction of the pAKT levels, which confirmed the inhibition of the PI3K. In both genotypes, the ERK phosphorylation was inhibited by the PI3K inhibitor upon 2 h of CD40 stimulation, while LY294002 treatment did not influence the pERK levels after 10 min of CD40 stimulation (Figure 31). Thus, in both genotypes long-term CD40 stimulation seemed to be PI3K dependent, while the initial peak of pERK after 10 min appears to be independent from PI3K.

3.3.3 Enhanced ERK phosphorylation in RafDKO/LC40 B cells

Next, we tested the ERK phosphorylation in B cells from LMP1/CD40//CD19-Cre (LC40) mice expressing a constitutive active CD40 in B cells. We have shown previously that ERK is constitutively activated in B cells and plays an important role in the B cell expansion of LC40 mice. To study whether ERK is still phosphorylated in the absence of B-Raf//Raf-1, the mouse strains B-Raf^{fl/fl}//Raf-1^{fl/fl} (184) and LMP1/CD40^{stopfl}//CD19-Cre (LC40) (52) were crossed to generate RafDKO/LC40 mice (Raf-1^{fl/fl}//B-Raf^{fl/fl}//LMP1/CD40^{flSTOP+/-}//CD19-Cre^{+/-}) mice (Figure 8). These mice exhibit a B cell specific B-Raf//Raf-1 inactivation and concomitant expression of the LC40 transgene. This fusion protein consists of the transmembrane domain of the viral LMP1 protein and the intracellular signaling domain of the CD40 receptor leading to constitutive active CD40 signaling (52). Isolated splenic B cells from LC40 and RafDKO/LC40 mice were examined concerning their nuclear and cytoplasmic pERK levels by Western blot.

The ERK phosphorylation was increased in RafDKO/LC40 compared to LC40 B cells (Figure 32) in both the cytoplasm and the nucleus. These results indicated an inhibitory function of the B-Raf and Raf-1 towards the ERK phosphorylation also in LC40 expressing B cells. Thus, the previously described PI3K dependent ERK phosphorylation in LC40 expressing B cells also appears to be negatively regulated by B-Raf and Raf-1.

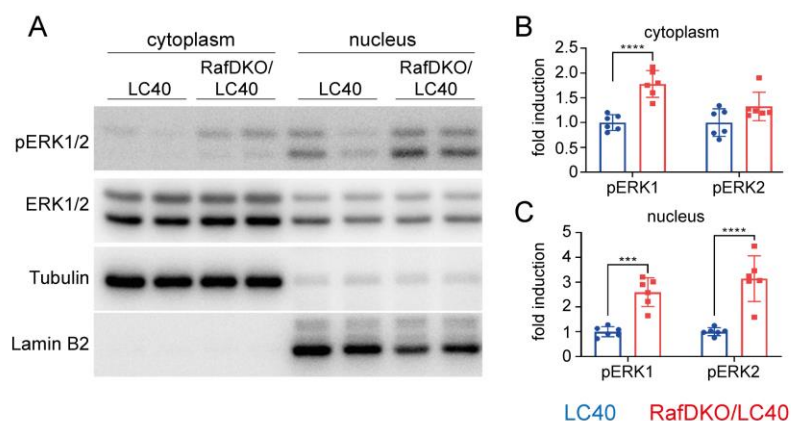


Figure 32: RafDKO/LC40 B cells exhibited higher ERK phosphorylation than LC40 B cells. Nuclear/cytoplasmic fractionation was performed on isolated splenic B cells from LC40 (n = 6) and RafDKO/LC40 (n = 6) mice. Total and phosphorylated ERK1/2 levels in the cytoplasmic and the nuclear fraction was analyzed by Western blot. Tubulin and Lamin B2 served as loading controls for the cytoplasmic and nuclear samples, respectively. (A) Representative Western blot of the LC40 and RafDKO/LC40 samples as indicated. (B+C) Fold induction of pERK1 and pERK2 in the cytoplasmic (B) and nuclear (C) fractions in RafDKO/LC40 compared to LC40 samples. The calculation of the fold induction is described in section 6.7.5. The dots represent individual mice, the bars and error bars represent the mean \pm standard deviation. The data were normally distributed and statistically analyzed using the Two-way ANOVA with Sidak's multiple comparisons test. ***p < 0.001; ****p < 0.0001.

3.4 Attenuated LC40 mediated phenotype upon B-Raf//Raf-1 inactivation

Although Raf-kinases seemed not to mediate ERK phosphorylation upon CD40 signaling, Raf-kinases might influence B cell activation and expansion. Therefore, phenotypical analyses of the RafDKO/LC40 mice were performed in comparison to LC40 mice, which are still Raf proficient. CD19-Cre^{+/-} and wildtype C57BL/6 mice were summarized under the term control (ctrl). In the following, some data of Laura Kuhn, a master student of our lab, were reevaluated or summarized with own data.

3.4.1 Diminished B cell expansion in RafDKO/LC40 mice

First, we focused on the phenotypical analyses of young (< 4 months) RafDKO/LC40 mice in comparison to age matched LC40 and control mice. As earlier described (52), LC40 mice displayed a splenomegaly (Figure 33A) due to a nearly five-fold expansion of B cells (Figure 33B) and a 3 fold increase of T cells (Figure 33C). RafDKO/LC40 mice featured significantly reduced splenic weights and B cell numbers compared to LC40 mice but they were still significantly higher than in controls. The number of T cells from RafDKO/LC40 mice also tended to be decreased in comparison to LC40 mice but still increased compared to controls (Figure 33A-C). Thus, in terms of cell expansion, RafDKO/LC40 revealed an intermediate phenotype between control and LC40 mice.

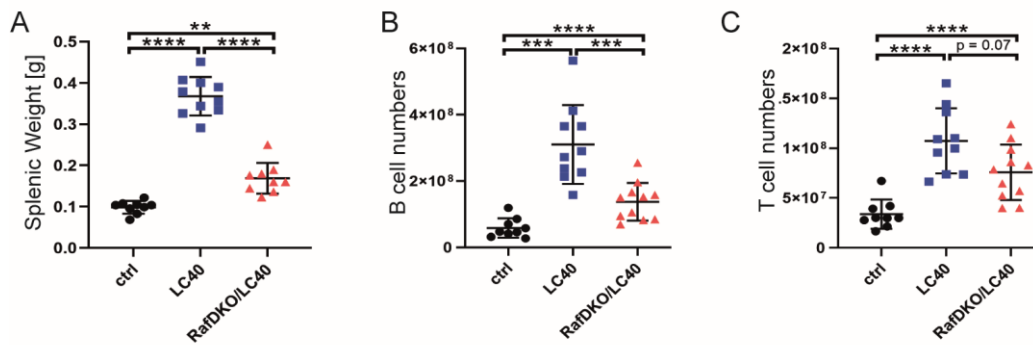


Figure 33: B-Raf//Raf-1 inactivation weakened the LC40 induced B and T cell expansion. Young (< 4 months) control (ctrl; n = 8), LC40 (n = 8) and RafDKO/LC40 (n = 9) mice were analyzed regarding their splenic weights (A), their B220⁺ B (B) and their Thy1.2⁺ T (C) cell numbers measured by flow cytometry. Each dot represents an individual mouse. Line and error bars depict the mean \pm standard deviation. (A-C) The splenic weight (A) was normal, and the B and T cell numbers (B+C) were lognormal distributed. After logarithmic transformation of the lognormal distributed data sets, all data were statistically analyzed by One-way ANOVA with Tukey's multiple comparison. **p < 0.01; ***p < 0.001; ****p < 0.0001. In these illustration FACS stainings performed by Laura Kuhn were reevaluated and summarized with own data.

Additionally, the two main B cell subsets in the spleen, Fo B and MZ B cells, were analyzed by CD21 and CD23 surface stainings. In LC40 mice, the boundaries between MZ B (CD23^{high}CD21^{high}) and Fo B (CD23^{high}CD21⁺) cells were blurred due to a significant increase of CD21 expression in LC40 B cells compared to controls. In RafDKO/LC40 mice, the upregulation of CD21 was significantly decreased in comparison to LC40 mice (Figure 34A-B). Nevertheless, MZ B and Fo B cell like cells of LC40 and RafDKO/LC40 mice were determined by transferring MZ B and Fo B gates of controls.

LC40 mice showed an expansion of Fo B and MZ B cells relative to controls with a stronger effect on MZ B than on Fo B cells, which confirmed previously published data by Hömig-Hölzel et al. in 2008 (52). This resulted in a shift in the proportion of Fo B and MZ B cells towards the MZ B cell compartment. This phenotype was weakened in RafDKO/LC40 mice (Figure 34C). MZ B cell numbers were significantly reduced in RafDKO/LC40 mice by nearly one sixth compared to LC40 mice, while Fo B cell numbers only tended to decrease (Figure 34D). These results suggested that B-Raf and Raf-1 are important for the strong expansion of MZ B cells in the LC40 mice.

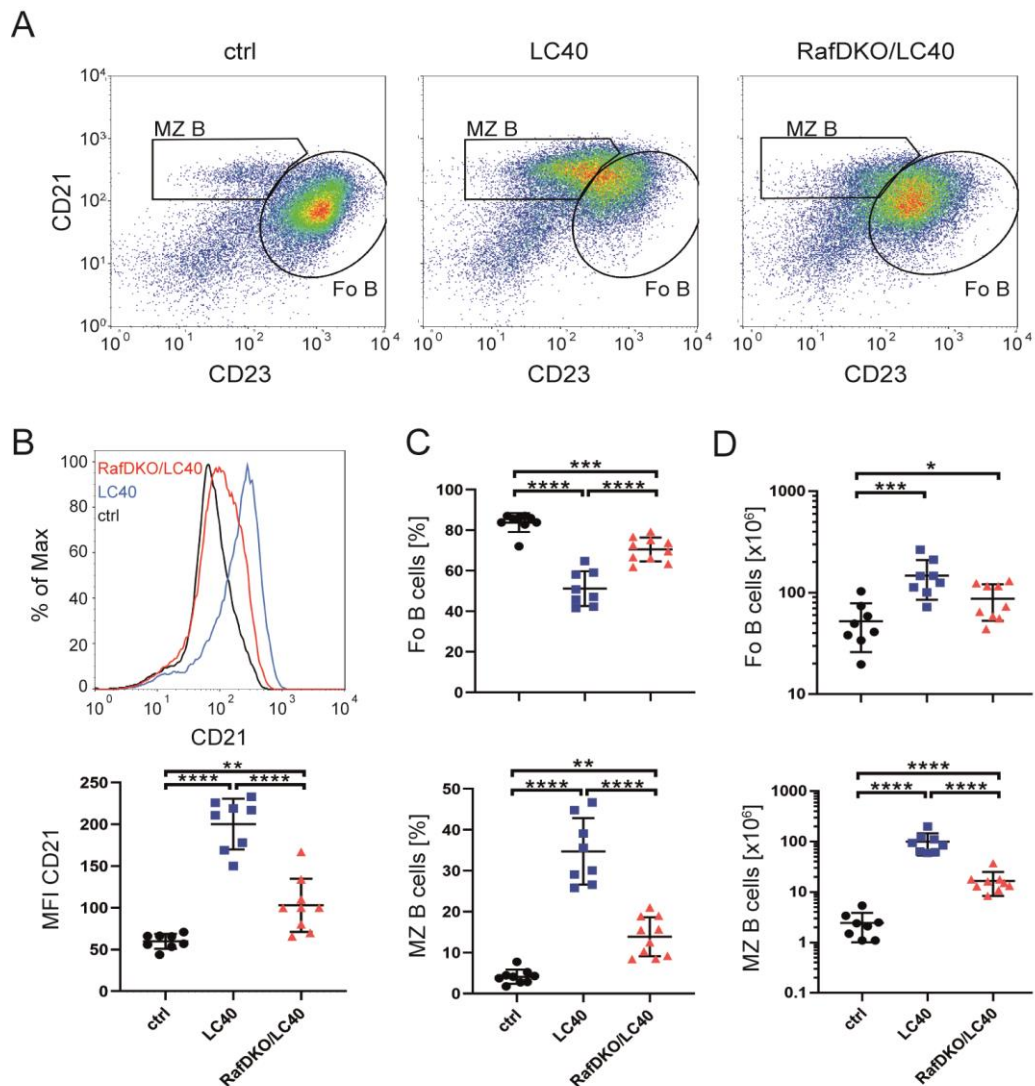


Figure 34: B-Raf/Raf-1 inactivation weakened the LC40 induced expansion of Fo B and MZ B cells. The surface CD21 and CD23 expression of young (< 4 months) control (ctrl; n = 8), LC40 (n = 8) and RafDKO/LC40 (n = 9) mice was analyzed by flow cytometry. (A) Representative plots for CD23/CD21 of B220⁺ splenic B cells illustrating the gating strategy of Fo B (CD23^{high}CD21⁺) and MZ B (CD23⁻CD21^{high}) cells. (B) Representative CD21 histogram overlay of control, LC40, and RafDKO/LC40 B220⁺ B cells and the summarized MFI. (C-D) The frequency (C) and the cell numbers (D) of Fo B and MZ B cells of the 3 genotypes, gated as described in (A). (B-D) Each dot represents an individual mouse. Line and error bars depict the mean \pm standard deviation. The CD21 MFI (B) and the Fo B and MZ B cell frequencies (C) were normal distributed, and the Fo B and MZ B cell numbers (D) were lognormal distributed. After logarithmic transformation of the lognormal distributed data sets of (D), all data were statistically analyzed by One-way ANOVA with Tukey's multiple comparison. * $p < 0.05$; ** $p < 0.01$; *** $p < 0.001$; **** $p < 0.0001$. In these illustration FACS staining performed by Laura Kuhn were reevaluated and summarized with own data.

3.4.2 Diminished pathological splenomegaly in old RafDKO/LC40 mice

In 2008, Hömig-Hölzel et al. described an LC40 induced transformation of B cells to an aberrant CD43⁺CD21^{low}CD23^{low} population during aging (52). The question arose whether Raf-kinases play a role in the development of this aberrant B cell population in LC40 mice, which finally develops to B cell lymphomas. To address this question, aged

control, LC40, and RafDKO/LC40 mice were analyzed. Again, these data were summarized with some previous results of Laura Kuhn.

It was noticed that the splenic weights in all 3 genotypes tended to increase during aging. While the increase in splenic weight was very low in control mice and moderate in RafDKO/LC40 mice, LC40 mice showed a strong variation in the splenic weights (Figure 35A). To get a better overview about the increase in the splenic weight in the three genotypes during aging, mice were categorized in three groups: Mice that had a splenic weight less than or equal to 0.2 g were referred to mice with normal splenic weight. If the splenic weight was between 0.2 g and 0.5 g the mice were designated as mice with a moderate splenomegaly. A splenic weight higher than 0.5 g was categorized as pathological splenomegaly.

All young control mice had a normal splenic weight and all young LC40 mice displayed a moderate splenomegaly. In contrast, only 14.3 % of the young RafDKO/LC40 mice exhibited a moderate splenomegaly. In control mice, aging resulted in a moderate splenomegaly in 4.2 % and pathological splenomegaly in 4.2 %. In LC40 mice, half of the old LC40 mice (56.5 %) featured a pathological and 30.4 % a moderate splenomegaly. In contrast, only 3.1 % of old RafDKO/LC40 mice displayed a pathological splenomegaly, and (37.0 %) a moderate splenomegaly. Opposite to the old LC40 mice, more than half of the old RafDKO/LC40 mice (59.4 %) exhibited a normal splenic weight (Figure 35B).

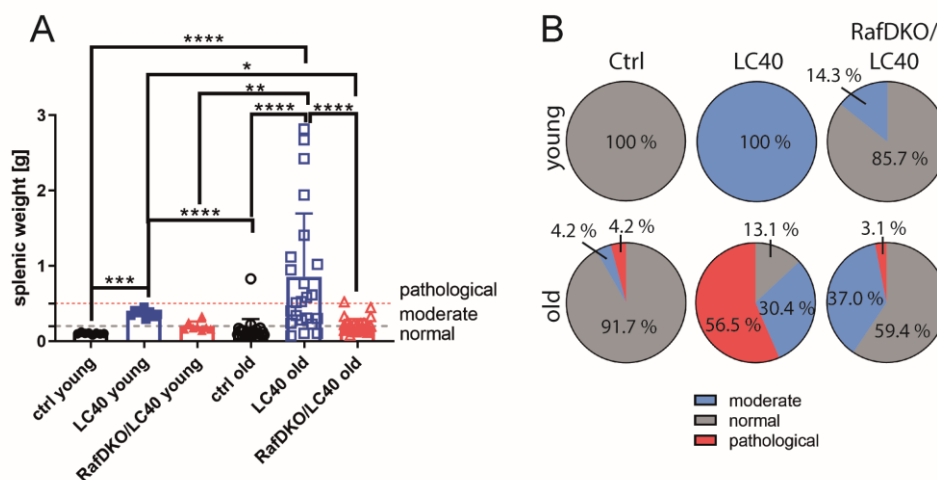


Figure 35: B-Raf//Raf-1 inactivation diminished the LC40 mediated pathological splenomegaly. (A) The splenic weight of young (< 4 months) control (ctrl; n = 9), LC40 (n = 10) and RafDKO/LC40 (n = 7) mice were compared to old (> 10 months) control (n = 24), LC40 (n = 23) and RafDKO/LC40 (n = 32) mice. Each dot represents an individual mouse. Bars and error bars depict the mean \pm standard deviation. After logarithmic transformation of the lognormal distributed data set, it was statistically analyzed by One-way ANOVA with Tukey's multiple comparison. * $p < 0.05$, ** $p < 0.01$; *** $p < 0.001$; **** $p < 0.0001$. (B) Pie charts illustrating the frequencies of mice with a normal splenic weight (< 0.2 g) or a moderate (between 0.2 g and 0.5 g) or pathological (> 0.5 g) splenomegaly per genotype. These illustrations summarize my data and reevaluated data of Laura Kuhn.

Next the splenic cell composition of old control, LC40, and RafDKO/LC40 mice were analyzed (Table 1). Splenic B (B220⁺, CD19⁺) and T cell numbers (Thy1.2⁺) were significantly expanded in old LC40 mice compared to controls. This LC40 mediated cell expansion was significantly reduced by B-Raf//Raf-1 inactivation.

Interestingly, LC40 expression in B cells did also affect the T cell expansion. Thereby, the two main T cell subsets, CD4⁺ and CD8⁺, were significantly increased in old LC40 compared to aged-matched controls. The LC40 mediated expansion affected more CD4⁺ than CD8⁺ T cells leading to a significant increase of the CD4⁺/CD8⁺ ratio. The B-Raf//Raf-1 inactivation reduced the LC40 mediated CD4⁺ and CD8⁺ T cell expansion to control levels resulting in a normalized CD4⁺/CD8⁺ ratio. Furthermore, LC40 expressing B cells significantly increased the number of activated CD4⁺CD69⁺ and CD8⁺CD69⁺ T cells compared to controls. Hereby, the B-Raf//Raf-1 inactivation significantly diminished the number of activated CD4⁺CD69⁺ and CD8⁺CD69⁺ T cells to control levels. FACS stainings for naïve (CD62L^{high}CD44^{low}), effector (CD62L^{low}CD44^{low}) and memory (CD62^{high}CD44^{high}) cells in the CD4 and CD8 positive T cell compartments revealed a significant expansion of effector and memory CD4⁺ T cells in LC40 mice compared to controls. Again, RafDKO/LC40 mice exhibited a control like cell composition of these T cell subsets (Table 1). Thus, Raf-kinases seemed to contribute to the LC40 mediated T cell expansion and activation also during aging.

Table 1: Splenic cell composition of old control, LC40 and RafDKO/LC40 mice. The cell composition of the spleen of old (> 10 months) control (ctrl; n = 19), LC40 (n = 18) and RafDKO/LC40 (n = 24) mice was determined by different FACS stainings. The most used markers are depicted in the table. Other markers: naïve (CD62L^{high}CD44^{low}), effector (CD62L^{low}CD44^{low}) and memory (CD62^{high}CD44^{high}) CD4 and CD8 positive T cells. Numbers illustrate the mean ± standard deviation. All data sets were logarithmically transformed due to lognormal distribution and were statistically analyzed by One-way ANOVA with Tukey's multiple comparison. *p < 0.05; **p < 0.01; ***p < 0.001; ****p < 0.0001. This table summarizes my data and reevaluated data of Laura Kuhn.

	ctrl	LC40	RafDKO/LC40	
cell number [x10 ⁷]	CD19 ⁺	6.8 ± 5.9	46.6 ± 55.5	11.8 ± 10.0
	B220 ⁺	6.7 ± 5.6	48.8 ± 55.3	11.4 ± 10.2
	Thy1.2 ⁺	4.2 ± 7.5	25.5 ± 20.9	5.4 ± 2.8
cell number [x10 ⁷]	CD3 ⁺ T cells	7.3 ± 15.4	30.4 ± 35.6	6.4 ± 3.7
	CD3 ⁺ CD4 ⁺ T cells	3.5 ± 8.8	14.0 ± 16.7	2.5 ± 1.4
	CD3 ⁺ CD8 ⁺ T cells	1.5 ± 2.6	3.9 ± 5.6	1.8 ± 1.4
ratio CD4/CD8	1.6 ± 0.8	3.9 ± 2.0	1.7 ± 1.0	
cell number [x10 ⁶]	CD3 ⁺ CD4 ⁺ CD69 ⁺ T cells	6.4 ± 11.4	51.3 ± 75.4	7.4 ± 5.2
	CD3 ⁺ CD8 ⁺ CD69 ⁺ T cells	2.1 ± 4.1	13.4 ± 22.0	2.7 ± 1.8
cell number [x10 ⁶]	CD4 ⁺ naive T cells	3.8 ± 6.7	12.1 ± 19.5	2.3 ± 2.4
	CD4 ⁺ effector T cells	31.8 ± 82.7	07.1 ± 139.1	20.2 ± 12.9
	CD4 ⁺ memory T cells	1.0 ± 1.8	3.6 ± 4.8	0.9 ± 1.0
	CD8 ⁺ naive T cells	3.6 ± 6.6	7.4 ± 1.5	4.0 ± 5.1
	CD8 ⁺ effector T cells	10.2 ± 1.8	22.6 ± 37.7	9.1 ± 6.4
	CD8 ⁺ memory T cells	1.7 ± 2.1	5.0 ± 7.0	4.0 ± 11.0

3.4.3 Diminished LC40 mediated outgrowth of the aberrant CD21^{low}CD23^{low}CD43⁺ B cell population by inactivation of B-Raf and Raf-1

As already mentioned, the lymphomagenesis of LC40 mice based on the outgrowth of an aberrant B1-like CD21^{low}CD23^{low}CD43⁺CD5^{low} B cell population. We found significantly increased proportions of B1b (B220^{low}CD5^{low}) cells in LC40 mice compared with controls, whereas RafDKO/LC40 mice displayed similar proportions of B1b cells like controls. B1a (B220^{low}CD5^{high}), B2 (B220^{high}CD5^{low}), and activated B2 (B220^{high}CD5^{high}) cells were similar distributed in old control, LC40 and RafDKO/LC40 mice (Table 2).

Table 2: Splenic B cell composition of old control, LC40 and RafDKO/LC40 mice. The frequencies of splenic B2 (B220^{high}CD5^{low}), activated B2 (B220^{high}CD5^{high}), B1a (B220^{low}CD5^{high}), B1b (B220^{low}CD5^{low}) cells of old (> 10 months) control (ctrl; n = 19), LC40 (n = 18) and RafDKO/LC40 (n = 24) mice was determined by different FACS stainings. Numbers illustrate the mean \pm standard deviation. All data sets were logarithmically transformed due to lognormal distribution and were statistically analyzed by One-way ANOVA with Tukey's multiple comparison. *p < 0.05; ***p < 0.001. This table summarizes my data and reevaluated data of Laura Kuhn.

	ctrl	LC40	RafDKO/LC40
frequencies [%] B2	60.8 \pm 21.8	57.3 \pm 14.8	56.1 \pm 19.0
act. B2	2.2 \pm 2.6	4.3 \pm 5.5	4.0 \pm 7.9
B1a	2.4 \pm 4.3	1.6 \pm 1.2	3.1 \pm 7.0
		**	
B1b	10.4 \pm 12.3	16.1 \pm 6.3	11.5 \pm 6.6

In young mice, no differences in the amount of CD21^{low}CD23^{low} B cells could be detected between the three genotypes. During aging both LC40 and RafDKO/LC40 mice featured an elevated CD21^{low}CD23^{low} population compared to control mice, but the increase was more prominent in B-Raf//Raf-1 proficient mice (Figure 36A). After similar categorization of the CD21^{low}CD23^{low} B cell population in aged mice of all three genotypes as for the splenic weight, the results became even clearer. In control mice 13.6 % developed a moderate (between 40 % and 60 %) and 4.5 % a pathological (> 60 %) expansion of the CD21^{low}CD23^{low} B cell population. In RafDKO/LC40 mice, the proportion of mice with moderate (22.2 %) and pathological (11.1 %) expansion of the CD21^{low}CD23^{low} B cells doubled in comparison to controls, but the majority (66.7 %) still displayed normal (< 40 %) amounts of CD21^{low}CD23^{low} B cells. In contrast, only 30.0 % of LC40 mice had normal percentages of the CD21^{low}CD23^{low} B cell population. In the majority of LC40 mice, the CD21^{low}CD23^{low} B cell population expanded to moderate (25.0 %) or pathological (45.0 %) proportions (Figure 36B).

A similar picture was obtained by analyzing the percentages of the CD43⁺CD23^{low} population in aged mice and categorizing them into mice with normal (< 25%), moderate increased (between 25% and 70%), and pathological increased (> 70%) percentages of the CD43⁺CD23^{low} population (Figure 36C and D).

In summary, both RafDKO/LC40 and LC40 mice developed higher amounts of the CD43^{high}CD23^{low}CD21^{low} aberrant B cell population than controls. But, in RafDKO/LC40 mice the outgrowth of the aberrant B cell population was less severe than in LC40 mice. These data suggested a participation of B-Raf and Raf-1 in the LC40 mediated outgrowth and expansion of the aberrant B cell population.

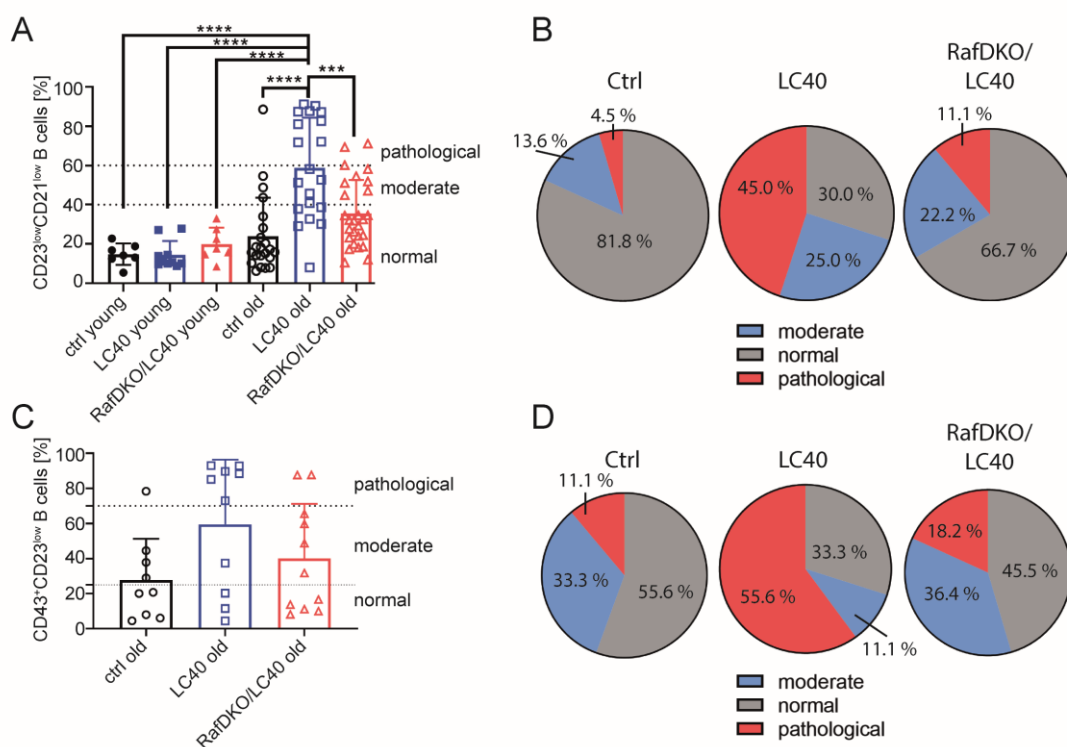


Figure 36: B-Raf/Raf-1 inactivation reduced the LC40 mediated outgrowth of the aberrant B cell population. The aberrant splenic B cell population was determined by flow cytometry. The FACS plots were pre-gated on B220⁺ and then the percentage of either CD21^{low}CD23^{low} or CD43⁺CD23^{low} was determined. (A) The graph compiles the percentages of the CD21^{low}CD23^{low} B cell population of young (< 4 months) control (ctrl; n = 7), LC40 (n = 10) and RafDKO/LC40 (n = 7) and old (> 10 months) control (n = 22), LC40 (n = 20) and RafDKO/LC40 (n = 27) mice. (B) Pie charts of old control, LC40, and RafDKO/LC40 mice illustrating the frequencies of mice with normal (< 40%), moderate (between 40% and 60%) or pathological (> 60%) amounts of CD21^{low}CD23^{low} B cells as depicted in (A). (C) The graph summarizes the percentages of the CD43⁺CD23^{low} B cell population of old (> 10 months) control (n = 9), LC40 (n = 10) and RafDKO/LC40 (n = 11) mice. (D) Pie charts of old control, LC40, and RafDKO/LC40 mice illustrating the frequencies of mice with normal (< 25%), moderate (between 25% and 70%) or pathological (> 70%) amounts of CD43⁺CD23^{low} B cells as depicted in (C). (A+C) Each dot represents an individual mouse. Bars and error bars depict the mean \pm standard deviation. Due to normal distribution the data were directly statistically analyzed by One-way ANOVA with Tukey's multiple comparison. *p < 0.05; ***p < 0.001; ****p < 0.0001. Here summarized data from me and reevaluated data of Laura Kuhn are illustrated.

3.4.4 Alteration of the LC40 mediated B cell activation upon B-Raf//Raf-1 inactivation

LC40 expression induces a B cell activation in young mice, which is heterogenous in B cells of aged LC40 mice (52). To investigate the effect of B-Raf//Raf-1 inactivation on LC40 mediated B cell activation, the expression of the activation markers CD95, ICAM-1, and ICOS-L was determined in B cells of young (< 4 months) and old (> 10 months) control, LC40, and RafDKO/LC40 mice.

CD95 and ICOS-L levels were significantly higher in LC40 whereas they were similar in RafDKO/LC40 mice in comparison to controls. Interestingly, the significantly increased expression of CD95 and ICOS-L decreased in aged LC40 mice and was then comparable among all three genotypes. In contrast, differences of ICAM-1 between the genotypes were hardly visible in young mice, but the expression of ICAM-1 increased significantly in LC40 and RafDKO/LC40 mice during aging resulting in significantly elevated ICAM-1 levels in both old LC40 and RafDKO/LC40 mice compared to old controls (Figure 37). These data revealed that B-Raf and Raf-1 are involved in the LC40 mediated increase in ICOS-L and CD95 in young but not old mice. In contrast, Raf-kinases do not seem to have an effect on increased ICAM-1 levels in old mice.

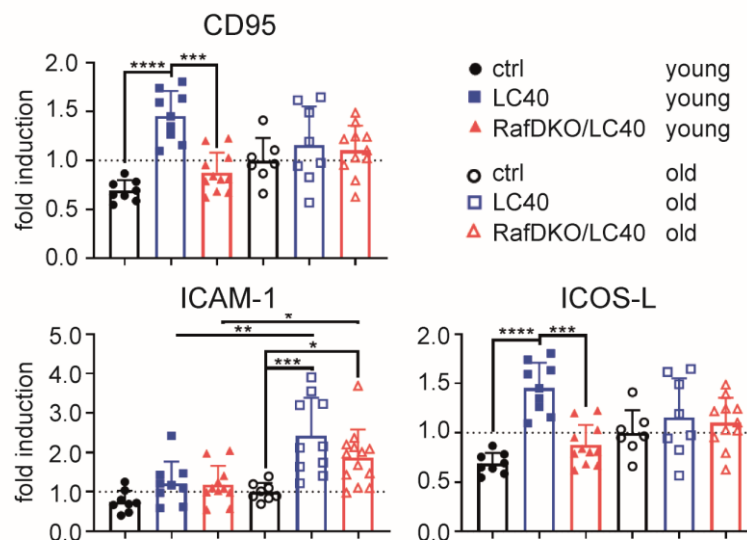


Figure 37: The expression pattern of the different B cell activation markers in control, LC40 and RafDKO/LC40 mice. The surface expression of the activation markers CD95, ICAM-1, and ICOS-L was analyzed on B220⁺ B cells of young (< 4 months) control (ctrl; n = 8), LC40 (n = 9) and RafDKO/LC40 (n = 11) and old (> 10 months) control (n = 7-8), LC40 (n = 8-10) and RafDKO/LC40 (n = 11-13) mice by FACS. The MFI was normalized to the mean of the old control mice leading to the fold induction of each marker. Each dot represents an individual mouse. Bars and error bars depict the mean ± standard deviation. All data sets were lognormal distributed. After logarithmic transformation the data sets were statistically analyzed by One-way ANOVA with Tukey's multiple comparison. *p < 0.05, **p < 0.01; ***p < 0.001; ****p < 0.0001. These illustrations summarized my own FACS stainings with reevaluated ones performed by Laura Kuhn.

3.4.5 Detection of Raf proficient B cells in old RafDKO/LC40 mice

Since in conditional mice the Cre mediated recombination of LoxP sites is never 100%, it could be possible that B cells with undeleted *Raf* genes grew out in the aged RafDKO/LC40 mice. To test this assumption, the B-Raf and Raf-1 levels of B cells from old control, LC40, and RafDKO/LC40 mice were investigated by Western blot. B-Raf was detected by a pB-Raf antibody recognizing the constitutive phosphorylated serine at position 445 (129,141). Additionally, the pERK levels were determined. B cells from young mice were analyzed in parallel, to test whether aging influences the expression levels of these proteins.

As expected, in young control and LC40 B cells, B-Raf and Raf-1 could be detected, whereas Raf-kinases were absent in young RafDKO/LC40 B cells. Despite some variations in the amounts, B-Raf and Raf-1 were detectable in all old control and LC40 mice. However, only 25 % of the old RafDKO/LC40 mice displayed a complete absence of B-Raf and Raf-1. The other RafDKO/LC40 samples of aged mice had intermediate to high B-Raf and Raf-1 levels. These data indicated a selection of B-Raf//Raf-1 proficient B cells in old RafDKO/LC40 mice (Figure 38A) during aging.

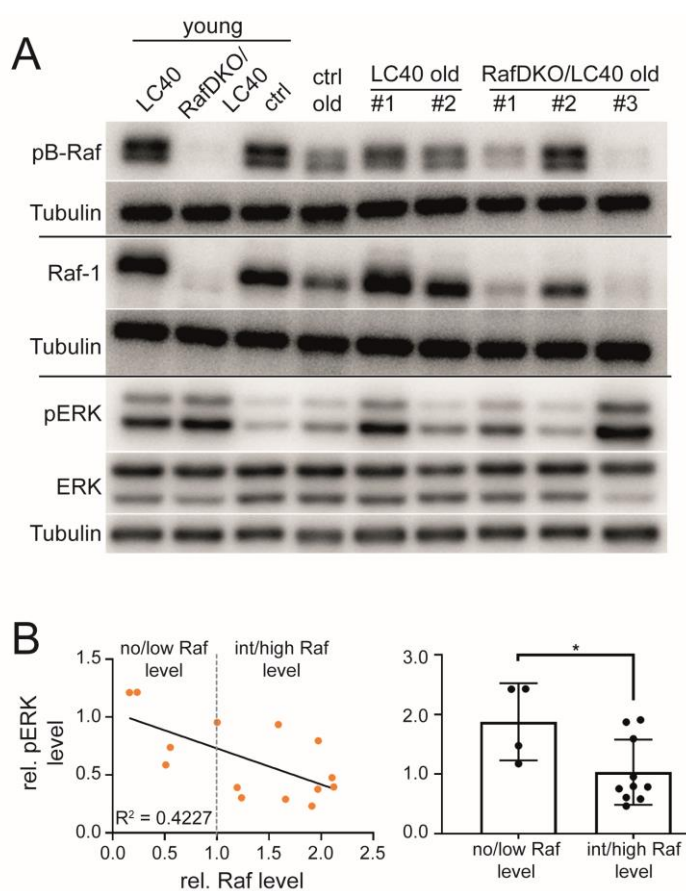


Figure 38: In old RafDKO/LC40 mice Raf proficient B cells are detectable. (A) Representative Western blot for pB-Raf, Raf-1, pERK, and ERK of isolated splenic B cells of old (> 10 months) control (ctrl; n = 5), LC40 (n = 4) and RafDKO/LC40 (n = 8) mice. Tubulin served as loading control. Young (< 4 months) control (n = 5), LC40 (n = 1) and RafDKO/LC40 (n = 1) mice were included as controls. (B) The left graph depicts the relative (rel.) Raf level (sum of pB-Raf and Raf-1 normalized to the loading control Tubulin) against the summarized rel. pERK level (sum of pERK1 and pERK2 each normalized to the loading control Tubulin), the linear regression, the correlation coefficient R^2 and the categorization of no/low Raf level (rel. Raf level < 1) and int/high Raf level (rel. Raf level > 1) regardless of the genotype. The right graph shows the rel. pERK level in B cells with no/low Raf level compared to B cells with int/high Raf level regardless of the genotype.

The dots represent individual mice, the bars and error bars represent the mean \pm standard deviation. The data were lognormal distributed. After logarithmic transformation the data were statistically analyzed using the Unpaired Student's test. * $p < 0.05$.

Next, the ERK phosphorylation of each sample was analyzed. As already described, in young mice LC40 expression increased the ERK phosphorylation in B cells compared to controls (52). This increased pERK levels were also present in RafDKO/LC40 mice compared to controls, which was already analyzed in section 3.3.3. ERK phosphorylation of old mice were very heterogeneous. It was noticed that in samples with high B-Raf and Raf-1 levels, ERK phosphorylation was lower than in samples with low B-Raf and Raf-1 amounts (Figure 38A). To investigate this in more detail, B-Raf and Raf-1 levels were summed for each sample. This normalized Raf levels were compared to the normalized pERK levels of the same sample regardless of genotype and age. The normalized pERK level was determined by summing the normalized pERK1 and pERK2 values. Here, an indirect correlation with $R^2 = 0.4227$ could be detected. Data Points without or with low Raf levels (< 1) exclusively represent RafDKO/LC40 mice, which showed significantly higher ERK phosphorylation than mice displaying intermediate or high Raf levels (Figure 38B).

In summary, these Western blot analyses demonstrated a selection advantage of Raf competent B cells compared with B-Raf//Raf-1 deficient B cells in aged RafDKO/LC40 mice. We did not test whether the stop-cassette upstream the *LMP1/CD40* transgene was deleted in those Raf proficient B cells of old RafDKO/LC40 mice. Nevertheless, these results indicated an important role of B-Raf and Raf-1 in B cell expansion. Thus, B cells featuring no/low Raf protein levels might reflect real RafDKO/LC40 B cells concomitantly expressing LC40 leading to increased pERK levels. The latter were even higher than in Raf proficient LC40 B cells included in the group with int/high Raf levels. These results confirmed our findings of section 3.3.3 also in aged mice.

3.5 Alteration of the LC40 induced gene expression pattern by B-Raf//Raf-1 inactivation

As previously demonstrated (see 3.3.3 and 3.4), it could be shown that B-Raf//Raf-1 inactivation in LC40 expressing B cells further increased the pERK levels and attenuated the LC40 mediated phenotypic changes. To investigate how B-Raf//Raf-1 inactivation influences the transcriptional profile of LC40 B cells, the RNA expression pattern of isolated splenic B cells from young RafDKO/LC40 and LC40 mice was analyzed by performing RNA sequencing analyses. The RNA was sequenced by the Research group of Dr. Helmut Blum of the Laboratory for Functional Genome Analysis (LAFUGA) in Munich. The gene alignments, analyses of the robustness, heatmap and bioinformatic analysis of the biological processes were executed in cooperation with Dr. Sonja Grath, Head of the Research group "Molecular Evolution and Functional Bioinformatics", LMU Munich and Daniel Strobl, Institute of Computational Biology, Helmholtz Center Munich. The

analyses of the Top25 differentially expressed protein-coding genes and the Gene Set Enrichment Analyses (GSEA) were performed in close collaboration with Dr. Lothar Strobl, a member of our own research group.

3.5.1 B-Raf//Raf-1 inactivation reduced the expression of genes with a tumor promoting function in LC40 B cells

Using the heat-map of all significantly differentially expressed genes, the robustness of RNA sequencing could be confirmed. This assumption based on the clustering of the individual genotypes and the similar RNA expression profiles of the different samples of one genotype. In LC40 B cells 807 genes were significantly upregulated and 466 genes significantly downregulated compared to RafDKO/LC40 B cells (Figure 39).

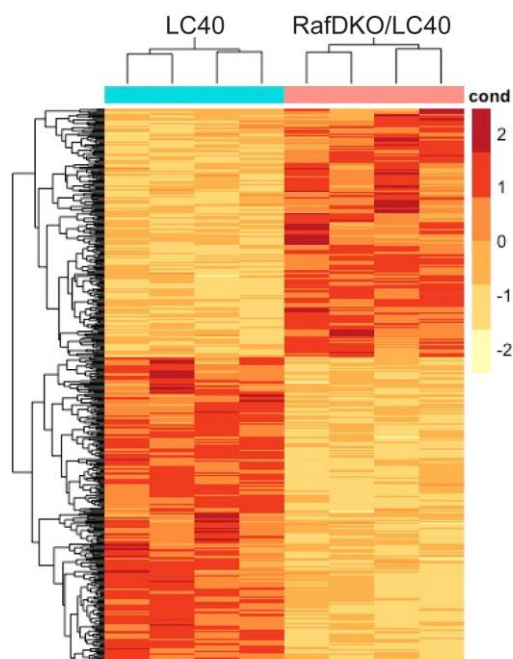


Figure 39: The B-Raf//Raf-1 inactivation changed the gene expression pattern in LC40 expressing B cells. Heatmap of all significant differentially expressed genes between young LC40 (n = 4) and RafDKO/LC40 (n = 4) mice after unsupervised clustering. The significantly differentially expressed genes were represented by the rows, the different samples were organized in the columns. Relative changes of the gene expression were illustrated by the color code. Upregulated genes were depicted in red and downregulated genes in yellow.

The top 25 differentially expressed protein-coding genes (Table 3 and Table 4) were analyzed in more detail. Among these, a clear majority (80%) showed a higher expression in LC40 than in RafDKO/LC40 B cells. Many differentially expressed genes were associated with survival, activation, immunosuppression and MZB cell development, or were described as tumorigenic or oncogenic. These findings may explain the increased cell expansion in LC40 mice (Table 3). The genes with a lower expression in LC40 than in RafDKO/LC40 B cells affected cell proliferation, as well as cell activation and apoptosis (Table 4).

Moreover, the reduced potential of RafDKO/LC40 mice for the expansion of aberrant B cells could be explained by higher *Ahnak* expression compared with LC40, as *Ahnak* could downregulate the oncogene *Myc* (201). Indeed, a significantly higher *Myc* expression in LC40 B cells than in the corresponding RafDKO/LC40 samples was detectable. Additionally, the expression of the *Myc* target gene *Odc1* (202) was sharply reduced in RafDKO/LC40 compared to LC40 B cells (Figure 40). These results supported the notion that RafDKO/LC40 B cells exhibit an alteration in LC40 induced gene expression, which might attenuate cell expansion and transformation during aging.

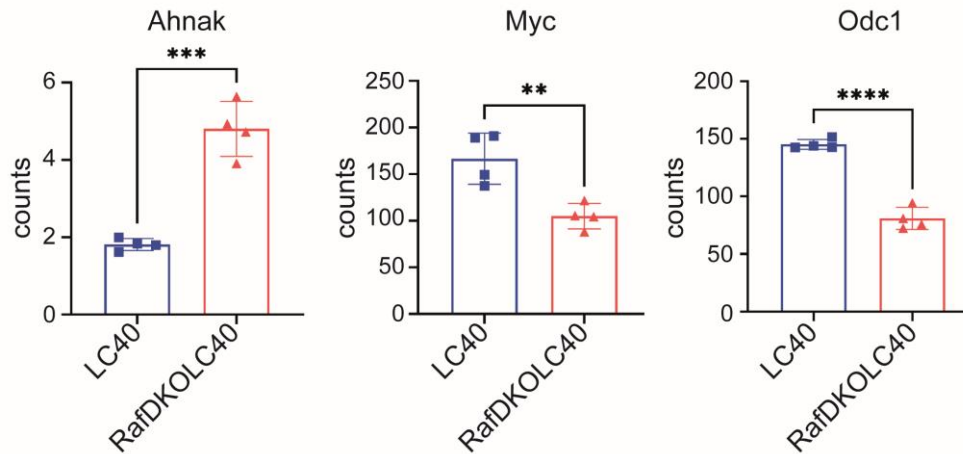


Figure 40: B-Raf//Raf-1 inactivation increased *Ahnak* and decreased *Myc* and *Odc1* RNA expression in LC40 expressing B cells. Normalized counts of *Ahnak*, *Myc* and *Odc1* of the RNA sequencing of LC40 ($n = 4$) and RafDKO/LC40 ($n = 4$) B cells. Dots represent individual mice. Bars and error bars illustrate the mean \pm standard deviation. Data were normal distributed and statistically analyzed using the Unpaired Student's test. ** $p < 0.01$; *** $p < 0.001$; **** $p < 0.0001$.

Table 3: Genes within the Top 25 significant differentially expressed protein coding genes with a higher expression in LC40 than in RafDKO/LC40 B cells. Gene symbols, a brief function with its corresponding references, the log2FoldChange and the adjusted p-values (padj) are listed.

gene symbol	function	log2FoldChange	padj	references
Lilrb4	immunosuppressive	-1,27805795	4,81E-59	(203)
Lilr4b	function in antigen capture and presentation, inhibits MHC class I signaling	-1,173419354	8,38E-53	https://www.genecards.org/cgi-bin/carddisp.pl?gene=LILRB4
Fosl2	oncogenic	-1,207805725	7,70E-50	(204)
Rsu1	regulation of cell adhesion	-1,143803723	2,18E-49	(205)
Cacna1e	calcium signaling	-0,938773216	1,64E-45	(206)
Mios	Upregulated in PCs compared to other B cell subsets	-1,423705688	2,14E-44	https://www.proteinatlas.org/ENSG00000164654-MIOS/immune+cell/B-cells
Myof	tumorigenesis and malignant progression	-0,944659212	3,60E-41	(207)
Cnr1	survival	-2,517946099	5,48E-40	(208)
Ccr1	Upregulated upon EBV infection and in lymphoblastoid cell lines	-1,571921635	2,09E-38	(209)
Sema7a	Activation/differentiation of lymphocytes	-0,939827064	3,51E-30	(210)
	Notch-target			(54)
Odc1	myc target	-0,85142519	1,69E-28	(202)
Asb2	Elevated in MZBs by Notch1 signaling	-1,554016811	2,55E-28	(211,212)
Cebpz	regulates heat shock protein 70 (HSP70) promoter; participates in cell growth and differentiation; contributes to leukemia	-0,816770644	4,28E-26	(213)
I830077J02Rik	electron carrier activity	-0,894703789	2,12E-25	https://www.ncbi.nlm.nih.gov/IEB/Research/Acembly/av.cgi?db=mouse&q=I830077J02Rik
Bhlhe40	negative regulator of B cell activation; upregulated in human anergic CD21 ^{low} B cells	-0,876967654	2,13E-25	(214)
Cr2	B lymphocytes activation; CD21; Notch target	-0,700305164	4,81E-25	(215,216)
Il21r	T cell mediated B cell proliferation, PC differentiation	-0,766560673	6,09E-25	(64,217)
Kit	lymphocyte development	-1,106802074	1,01E-24	(218)
Utrn	Cell motility/adhesion	-0,696973379	1,15E-24	(219)
Nr4a3	induced by BCR signaling; dampening B cell proliferation	-0,792244651	1,08E-23	(220)

Table 4: Genes within the Top 25 significant differentially expressed protein coding genes with a lower expression in LC40 than in RafDKO/LC40 B cells. Gene symbols, a brief function with its corresponding reference, the log2FoldChange and the adjusted p-values (padj) are listed.

gene symbol	function	log2FoldChange	padj	references
Cacna1i	Voltage-sensitive calcium channels; not described in immune cells so far	1,940105148	9,12E-41	https://www.proteinatlas.org/ENSG00000100346-CACNA1I
Ahnak	growth retardation and cell cycle arrest through downregulation of c-Myc and cyclin D1/D2 (mamma-carcinoma)	1,310778809	1,14E-40	(201)
Sh2b2	modulation of BCR signaling; APS-KO mice > increased B1 cells	2,502443232	4,71E-40	(221,222)
Cmah	Cmah knockout mice > hyperactive B cells	0,8773423	5,11E-32	(223)
A430078G23Rik	regulating cell death and apoptosis	1,03852376	1,08E-23	(224)

3.5.2 Alterations of biological processes upon B-Raf//Raf-1 inactivation

The gene expression pattern of RafDKO/LC40 and LC40 B cells was checked for significantly enriched biological processes. Making use of the online platform PANTHER (Protein Analysis Through Evolutionary Relationships, <http://pantherdb.org>) (225), biological processes with respect to the direction of the gene regulation (up- or downregulated) were examined. Within the biological process "positive regulation of cell adhesion" 14 of the 410 genes were significantly lower expressed in LC40 compared to RafDKO/LC40 B cells (Suppl. Table 1). Also, the process "immune response" was significantly enriched with genes presenting a lower expression in LC40 in comparison to RafDKO/LC40 B cells (

Suppl. Table 2). In contrast, the biological process "semaphorin interactions" showed an enrichment of genes with a higher expression in the LC40 compared to the RafDKO/LC40 genotype (Suppl. Table 3). Thus, B-Raf//Raf-1 inactivation seemed to modify the kind of cell-cell and cell-matrix interactions of LC40 expressing B cell, which also play a role in the immune response.

3.5.3 Increased MZ B cell differentiation in LC40 mice is reverted in the absence of B-Raf and Raf-1

LC40 mice displayed increased amounts of MZ B cells compared to controls and RafDKO/LC40 mice (see section 3.4.1). To determine whether the expanded B cells in LC40 mice are indeed MZ B cells or whether only the expression of some surface molecules is altered, the differentially expressed genes of LC40 and RafDKO/LC40 mice were compared with the gene sets of MZ B and Fo B cells using GSEA. The ImmGen Population Comparison Tool based on microarray data (<http://rstats.immgen.org/PopulationComparison/index.html>) (226) was used to assemble genes into gene sets that are differentially expressed between MZ B and Fo B cells (Suppl. Table 4 and 5). Subsequent GSEA highlighted a strong significant enrichment of genes upregulated in MZ B cells in LC40 in comparison to RafDKO/LC40 samples. In contrast, Fo B cell associated genes were found to be significantly enriched in RafDKO/LC40 B cells (Figure 41). These results suggested that LC40 expression induces enhanced differentiation towards MZ B cells. This phenotype is attenuated in the absence of B-Raf and Raf-1.

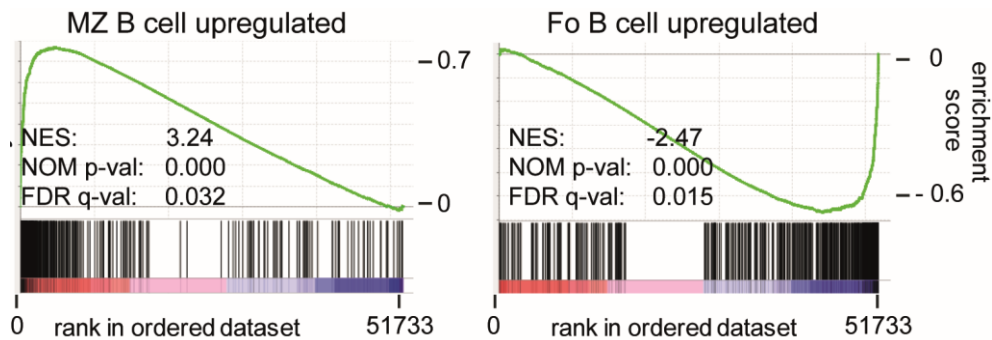


Figure 41: LC40 B cells exhibit predominantly a MZ B cell gene signature, which is abrogated in RafDKO/LC40 B cells. GSEA Enrichment plots performed on the ranked differentially expressed gene list of LC40 compared to RafDKO/LC40 B cells with gene sets for genes upregulated in MZ B and Fo B cells. The normalized enrichment score (NES), the nominal p-value (NOM p-val) and the False discovery rate (FDR q-val) are recorded in the corresponding graphs. The gene sets (Suppl. Table 4 and 5) were generated using the micro-array data of the ImmGen database (226).

3.5.4 Reduced Notch2 and non-canonical NF κ B mediated gene expression in RafDKO/LC40 mice

As described in Section 1.2.1, MZ B cell differentiation is controlled by the interplay of multiple signaling pathways. Thus, BCR, BAFFR, and Notch2 signaling have been described to participate in this cell fate decision (11). Our group showed recently that Notch2 signaling is sufficient to induce the transdifferentiation of Fo B cells into functional MZ B cells (54) highlighting the importance of the Notch2 pathway in differentiation to MZB cells. As depicted in section 3.4.1, LC40 B cells displayed a higher CD21 expression compared to RafDKO/LC40 B cells, which has been described as a typical Notch target gene (*Cr2*) (32,227). Additionally, among the top 25 differentially expressed protein-coding genes the Notch target genes *Cr2*, *Asb*, and *Sema7a* displayed a significantly higher expression in LC40 compared to RafDKO/LC40 B cells (Table 3). Thus, the question arose if B-Raf//Raf-1 inactivation reduces Notch2 signaling in LC40 expressing B cells.

To address this question, we used RNA sequencing data from Lechner et al., who induced constitutive active Notch2 signaling by tamoxifen administration in Fo B cells. At day 3 after tamoxifen treatment, a Notch2 dependent change in the gene expression profile could already be detected without causing a change in the Fo B cell phenotype or localization. At day 14 after Notch2 induction Fo B cells transdifferentiated to real MZ B cells (54). These RNA Seq data were used to generate different gene sets for GSEA. First, the gene expression profile of Notch2IC expressing (Notch2IC⁺) Fo B cells was compared to normal Fo B cells at day three after tamoxifen treatment to extract a gene set for the immediate early (Notch2 up- (Suppl. Table 6) and downregulated (Suppl. Table 7) genes. Next, the differentially expressed genes of Notch2IC⁺ B cells after 14 days

and 3 days after tamoxifen induction were compared to obtain late Notch2 up- (Suppl. Table 8) and downregulated (Suppl. Table 9) genes.

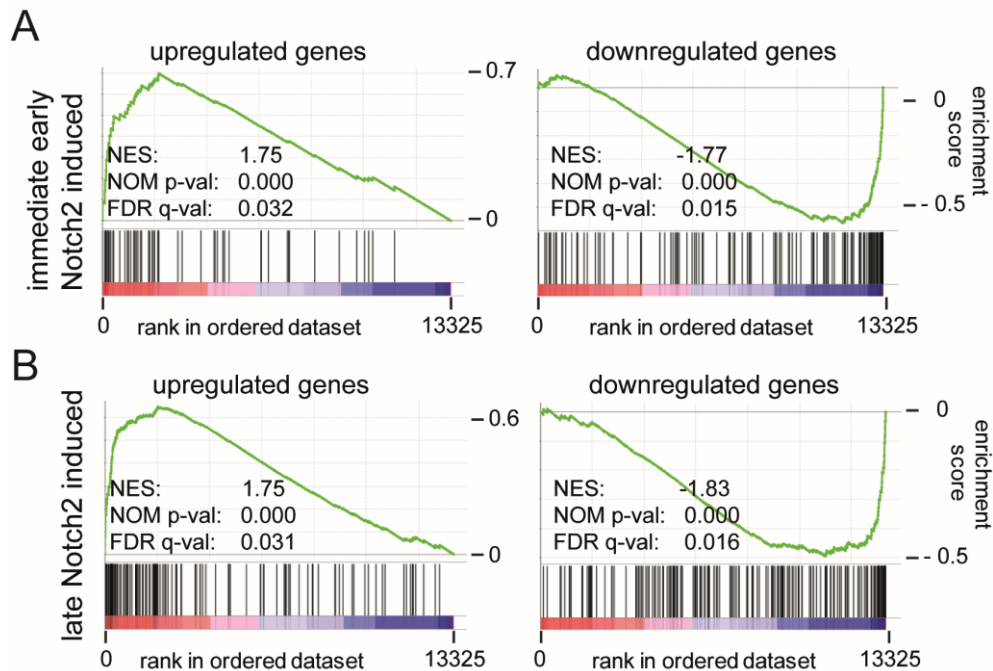


Figure 42: The Notch2 induced gene signature of LC40 expressing B cells was diminished in RafDKO/LC40 B cells. GSEA enrichment plots performed on the ranked differentially expressed gene list of LC40 compared to RafDKO/LC40 B cells with gene sets for up- (left column) and downregulated (right column) immediate early (A) and late (B) Notch2 responding genes (Suppl. Table 6 to 9). The normalized enrichment score (NES), the nominal p-value (NOM p-val) and the False discovery rate (FDR q-val) are recorded in the corresponding graphs. The gene sets were generated using the RNA-Seq data of Lechner et al., 2021 (54).

GSEA of immediate early and late Notch2 induced genes discovered an enrichment of genes upregulated by Notch2 activation in LC40 and in parallel an enrichment of Notch2 downregulated genes in RafDKO/LC40. (Figure 42). These results indicated a LC40 mediated activation of Notch2 signaling in B cells, which is attenuated by the B-Raf//Raf-1 inactivation in RafDKO/LC40 B cells.

In addition to Notch2, BAFFR signaling plays an essential role in the development of MZ B cells (11). Stimulation of the BAFF receptor leads mainly to the activation of the non-canonical NF κ B signaling pathway (11,47). In LC40 expressing B cells, hyperactive non-canonical NF κ B signaling in addition to increased ERK and JNK phosphorylation was detected (52). A direct target of the non-canonical NF κ B signaling pathway is ICOS-L (228). As mentioned above, young LC40 mice displayed upregulated ICOS-L compared to controls, which was significantly decreased by B-Raf//Raf-1 inactivation in young RafDKO/LC40 B cells (see section 3.4.4). These observations led to the question, if the B-Raf//Raf-1 deficiency could reduce the activity of the non-canonical NF κ B signaling pathway in LC40 expressing B cells. To analyze this, GSEA were performed using gene

sets designed from gene expression data of different mouse models displaying hyperactivated non-canonical NF κ B signaling.

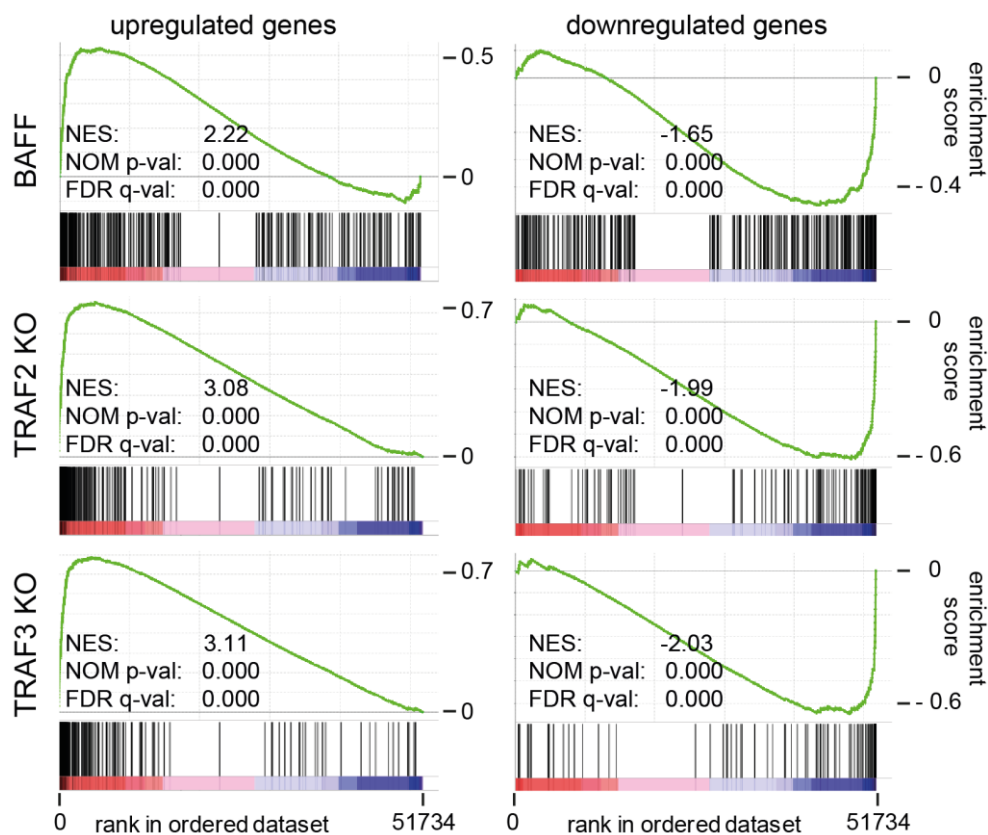


Figure 43: The non-canonical NF κ B induced gene signature of LC40 expressing B cells was diminished in RafDKO/LC40 B cells. GSEA Enrichment plots performed on the ranked differentially expressed gene list of LC40 compared to RafDKO/LC40 B cells with gene sets for up- (left column) and downregulated (right column) genes of BAFF-tg (BAFF), TRAF2KO and TRAF3KO B cells displaying a hyperactive non-canonical NF κ B signal were generated using the micro-array data of Gardam et al., 2008 (48) (Suppl. Table 10 to 15). The normalized enrichment score (NES), the nominal p-value (NOM p-val) and the False discovery rate (FDR q-val) are recorded in the corresponding graphs.

Gardam et al. published micro-array data of B cells from transgenic BAFF overexpressing mice compared to controls (48). These data were used to generate BAFF upregulated (BAFF-UP; Suppl. Table 10) and BAFF downregulated (BAFF-DOWN; Suppl. Table 11) gene sets. Within the same publication, data sets of TRAF2KO or TRAF3KO compared to control B cells were published (48). These knockouts result in a hyperactivation of the non-canonical NF κ B signaling pathway (46,48). Thus, gene sets for up- and downregulated genes of TRAF2KO and TRAF3KO mice were extracted (Suppl. Table 12 to 15).

All GSEA with gene sets reflecting genes upregulated by non-canonical NF κ B signaling were enriched in samples of the LC40 in comparison to the RafDKO/LC40 genotype. In contrast, genes downregulated by non-canonical NF κ B were enriched in the

RafDKO/LC40 genotype (Figure 43). These results implied the participation of B-Raf and Raf-1 in the LC40 induced non-canonical NF κ B signaling.

3.5.5 Requirement of B-Raf and Raf-1 for LC40 induced activation of the Notch2 and non-canonical NF κ B signaling pathways

To test, if B-Raf//Raf-1 inactivation leads to a reduction of LC40 mediated Notch2 and non-canonical NF κ B signaling, RNA-Seq data of young LC40 and RafDKO/LC40 B cells were used. First, RNA levels of *Notch2* and its downstream targets *HES1* and *CD21* were examined. No significant differences in the normalized counts of *Notch2* between LC40 and RafDKO/LC40 B cells could be detected. Thus, *Notch2* did not appear to be downregulated at the level of RNA transcription upon B-Raf//Raf-1 inactivation. However, the Notch2 target genes *HES1* and *CD21* displayed higher RNA levels in LC40 than in RafDKO/LC40 B cells (Figure 44A). The lower *CD21* RNA levels in RafDKO/LC40 B cells confirmed the previous results of reduced CD21 surface expression in RafDKO/LC40 B cells measured by flow cytometry (see section 3.4.1). In summary, decreased expression of Notch2 target genes in RafDKO/LC40 compared with LC40 B cells referred to reduced LC40 mediated Notch2 signaling upon B-Raf//Raf-1 inactivation, but this seemed not to be caused by decreased *Notch2* RNA expression.

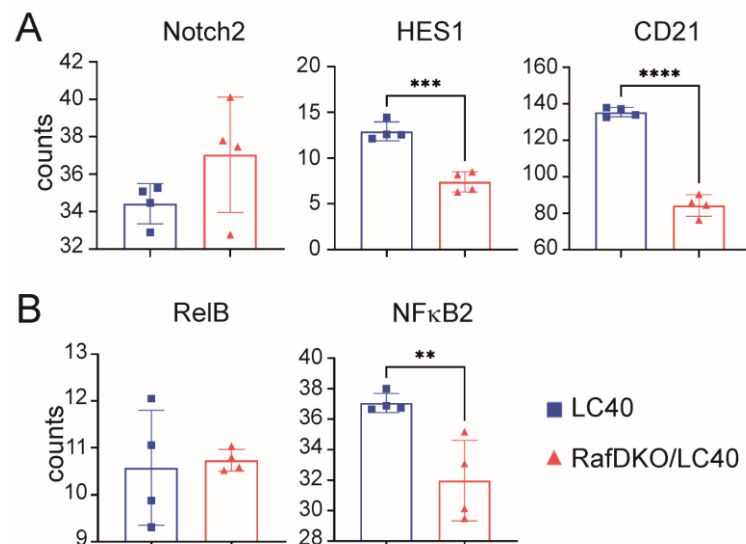


Figure 44: B-Raf//Raf-1 inactivation decreased HES1, CD21 and NF κ B2 RNA expression in LC40 expressing B cells. The normalized counts of the components of the Notch2 signaling pathway Notch2, HES1, and CD21 (A) and of the non-canonical NF κ B signaling pathway RelB and NF κ B2 (B) of the RNA sequencing of LC40 (n = 4) and RafDKO/LC40 (n = 4) B cells. Dots represent individual mice. Bars and error bars illustrate the mean \pm standard deviation. Data were normal distributed and statistically analyzed using the Unpaired Student's test. **p < 0.01; ***p < 0.001; ****p < 0.0001.

To analyze the activity of non-canonical NF κ B signaling, the RNA levels of the two components of the non-canonical NF κ B signaling pathway, *RelB* and *NF κ B2* (p100/p52), were analyzed. A significant reduction in *NF κ B2* RNA was observed in RafDKO/LC40 compared with LC40 B cells, but no differences were observed in the RNA levels of *RelB* (Figure 44B). These results indicated a contribution of B-Raf and Raf-1 in LC40 mediated *NF κ B2* expression, which might lead to the reduced non-canonical NF κ B activation in RafDKO/LC40 compared to LC40 B cells detected by the GSEA.

The normalized counts underlined the results of the GSEA that B-Raf and Raf-1 might contribute to Notch2 and non-canonical NF κ B signaling. To confirm these findings on protein level, Western blots for Notch2, HES1, RelB and p100/p52 (protein of the *NF κ B2* gene) were performed with *ex vivo* isolated B cells from young control, LC40, and RafDKO/LC40 mice.

A significant LC40 mediated upregulation of Notch2 protein expression could be observed in LC40 and RafDKO/LC40 B cells compared to controls. However, LC40 and RafDKO/LC40 B cells featured similar Notch2 protein levels. Similarly, an increased HES1 signal was detected in LC40 B cells in comparison to controls. But here RafDKO/LC40 B cells tended to have reduced amounts of HES1 compared to LC40 B cells (Figure 45A). This confirmed the lower gene expression of *HES1* in RafDKO/LC40 than in LC40 B cells analyzed by RNA sequencing. These results indicated reduced Notch2 signaling in RafDKO/LC40 compared to LC40 B cells, which is not caused by reduced Notch2 transcription or protein expression.

RelB did not display any differences regarding the RNA levels between LC40 and RafDKO/LC40 B cells. However, there was a tendency for decreased RelB protein levels in RafDKO/LC40 B cells in comparison to control and LC40 B cells. Interestingly, a significantly increased RelB cleavage was observed in LC40 B cells compared to control and RafDKO/LC40 B cells. In addition, we could detect diminished p52 levels in RafDKO/LC40 B cells in comparison to LC40 B cells (Figure 45B).

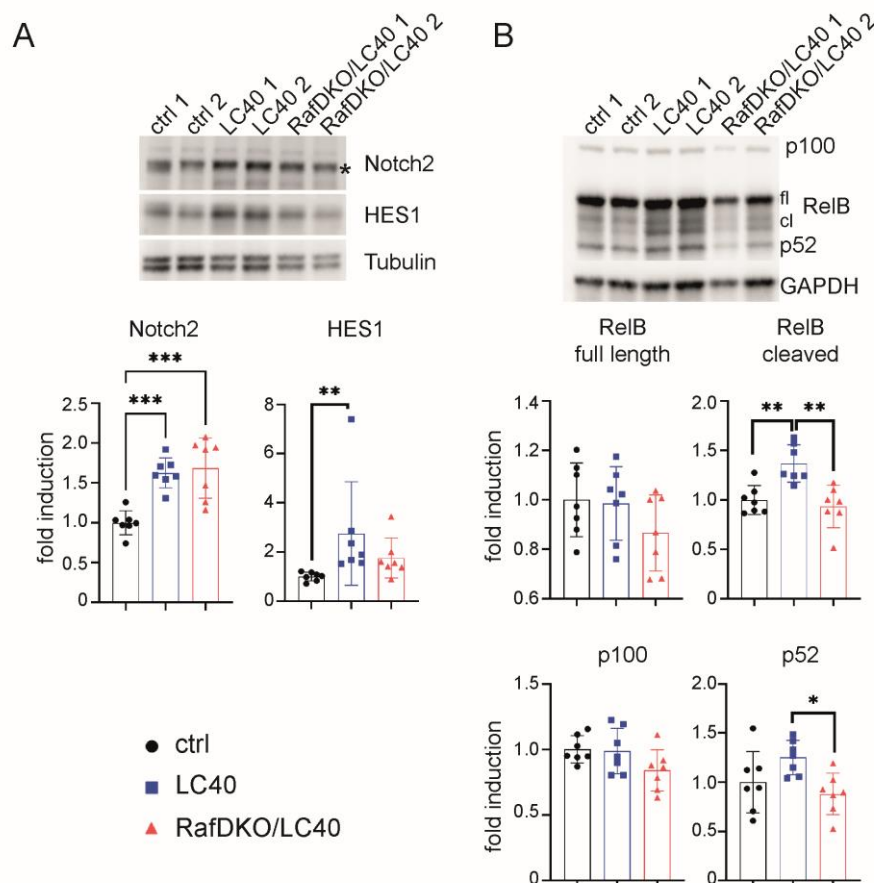


Figure 45: RafDKO/LC40 B cells displayed significantly reduced HES1 and p52 protein expression. Representative Western blots and the quantified fold induction of Notch2 and HES1 (A) and RelB and p100/p52 (B) of isolated splenic B cells of control (ctrl; n = 7), LC40 (n = 7) and RafDKO/LC40 (n = 7) mice in comparison to control B cells. The calculation of the fold induction is described in section 6.7.5. The dots represent individual mice, the bars and error bars represent the mean \pm standard deviation. The data for Notch2, RelB and p52 were normal, the data for HES1 and p100 were lognormal distributed. After logarithmic transformation of the lognormal distributed data sets, all data sets were statistically analyzed using the One-way ANOVA with Tukey's multiple comparisons test. *p < 0.05; **p < 0.01; ***p < 0.001.

Taken together, not only the results of the GSEA, but also the reduced amounts of HES1 RNA and protein levels, as well as the diminished CD21 expression in RafDKO/LC40 compared to LC40 B cells revealed a reduction of Notch2 signaling by B-Raf//Raf-1 inactivation in LC40 expressing B cells. Similarly, the non-canonical NF κ B signaling pathway was less active in RafDKO/LC40 B cells than in LC40 B cells. Evidence for this was the enrichment of non-canonical NF κ B upregulated genes in LC40 B cells and downregulated genes in RafDKO/LC40 B cells detected by GSEA. Furthermore, the reduced NF κ B2 RNA level and the decreased p52 protein level supported the assumption of less non-canonical NF κ B signaling in RafDKO/LC40 than in LC40 B cells. In summary, B-Raf and Raf-1 seemed to promote the LC40 mediated activation of the non-canonical NF κ B and Notch2 signaling pathways.

4. Discussion

B cells need to translate various extracellular signals into the corresponding cellular functions. The latter can range from proliferation and differentiation to cell cycle arrest and apoptosis. Many different signaling pathways play important roles in the corresponding signal transduction. It is known that BCR as well as CD40 and TLR4 activate the Ras-Raf-MEK-ERK signaling pathway (52,85,100,114,118,181). This signaling pathway is described as a linear signaling cascade (120,129,136). An essential involvement of the Ras-Raf-MEK-ERK signaling pathway in B cell development, as well as in lymphoma development, has been demonstrated through the Ras and ERK components. The various Raf-kinases have often not been studied in this regard (181–183). Thus, their roles in terms of mammalian B cell development, activation, differentiation, and lymphoma generation remained to be explored. To analyze this, a mouse model was developed with a conditional knockout of B-Raf and Raf-1 specifically in B cells from the pro-B cell stage onwards. Regarding B cell development, a redundant function of B-Raf and Raf-1 was demonstrated at the transition from pro- to large pre-B cells and the development of transitional B cells into mature B cells. In addition, these mice exhibited an impaired TD immune response (184). The role of B-Raf and Raf-1 in B cell activation, differentiation and lymphoma generation were investigated within this thesis by examining (I) the mechanisms of BCR induced ERK phosphorylation, (II) the participation of B-Raf and Raf-1 to PC differentiation, and (III) the influence of B-Raf//Raf-1 inactivation on short-term or constitutive CD40 signaling.

4.1 Negative regulation of BCR mediated pERK levels by Raf-kinases in mature B cells

During analyses of basal ERK phosphorylation in control and DKO B cells, the following observations were made: Although, B cell development was impaired in B-Raf//Raf-1 deficient B cells and was described to be highly dependent on ERK1/2 in mice (184,185), ERK phosphorylation was similar between developing B cells of DKO and control mice. This could be due to the presence of a certain pERK threshold for cell survival or differentiation, or low amounts of developing B cells exhibiting a change in ERK phosphorylation to pass certain checkpoints. Additionally, MZ B cells exhibited higher basal pERK than Fo B cells, which could be due to higher BCR expression and tonic BCR signaling in MZ B compared to Fo B cells (11,229).

In contrast to the previous results of Brummer et al. in 2002, which were obtained in chicken DT40 cells (178), no Raf dependence of BCR mediated ERK activation could be

detected in mature murine B cells. Unexpectedly, B-Raf//Raf-1 inactivation led to increased pMEK and pERK levels with and without anti-IgM treatment, indicating a negative regulatory function of B-Raf and Raf-1 in mature murine B cells. B-Raf//Raf-1 inactivation further led to increased pERK levels in recirculating B cells of the bone marrow, underlining the negative regulatory function of Raf-kinases in mature B cells. This negative regulatory function seemed to be restricted to MEK/ERK phosphorylation, since no alterations in the BCR mediated activation of SYK and the downstream signaling pathways NF κ B, PI3K/AKT, and PLC γ 2/JNK/p38 could be observed in mature DKO B cells. Up to now, MEK1/2 is the only accepted Raf target protein (120,127). Furthermore, the only known MEK substrate is ERK (230). The negative regulatory function of Raf towards pMEK and pERK could be caused by Raf mediated activation of repressors of pMEK and pERK. Well known repressors of ERK phosphorylation are the dual-specificity MAP kinase phosphatases (DUSP) (231–233). Kidger et al. published in 2017 a regulating function of the Raf-kinases on DUSP5 (232). Thus, in mature B cells Raf-kinases might regulate DUSPs to fine-tune the ERK phosphorylation upon tonic or initial BCR signaling. The mechanisms of how ERK could be phosphorylated in DKO B cells were investigated by several inhibition experiments. Incubation with different pan-Raf inhibitors (Sorafenib, Dabrafenib and LY3009120) resulted in a dose-dependent increase of pERK amounts in unstimulated and BCR stimulated control and DKO B cells. The dose-dependency of pERK already at low inhibitor concentrations, the use of high saturating inhibitor concentrations, and the pERK inducing effect of the paradox-breaking pan-Raf inhibitor LY3009120 argued against paradoxical ERK activation in our experiments (172,174–177). In addition, a compensatory ERK phosphorylation by A-Raf could be excluded. These data confirmed an inhibitory function of Raf-kinases with respect to the basal and initial BCR mediated ERK phosphorylation. Furthermore, these results showed that ERK is activated independently of Raf-kinases in resting and activated mature B cells. Additional inhibitor experiments against various signaling pathways revealed the involvement of SYK, PI3K and Rac/PAK in basal and initial BCR mediated ERK phosphorylation. PI3K dependent pERK upregulation was previously described (107,234). Furthermore, the phosphorylation of ERK by the serine-threonine kinase PAK was published as either PI3K dependent or independent in various cell types (154,235–237). Additionally, PLC γ 2 signaling was postulated to increase pERK (197,238). Thus, we hypothesized that BCR mediated SYK activation transmitted ERK phosphorylation via an interplay of PI3K, Rac/PAK and PLC γ 2 signaling. Thereby, Raf-kinases seemed to negatively regulate these processes. The PLC γ 2 participation has to be further elucidated in future experiments.

Since ERK phosphorylation was unaltered in developing and increased in mature DKO B cells, BCR mediated signaling could be elicited differently in developing and mature B cells. It has been hypothesized that the BCR localization within or outside of lipid rafts may influence the type and outcome of BCR mediated signaling. The pre-BCR is permanently localized in lipid rafts (29,239), while the BCR of transitional B cells is constantly excluded from lipid rafts even upon antigen binding (240,241). In mature B cells antigen crosslinking of the BCR mediates its recruitment to lipid rafts leading to proliferation, activation, and differentiation (29,242,243). Thus, B-Raf and Raf-1 might negatively regulate the pERK level upon BCR signaling outside of the lipid rafts in transitional, resting mature B cells, or initially activated mature B cells. But a B-Raf//Raf-1 dependence of the ERK phosphorylation could still be present in signaling processes induced by BCRs localized within lipid rafts, such as pre-BCR signaling of developing B cells or antigen-induced BCR signaling in pre-PBs and PBs. To analyze the BCR localization within the plasma membrane and the corresponding pERK signaling in the presence or absence of B-Raf and Raf-1, AMNIS imaging flow cytometry for the ganglioside GM1 of lipid rafts, the BCR component CD79b and pERK in control and DKO B cell subsets could be performed (17,244–247).

4.2 Impaired PC differentiation upon B-Raf//Raf-1 inactivation

DKO mice showed a significant impairment of the TI type II immune response induced by NP-FicolI immunization. Similar results were observed upon TD and TI type I immunizations (184). Thus, in DKO mice, a defect in the generation of ASCs and the resulting antibody production is generally evident. *In vitro* differentiation by LPS revealed defects in the differentiation of activated B cells to pre-PBs and further to PBs. Proliferation of activated B cells is a prerequisite of PC differentiation because it enables epigenetic changes. These allow the accessibility of BLIMP1 and other transcription factors to the DNA, which lead to the alteration of the gene expression necessary for PC differentiation (198,248). CFSE experiments revealed that in DKO B cells, not only proliferation but also PC differentiation were impaired (184).

Comparable to short-term BCR stimulation, a PI3K dependence of ERK phosphorylation could be detected in the initial B cell activation by LPS, whereas an involvement of SYK, Rac/PAK and PLC γ 2 remains to be investigated. The negative regulation of the Raf-kinases towards pERK detected upon BCR stimulation was also present upon LPS short-term stimulation. Besides the increased pERK level in DKO B cells, a prolonged ERK phosphorylation in the nucleus of DKO B cells was observed. Nuclear localization of DUSP5 was described to lead to nuclear dephosphorylation of pERK (232). Thus, decreased nuclear DUSP5 activity in DKO B cells might cause an increased and prolonged

amount of nuclear pERK. The latter might contribute to the impairment of PC differentiation of DKO B cells, since not only the absolute pERK levels but also the spatiotemporal dynamics of pERK seemed to translate specific effector functions, such as proliferation or differentiation (152,232,249,250). In PC12 cells a transient and sharp increase of pERK mediates proliferation, while sustained pERK signaling leads to neuronal differentiation (251–253). Furthermore, anergic B cells exhibit increased pERK levels but fail to further increase pERK and to differentiate into PC. That indicated a requirement of low pERK levels in quiescent B cells with a potential to spatiotemporally increase upon stimulation (19,192,254,255).

Additionally, our results provided evidence that a moderate ERK phosphorylation in activated B cells might evoke proliferation, while sharply increased pERK level in pre-PBs and PBs could cause differentiation. The latter is underlined by the link of increasing pERK to the upregulation of BLIMP1 required for PC differentiation (198). The sharp increase of pERK in pre-PBs and PBs was attenuated in DKO B cells. The negative regulatory function of Raf might keep pERK at low levels in resting and activated B cells, but Raf-kinases might mediate ERK phosphorylation in pre-PBs and PBs. This possible switch in the function of Raf-kinases could be caused by alterations in the phosphorylation, the dimerization, and the subcellular localization of Raf as well as differences in the interaction with distinct scaffolding proteins (127,136,142,250). Which of these mechanisms regulate the Raf functions needs to be further explored in the future. Analyses of the phosphorylation patterns of Raf by mass spectrometry, or determination of their subcellular localization by AMNIS imaging flow cytometry or immunohistochemistry may help to answer this question. In addition, dimerization of Raf molecules could be investigated by non-denaturing gel electrophoresis, while immunoprecipitation could reveal interaction partners of Raf.

4.3 Negative regulation of CD40 mediated pERK by Raf-kinases

In addition to BCR and TLR signaling, costimulatory signals through TNFR also participate in B cell activation and differentiation (46,101). Therefore, the role of Raf-kinases was also investigated upon CD40 stimulation. Although control and DKO B cells exhibited comparable pERK kinetics, the negative regulatory function of Raf-kinases detected upon short-term BCR and TLR4 stimulation, was also evident upon CD40 stimulation. The use of the LY3009120 pan-Raf inhibitor confirmed a redundant negative regulatory function of all 3 Raf-kinases upon CD40 stimulation.

Furthermore, our experiments revealed a PI3K dependent ERK phosphorylation upon 2 h of CD40 stimulation in control and DKO B cells. These data confirmed the published

results that constitutive CD40 signaling in LC40 B cells causes a CD19/PI3K dependent increase of pERK mediating B cell survival and proliferation (107). Introducing a B cell specific deletion of B-Raf and Raf-1 in this LC40 mouse model revealed a negative regulatory function of B-Raf and Raf-1 even upon constitutive CD40 signaling, since pERK levels were even higher in RafDKO/LC40 B cells compared to LC40 B cells. This was true for the cytoplasmic and the nuclear fraction, which suggested an unaltered translocation of pERK upon Raf inactivation. Thus, we could not confirm the postulated function of nuclear B-Raf as a stabilizer for nuclear pERK by preventing DUSP5 mediated dephosphorylation of pERK (200).

In contrast to the PI3K dependent upregulation of pERK after 2 h or constitutive CD40 signaling, our data suggested a different mechanism of ERK phosphorylation after 10 min of CD40 stimulation. Hereby, ERK activation was still negatively regulated by Raf-kinases but was induced without the participation of PI3K signaling. One possible mechanism of initial CD40 mediated ERK phosphorylation would be PI3K independent phosphorylation of ERK by Rac/PAK signaling (237), as described upon short-term BCR stimulation (see section 4.1). Furthermore, TPL2 signaling could lead to ERK phosphorylation upon 10 min of CD40 stimulation (256). Which signaling pathways are responsible for the early CD40 induced pERK peak remains to be investigated.

The different mechanisms leading to ERK phosphorylation upon CD40 stimulation might be influenced by the localization of CD40 receptors within the plasma membrane and the association with different TRAF molecules. The initial pERK peak after 10 min of CD40 stimulation might be mediated by TRAF6/TPL2 signalosomes outside of lipid rafts (247,256). In contrast, long-term CD40 stimulation might require the recruitment of the CD40 receptor to lipid rafts by the association with TRAF2 and TRAF3 (101,110,247) leading to Lyn/PI3K dependent ERK phosphorylation (107,247,257–259). These hypotheses need to be confirmed either by Western blot analyses of plasma membrane fractions or by AMNIS imaging flow cytometry.

4.4 Diminished LC40 phenotype upon B-Raf//Raf-1 inactivation

4.4.1 Reduced cell expansion in young RafDKO/LC40 mice

Additional to its role in ERK phosphorylation, effects of B-Raf//Raf-1 inactivation on cell activation, expansion, and transformation by constitutive CD40 signaling in B cells were investigated comparing RafDKO/LC40 mice to control and LC40 mice. B cell specific LC40 expression leads to a splenomegaly already in young mice due to a B and T cell expansion. LC40 mediated B cell expansion affected MZ B cells more than Fo B cells,

shifting the ratio of these two cell populations toward MZ B cells (52). The B-Raf//Raf-1 inactivation in LC40 expressing B cells diminished not only the MZ B and Fo B but also the T cell expansion. This resulted in a significantly reduced splenomegaly in RafDKO/LC40 mice compared to LC40 mice.

In LC40 B cells, increased survival and proliferation compared to wildtype B cells is dependent on the hyperactivation of the CD19/PI3K/ERK signaling pathway (107). As already mentioned, RafDKO/LC40 B cells displayed increased pERK levels in both the cytoplasm and nucleus compared with LC40 B cells. Retention of pERK in the cytoplasm by binding to cytoplasmic anchor proteins has been described to mediate apoptosis (260–262). Thus, the increased pERK levels in the cytoplasm of RafDKO/LC40 in comparison to LC40 might mediate increased apoptosis instead of proliferation. This could contribute to the reduced B cell expansion in RafDKO/LC40 compared to LC40 mice.

Besides the direct influence of pERK on proapoptotic proteins, cross-talks to other signaling pathways could also influence B cell expansion. For example, upregulation of CD21 by LC40 expression was observed, blurring the boundaries between Fo B and MZ B cells. B-Raf//Raf-1 inactivation in RafDKO/LC40 mice significantly reduced the amount of MZ B cell-like cells and significantly decreased the CD21 expression compared to LC40 mice. Since Notch2 signaling drives transitional B cells into MZ B cells (11,32–34,54) and CD21 has been described as a typical Notch target gene (32,227,263), our results suggested that B-Raf//Raf-1 inactivation reduced the LC40 induced Notch2 signaling. Furthermore, a synergistic effect of Notch2 signaling on CD40 mediated proliferation was described (264). Therefore, the interplay of Notch and CD40 signaling in LC40 B cells could promote proliferation leading to B cell expansion. Decreased Notch activity in RafDKO/LC40 compared to LC40 B cells might contribute to the reduced B cell expansion in RafDKO/LC40 mice. The influence of Raf inactivation on Notch signaling will be further discussed in section 4.5.4.

4.4.2 Reduced LC40 mediated aberrant B cell expansion in old RafDKO/LC40 mice

While in young LC40 mice both MZ B and Fo B cells were expanded, an aberrant B1b cell-like population $CD21^{low}CD23^{low}CD43^{+}CD5^{low}$ grew out in aged LC40 mice (52,265). This correlated with the appearance of mono- and oligoclonal bands in Southern blots of aged LC40 mice (265). The role of B-Raf and Raf-1 on the LC40 mediated expansion of aberrant B cells was analyzed using aged RafDKO/LC40, LC40 and control mice.

The majority of old LC40 mice developed a pathological splenomegaly, while most of the aged control mice displayed normal splenic weights. Compared to LC40 mice, fewer

RafDKO/LC40 mice exhibited a pathological splenomegaly during aging. Similar results were obtained analyzing the so-called aberrant B cell population CD21^{low}CD23^{low}CD43⁺CD5^{low} B cells. Some preliminary results of other organs of aged RafDKO/LC40 mice indicated that the B-Raf//Raf-1 inactivation did not alter the homing of aberrant B cells. These data reflect the importance of B-Raf and Raf-1 for the LC40 mediated aberrant B cell expansion in the spleens of aged mice.

4.4.3 Altered LC40 mediated B cell activation in RafDKO/LC40 mice

Upregulation of CD95 reflects B cell activation. CD95 is important for negative selection of autoreactive B cell clones by inducing apoptosis as a death receptor (256,266–268). Besides its function in apoptosis, the induction of non-apoptotic signaling pathways by CD95 and its beneficial role in proliferation and cancer progression is discussed (269,270). Thus, CD95 was analyzed with respect to B cell activation in young and old LC40, RafDKO/LC40 and control mice. While young LC40 B cells displayed increased CD95 expression compared to young control and RafDKO/LC40 mice, aged mice showed similar CD95 level in all three genotypes. These data indicated that B cells of young LC40 mice might profit from high CD95 expression, while in aberrant B cells the pro-apoptotic function of CD95 might dominate. This might lead to a positive selection of aberrant B cells exhibiting lower CD95 expression level. These ambivalent functions of CD95 might cause the high heterogeneity of CD95 in aged LC40 mice (52). A participation of Raf-1 in the switch of the CD95 function from apoptosis to metastasis in colorectal cancer cells had already been described. The authors have shown that CD95 mediates apoptosis in the absence of Raf-1, while it leads to metastasis in Raf-1 proficient cells (271). Thus, the reduced CD95 expression level in young RafDKO/LC40 B cells compared to LC40 B cells could be due to increased apoptosis of CD95^{high} cells in the absence of Raf-1 in RafDKO/LC40 B cells. This could also contribute to the reduced B cell expansion detected in RafDKO/LC40 mice compared to LC40 mice.

In addition to B cell expansion, LC40 expression led to marked T cell expansion in young and aged LC40 mice (52). T cells in aged LC40 mice also exhibited a high level of activation, as reflected by the increased proportions of CD69⁺ T cells and differentiated effector and memory T cells. Here, LC40 had a stronger effect on CD4⁺ T cells than on CD8⁺ T cells, as indicated by the significant increase in CD4⁺/CD8⁺ ratio in LC40 mice compared with controls. B-Raf//Raf-1 inactivation significantly attenuated the LC40 induced T cell phenotype to control levels. Since leakiness of the expression of the Cre-recombinase in T cells is unlikely (52), T cell expansion is most likely elicited as a bystander effect. B cell depletion experiments revealed an important role of B cells in the activation and maintenance of T cells (52,272–274). In this context, B-T cell interactions

could provide certain co-stimulatory signals to promote T cell expansion. Thereby, B cell activation might play an important role.

Binding of ICOS-L on activated B cells to ICOS on T cells promotes proliferation and differentiation into follicular T helper cells (275,276). Thus, increased ICOS-L expression on B cells of young LC40 mice, which was reduced in young RafDKO/LC40 mice, might contribute to the T cell activation and expansion. This might explain why the T cells are less expanded in RafDKO/LC40 mice compared to LC40 mice.

Other protein interactions mediating B-T cell interactions would be CD40/CD40-L, MHC II/TCR, CD80/CD28, and CD86/CD28 (276–279). Preliminary results regarding CD80 and CD86 expression on B cells of aged control, LC40, and RafDKO/LC40 B cells indicate that CD80 and CD86 were more highly expressed on LC40 than on control and RafDKO/LC40 B cells. This could explain the differences in T cell expansion between aged LC40 and RafDKO/LC40 animals but should be confirmed by additional experiments. Previous FACS stainings published by Hömig-Hölzel et al. in 2008 revealed that MHC II is upregulated in LC40 B cells compared to controls (52), but the effect of genetic B-Raf//Raf-1 inactivation remains unanswered. Furthermore, the effect of LC40 signaling on the expression of endogenous CD40 on the B cell surface and the influence of a B-Raf//Raf-1 inactivation on this expression pattern should be examined.

4.4.4 Detection of Raf proficient B cells in old RafDKO/LC40 mice

The decreased B and T cell expansion and the reduced aberrant B cell development in RafDKO/LC40 compared to LC40 mice indicated an essential function of B-Raf and Raf-1 in constitutive CD40 signaling in B cells. Cre-recombinase under the control of the CD19 promotor led to a high deletion efficiency in peripheral B cells and a moderate one in developing ones in the bone marrow (52,190). A high deletion efficiency of the floxed DNA regions in young RafDKO/LC40 mice was substantiated by the absence of B-Raf and Raf-1 in Western blot analysis, and the clear phenotype induced by B-Raf//Raf-1 inactivation such as decreased splenomegaly, decreased B cell expansion and increased ERK phosphorylation compared to LC40 cells.

Despite the high CD19-Cre mediated deletion efficiency in mature B cells, the latter is never 100%. Thus, an outgrowth of undeleted Raf proficient B cells in RafDKO/LC40 mice during aging was possible. Indeed, Western blot analyses revealed a growth advantage of Raf proficient B cells in old RafDKO/LC40 mice, which could not be detected in young RafDKO/LC40 mice. Since the recombination of the loxP-flanked exons of B-Raf and Raf-1 as well as the deletion of the STOP-cassette of the LC40 fusion protein is mediated by the same Cre-recombinase under the control of the CD19 promoter, it is likely that the Raf proficient B cells growing out in old RafDKO/LC40 mice might also fail

to express LC40. However, this should be confirmed by Western blot using a human anti-CD40 antibody as published by Hömig-Hölzel et al. (52). The re-expression of Raf1 and B-Raf in B cells of RafDKO/LC40 mice during aging supports the importance of B-Raf and Raf-1 for B cell maintenance and/or expansion. Reasons could be increased survival, elevated proliferation, or reduced immune surveillance of Raf proficient B cells compared to the RafDKO/LC40 ones.

In addition to the Raf expression, the ERK phosphorylation in B cells of aged RafDKO/LC40, LC40 and control mice was investigated. An indirect correlation between the expression of B-Raf and Raf-1 and the ERK phosphorylation was found. The fact that Raf deficient B cells showed the highest pERK level might be due to the CD19-Cre mediated deletion of the loxP-flanked regions in the *B-Raf*, *Raf-1* and *LC40* genes in these B cells. Consequently, these cells presumably exhibited concomitant LC40 expression in addition to inactivation of B-Raf and Raf-1, which, as has already been shown in young mice, leads to higher ERK phosphorylation than in B cells of LC40 mice (see section 3.3.3). Despite this, the indirect correlation of Raf expression and ERK phosphorylation was also present in Raf expressing B cells of all genotypes. This supported the results of a negative regulatory function of B-Raf and Raf-1 with respect to the ERK phosphorylation already discussed in the section 4.3.

4.5 Changed LC40 mediated gene expression pattern upon B-Raf//Raf-1 inactivation

In addition to the increased pERK levels in RafDKO/LC40 B cells, ERK independent functions of B-Raf and Raf-1 may contribute to the attenuated LC40 mediated phenotype. Therefore, transcriptomic analyses of young RafDKO/LC40 and LC40 B cells were performed to identify mechanisms for the decreased B and T cell expansions and B cell transformation in RafDKO/LC40 compared to LC40 mice. Because of the blurred boundaries of MZ B and Fo B cells in LC40 mice, the whole splenic B2 cell population was used. As a result, a higher proportion of MZ B cells was presumably present in the LC40 samples than in the RafDKO/LC40 samples. Apart from this, however, this strategy offers the possibility to show differences in the gene expression patterns of splenic B2 cells of RafDKO/LC40 and LC40 mice. In future experiments the expression of genes of interest and of the corresponding proteins should be examined on isolated MZ B and Fo B cells. In addition, it may be interesting to compare the transcriptional profile of the two genotypes with control samples.

4.5.1 Diminished expression of tumor associated genes in RafDKO/LC40 B cells

By analyzing the top 25 differentially expressed genes between LC40 and RafDKO/LC40, the high occurrence of tumor-associated genes such as *Myof*, *Cebpz*, and *Fosl2* was noticed (204,207,213,280). These genes were all significantly higher expressed in LC40 than in RafDKO/LC40 B cells and might contribute to the increased occurrence of pathological splenomegaly and greater cell expansion in LC40 mice.

Furthermore, two *Myc* associated genes *Ahnak* and *Odc1* were detected among the top 25 differentially expressed genes. While *Ahnak* was higher expressed in RafDKO/LC40 B cells, they displayed significantly lower RNA levels of *Odc1*. *Myc* itself was significantly higher expressed in LC40 compared to RafDKO/LC40 B cells. Low *Ahnak* expression in Burkitt-lymphomas suggested a tumor suppressing function of *Ahnak* in B cells (281), which might base on the *Ahnak* mediated repression of *Myc* (201).

Myc itself exhibits a wide range of cellular functions causing tumor progression and gene instability when hyperactivated (282–284). A correlation between Raf-kinases and the *Myc* RNA expression has rarely been investigated in murine mature B cells. In pro-B cells an ERK dependency of the *Myc* RNA expression was described by Yasuda et al. in 2008, but the role of Raf-kinases was not investigated in this context (185). In 1998, Kerkhoff et al. established a direct link between Ras/Raf signaling and *Myc* RNA expression in a fibroblast cell line (285). With a higher *Myc* expression in LC40 compared to RafDKO/LC40 B cells, our results suggested a Raf dependent *Myc* expression also in mature murine B cells. In contrast to the described ERK dependency published by Yasuda et al., in 2008 (185), our RafDKO/LC40 B cells displayed lower *Myc* expression but higher pERK levels than LC40 B cells. However, Yasuda et al. did not investigate the effects of the ERK1/2 double knockout on Raf-kinases. Thus, the ERK dependence of the *Myc* expression described by Yasuda et al. may in fact be due to reduced Raf expression or activity. Thus, our data revealed that in mature B cells with a constitutive CD40 signal the *Myc* expression might be regulated in a Raf dependent but ERK independent mechanism.

Furthermore, synergies between *Myc* and Raf and between *Myc* and CD19 in tumor development and progression have been described in B cells (286–288). Based on the reduction of the *Myc* expression in RafDKO/LC40 compared to LC40 B cells, it could be hypothesized, that LC40 B cells would exhibit an increased activity of the *Myc*:CD19 amplification loop. This might result in a greater predisposition to B cell transformation and lymphoma development in LC40 than in RafDKO/LC40 B cells.

Odc1 is described as a direct *Myc* target (202,289,290). Thus, the lower *Odc1* expression in RafDKO/LC40 compared to LC40 B cells could give an indication of reduced *Myc* protein levels upon B-Raf//Raf-1 inactivation. This assumption should be proven by future Western blot analyses. *Odc1* encodes for the ornithine decarboxylase 1 mediating the rate-limiting step in polyamine biosynthesis (291,292). Polyamines play a crucial role in cell proliferation, survival, and apoptosis (292–294). Thus, *Odc1* might participate to tumor development, since inhibiting *Odc1* prevents tumor progression (290,292,295). Taken together, B-Raf//Raf-1 inactivation appeared to cause a decreased *Ahnak* expression, which could explain the reduced RNA levels of *Myc* and *Odc1* in RafDKO/LC40 compared to LC40 B cells. Thus, the altered expression pattern of *Ahnak*, *Myc*, and *Odc1* in RafDKO/LC40 B cells compared with LC40 B cells could contribute to the reduced B cell expansion and transformation upon B-Raf//Raf-1 inactivation in LC40 B cells.

4.5.2 Changed expression of genes involved in immune responses and cell adhesion in RafDKO/LC40 B cells

Genes of the biological processes "positive regulation of cell adhesion" and "immune response" were higher expressed in RafDKO/LC40 compared to LC40 samples. In these two biological processes a certain overlap of genes was present pointing to the close connection between cell adhesion and adequate immune responses (296,297). Genes occurring in both biological processes were *CD27* and *Tnfrsf13c*. *CD27* was described to play a critical role in germinal center formation (298,299). Lower *CD27* level in LC40 B cells might contribute to the impaired germinal center reaction in LC40 B cells compared to controls (52). RafDKO/LC40 mice might be able to form germinal centers due to higher *CD27* expression, which needed to be examined in future experiments. Additionally, *Tnfrsf13c* was higher expressed in RafDKO/LC40 than in LC40 B cells. *Tnfrsf13c* encodes for the BAFF receptor, which mediates survival signals in B cells predominantly via non-canonical NF κ B signaling (46–48,300–302). Because B-Raf//Raf-1 inactivation might reduce cell survival, as discussed in section 4.4, the increased *Tnfrsf13c* levels could result from positive selection of RafDKO/LC40 B cells displaying a high BAFF receptor expression.

Furthermore, differentially expressed genes of the biological process "semaphorin interactions" were higher expressed in LC40 compared to RafDKO/LC40 B cells. The significantly changed genes of the biological process "semaphorin interactions" includes semaphorin 7a (*Sema7a*) and some plexins (e.g., *Plxna1*, *Plxnd1*), which serves as semaphorin receptors. Initially, semaphorin interactions were described in the context of axon guidance, but later have been published playing a crucial role in the immune response (210,303–306). *Sema7a* can be promoted by stimulation in B cells (307) and is thought

to play an important role in their activation and differentiation (210). Furthermore, Plexin d1 (*Plxnd1*) was described to play a crucial role in MZ B cells and was upregulated in CD40 stimulated Fo B cells (308). Additionally, Semaphorins also appear to be important in tumorigenesis and metastasis. They have been identified in different cancer types, although no aberrant expression of semaphorins were detected in B cell lymphomas so far (309–311). Thus, Raf-kinases might take part in an LC40 induced upregulation of semaphorins and its receptors (plexins) leading to increased semaphorin interactions in LC40 compared to RafDKO/LC40 B cells. This higher expression of genes of "semaphorin interactions" in LC40 B cells might contribute to the LC40 mediated MZ B cell expansion and tumorigenesis. The B-Raf//Raf-1 inactivation seemed to decrease the semaphorin interactions, which might explain the decreased B cell expansion and transformation in RafDKO/LC40 mice compared to LC40 mice.

4.5.3 Contribution of B-Raf and Raf-1 to the LC40 induced MZ B cell expansion

Among the top 25 differentially expressed genes MZ B related ones appeared. These results had to be interpreted carefully, since they could either be causative or a consequence of increased MZ B cell expansion in LC40 compared to RafDKO/LC40 mice. Thus, the following results should be analyzed in future experiments by single cell sequencing or sorting of MZ B cell like and Fo B cell like cells followed by qPCR.

Nevertheless, LC40 B cells displayed a higher expression of *Cr2*, encoding the CD21 protein. This confirmed the results of the CD21 FACS (see section 3.4.1 and 4.4.1). LC40 B cells also possessed significantly higher *Asb2* amounts, which is induced by Notch signaling and is typical for MZ B cells (211,212). These results indicated that constitutive CD40 signaling pushes splenic B2 cells into a MZ B cell like phenotype.

Since Hömig-Hölzel et al. showed by histological analysis that the expanded MZ B cell population in LC40 mice was intrafollicular and not localized in the marginal zone (52), the question arose to what extent MZ B cells of LC40 mice correspond to true MZ B cells and whether B-Raf//Raf-1 inactivation affects only single genes or the "true" generation of MZ B cells. To investigate this, GSEA with respect to Fo B and MZ B gene sets were performed. These revealed a significant enrichment of MZ B cell associated genes in LC40 samples and of Fo B cell associated genes in RafDKO/LC40 samples. This argued for a true induction of the MZ B cell phenotype by LC40 signaling, which is alleviated by B-Raf//Raf-1 inactivation. Since both Notch and non-canonical NFκB signaling participate to the cell fate decision towards MZ B cells (11,32,33,52,53), their activations were investigated and discussed in the following section 4.5.4.

4.5.4 Reduced LC40 mediated Notch2 and non-canonical NFκB signaling in RafDKO/LC40 mice

GSEA of the RNA-Seq data revealed an increased activation of Notch2 and non-canonical NFκB signaling in LC40 compared to RafDKO/LC40 B cells. Thus, inactivation of B-Raf and Raf-1 seemed to negatively affect LC40 mediated activation of Notch2 and non-canonical NFκB signaling.

Normalized counts of the RNA-Seq and Western blots showed that Notch2 was more highly expressed in LC40 and RafDKO/LC40 B cells than in controls. In contrast, both Notch2 targets CD21 and HES1 were reduced at gene and protein levels in RafDKO/LC40 compared with LC40 B cells. Thus, B-Raf//Raf-1 inactivation did not appear to affect the LC40 induced Notch2 transcription and translation, but the Raf-kinases seemed to influence the expression of Notch2 targets. The Notch mediated expression of its target genes depends on the interaction between the intracellular domain of Notch (NotchIC) and the DNA-binding protein RBPJ. The RBPJ-NotchIC complex associates with transcriptional activators. In contrast, in the absence of NotchIC, RBPJ inhibits transcription by binding corepressors (312,313). AKT1 mediated phosphorylation of RBPJ was shown to promote this transcriptional repression, thereby reducing the expression of Notch1 target genes (314). By a similar mechanism, B-Raf//Raf-1 inactivation could AKT-dependently or -independently increase RBPJ phosphorylation and thereby reduce LC40 mediated expression of Notch target genes without affecting Notch2. To study the RBPJ-NotchIC interaction in RafDKO/LC40 compared to LC40 B cells, immunoprecipitation or DNA chip experiments could be performed.

No differences of the normalized counts of RelB could be detected between LC40 and RafDKO/LC40. However, protein expression of full-length RelB was moderately increased in LC40 compared to RafDKO/LC40 B cells. These results supported the hypothesis of higher non-canonical NFκB activation in LC40 compared to RafDKO/LC40 B cells. In addition, LC40 B cells displayed more RelB cleavage than control and RafDKO/LC40 B cells. RelB cleavage has mostly been described in context with subsequent proteasomal degradation. This might suggest a compensatory mechanism in LC40 B cells to counteract hyperactivation of non-canonical NFκB signaling. In 2008, Hömig-Hölzel et al. observed a reduced capacity to activate the canonical NFκB signaling pathway in LC40 compared to control B cells (52). This could be due to the negative regulatory function of RelB on RelA and cRel, which has already been described in T cells and could be alleviated by RelB cleavage (315).

NFκB2 encodes p100 the cytoplasmic p52 precursor, which is also an important component of the non-canonical NFκB signaling pathway. LC40 B cells exhibited increased normalized counts of *NFκB2* and p52 protein compared to RafDKO/LC40 B cells. Thus,

B-Raf and Raf-1 appeared to be essential contributors of the LC40 mediated induction of p52. The latter was already published in 2008 by Hömig-Hölzel et al. (52). Since *NFκB2* expression can be induced by Notch signaling (316–318), the reduced activation of the non-canonical NFκB pathway in RafDKO/LC40 B cells could also result from reduced Notch activation as previously discussed. This could be investigated, for example, by using γ-secretase inhibitors in LC40 B cells with subsequent analysis of p52 levels.

4.6 Raf-kinases: more than a kinase towards MEK/ERK

Within this thesis, we could establish that Raf-kinases play a crucial role in PC differentiation, cell expansion and B cell transformation with only a minor effect on the initial B cell activation. In activated B cells BCR, TLR4 and CD40 induced ERK phosphorylation might probably be mediated by SYK activation followed by PI3K, Rac/PAK and PLCγ2 signaling. Hereby, Raf-kinases did not phosphorylate MEK/ERK, but rather negatively regulate the pERK level in unstimulated and activated B cells. In contrast, Raf-kinases seemed to be essential for the dramatic increase of pERK in pre-PBs and PBs, which resulted in BLIMP1 expression followed by the initiation and implementation of the PC differentiation. Thus, the function of Raf-kinases seemed to depend on the differentiation state of the B cell by switching from a negative regulator of pERK in unstimulated and activated B cells to a MEK/ERK phosphorylating kinase in pre-PBs and PBs.

The expression of LC40 elicits a constitutive CD40 signaling in B cells, which led to activation, expansion, and transformation, but fail to induce differentiation. Thus, our results of increased pERK in RafDKO/LC40 compared to LC40 B cells supported our theory of a negative regulatory function of B-Raf and Raf-1 on pERK in activated B cells. Nonetheless, B-Raf//Raf-1 inactivation in LC40 expressing B cells, led to a diminished LC40 mediated phenotype. The RNA-Seq analyses revealed changes in the gene expression pattern in LC40 expressing B cells by the inactivation of B-Raf and Raf-1. These changes could explain the reduced B cell expansion and transformation in RafDKO/LC40 compared to LC40 mice, which might be due to cross talks of B-Raf and Raf-1 with other signaling pathways upon constitutive CD40 signaling. B-Raf and Raf-1 seemed to contribute to LC40 mediated Notch2 signaling probably by altering the RBPJ binding capacity. Furthermore, B-Raf//Raf-1 inactivation diminished the LC40 induced non-canonical NFκB activation predominantly by reducing the *NFκB2* expression either Notch2-dependently or -independently.

In contrast to literature, Raf-kinases might not only phosphorylate MEK and ERK but further negatively regulate the pERK levels depending on the differentiation state of the B cell. Furthermore, B-Raf and Raf-1 seemed to contribute to Notch2 and non-canonical NFκB signaling during LC40 mediated B cell activation. Thus, our results supported the

hypothesis of B-Raf and Raf-1 as a regulator of B cell activation by fine-tuning not only the MEK/ERK but also Notch2 and non-canonical NF κ B activation.

5. Material

5.1 Mouse strains

The activation and differentiation of the B-Raf//Raf-1 double knockout B cells was investigated using young (8-20 weeks) RafDKO//mb1-Cre and control mice. RafDKO//LMP1/CD40//CD19-Cre mice and its corresponding controls up to an age of 4 month were defined as young mice. Aged RafDKO/LC40, LC40 and control mice (10-20 months) were analyzed for the investigation of the outgrowth of an aberrant cell proliferation depending on the constitutive CD40 signaling in combination with and without the B-Raf//Raf-1 inactivation.

All mice were maintained under specific pathogen-free housing conditions. Agreeable to the German Animal Welfare Act, all experiments were authorized by the institutional committee on animal experimentation and the Government of Upper-Bavaria.

5.1.1 C57BL/6

The C57BL/6 mouse strain was obtained from Charles River Laboratories. Mice of this strain were used for breeding and as control mice in our experiments.

5.1.2 mb1-Cre

The *mb1*-locus encodes for the *Igα* gene. *Igα* is involved in the BCR signaling and is expressed very early during B cell development. The integration of a humanized *Cre-recombinase* into the exon 2 and 3 of the *Igα* gene leads to the B cell specific expression of the *Cre-recombinase* already at the early pro-B cell stage (188). No homozygous mb1-Cre^{+/+} mice were used, because homozygous insertion of the *Cre* gene led to a knockout of the *Igα* gene leading to a B cell deficiency (189). Heterozygous mb1-Cre^{+/-} mice displayed a wildtype like phenotype and were used for breeding and as control mice.

5.1.3 RafDKO//mb1-Cre (DKO)

This mouse strain has its origin in the cross breeding of the *Raf-1^{fl/fl}* mice (186) with the *B-Raf^{fl/fl}* mice (187) resulting in a *Raf-1^{fl/fl}//B-Raf^{fl/fl}* mouse strain. Here, the exon 3, encoding for the Ras-binding domain and exon 12, encoding for parts of the kinase domain, were flanked by loxP sites. Both the floxed *Raf-1* and *B-Raf* alleles were bred to homozygosity. Subsequent cross breeding of these mice to the mb1-Cre mouse strain led to a B cell specific deletion of the loxP flanked exons of *B-Raf* and *Raf-1* very early during B cell development. Deletion of the exons leads to a knockout of *Raf-1* and *B-Raf*.

5.1.4 CD19-Cre

CD19 is a B cell specific surface molecule. It is already detectable during B cell development and highly expressed in mature B cells (93). The CD19-Cre mouse strain (C57BL/6 background) expresses the *Cre-recombinase* under the control of the *CD19* promoter (190). *CD19* alleles containing the *Cre* gene lose the ability of CD19 expression. Therefore, a homozygous *CD19-Cre^{+/+}* mouse displays a CD19 deficiency (93) and was not used in our experiments.

5.1.5 LMP1/CD40//CD19-Cre (LC40)

LMP1/CD40 (LC40) is an artificial fusion protein. It contains the transmembrane domain of the viral EBV protein LMP1 fused to the cytosolic domain of CD40. The LMP1 part leads to a ligand independent accumulation of LMP1/CD40 and the constitutive activation of the CD40 signaling. The *LMP1/CD40* gene construct additionally contains a loxP flanked *STOP-cassette* in front of the fusion protein coding region. The whole construct is integrated into the *rosa26* locus. A *STOP-cassette*, cloned upstream of *LMP1/CD40* transgene prevents expression of the fusion protein. Cre-recombinase mediated excision of the *STOP-cassette* enables expression of the *LMP1/CD40* gene. Cross breeding of the LMP1/CD40 mice to CD19-Cre mice leads to a B cell specific excision of the *STOP-cassette* resulting in an B cell specific expression of LMP1/CD40 (52). We backcrossed the original LMP1/CD40//CD19-Cre (Balb/c) to a C57BL/6 background. Therefore, in some experiments mice with a mixed background had to be used. Only LMP1/CD40//CD19-Cre^{+/-} (LC40) mice were used for analyses.

5.1.6 RafDKO//LMP1/CD40//CD19-Cre (RafDKO/LC40)

The RafDKO//LMP1/CD40//CD19-Cre (RafDKO/LC40) mouse strain results of cross breeding of the Raf-1^{fl/fl}//B-Raf^{fl/fl} (see section 5.1.3) mouse strain with the LMP1/CD40//CD19-Cre (see section 5.1.5) mouse strain on a C57BL/6 background. After CD19-Cre mediated excision of the loxP flanked regions, B cells of these mice display a concomitant B-Raf//Raf-1 knockout and an expression of the LMP1/CD40 fusion protein.

5.2 Antibodies

Table 5: Antibodies used in FACS with its corresponding conjugates, clones, the company and its used dilution.

	Antibody	Conjugate	Clone	Company	Dilution
FACS	CD43	Biotin; BV421; FITC	S7	BD Biosciences	1:100
	SA-APC			BD Biosciences	1:400
	SA-PerCP			BD Biosciences	1:100
	B220	PerCP; FITC	RA3-6B2	BD Biosciences	1:400
	CD21	APC; BV421	7G6	BD Biosciences	1:100
	CD23	PE; FITC	B3B4	BD Biosciences	1:200
	CD5	APC; BV450	53-7.3	BD Biosciences	1:500
	CD95	PE; V450	JO2	BD Biosciences	1:75
	CD138	PE; BV421	281-2	BD Biosciences	1:600; 1:200
	BLIMP1	AlexaFluor 647	5E7	BD Biosciences	1:100
	PAX5	PE	1H9	BD Biosciences	1:2000
	IRF4	APC	3E4	BD Biosciences	1:200
	Phospho-ERK1/2 (Thr202/Tyr204)			Cell signaling (#9101S)	1:100
	ERK1/2			Cell signaling (#9102S)	1:100
	Rabbit mAb IgG XP Isotype Control		DA1E	Cell signaling (#3900S)	1:100
	goat-anti-rabbit	AlexaFluor 488; PE		invitrogen	1:100
	CD19	PE; APC; FITC		BD Biosciences	1:600; 1:200
	Thy1.2	Biotin		BD Biosciences	1:1000
	CD3	FITC		BD Biosciences	1:200
	CD4	APC		eBioscience™	1:400
	CD8	PerCP		BD Biosciences	1:80
	CD25	PE	PC61	BD Biosciences	1:400
	CD62-L	FITC		BD Biosciences	1:100
	CD44	PE		BD Biosciences	1:500
	CD69	PE		BD Biosciences	1:50
	ICAM-1	FITC		BD Biosciences	1:200
	ICOS-L	PE		eBioscience™	1:100
	TOPRO-3			Molecular Probes	1:40000
	Fixable Live/Dead	FITC; UV		Life technologies	1:1000

Table 6: Antibodies used in ELISpot with its corresponding clones, the company, and its used dilution.

Antibody	Clone	Company	Dilution
rat-anti-mouse IgM	R6-60.2	BD Biosciences	1:500
rat-anti-mouse IgG3	R40-82	BD Biosciences	1:500
Avidin D - HRP		Vector	1:2000

Table 7: Antibodies used in ELISA with its corresponding clones, the company, and its used dilution.

Antibody	Clone	Company	Dilution
goat-anti-mouse-IgM-HRP	YF97	Southern Biotech	1:5000
rat-anti-mouse IgG3	R40-82	BD Biosciences	1:350
Avidin D - HRP		Vector	1:2000

Table 8: Antibodies used in protein analyses (Western blot and WES) with its corresponding clones, the company, and its used dilution.

	Antibody	Conjugate	Clone	Company	Dilution
Western blot	Phospho-ERK1/2 (Thr202/Tyr204)			Cell signaling (#9101S)	1:2500
	ERK1/2			Cell signaling (#9102S)	1:2500
	alpha/beta-Tubulin			Cell signaling (#2148S)	1:2500
	Phospho-AKT (Ser473) XP		D9E	Cell signaling (#4060S)	1:2500
	AKT			Cell signaling (#9272S)	1:2500
	Phospho-MEK (Ser217/221)		41G9	Cell signaling (#9154S)	1:1000
	MEK		47E6	Cell signaling (#9126S)	1:1000
	Phospho-SYK (Tyr525/526)			Cell signaling (#2711S)	1:1000
	Phospho-p38 MAPK (Thr180/Tyr182) XP		D3F9	Cell signaling (#4511S)	1:1000
	Phospho-IkBalpa (Ser32/36)		5A5	Cell signaling (#9246S)	1:1000
	IkBalpa		44D4	Cell signaling (#4812S)	1:1000
	Phospho-PLC-gamma-2 (Tyr1217)			Cell signaling (#3871S)	1:1000
	Phospho-SAPK/JNK (T183/Y185)		81E11	Cell signaling (#4668S)	1:1000
	GAPDH		6C5	Merck (#CB1001-500UG)	1:20000
	A-Raf			Cell signaling (#4432S)	1:1000
	Raf-1 (C-Raf)			Cell signaling (#9422S)	1:1000
	pB-Raf			Cell signaling (#2696S)	1:1000
	Lamin B2			Cell signaling (#13823)	1:1000
	Notch2		C651.DbHN	Dr. Artavanis-Tsakonas, Developmental Studies Hybridoma Bank, University of Iowa	1:2
	HES1			SantaCruz (#sc-25392)	1:500
	p100/p52			Cell signaling (#4882S)	1:1000
	RelB			Cell signaling (#4922S)	1:1000
	Anti-mouse IgG-HRP	HRP-linked		Cell signaling (#7076S)	1:2500
Anti-rabbit IgG-HRP	HRP-linked		Cell signaling (#7074S)	1:2500	
Anti-rat IgG-HRP	HRP-linked		SantaCruz (#sc-2006)	1:2000	
WES	Tubulin			Cell signaling (#2148S)	1:20
	LaminB2		E1S1Q	Cell signaling (#13823S)	1:50
	Phospho-Erk1/2 (Thr202/Tyr204)			Cell signaling (#9101S)	1:20

5.3 Chemicals, enzymes, commercial kits and consumable material

Table 9: Material/Chemicals/Enzymes/Commercial kits and the company the products were obtained from.

Material/Chemicals/Enzymes/Commercial kits	Company
4 % PFA (Roti Histofix 4%)	Roth
Acrylamide (Rotiphorese Gel 30)	Roth
APS	AppliChem
BSA (ELISpot coating)	New England BioLabs
BSA (Westernblot)	Sigma Life Science
DC Protein Assay Kit	BioRad

**Material/Chemicals/Enzymes/
Commercial kits**

	Company
CD43 depletion Kit	Mitenyi Biotec
DMSO	Sigma Life Science
DNA loading buffer	ThermoScientific
DNA marker (gene ruler)	ThermoScientific
dNTPs	ThermoFisher
DTT	Sigma Life Science
ECL Western Blotting Detection Reagents	GE Healthcare
EDTA	Merck
FACS tubes (MP32022)	Micronic
Fetal calf serum (FCS)	PAA Cell culture Company
Glycine	Sigma Life Science
Halt Phosphatase Inhibitor Cocktail	Pierce
IGEPAL	Sigma Life Science
L-glutamine	Gibco
LIVE/DEAD Fixable Blue Cell Stain Kit	Life technologies
MACS buffer	Mitenyi Biotec
MgCl ₂ (50 mM)	ThermoFisher
Microplate, 96-well, PS, roundbottom (FACS)	Greiner Bio One
Mini Compete protease inhibitor	Roche
Mini-Protean TGX Protein Gels (10%)	Bio Rad
NE-PER Kit	Life technologies
Non-essential amino acids (NEAA)	Gibco
NP13-BSA	Biosearch Technologies
PAGE ruler Prestained Protein ladder	Thermo Scientific
Pan-B cell isolation kit	Mitenyi Biotec
Penicillin	Gibco
Ponceau S Solution	Sigma Life Science
Powdered milk	Roth
RBC lysis buffer	eBioscience TM
Reaction tube 1.5ml	Eppendorf
Reaction tube 15ml	Sarstedt
Reaction tube 2ml	Eppendorf
Reaction tube 50ml	Sarstedt
RPMI	Gibco
SDS	Sigma Aldrich
Sodium pyruvat	Gibco
Streptomycin	Gibco
Taq buffer	ThermoFisher
Taq polymerase	ThermoFisher
TEMED	Roth
TOPRO-3	Molecular Probes
Tris	AppliChem

**Material/Chemicals/Enzymes/
Commercial kits**

	Company
Trizol	invitrogen
Tween	AppliChem
Wes Anti-rabbit detection module	protein simple
WES Separation Kit	proteinsimple (#SM-W004)
WES Separation Module, 12-230 kDa, 8x25 capillary cartidges	protein simple
β -Mercaptoethanol (cell culture)	Gibco
β -Mercaptoethanol (Western blot)	Merck

5.4 Inhibitors

Table 10: Inhibitors with its corresponding target, the company, and its used concentration.

Inhibitor	Company	Target	Concentration
LY294002	Cell Signaling Technology	PI3K	6 μ M or 20 μ M
Sorafenib	Bayer HealthCare	Raf	1 μ M to 10 μ M
Dabrafenib	Selleckchem	Raf	1 μ M to 10 μ M
LY3009120	Selleckchem	Raf	0.1 μ M to 10 μ M
p505-15	Selleckchem	SYK	0.5 μ M
PF-3758309	Selleckchem	PAK	5 μ M or 10 μ M
Akt8= Akti 1/2	Merck	AKT	5 μ M
IKK2-inhibitor 8	Merck	IKK2	5 μ M
DMSO	SigmaLife Science	solvent control	0.1 μ M to 20 μ M

5.5 Stimuli

Table 11: Stimuli with its corresponding company, its used concentration, and the incubation time points. Mostly used timepoints are marked with bolt type.

Inhibitor	Company	Concentration	Timepoints
LPS long-term	Sigma-Aldrich	50 μ g/ml	1 - 3 d
LPS short-term			1/ 2.5/ 5/ 10/ 20 min
anti-IgM	115-006-020 Jackson Immunology Research	15 μ g/ml	0.5/ 2.5 /5 /15 min
anti-CD40	HM40-3 eBioscience	2.5 μ g/ml	10/ 20/ 30/ 120 min

5.6 Buffer and media composition

Table 12: Formula of media and uncommercial buffers

Buffer	Composition
Lysis buffer DNA isolation	100 mM Tris/HCl (pH 8), 5 mM EDTA, 0.2 % SDS, 200 nM NaCl, 100 µg/ml Proteinase K
1x TAE	40 mM Tris/HCl, 20 mM acetic acid, 1 mM EDTA (pH 8.5)
TE	10 mM Tris (pH 7.9), 1 mM EDTA
1 % B cell media (1 % BCM)	1x RPMI 1640 containing 1% (v/v) heat-inactivated FCS, 100 U/ml penicillin, 100 µg/ml streptomycin, 1 mM sodium pyruvate, 2 mM L-glutamine, 1x NEAA, and 52 µM β-mercaptoethanol
10 % B cell media (10 % BCM)	1x RPMI 1640 containing 10% (v/v) heat-inactivated FCS, 100 U/ml penicillin, 100 µg/ml streptomycin, 1 mM sodium pyruvate, 2 mM L-glutamine, 1x NEAA, and 52 µM β-mercaptoethanol
2x Laemmli buffer	120 mM Tris (pH 6.8), 4 % SDS, 20 % Glycerin, 0.01% bromphenol blue
2x NP40 lysis buffer	100 mM Tris (pH 7.4), 300 mM NaCl, 4 mM EDTA, 2 % NP40, 1/100 Phosphatase Inhibitor, 1/7 Protease inhibitor
Buffer A (nuc-cyt fractionation)	10 mM HEPES (pH 7.9), 10 mM KCl, 0.1 mM EDTA, 0.1 mM EGTA, 1 mM DTT (add fresh), 1/100 Phosphatase Inhibitor, 1/7 Protease inhibitor
Buffer C (nuc-cyt fractionation)	20 mM HEPES (pH 7.9), 0.4 M NaCl, 1 mM EDTA, 1 mM EGTA, 1 mM DTT (add fresh), 1/100 Phosphatase Inhibitor, 1/7 Protease inhibitor
Stacking gel	5 % acrylamide, 6,25 % 2 M Tris (pH 6.8), 10 % SDS, 10 % APS, 10 % TEMED in distilled water
Running gel 7.5 %	7.5 % acrylamide, 25 % 1.5 M Tris (pH 8.8), 10 % SDS, 10 % APS, 10 % TEMED in distilled water
Running gel 12 %	12 % acrylamide, 25 % 1.5 M Tris (pH 8.8), 10 % SDS, 10 % APS, 10 % TEMED in distilled water
10x Running buffer	30.3 g Tris, 144.2 g glycine, 10 g SDS in 1l membrane pure water
10x Blotting buffer	30.3 g Tris, 144.2 g glycine in 1l membrane pure water
TBST	0.1 M Tris/HCl (pH 7.5) , 0.1 M NaCl, 0.02 % (v/v) Tween
PBS	137 mM NaCl, 2.7 mM KCl, 10 mM Na ₂ HPO ₄ , 1.8 mM KH ₂ PO ₄
Stripping solution	8 g SDS, 3,125 % 2 M Tris (pH 6.8) in 400 ml membrane pure water
Carbonate buffer	0.1 M NaHCO ₃ (pH 9.5)
ELISA substrate buffer	0.1 M citric acid, 0.1 M Tris with freshly added 0.015% H ₂ O ₂

5.7 Software

The specific software programs are mentioned in the description of the specific methods. Commonly used software programs were Microsoft Excel for organization and calculation of data sets. Microsoft Word and PowerPoint were used to generate the text and illustrations. Most figures were designed using the Adobe Illustrator and BioRender Basic (biorender.com).

6. Methods

The used Antibodies (see section 5.2), chemicals, commercial kits, and consumable material (see section 5.3) were summarized in different tables in the material section. Furthermore, the different inhibitors (see section 5.4) and stimuli (see section 0) as well as the buffer and media composition (see section 5.6) were listed in the material section.

6.1 Mouse genotyping

6.1.1 Isolation of genomic DNA

To analyze the genotypes of the transgenic mice, DNA from tissue samples (ear or tail clippings) was isolated. Tissue samples were shaken in 500 µl lysis buffer at 56 °C overnight. Precipitation of the proteins was accomplished by adding 170 µl saturated NaCl solution (> 5 M) to the lysed tissue samples and subsequent inversion. The proteins and tissue remnants were pelletized by centrifugation (Eppendorf; Centrifuge 5424 R; 10 min, 15000 rpm, 4 °C). By transferring the supernatant into tubes containing 500 µl (100 %) isopropyl alcohol and subsequent inversion, the DNA was precipitated. After pelletizing the DNA by centrifugation, the DNA pellet was washed by adding 500 µl (70 %, v/v) ethanol, followed by another round of centrifugation. The supernatant was discarded afterwards, and the DNA pellet was dried first at room temperature and then at 37 °C for 30 min in the heater. The dried DNA pellet was dissolved in 100 µl TE buffer by shaking for 2-3 h at 37 °C. The dissolved DNA was stored at 4 °C.

6.1.2 Polymerase chain reaction and gel electrophoreses

After the isolation of the genomic DNA of the transgenic mice (see section 6.1.1), the genotype of each mouse was determined by specific polymerase chain reactions (PCRs) and additional gel electrophoreses. The set of PCRs needed to be performed for each mouse strain (Table 13) and the corresponding primer (Table 14; purchased from metabion), PCR mixtures (Table 15) and PCR programs (Table 16) are listed below. The PCRs were run in the thermal cycler from Biometra.

The amplified gene products were detected by gel electrophoreses. Therefore, the amplified PCR probes were mixed with DNA loading buffer and loaded onto agarose gels [1x TAE, 5 µg/ml ethidium bromide, 1.5 - 2% (w/v) agarose (Biozym)]. For gel electrophoresis gel chambers from PEQLAB Biothechnologie containing 1x TAE buffer were used. After running the electrophoreses at 80 V to 100 V for 1.5 h, the DNA products were detected by the UV luminescence screen Quantum ST-4. With UV light DNA intercalated ethidium bromide could be visualized. Additionally, a gene ruler was loaded onto

each gel prior electrophoreses to analyze the size of the DNA bands. The specific product size of each PCR product is shown in

Table 17.

Table 13: Specific PCRs needed to be performed for the indicated mouse strains

mb1cre	RafDKO//mb1cre	CD19cre	LMP1/CD40//CD19cre	RafDKO/LMP1/CD40//CD19cre
mb1cre	mb1cre	CD19cre	CD19cre	CD19cre
	Raf-1		LMP1/CD40	LMP1/CD40
	B-Raf		rosa26	rosa26
	B-Raf Δ			Raf-1
				B-Raf
				B-Raf Δ

Table 14: Primer and primer sequences used in the different PCRs

PCR	Primer	Primer sequence 5'-3'
mb1cre	Mb1-Cre P54	GGAGATGTCTTCACTCTGATTCT
	Mb1-Cre P55	ACCTCTGATGAAGTCAGGAAGAAC
B-Raf	B-Raf 9	GCATAGCGCATATGCTCACA
	B-Raf 11	CCATGCTCTAACTAGTGCTG
B-Raf Δ	B-Raf 9	GCATAGCGCATATGCTCACA
	B-Raf 17	GTTGACCTTGAACCTTCTCC
Raf-1	Raf-1 US-Lox	TGGCTGTGCCCTTGG AACCTCAGCACC
	Raf-1 DS-Lox	AACATGAAGTGGTGTCTCCGGGCGCC
	Raf-1 CT-U	ATGCACTGAAATGAAAACGTGAAGACGACG
CD19cre	CD19c	AACCAGTCAACACCCTTCC
	CD19d	CCAGACTAGATACAGACCAG
	Cre 7	TCAGCTACACCAGAGACGG
LMP1/CD40	CD40 PCR3	CTGAGATGCGACTCTCTTTGCCAT
	Ex1Fw1LMP1	AGGAGCCCTCCTTGTCTCTA
rosa26	Rosa fw 1(60)	CTCTCCCAAAGTCGCTCTG
	Rosa rev2 (62)	TACTCCGAGGCGGATCACAAGC

Table 15: PCR mixtures specific for each PCR

	mb1cre	B-Raf	B-Raf- Δ	Raf-1	CD19cre	LMP1/CD40	rosa26
dH ₂ O	18.85 μ l	18.35 μ l	18.35 μ l	18.1 μ l	19.1 μ l	19.65	18.4 μ l
Taq buffer (10x)	2.5 μ l	2.5 μ l	2.5 μ l	2.5 μ l	2.5 μ l	2.5 μ l	2.5 μ l
MgCl ₂ (50mM)	1 μ l	1 μ l	1 μ l	1 μ l	1 μ l	1 μ l	1.5 μ l
dNTP	0.5 μ l	0.5 μ l	0.5 μ l	0.5 μ l	0.5 μ l	0.5 μ l	0.5 μ l
primer	0.25 μ l	0.25 μ l	0.25 μ l	0.25 μ l	0.25 μ l	0.1 μ l	0.1 μ l
DMSO	-	-	-	-	-	-	0.25 μ l
Taq polymerase (5U/ μ l)	0.15 μ l	0.15 μ l	0.15 μ l	0.15 μ l	0.15 μ l	0.15 μ l	0.15 μ l
DNA (5-10ng)	1.5 μ l	2 μ l	2 μ l	2 μ l	1 μ l	1 μ l	1.5 μ l

Table 16: PCR programs of the thermal cycler specific for each PCR

	mb1cre	B-Raf	B-Raf-Δ	Raf-1	CD19cre	LMP1/CD40	rosa26
initial denaturation	4min, 94°C	5min, 94°C	5min, 94°C	4min, 94°C	2.5min, 95°C	5min, 95°C	3min, 95°C
cyclic denaturation	45sec, 94°C	45sec, 94°C	45sec, 94°C	45sec, 94°C	45sec, 94°C	45sec, 95°C	45sec, 95°C
cyclic hybridization	1min, 58°C	1min, 60°C	1min, 60°C	30sec, 58°C	45sec, 59°C	45sec, 55°C	45sec, 58°C
cyclic elongation	1min, 72°C	1min, 72°C	1min, 72°C	2min, 72°C	2min, 72°C	1.25min, 72°C	1min, 72°C
final elongation	10min, 72°C	10min, 72°C	10min, 72°C	10min, 72°C	10min, 72°C	10min, 72°C	10min, 72°C
number of cycles	35	30	30	40	30	32	33

Table 17: Sizes of the different PCR products of the specific PCRs

	mb1cre	B-Raf	B-Raf-Δ	Raf-1	CD19cre	LMP1/CD40	rosa26
wt		357bp		165bp	500bp		500bp
fl/fl		413bp		220bp		600bp	
del			280bp	360bp			
cre	500bp				700bp		

6.2 Mouse immunization

To induce a TI immune reaction, RafDKO//mb1-Cre and control (mb1-Cre^{+/-} or wildtype C57BL/6) mice were injected intraperitoneally (i.p.) with 50 µg NP-Ficoll (Biosearch Technologies) in 200 µl DPBS (Gibco). NP-Ficoll induces a TI type 2 immune response (6) resulting predominantly in IgM and IgG3 antibody production (319). The NP-specific immune reaction regarding the predominant isotypes (IgM and IgG3) was analyzed 14 days after immunization by ELISpot (see section 6.10) and ELISA (see section 6.9).

6.3 Organ preparation

The phenotype of the different transgenic mice was studied by analyzing the serum, the bone marrow, and the spleen. For collection of serum, mice were killed by CO₂-inhalation. Subsequently, the blood was taken by cardiopuncture with a syringe. For extraction of the serum, the blood was directly stored on ice without additives for 3 h. After 3 h on ice, the coagulated component of the blood was pelletized by centrifugation (Eppendorf; Centrifuge 5424 R; 15 min, 14000 rpm, 4 °C). The supernatant was transferred into a new tube and centrifuged another time. Afterwards the supernatant (serum) was transferred into a new tube. The sera were frozen at -80 °C until ELISA (see section 6.9) was performed. For the preparation of the other organs, mice could either be euthanized by CO₂-inhalation or by cervical dislocation. The spleen was collected in tubes containing 1 % BCM. The bone marrow cells were flushed out of the tibia with 1 % BCM. All samples were stored on ice until cell or serum preparation.

6.4 Single cell suspensions

To generate single cell suspensions the spleen was ground through a 70 μ M cell strainer and pelletized for 10 min, at 1200 rpm, and 4°C using the Rotanta 460R, Hettich Centrifuge. Because of the containment of erythrocytes, the cell suspensions of the spleen and the bone marrow needed to be treated with RBC (Red Blood Cell) lysis buffer (eBioscience™) for 3 min at room temperature. RBC lysis was stopped by adding twice the volume of 1 % BCM and subsequent centrifugation (10 min, at 1200 rpm, and 4°C, Rotanta 460R, Hettich Centrifuge). After lysis, all cells were resuspended in 1 % BCM and stored on ice.

6.5 B cell enrichment with MACS purification

To enrich B cells in the single cell suspensions of the spleens of the transgenic mice (see sections 6.3 and 6.4) magnetic cell sorting (MACS; Miltenyi Biotec) was performed following the manufacturer's instructions. Usually, naïve B cells were isolated by the CD43 depletion kit (Miltenyi Biotec). Only for B cell enrichment of aged mice the pan-B cell isolation kit (Miltenyi Biotec) was used, because some old mice exhibited a CD43⁺ B cell population, which would be sorted out by CD43-depletion.

6.6 B cell culture, stimulation, and inhibitor treatment

6.6.1 Short-term stimulation

For short-term stimulation (up to 2 h) B cells could be kept under unsterile conditions. Isolated splenic B cells (see section 6.5) were seeded (3 - 5 x 10⁶ cells in 100 μ l 1 % BCM) in 1.5 ml reaction tubes. To get enough B cells for each sample per experiment, B cells of 2 or 3 mice per genotype were pooled before seeding. Cells were rested at least for 30 min at 37 °C in the heater (Eppendorf; Thermomixer compact) without shaking. After resting, B cells were either directly stimulated or incubated with the different inhibitors (see Table 10) for 1.5 h diluted in 1 % BCM. As solvent control of the inhibitors served DMSO at the highest inhibitor concentration used for each experiment. For stimulation, untreated or inhibitor treated B cells were gently mixed with the different stimuli (see section 0) diluted in pre-heated 1 % BCM. After incubation for the different time points, the reaction was stopped by adding 1 ml ice-cold PBS to the sample, inverting the tube, and storing the sample on ice.

6.6.2 Long-term stimulation with LPS

Long-term stimulation was performed with B cells of DKO and the corresponding control mice. Here, long-term stimulation was defined as a time frame of 1 up to 3 days. Cultivation took place in an incubator (Binder) at 37 °C, 5 % CO₂ and 95 % humidity. B cells were enriched (see section 6.5) under sterile conditions. Cultivation of the different samples took place in round bottom 96-well plates. In each well 5 x 10⁵ cells were seeded in 50 µl 1 % BCM. For each condition and genotype 3 to 5 wells were seeded, which were pooled during harvesting. All samples rested for 30 min in the incubator to establish a resting state upon normothermic conditions (37 °C) after isolating the B cells on ice. To be able to compare the stimulated B cell samples to the unstimulated initial state of the seeded cells, 3 wells per genotype were pooled, washed with ice-cold PBS, stained with fixable Live/Dead staining, fixed and permeabilized and stored at -20 °C (see section 6.8). The residual samples were used for long-term stimulation with LPS. Therefore, the seeded B cells were mixed with 11 µl 1 % BCM, 50 µl LPS (100 µg/ml in 1 % BCM), and 14 µl FCS (fetal calve serum) to increase the FCS concentration of the B cell media to 10 %. Each sample was cautiously mixed by pipetting and incubated for 1 to 3 days depending on the used time points of the experiment. Afterwards, the samples of one condition and genotype were pooled and washed with ice-cold PBS. After fixable Live/Dead staining, fixation and permeabilization, the samples were stained for intracellular FACS together with the unstimulated samples of day 0 (see section 6.8).

6.7 Protein analysis

6.7.1 Protein extraction of whole cell lysates

For protein analyses *ex vivo* isolated B cells or short-term stimulated B cells (6.6.1) were used. For each sample 3 to 5 x 10⁶ cells were used. After resting at 37 °C for 1h or short-time stimulation the cells were washed twice with ice-cold PBS and then centrifuged (Eppendorf; Centrifuge 5424 R; 10 min, 4 °C, 2600 rpm). Cells were lysed by adding 10 µl 2x NP40 lysis buffer to the cell pellet followed by a 20 min incubation on ice. To support cell lysis, samples were vortexed every 5 min for approximately 1 min during NP40 incubation. Subsequently, the samples were centrifuged (15 min, 4 °C, 15000 rpm) to separate the proteins from cell fragments and the DNA. Afterwards, the protein containing supernatant was transferred into a new tube and stored at -80 °C.

6.7.2 Nuclear cytoplasmic fractionation

The NE-PER extraction Kit (Thermo Scientific) was used for nuclear cytoplasmic fractionation of short-time LPS stimulated control and DKO B cells following the manufacturer's instructions. The nuclear cytoplasmic fractionations of RafDKO/LC40, LC40 and the corresponding control B cells were performed by a non-commercial protocol. After B cell isolation (see section 6.5), 2×10^7 B cells were rested in 500 μ l 1 % BCM in a tube in a heater at 37 °C. After washing the cells twice with ice-cold PBS and subsequent centrifugation (Eppendorf; Centrifuge 5424 R; 10 min, 4 °C, 2600 rpm), the cell pellet was dissolved in 100 μ l of buffer A. After incubation for 15 min on ice, 6.75 μ l NP40 (Sigma) was added. To increase the rupture of the cell membrane, the samples were harshly mixed at 4 °C on a vortexer for 5 min. The cytoplasmic fraction was separated from the nuclei and other cell fragments by centrifugation (Eppendorf; Centrifuge 5424 R; 10 min, 4 °C, 15000 rpm). The supernatant containing the cytoplasmic fraction was transferred into a new reaction tube and stored on ice for a short time. The remaining pellet was washed once with 1.5 ml buffer A and subsequently pelleted by centrifugation (5 min, 4 °C, 13000 rpm). The supernatant was discarded and 40 μ l buffer C was added to the pellet. The nuclei were broken by harshly mixing the samples on the vortexer for 30 min at 4 °C. After centrifugation (10 min, 4 °C, 15000 rpm) the supernatant containing the nuclear fraction was transferred into a new reaction tube and was stored on ice for a short time. For long-term storage both fractions were frozen at -80 °C.

6.7.3 Protein quantification

Protein quantification in the nuclear and cytoplasmic fractions was performed in two different ways. Because of the low protein concentrations and the buffer composition, the concentration of the proteins isolated with the NE-PER Kit were measured with the NanoDrop (ND-1000 Spectrophotometer) at 280 nm.

The protein concentrations of whole cell lysates (see section 6.7.1) and nuclear/cytoplasmic fractionations prepared with the "non-commercial" method (see section 6.7.2) were determined using the DC Protein Assay Kit (BioRad) following the manufacturer's instructions. As protein standard, different defined concentrations of bovine serum albumin were used. This method bases on the Bradford Assay measuring the shift of the absorption maximum from 480 nm to 595 nm, induced by protein binding to the added dye.

6.7.4 SDS-PAGE and Western blot

SDS-PAGE

The proteins of the whole cell lysates (see section 6.7.1) and the non-commercially prepared nuclear cytoplasmic fractionations (see section 6.7.2) were separated by SDS-PAGE (sodium dodecyl sulfate polyacrylamide gel electrophoresis) followed by a Western blot analysis. After protein quantification 10 µg to 20 µg protein sample were incubated with 2 x Laemmli buffer and a tenth DTT at 70 °C for 10 min. This led to the denaturation of the proteins, allowing their separation only by the molecular weight. After denaturation, the samples, and a protein marker (PAGE ruler) were loaded onto an acrylamide gel. For most of the proteins 12 % non-commercial gels or 10 % commercial gels (Mini-Protean TGX Protein Gels 10%) were used. Only the detection of Raf-1 and B-Raf was performed with 7.5 % non-commercial gels. All gels contain a stacking and a running gel, which are used to focus and separate the samples, respectively. For gel running the chambers from BioRad (Mini Protean Tetra Cell, Bio Rad) filled with running buffer were used following the manufacturer's instructions. The stacking gel ran at 30 mA until samples passed over to the running gel. Then the power was set to 60 mA for 30 min and then to 90 mA until the 15 kDa band of the marker just left the bottom of the gel.

Western blot

After SDS-PAGE the proteins were transferred to and immobilized on a PVDF membrane (polyvinylidene fluoride; Immobilon-P Transfer Membrane). Prior transfer the PVDF membrane was activated in methanol and equilibrated in distilled water followed by an incubation step in blotting buffer. The proteins were transferred to the membrane by wet blotting in the BioRad chamber (Mini Protean Tetra Cell, Bio Rad) filled with blotting buffer at 80 mA at 4 °C over night.

Blocking and antibody incubation

To prove the protein transfer, the membrane was stained by Ponceau S solution for 1 min followed by washing with deionized water. To avoid unspecific antibody binding to the proteins the membranes were blocked for 1 h at room temperature with a high concentrated protein solution. Thereby, whole cell lysates were blocked with 5 % (w/v) BSA (bovine serum albumin)/TBST (Tris-buffered saline with Tween20). For Lamin B2 and Notch2 detection membranes were incubated in 5 % (w/v) milk/TBST. After blocking, the membranes were incubated with the primary antibodies (see Table 8) diluted in the blocking solution at 4 °C over night. The primary antibody bound specifically to the protein of interest and was recognized HRP (horseradish peroxidase) conjugated secondary antibodies (see

Table 8). The latter were specific for the species dependent Fc-part of the primary antibody. The secondary antibodies were always diluted in 5 % (w/v) milk/TBST and incubated for 2 h at room temperature. After each antibody incubation the membranes were washed three times with TBST.

Development

The specific antibody binding to the protein of interest was detected by chemiluminescence. For this development the membranes were wetted with a freshly mixed ECL-solution according to the manufacturer's instructions. ECL served as a substrate for the HRP. The ECL conversion by HRP led to a light emission, which was either detected by film (Agfa HealthCare) exposition and subsequent film development (Cawomat 2000 IR processor, Ernst Christiansen) or by the Vilber Fusion FX6 Edge imager. By these methods the proteins of interest were depicted as bands. After development, the ECL-solution was removed by washing the membranes three times with TBST. Afterwards, membranes could be dried at room temperature and subsequently stored at 4 °C or the bound antibodies could be removed from the membranes by stripping (see below).

Stripping

Due to the low amounts of protein samples in our experiments, we had to test several proteins of interest on one membrane, consecutively. Proteins with different sizes, e.g. ERK and tubulin, could be detected sequentially without removing the previous antibodies. To detect proteins of a similar size, e.g. ERK and MEK, the membrane had to be stripped in between. This stripping procedure removed the previously bound antibodies. For this purpose, the membranes were incubated with 7.5 ml stripping buffer freshly mixed with 51.5 μ l β -mercaptoethanol for 35 min in a 50 ml reaction tube rotating in a hybridization oven (Mini 10, Thermo Hybaid) at 56 °C. Subsequently, the membranes were washed five times with TBST. Thereafter, the previously described working steps of blocking, antibody incubation, and development were performed.

6.7.5 Western blot quantification

As described above in a Western blot, the proteins of interest were depicted as bands. The width and darkness of the bands represented the amount of protein. The analogous films were scanned (EPSON Expression 1680 Pro Scanner) and quantified using ImageJ/Fiji. The digital images developed by the Fusion FX6 Edge imager were quantified by the Vilber Bio-1D software. To exclude the impact of different loading or blotting of the different samples on one membrane, all quantified values were normalized by divi-

sion through the corresponding values of their inherent loading control. As loading controls, Tubulin, GAPDH or Lamin B2 were used. To calculate the fold induction, the normalized protein amounts of each sample and condition were divided by the mean of the normalized protein amounts of the unstimulated control samples.

6.7.6 Protein Simple WES

DKO mice displayed low amounts of B cells. Therefore, LPS kinetics (see section 6.6.1) with subsequent nuclear cytoplasmic fractionation (see section 6.7.2) led to very low protein amounts, which were not sufficient for a conventional Western blot.

Thus, to detect and quantify different proteins of interest in those samples, WES from Protein Simple was used following the manufacturer's instructions. WES is a fully automated system specialized on a low protein input and a fast data generation. In this system a matrix is constructed within a capillary for size separation of proteins. After separation of the proteins, the proteins are immobilized on the capillary wall by UV radiation. Next, the matrix is removed from the capillary. Afterwards, immunoblotting with primary antibodies and HRP-conjugated secondary antibodies was performed. WES also fully automatically performs the development by chemiluminescence. Using the associated protein simple Compass software, the proteins could be detected and quantified.

For WES the above described primary Western blot antibodies pERK, Tubulin and Lamin B2 were used with deviating dilutions, which will be described in the following (see Table 8). To ensure a correct measurement, the protein concentration must be in a linear regression of the chemiluminescence signal. Therefore, the optimal protein concentration for each antibody was determined by a dilution series (0.03-1.5 $\mu\text{g}/\mu\text{l}$) with a fixed antibody dilution (pERK 1:50; LamB2 1:50; Tub 1:20). Additionally, the used amounts of primary antibodies must lead to a saturated binding on the immobilized proteins. Thus, the antibody dilutions for each determined protein concentration were optimized in a second round of antibody dilution series (1:200 to 1:20). In our case we established the following settings: We used 0.3 $\mu\text{g}/\mu\text{l}$ of the nuclear fraction in combination with the pERK (1:20) and the LamB2 (1:50) antibodies. To detect Tubulin (1:20) 0.3 $\mu\text{g}/\mu\text{l}$ of the cytoplasmic fraction was applied. For pERK (1:20) a protein concentration of 0.5 $\mu\text{g}/\mu\text{l}$ of the cytoplasmic fraction was used. To compare the different WES runs among each other, each run of the WES contained the same sample of anti-IgM stimulated control B cells followed by a nuclear cytoplasmic fractionation with the NE-PER Kit.

6.8 Flow Cytometry (FACS)

Flow cytometry was performed to analyze the cell composition of different organs of the transgenic mice *ex vivo* or the activation and differentiation of B cells upon *in vitro* stimulation. Thereby, different marker proteins for the different cell subsets, for activation, and for differentiation were stained with fluorochrome-coupled antibodies. Only ERK, pERK and its isotype control were stained with primary antibodies and fluorochrome-coupled secondary antibodies. All antibodies and the corresponding dilutions are listed above (see Table 5).

For each staining 5×10^5 to 1×10^6 cells were seeded into one well of a 96-well plate. To remove the B cell media, cells were washed with 150 μ l MACS buffer and pelletized by centrifugation (5 min, 1200 rpm, 4 °C; Rotanta 460-R, Hettich centrifuge). Up to 5 wells of long-term stimulated samples (see section 6.6.2) were pooled during the washing step to have enough cells for FACS staining. The following staining protocols (surface or intracellular staining) depend on the cellular localization of the different marker proteins:

Surface staining

If all the marker proteins used for one staining are localized on the cell surface, the proteins could be directly stained and no fixation and permeabilization was needed. For surface staining the washed cells of one well were mixed with 25 μ l of the antibodies diluted in MACS buffer. After incubation (20 min, in the dark, on ice) cells were washed by adding 150 μ l MACS buffer and subsequent centrifugation (5 min, 1200 rpm, 4 °C; Rotanta 460-R, Hettich centrifuge). Cells were either resuspended in 80–100 μ l of MACS buffer or in a TOPRO-3 dilution (1:40000) to stain dead cells. The resuspended cells were transferred to a FACS tube. Stained cells were kept in the dark on ice until the FACS measurement was performed.

Intracellular staining

For some of the plasmablast marker, e.g. IRF4 and PAX5, but also for pERK, ERK, and its isotype controls, cells needed to be fixed and permeabilized to stain these intracellular proteins. *Ex vivo* isolated cells were highly vital and could directly be fixed by incubating the washed cells 10 min with 2 % PFA (4 % Histofix diluted 1:2 with PBS) at room temperature. Compared to that, long-term stimulated (see section 6.6.2) cell samples contained a lot of dead cells. To be able to exclude these in the following analysis, a live/dead staining was necessary. The live/dead staining was performed prior the fixation and permeabilization of the cells. Therefore, the previously described seeded cells were washed again with PBS to remove the MACS buffer. MACS buffer contains BSA, which would

trap and weaken the live/dead staining. After washing, cells were stained in 75 μ l live/dead stain (dilution 1:1000 in PBS) for 5 min on ice in the dark. Thereafter, 75 μ l 4 % PFA was added to each sample to fix the live/dead stained cells. Cells were incubated for 10 min at room temperature in the dark. Afterwards cells were centrifuged (5 min, 1200 rpm, 4 °C; Rotanta 460-R, Hettich centrifuge) and permeabilized by resuspending the cell pellets in 100 μ l ice-cold methanol. These permeabilized cells could either be directly used for staining or could be covered with a foil and then stored up to one week in the freezer (-20 °C).

To remove the methanol, cells were consecutively washed with PBS and MACS buffer. Next, cells were stained with 30-80 μ l (depending on pellet size) of a mixture of the directly fluorochrome coupled antibodies and the primary antibodies for 1 h at room temperature in the dark. After washing the cells with MACS buffer, cells were incubated with 30-80 μ l of the secondary antibody for 30 min at room temperature in the dark. Then cells were washed with MACS buffer and transferred into FACS tubes. Until the FACS measurement was performed, the stained cells were kept on ice in the dark.

FACS measurement

All stained cells were measured using the FACS Calibur or the LSR Fortessa (Beckton Dickinson). To evaluate the data the FlowJo10 Software was used. For quantification of the expression of proteins by FACS either the Median fluorescent intensity (MFI) is depicted or the fold induction of the MFI in comparison to controls. To calculate the fold induction the MFI of the protein of interest of each sample and condition were divided by the mean of the MFIs of the protein of interest of the unstimulated control samples.

6.9 ELISA

Enzyme linked immunosorbent assay (ELISA) was used to detect NP-specific antibodies in the sera (see Section 6.3) of immunized mice and their controls (see Section 6.2). As described above the predominant isotypes of the TI type 2 reaction, IgM and IgG3, were analyzed.

For ELISA 96-well plates (NUNCTM plates, Nunc) were coated with 5 μ g/ml NP13-BSA in carbonate buffer (50 μ l/well) over night at 4 °C. As washing solution, PBS was used for the IgG3-ELISA and 0.05 % (v/v) PBS-Tween for the IgM-ELISA. After washing the plates three times with 200 μ l of washing solution per well, the plates were blocked by incubating each well with 50 μ l of blocking buffer at room temperature. IgG3-plates were blocked for 1 h with 1 % milk/PBS and IgM-plates for 2 h with 5 % milk/PBS. To avoid a signal saturation and to ensure a correct calculation of the relative units, the serum incubation was performed with a dilution series. Additionally, an internal standard composed

of pooled sera of NP-Ficoll immunized mice was carried along next to the individual samples. Thus, the sera and the standard were diluted 1:10 in 1 % milk/PBS for the starting dilutions. Then these starting dilutions were serially diluted 1:2 in 1 % milk/PBS for eight times. After an incubation for 1 h at room temperature, unspecifically bound antibodies of the sera were removed by washing the plates three times with the corresponding washing solution. The NP-specific antibodies were then detected by isotype specific antibodies listed in Table 7 (diluted in 1 % milk/PBS). The IgG3 NP-specific serum antibodies were bound by consecutive incubation of the plates with a biotinylated anti-IgG3 specific antibody (50 μ l/well; 30 min; room temperature) and HRP-conjugated streptavidin (50 μ l/well; 1 h; room temperature). By any incubation the plates were washed three times with PBS. For linking the HRP enzyme to NP-specific IgM serum antibodies, directly HRP-coupled anti-IgM antibodies (50 μ l/well; 1 h; room temperature) were used. After their incubation, these plates were washed three times with 0.05 % PBS-Tween. Both the IgG3- and the IgM-ELISA were developed by adding 100 μ l o-phenylenediamine (P-7288, Sigma) in ELISA substrate buffer per well. The substrate reaction started right away. Thus, after slightly shaking, the plates were directly measured by the ELISA reader (Photometer infinite F200 Pro, Tecan). The ELISA reader measured the optical density (OD) of the product at a wavelength of 405 nm. As a reference the OD 620 nm was used. The amount of product and in the following the OD 405 nm correspond to the amounts of NP-specific antibodies in the sera of the immunized and unimmunized mice.

6.10 ELISpot Assay

With the Enzyme Linked Immuno Spot (ELISpot) Assay antibody secreting cells (ASCs) of immunized and unimmunized mice (see section 6.2) were detected *in vitro*. Because the TI type 2 reaction mainly causes an IgM and IgG3 immune response (319), these NP-specific ASCs were determined isotype specifically.

Because vital cells were cultivated in this assay for 24 h, the coating, blocking and cell cultivation had to be proceeded under sterile conditions. For the ELISpot special membrane plates (MultiScreen HTS, 96-well, MCE-membrane, Merck Millipore) were coated with 50 μ l of sterile filtered 25 μ g/ml NP13-BSA in carbonate buffer. For each sample and antibody isotype triplicates were coated. One additional well per sample and isotype was coated with NP13-BSA, which was later used as a media control. As a background control one well per sample and isotype was coated with sterile filtered 25 μ g/ml BSA in carbonate buffer.

After an incubation over night at 4 °C the unbound NP13-BSA and BSA was removed by washing the plates three times with PBS. Afterwards, the plates were blocked with 10 % BCM for at least 2 h at 37 °C. For IgM ASC detection, 5×10^5 splenocytes/well were

seeded in 10 % BCM, whereas 1×10^6 splenocytes/well were applied to analyze IgG3 ASCs. As a media control one NP13-coated well per sample was incubated with 10 % BCM instead of splenocytes. The splenocytes were cultivated for 24 h in the incubator (Binder; 37 °C, 5 % CO₂, 95 % humidity). During that time the ASCs produce antibodies. The NP-specific ones would bind to the NP13-coated membrane. To remove the splenocytes and the unspecifically bound antibodies, the plates were washed six times with 0.025 % PBS/Tween. The NP-specific antibodies were then recognized by biotinylated anti-IgM and anti-IgG3 antibodies diluted in 1 % PBS/BSA (see Table 6) incubated for 2 h at 37 °C in the incubator. After that, the ELISpot plates were washed six times with 0.025 % PBS/Tween. After incubation with Avidin-HRP diluted in 1 % PBS/BSA (see Table 6) for 45 min at room temperature, the plates were washed three times with 0.025 % PBS/Tween and subsequently three times with PBS. To develop the spots 3,3'-Diaminobenzidin peroxidase-substrate (0.7 mg/ml, Sigma-Aldrich) was used in combination with UREA H₂O₂ (2.0 mg/ml, Sigma-Aldrich). Both tablets were solved in 5 ml of distilled water and added to the plates (50 µl/well). The incubation time until the spots become visible was about 10 min. The reaction was stopped by adding distilled water to each well. Afterwards, the plates were washed intensively with deionized water. Afterwards the plates were fully dried over night, the ImmunoSpot Series 5 UV Analyzer (CTL Europe) was used to analyze and count the spots.

6.11 RNA-Sequencing

To investigate differences in the B cell transcriptome of RafDKO//LC40 and LC40 mice, RNA sequencing (RNA-Seq) analyses were performed. B cells were isolated by CD43-depletion (see section 6.5). 1×10^7 B cells were resuspended in 100 µl 1 % BCM. After adding 900 µl Trizol the samples were immediately mixed for 1 min by the vortexer. Afterwards the samples were incubated at room temperature for 5 min. After incubation, the samples were directly frozen using dry ice and stored at -80 °C.

In cooperation with the research group Laboratory for Functional Genome Analysis (LA-FUGA; LMU Munich) of Dr. Helmut Blum the RNA isolation and the RNA sequencing (RNA-Seq) was performed. 75 µg of each isolated RNA were inserted to construct a strand-specific rRNA-depleted cDNA-library applying the Encore® complete RNASeq Library system (NuGen Technologies, Inc) in the Illumina HiSeq1500. The RNA-Seq of the cDNA library fragments resulted in the read counts.

The data pre-processing including general read statistic, count normalization, and quality control were performed in cooperation with Dr. Sonja Grath, Head of the Research group "Molecular Evolution and Functional Bioinformatics", LMU Munich using the software R (version 3.5.1). Alignment, normalization, and subsequent statistical analyses led to the

generation of different values, important for the interpretation of the RNA-Seq results. The adjusted p-value (p_{adj}) corrects the statistical p-value for the False Discovery Rate, which reflects the probability that the initial hypothesis is incorrectly rejected. Additionally, the difference of a gene expression between the two genotypes (LC40 and RafDKO/LC40) was represented by the log₂fold change. Thereby, the fold induction of the gene expression in LC40 in comparison to RafDKO/LC40 is logarithmized to the base of 2. For analyzing the significantly differentially expressed genes the cutoffs were set to an adjusted p-value lower than 0.05 and a log₂fold change greater than or equal to 0.585 or smaller or equal to -0.585. The latter refers to an actual 1.5 fold change in the gene expression. All significantly differentially expressed genes were visualized in a heatmap using the R software. To analyze the biological processes regarding the direction of the gene regulation (up- or downregulated) the online platform PANTHER (Protein Analysis Through Evolutionary Relationships, <http://pantherdb.org>) (225), was used.

The Top 25 protein coding genes refer to the 25 differentially protein coding genes with the highest adjusted p-values based on the alignment, normalization, and subsequent statistical analyses of Daniel Strobl, Institute of Computational Biology, Helmholtz Center Munich using R (version 3.5.1). This statistical evaluation of the RNA-Seq data by Daniel Strobl also established the basis of the ranked list of differentially expressed genes between LC40 and RafDKO/LC40 B cells, which was used in the Gene Set Enrichment Analyses (GSEA). The GSEA allows the comparison of a defined gene set to the ranked list of the detected genes between LC40 and RafDKO/LC40 B cells. The gene sets were generated using the ImmGen Population Comparison Tool based on microarray data ([http://rstats.immgen.org/Population Comparison/index.html](http://rstats.immgen.org/Population%20Comparison/index.html)) (226) for the MZ B and Fo B gene sets (see Suppl. Table 4-5), the RNA sequencing data from Lechner et al. (54) for the different Notch2 regulated gene sets (see Suppl. Table 6-9), and the micro-array data of B cells of transgenic BAFF-overexpressing, TRAF2KO or TRAF3KO of Gardam et al. (48) for the different gene sets of the non-canonical NF κ B pathway (see Suppl. Table 10-15). The GSEA software 4.1.0 examined every gene of the gene sets for its position within the ranked gene list of LC40 and RafDKO/LC40, thereby generating the normalized enrichment score (NES). If there is a match, an enrichment score is determined regarding the position in the ranked gene list. If there is no match for genes of the gene sets within the ranked gene list, this reduces the enrichment score. The enrichment score is then normalized for variation in the gene set size (NES). In our case a positive NES reflects an enrichment in the beginning of the ranked gene list representing genes highly expressed in LC40 B cells, while a negative NES indicated an enrichment of genes in the RafDKO/LC40. A significant enrichment is also defined by a nominal p-value below 1 % and a False discovery q-value below 25 %. The bases for the GSEA (gene sets,

ranked gene list, software skills) were established in close collaboration with Dr. Lothar Strobl, a member of our own research group.

6.12 Statistics

All experiments were performed unblinded. The statistics were all calculated using the Prism software version 9 (Graph Pad). First the distribution and equal variance was analyzed. If samples followed a log-normal distribution, the corresponding data set was logarithmically transformed prior to further evaluations. Additionally, the means and standard deviations (SDs) were analyzed. The distribution of the data sets and the exact statistical tests were indicated in the legend of the Figures and Tables. * $p \leq 0.05$, ** $p \leq 0.01$, *** $p \leq 0.001$, and **** $p \leq 0.0001$. Furthermore, the statistical plots were drawn up with the prism software.

References

1. Parkin J, Cohen B. An overview of the immune system. Vol. 357, *Lancet*. Elsevier B.V.; 2001. p. 1777–89.
2. Murphy KM. *Janeway's Immunobiology*. 8th ed. New York: Garland Science, Taylor & Francis Group; 2012.
3. Chaplin DD. Overview of the immune response. *Journal of Allergy and Clinical Immunology*. 2010 Feb;125(2 SUPPL. 2).
4. Parker DC. T CELL-DEPENDENT B CELL ACTIVATION. *Annu Rev Immunol*. 1993;11:331–60.
5. Allman D, Wilmore JR, Gaudette BT. The continuing story of T-cell independent antibodies. *Immunol Rev*. 2019;288(1):128–35.
6. Obukhanych T V., Nussenzweig MC. T-independent type II immune responses generate memory B cells. *Journal of Experimental Medicine*. 2006;203(2):305–10.
7. Mond JJ, Lees A, Ord C, Snapper M. T CELL-INDEPENDENT ANTIGENS TYPE 2 [Internet]. Vol. 13, *Annu. Rev. Immunol*. 1995. Available from: www.annualreviews.org
8. Martin F, Kearney JF. Marginal-zone B cells. Vol. 2, *Nature Reviews Immunology*. 2002. p. 323–35.
9. Stall AM, Wells SM, Lam KP. B-1 cells: Unique origins and functions. *Semin Immunol*. 1996;8(1):45–59.
10. Montecino-Rodriguez E, Dorshkind K. B-1 B Cell Development in the Fetus and Adult. *Immunity*. 2012;36(1):13–21.
11. Pillai S, Cariappa A. The follicular versus marginal zone B lymphocyte cell fate decision. Vol. 9, *Nature Reviews Immunology*. 2009. p. 767–77.
12. Cerutti A, Cols M, Puga I. Marginal zone B cells: Virtues of innate-like antibody-producing lymphocytes. Vol. 13, *Nature Reviews Immunology*. 2013. p. 118–32.
13. Allman D, Pillai S. Peripheral B cell subsets. Vol. 20, *Current Opinion in Immunology*. 2008. p. 149–57.
14. Srivastava B, Quinn WJ, Hazard K, Erikson J, Allman D. Characterization of marginal zone B cell precursors. *Journal of Experimental Medicine*. 2005;202(9):1225–34.
15. Cinamon G, Zachariah MA, Lam OM, Foss FW, Cyster JG. Follicular shuttling of marginal zone B cells facilitates antigen transport. *Nat Immunol*. 2008;9(1):54–62.
16. Meffre E, Casellas R, Nussenzweig MC. Antibody regulation of B cell development. *Nat Immunol*. 2000;1(5):379–85.
17. Treanor B. B-cell receptor: From resting state to activate. *Immunology*. 2012;136(1):21–7.
18. Hardy RR, Hayakawa K. B cell development pathways. Vol. 19, *Annual Review of Immunology*. 2001. p. 595–621.
19. Cambier JC, Gauld SB, Merrell KT, Vilen BJ. B-cell anergy: From transgenic models to naturally occurring anergic B cells? *Nat Rev Immunol*. 2007;7(8):633–43.

20. Winkler TH, Martensson IL. The role of the pre-b cell receptor in b cell development, repertoire selection, and tolerance. *Front Immunol.* 2018;9(NOV):1–10.
21. Vettermann C, Schlissel MS. Allelic exclusion of immunoglobulin genes: Models and mechanisms. *Immunol Rev.* 2010;237(1):22–42.
22. Levin-Klein R, Bergman Y. Epigenetic regulation of monoallelic rearrangement (allelic exclusion) of antigen receptor genes. *Front Immunol.* 2014;5(DEC):1–6.
23. Grawunder U, Leu TMJ, Schatz DG, Werner A, Rolink AG, Melchers F, et al. Down-regulation of RAG1 and RAG2 gene expression in PreB cells after functional immunoglobulin heavy chain rearrangement. *Immunity.* 1995;3(5):601–8.
24. Akamatsu Y, Oettinger MA. Distinct Roles of RAG1 and RAG2 in Binding the V(D)J Recombination Signal Sequences. *Mol Cell Biol.* 1998;18(8):4670–8.
25. Clark MR, Mandal M, Ochiai K, Singh H. Orchestrating B cell lymphopoiesis through interplay of IL-7 receptor and pre-B cell receptor signalling. *Nat Rev Immunol.* 2014;14(2):69–80.
26. Allman D, Lindsley RC, DeMuth W, Rudd K, Shinton SA, Hardy RR. Resolution of Three Nonproliferative Immature Splenic B Cell Subsets Reveals Multiple Selection Points During Peripheral B Cell Maturation. *The Journal of Immunology.* 2001 Dec 15;167(12):6834–40.
27. Chung JB, Sater RA, Fields ML, Erikson J, Monroe JG. CD23 defines two distinct subsets of immature B cells which differ in their responses to T cell help signals. *Int Immunol.* 2002;14(2):157–66.
28. Kraus M, Alimzhanov MB, Rajewsky N, Rajewsky K. Survival of resting mature B lymphocytes depends on BCR signaling via the Ig α / β heterodimer. *Cell.* 2004;117(6):787–800.
29. Niiro H, Clark EA. Regulation of B-cell fate by antigen-receptor signals. Vol. 2, *Nature Reviews Immunology.* 2002. p. 945–56.
30. Teague BN, Pan Y, Mudd PA, Nakken B, Zhang Q, Szodoray P, et al. Cutting Edge: Transitional T3 B Cells Do Not Give Rise to Mature B Cells, Have Undergone Selection, and Are Reduced in Murine Lupus. *The Journal of Immunology.* 2007;178(12):7511–5.
31. Liubchenko GA, Appleberry HC, Holers VM, Banda NK, Willis VC, Lyubchenko T. Potentially autoreactive naturally occurring transitional T3 B lymphocytes exhibit a unique signaling profile. *J Autoimmun.* 2012 Jun;38(4):293–303.
32. Saito T, Chiba S, Ichikawa M, Kunisato A, Asai T, Shimizu K, et al. Notch2 Is Preferentially Expressed in Mature B Cells and Indispensable for Marginal Zone B Lineage Development. Vol. 18, *Immunity.* 2003.
33. Hampel F, Ehrenberg S, Hojer C, Draeseke A, Marschall-Schröter G, Kühn R, et al. CD19-independent instruction of murine marginal zone B-cell development by constitutive Notch2 signaling. *Blood.* 2011 Dec 8;118(24):6321–31.
34. Radtke F, Fasnacht N, MacDonald HR. Notch Signaling in the Immune System. *Immunity.* 2010;32(1):14–27.
35. Hayden M, Ghosh S. Signaling to NF- κ B. *Genes Dev.* 2004;18(18):2195–224.

36. Liu T, Zhang L, Joo D, Sun SC. NF- κ B signaling in inflammation. *Signal Transduct Target Ther.* 2017;2(March).
37. Sun SC, Chang JH, Jin J. Regulation of nuclear factor- κ B in autoimmunity. Vol. 34, *Trends in Immunology.* 2013. p. 282–9.
38. Baeuerle PA, Henkel T. FUNCTION AND ACTIVATION OF NF- κ B IN THE IMMUNE SYSTEM [Internet]. Vol. 12, *Annu. Rev. Immunol.* 1994. Available from: www.annualreviews.org
39. Kamata H, Tsuchiya Y, Asano T. I κ B β is a positive and negative regulator of NF- κ B activity during inflammation. *Cell Res.* 2010;20(11):1178–80.
40. Rickert RC, Jellusova J, Miletic A V. Signaling by the tumor necrosis factor receptor superfamily in B-cell biology and disease. Vol. 244, *Immunological Reviews.* 2011. p. 115–33.
41. Senftleben U, Cao Y, Xiao G, Greten FR, Krähn G, Bonizzi G, et al. Activation by IKK α of a second, evolutionary conserved, NF- κ B signaling pathway. *Science* (1979) [Internet]. 2001;293(5534):1495–9. Available from: <https://www.science.org>
42. Sasaki Y, Derudder E, Hobeika E, Pelanda R, Reth M, Rajewsky K, et al. Canonical NF- κ B Activity, Dispensable for B Cell Development, Replaces BAFF-Receptor Signals and Promotes B Cell Proliferation upon Activation. *Immunity.* 2006;24(6):729–39.
43. Siebenlist U, Brown K, Claudio E. Control of lymphocyte development by nuclear factor- κ B. *Nat Rev Immunol* [Internet]. 2005;5(6):435–45. Available from: <https://doi.org/10.1038/nri1629>
44. Bonizzi G, Karin M. The two NF- κ B activation pathways and their role in innate and adaptive immunity. Vol. 25, *Trends in Immunology.* 2004. p. 280–8.
45. Ghosh S, Karin M. Missing pieces in the NF- κ B puzzle. *Cell.* 2002;109(2 SUPPL. 1):81–96.
46. Grech AP, Amesbury M, Chan T, Gardam S, Basten A, Brink R. TRAF2 differentially regulates the canonical and noncanonical pathways of NF- κ B activation in mature B cells. *Immunity.* 2004;21(5):629–42.
47. Gardam S, Brink R. Non-canonical NF- κ B signaling initiated by BAFF influences B cell biology at multiple junctures. Vol. 4, *Frontiers in Immunology.* Frontiers Media S.A.; 2013.
48. Gardam S, Sierro F, Basten A, Mackay F, Brink R. TRAF2 and TRAF3 Signal Adapters Act Cooperatively to Control the Maturation and Survival Signals Delivered to B Cells by the BAFF Receptor. *Immunity.* 2008 Mar 14;28(3):391–401.
49. Dejardin E, Droin NM, Delhase M, Haas E, Cao Y, Makris C, et al. The Lymphotoxin-Receptor Induces Different Patterns of Gene Expression via Two NF- κ B Pathways. *Immunity.* 2002;17:525–35.
50. Xiao G, Harhaj EW, Sun SC. NF- κ B-Inducing Kinase Regulates the Processing of NF- κ B2 p100. *Mol Cell.* 2001;7:401–9.
51. Hostager BS, Bishop GA. CD40-mediated activation of the NF- κ B2 pathway. *Front Immunol.* 2013;4(NOV):2–5.

52. Hömig-Hölzel C, Hojer C, Rastelli J, Casola S, Strobl LJ, Müller W, et al. Constitutive CD40 signaling in B cells selectively activates the noncanonical NF- κ B pathway and promotes lymphomagenesis. *J Exp Med* [Internet]. 2008;205(6):1317–29. Available from: <http://www.jem.org/lookup/doi/10.1084/jem.20080238>
53. Li Z, Wang H, Xue L, Shin DM, Roopenian D, Xu W, et al. E μ -BCL10 mice exhibit constitutive activation of both canonical and noncanonical NF- κ B pathways generating marginal zone (MZ) B-cell expansion as a precursor to splenic MZ lymphoma. *Blood*. 2009;114(19):4158–68.
54. Lechner M, Engleitner T, Babushku T, Schmidt-Supprian M, Rad R, Strobl LJ, et al. Notch2-mediated plasticity between marginal zone and follicular B cells. *Nat Commun*. 2021 Dec 1;12(1).
55. Oracki SA, Walker JA, Hibbs ML, Corcoran LM, Tarlinton DM. Plasma cell development and survival. Vol. 237, *Immunological Reviews*. 2010. p. 140–59.
56. Smith' KGC, Hewitson' TD, Nossal' GJ V, Tarlinton' DM, Hall E. The phenotype and fate of the antibody-forming cells of the splenic foci. Vol. 26, *Eur. J. Immunol*. 1996.
57. MacLennan ICM, Toellner KM, Cunningham AF, Serre K, Sze DMY, Zúñiga E, et al. Extrafollicular antibody responses. Vol. 194, *Immunological Reviews*. 2003. p. 8–18.
58. Shapiro-Shelef M, Calame KC. Regulation of plasma-cell development. Vol. 5, *Nature Reviews Immunology*. 2005. p. 230–42.
59. Scandella E, Fink K, Junt T, Senn BM, Lattmann E, Förster R, et al. Dendritic Cell-Independent B Cell Activation During Acute Virus Infection: A Role for Early CCR7-Driven B-T Helper Cell Collaboration. *The Journal of Immunology*. 2007;178(3):1468–76.
60. Garside P, Ingulli E, Merica RR, Johnson JG, Noelle RJ, Jenkins MK. Visualization of specific B and T lymphocyte interactions in the lymph node. *Science* (1979). 1998;281(5373):96–9.
61. Roco JA, Mesin L, Binder SC, Nefzger C, Gonzalez-Figueroa P, Canete PF, et al. Class-Switch Recombination Occurs Infrequently in Germinal Centers. *Immunity*. 2019;51(2):337-350.e7.
62. Muramatsu M, Kazuo K, Sidonia F, Shuichi Y, Yoichi S, Tasuku H. Class Switch Recombination and Hypermutation Require Activation-Induced Cytidine Deaminase (AID), a Potential RNA Editing Enzyme. *Cell*. 2000;102(5):553–63.
63. Teng G, Papavasiliou FN. Immunoglobulin somatic hypermutation. Vol. 41, *Annual Review of Genetics*. 2007. p. 107–20.
64. Dvorscek AR, Mckenzie CI, Robinson MJ, Ding Z, Pitt C, O'donnell K, et al. IL-21 has a critical role in establishing germinal centers by amplifying early B cell proliferation. *EMBO Rep*. 2022;23.
65. Vinuesa CG, Sanz Í, Cook MC. Dysregulation of germinal centres in autoimmune disease. Vol. 9, *Nature Reviews Immunology*. 2009. p. 845–57.
66. Klein U, Dalla-Favera R. Germinal centres: Role in B-cell physiology and malignancy. Vol. 8, *Nature Reviews Immunology*. 2008. p. 22–33.

67. Tarlinton DM, Smith KGC. Dissecting affinity maturation: A model explaining selection of antibody-forming cells and memory B cells in the germinal centre. Vol. 21, *Immunology Today*. 2000. p. 436–41.
68. Allen CD, Okada T, Cyster JG. Germinal Center Organization and Cellular Dynamics Role of the GC in Antibody Responses. *Immunity*. 2008;27(2):190–202.
69. Elgueta R, Marks E, Nowak E, Menezes S, Benson M, Raman VS, et al. CCR6-Dependent Positioning of Memory B Cells Is Essential for Their Ability To Mount a Recall Response to Antigen. *The Journal of Immunology*. 2015;194(2):505–13.
70. Suan D, Sundling C, Brink R. Plasma cell and memory B cell differentiation from the germinal center. Vol. 45, *Current Opinion in Immunology*. Elsevier Ltd; 2017. p. 97–102.
71. Nutt SL, Vambrie S, Steinlein P, Kozmik Z, Rolink A, Weith A, et al. Independent regulation of the two Pax5 alleles during B-cell development. *Nat Genet*. 1999;21(4):390–5.
72. Reimold AM, Ponath PD, Li YS, Hardy RR, David CS, Strominger JL, et al. Transcription factor B cell lineage-specific activator protein regulates the gene for human X-box binding protein 1. *Journal of Experimental Medicine*. 1996;183(2):393–401.
73. Delogu A, Schebesta A, Sun Q, Aschenbrenner K, Perlot T, Busslinger M. Gene repression by Pax5 in B cells is essential for blood cell homeostasis and is reversed in plasma cells. *Immunity*. 2006;24(3):269–81.
74. Kallies A, Hasbold J, Fairfax K, Pridans C, Emslie D, McKenzie BS, et al. Initiation of Plasma-Cell Differentiation Is Independent of the Transcription Factor Blimp-1. *Immunity*. 2007;26(5):555–66.
75. Lin KI, Angelin-Duclos C, Kuo TC, Calame K. Blimp-1-Dependent Repression of Pax-5 Is Required for Differentiation of B Cells to Immunoglobulin M-Secreting Plasma Cells. *Mol Cell Biol*. 2002;22(13):4771–80.
76. Shaffer AL, Shapiro-Shelef M, Iwakoshi NN, Lee AH, Qian SB, Zhao H, et al. XBP1, downstream of Blimp-1, expands the secretory apparatus and other organelles, and increases protein synthesis in plasma cell differentiation. *Immunity*. 2004;21(1):81–93.
77. Kallies A, Hasbold J, Tarlinton DM, Dietrich W, Corcoran LM, Hodgkin PD, et al. Plasma Cell Ontogeny Defined by Quantitative Changes in Blimp-1 Expression. *The Journal of Experimental Medicine*. 2004;200(8).
78. Sciammas R, Shaffer AL, Schatz JH, Zhao H, Staudt LM, Singh H. Graded Expression of Interferon Regulatory Factor-4 Coordinates Isotype Switching with Plasma Cell Differentiation. *Immunity*. 2006;25(2):225–36.
79. Sanchez M, Misulovin Z, Burkhardt AL, Mahajan S, Costa T, Franke R, et al. Signal transduction by immunoglobulin is mediated through Ig α and Ig β . *Journal of Experimental Medicine*. 1993;178(3):1049–55.
80. Kurosaki T. Genetic Analysis of B Cell Antigen Receptor Signaling. *Annu Rev Immunol*. 1999;17(1):555–92.

81. Kurosaki BT, Takata M, Yamanashi Y, Inazu T, Taniguchi IIT, Yamamoto IT, et al. Syk Activation by the Src-family Tyrosine Kinase in the B Cell Receptor Signaling. *Journal of Experimental Medicine*. 1994;179(May):0–4.
82. Fu C, Turck CW, Kurosaki T, Chan AC. BLNK: A central linker protein in B cell activation. *Immunity*. 1998;9(1):93–103.
83. Wienands J, Schweikert J, Wollscheid B, Jumaa H, Nielsen PJ, Reth M. SLP-65: A new signaling component in B lymphocytes which requires expression of the antigen receptor for phosphorylation. *Journal of Experimental Medicine*. 1998;188(4):791–5.
84. Crespo P, Schuebel KE, Ostrom AA. activation of Rac-1 GDP / GTP exchange by the vav proto-oncogene product. *Nature*. 1997;385:169–72.
85. Dal Porto JM, Gauld SB, Merrell KT, Mills D, Pugh-Bernard AE, Cambier J. B cell antigen receptor signaling 101. *Mol Immunol*. 2004;41(6–7):599–613.
86. Pearson G, Robinson F, Gibson TB, Xu BE, Karandikar M, Berman K, et al. Mitogen-Activated Protein (MAP) Kinase Pathways: Regulation and Physiological Functions*. *Endocr Rev* [Internet]. 2001;22(2):153–83. Available from: <https://academic.oup.com/edrv/article/22/2/153/2423864>
87. Philip Cohen. The search for physiological substrates of MAP and SAP kinases in mammalian cells. *Trends Cell Biol*. 1997;8924(97):353–61.
88. Ishiai M, Kurosaki M, Pappu R, Okawa K, Ronko I, Chong F, et al. BLNK required for coupling syk to PLC γ 2 and rac1-JNK in B cells. *Immunity*. 1999;10(1):117–25.
89. Cambier JC, Pleiman CM, Clark MR. Signal Transduction by the B Cell Antigen Receptor. *Annu Rev Immunol*. 1994;12:457–86.
90. DeFranco AL. The complexity of signaling pathways activated by the BCR. *Curr Opin Immunol*. 1997;9(3):296–308.
91. Jiang A, Craxton A, Kurosaki T, Clark EA. Different protein tyrosine kinases are required for B cell antigen receptor-mediated activation of extracellular signal-regulated kinase, c-Jun NH₂-terminal kinase 1, and p38 mitogen-activated protein kinase. *Journal of Experimental Medicine*. 1998;188(7):1297–306.
92. Shinohara H, Yasuda T, Aiba Y, Sanjo H, Hamadate M, Watarai H, et al. PKC β regulates BCR-mediated IKK activation by facilitating the interaction between TAK1 and CARMA1. *Journal of Experimental Medicine*. 2005;202(10):1423–31.
93. Tedder TF, Inaoki M, Sato S. The CD19-CD21 Complex Regulates Signal Review Transduction Thresholds Governing Humoral Immunity and Autoimmunity. Vol. 6, *Immunity*. 1997.
94. Srinivasan L, Sasaki Y, Calado DP, Zhang B, Paik JH, DePinho RA, et al. PI3 Kinase signals BCR dependent mature B cell survival. *Cell*. 2009;139(3):573–86.
95. Gruss H, Duyster J, Herrmann F. Structural and biological features of the TNF receptor and TNF ligand superfamilies : Interactive signals in the pathobiology of Hodgkin ' s disease. *Annals of Oncology*. 1996;7:19–26.
96. Dallman C, Johnson PWM, Packham G. Differential regulation of cell survival by CD40. Vol. 8, *Apoptosis*. 2003.
97. Harnett MM. CD40: a growing cytoplasmic tale. *Sci STKE*. 2004;237.

98. Kawabe T, Naka T, Yoshida K. The Immune Responses in CD40-Deficient Mice: Impaired Immunoglobulin Class Switching and Germinal Center Formation. *Immunity*. 1994;1:167–78.
99. Banchereau J, Blanchard D, Galizzi JP, Kooten C van, Rousset F, Saeland S, et al. The CD40 Antigen And Its Ligand. *Annu Rev Immunol*. 1994;12:881–922.
100. Elgueta R, Benson MJ, De Vries VC, Wasiuk A, Guo Y, Noelle RJ. Molecular mechanism and function of CD40/CD40L engagement in the immune system. *Immunol Rev*. 2009;229(1):152–72.
101. Bishop GA, Hostager BS. The CD40-CD154 interaction in B cell-T cell liaisons. Vol. 14, *Cytokine and Growth Factor Reviews*. Elsevier BV; 2003. p. 297–309.
102. Ren CL, Morio T, Fu SM, Geha RS. Signal Transduction via CD40 Involves Activation of lyn kinase and Phosphatidylinositol-3-kinase, and Phosphorylation of Phospholipase Cgamma2. *J Exp Med*. 1994;179(February):673–80.
103. Vidalain PO, Azocar O, Servet-Delprat C, Rabourdin-Combe C, Gerlier D, Manié S. CD40 signaling in human dendritic cells is initiated within membrane rafts. *EMBO Journal*. 2000;19(13):3304–13.
104. Kashiwada BM, Shirakata Y, Inoue J ichiro, Yamamoto T, Nagaoka H, Takemori T. Tumor Necrosis Factor Receptor-associated Factor 6 (TRAF6) Stimulates Extracellular Signal-regulated Kinase (ERK) Activity in CD40 Signaling Along a Ras-independent Pathway. *J Exp Med*. 1998;187(2):237–44.
105. Nair A, Chakraborty S, Banerji LA, Srivastava A, Navare C, Saha B. Ras isoforms: Signaling specificities in CD40 pathway. *Cell Communication and Signaling*. 2020;18(1):1–12.
106. Gulbins E, Brenner B, Schlottmann K, Koppenhoefer U, Linderkamp O, Coggeshall KM, et al. Activation of the Ras signaling pathway by the CD40 receptor. *The Journal of Immunology [Internet]*. 1996 Oct 1;157(7):2844 LP – 2850. Available from: <http://www.jimmunol.org/content/157/7/2844.abstract>
107. Hojer C, Frankenberger S, Strobl LJ, Feicht S, Djermanovic K, Jagdhuber F, et al. B-cell expansion and lymphomagenesis induced by chronic CD40 signaling is strictly dependent on CD19. *Cancer Res*. 2014;74(16):4318–28.
108. Gallagher E, Enzler T, Matsuzawa A, Anzelon-Mills A, Otero D, Holzer R, et al. Kinase MEKK1 is required for CD40-dependent activation of the kinases Jnk and p38, germinal center formation, B cell proliferation and antibody production. *Nat Immunol*. 2007;8(1):57–63.
109. Hanissian SH, Geha RS. Jak3 Is Associated with CD40 and Is Critical for CD40 Induction of Gene Expression in B Cells. Vol. 6, *Immunity*. 1997.
110. Bishop GA. The multifaceted roles of TRAFs in the regulation of B-cell function. *Nat Rev Immunol*. 2004;4(10):775–86.
111. Iwasaki A, Medzhitov R. Control of adaptive immunity by the innate immune system. *Nat Immunol*. 2015;16(4):343–53.
112. Lu YC, Yeh WC, Ohashi PS. LPS/TLR4 signal transduction pathway. *Cytokine*. 2008;42(2):145–51.

113. Peng SL. Signaling in B cells via Toll-like receptors. Vol. 17, *Current Opinion in Immunology*. 2005. p. 230–6.
114. Schweighoffer E, Nys J, Vanes L, Smithers N, Tybulewicz VLJ. TLR4 signals in B lymphocytes are transduced via the B cell antigen receptor and SYK. *J Exp Med* [Internet]. 2017;214(5):1269–80. Available from: <http://www.jem.org/lookup/doi/10.1084/jem.20161117>
115. Kawasaki T, Kawai T. Toll-like receptor signaling pathways. *Front Immunol*. 2014;5(SEP):1–8.
116. Häcker H, Tseng PH, Karin M. Expanding TRAF function: TRAF3 as a tri-faced immune regulator. *Nat Rev Immunol* [Internet]. 2011;11(7):457–68. Available from: <http://dx.doi.org/10.1038/nri2998>
117. Ciesielska A, Matyjek M, Kwiatkowska K. TLR4 and CD14 trafficking and its influence on LPS-induced pro-inflammatory signaling. *Cellular and Molecular Life Sciences* [Internet]. 2021;78(4):1233–61. Available from: <https://doi.org/10.1007/s00018-020-03656-y>
118. Minguet S, Dopfer EP, Pollmer C, Freudenberg MA, Galanos C, Reth M, et al. Enhanced B-cell activation mediated by TLR4 and BCR crosstalk. *Eur J Immunol*. 2008;38(9):2475–87.
119. Kuriakose T, Rada B, Watford WT. Tumor progression locus 2-dependent oxidative burst drives phosphorylation of extracellular signal-regulated kinase during TLR3 and 9 signaling. *Journal of Biological Chemistry* [Internet]. 2014;289(52):36089–100. Available from: <http://dx.doi.org/10.1074/jbc.M114.587121>
120. Wellbrock C, Karasarides M, Marais R. The RAF proteins take centre stage. *Nat Rev Mol Cell Biol*. 2004;5(11):875–85.
121. Nassar N, Horn G, Herrmann CA, Scherer A, McCormick F, Wittinghofer A. The 2.2 Å crystal structure of the Ras-binding domain of the serine/threonine kinase c-Raf1 in complex with Rap1A and a GTP analogue. *Nature*. 1995;375(6532):554–60.
122. Marshall CJ. Ras effectors. *Curr Opin Cell Biol*. 1996;8:197–204.
123. Rapp UR, Goldsborough MD, Mark GE, Bonner TI, Groffen J, Reynolds FH, et al. Structure and biological activity of v-raf, a unique oncogene transduced by a retrovirus. *Proc Natl Acad Sci U S A*. 1983;80(14 I):4218–22.
124. Jansen HW, Rückert B, Lurz R, Bister K. Two unrelated cell-derived sequences in the genome of avian leukemia and carcinoma inducing retrovirus MH2. *EMBO J*. 1983;2(11):1969–75.
125. Davies H, Bignell GR, Cox C, Stephens P, Edkins S, Clegg S, et al. Mutations of the BRAF gene in human cancer. *Nature*. 2002;417(6892):949–54.
126. Sridhar SS, Hedley D, Siu LL. Raf kinase as a target for anticancer therapeutics. *Mol Cancer Ther*. 2005;4(4):677–85.
127. Matallanas D, Birtwistle M, Romano D, Zebisch A, Rauch J, von Kriegsheim A, et al. Raf family kinases: old dogs have learned new tricks. *Genes Cancer*. 2011;2(3):232–60.

128. Tran NH, Wu X, Frost JA. B-Raf and Raf-1 are regulated by distinct autoregulatory mechanisms. *Journal of Biological Chemistry*. 2005;280(16):16244–53.
129. Terrell EM, Morrison DK. Ras-mediated activation of the Raf family kinases. *Cold Spring Harb Perspect Med*. 2019 Jan 1;9(1).
130. Dhillon AS, Meikle S, Yazici Z, Eulitz M, Kolch W. Regulation of Raf-1 activation and signalling by dephosphorylation. *EMBO Journal*. 2002;21(1–2):64–71.
131. Tzivion G, Luo Z, Avruch J. A dimeric 14-3-3 protein is an essential cofactor for Raf kinase activity. *Nature*. 1998;394(6688):88–92.
132. Chong H, Lee J, Guan KL. Positive and negative regulation of Raf kinase activity and function by phosphorylation. *EMBO Journal*. 2001;20(14):3716–27.
133. Nan X, Collisson EA, Lewis S, Huang J, Tamgüney TM, Liphardt JT, et al. Single-molecule superresolution imaging allows quantitative analysis of RAF multimer formation and signaling. *Proc Natl Acad Sci U S A*. 2013;110(46):18519–24.
134. Lavoie H, Therrien M. Regulation of RAF protein kinases in ERK signalling. *Nat Rev Mol Cell Biol*. 2015;16(5):281–98.
135. Clark GJ, Drugan JK, Rossman KL, Carpenter JW, Rogers-Graham K, Fu H, et al. 14-3-3 ζ negatively regulates Raf-1 activity by interactions with the Raf-1 cysteine-rich domain. *Journal of Biological Chemistry*. 1997;272(34):20990–3.
136. Shin SY, Rath O, Choo SM, Fee F, McFerran B, Kolch W, et al. Positive- and negative-feedback regulations coordinate the dynamic behavior of the Ras-Raf-MEK-ERK signal transduction pathway. *J Cell Sci*. 2009;122(3):425–35.
137. Mott HR, Carpenter JW, Zhong S, Ghosh S, Bell RM, Campbell SL. The solution structure of the Raf-1 cysteine-rich domain: A novel Ras and phospholipid binding site. *Proc Natl Acad Sci U S A*. 1996;93(16):8312–7.
138. Ghosh S, Strum JC, Sciorra VA, Daniel L, Bell RM. Raf-1 kinase possesses distinct binding domains for phosphatidylserine and phosphatidic acid. *Journal of Biological Chemistry* [Internet]. 1996;271(14):8472–80. Available from: <http://dx.doi.org/10.1074/jbc.271.14.8472>
139. Rodriguez-Viciano P, Oses-Prieto J, Burlingame A, Fried M, McCormick F. A Phosphatase Holoenzyme Comprised of Shoc2/Sur8 and the Catalytic Subunit of PP1 Functions as an M-Ras Effector to Modulate Raf Activity. *Mol Cell*. 2006;22(2):217–30.
140. Abraham D, Podar K, Pacher M, Kubicek M, Welzel N, Hemmings BA, et al. Raf-1-associated protein phosphatase 2A as a positive regulator of kinase activation. *Journal of Biological Chemistry*. 2000;275(29):22300–4.
141. Mason CS, Springer CJ, Cooper RG, Superti-Furga G, Marshall CJ, Marais R. Serine and tyrosine phosphorylations cooperate in Raf-1, but not B-Raf activation. *EMBO Journal*. 1999;18(8):2137–48.
142. Tran NH, Frost JA. Phosphorylation of Raf-1 by p21-activated kinase 1 and Src regulates Raf-1 autoinhibition. *Journal of Biological Chemistry*. 2003;278(13):11221–6.
143. Cutler RE, Stephens RM, Saracino MR, Morrison DK. Autoregulation of the Raf-1 serine/threonine kinase. *Proc Natl Acad Sci U S A*. 1998;95(16):9214–9.

144. Rushworth LK, Hindley AD, O'Neill E, Kolch W. Regulation and Role of Raf-1/B-Raf Heterodimerization. *Mol Cell Biol*. 2006;26(6):2262–72.
145. Rajakulendran T, Sahmi M, Lefrançois M, Sicheri F, Therrien M. A dimerization-dependent mechanism drives RAF catalytic activation. *Nature*. 2009;461(7263):542–5.
146. Garnett MJ, Rana S, Paterson H, Barford D, Marais R. Wild-type and mutant B-RAF activate C-RAF through distinct mechanisms involving heterodimerization. *Mol Cell*. 2005;20(6):963–9.
147. Alessi DR, Saito Y, Campbell DG, Cohen P, Sithanandam G, Rapp U, et al. Identification of the sites in MAP kinase kinase-1 phosphorylated by p74(raf-1). *EMBO Journal*. 1994;13(7):1610–9.
148. Marais R, Light Y, Paterson HF, Mason CS, Marshall CJ. Differential regulation of Raf-1, A-Raf, and B-Raf by oncogenic Ras and tyrosine kinases. *Journal of Biological Chemistry* [Internet]. 1997;272(7):4378–83. Available from: <http://dx.doi.org/10.1074/jbc.272.7.4378>
149. Déléris P, Trost M, Topisirovic I, Tanguay PL, Borden KLB, Thibault P, et al. Activation loop phosphorylation of ERK3/ERK4 by group I p21-activated kinases (PAKs) defines a novel PAK-ERK3/4-MAPK-activated protein kinase 5 signaling pathway. *Journal of Biological Chemistry*. 2011;286(8):6470–8.
150. Roskoski R. ERK1/2 MAP kinases: Structure, function, and regulation. *Pharmacol Res*. 2012;66(2):105–43.
151. Gold MR. B Cell Development: Important Work for ERK. *Immunity*. 2008;28(4):488–90.
152. Kholodenko BN, Hancock JF, Kolch W. Signalling ballet in space and time. *Nat Rev Mol Cell Biol*. 2010;11(6):414–26.
153. Pritchard CA, Samuels ML, Bosch E, McMahon M. Conditionally oncogenic forms of the A-Raf and B-Raf protein kinases display different biological and biochemical properties in NIH 3T3 cells. *Mol Cell Biol*. 1995;15(11):6430–42.
154. Chu JY, Dransfield I, Rossi AG, Vermeren S. Non-canonical PI3K-Cdc42-Pak-Mek-Erk Signaling Promotes Immune-Complex-Induced Apoptosis in Human Neutrophils. *Cell Rep*. 2016;17(2):374–86.
155. Ben-Addi A, Mambole-Dema A, Brender C, Martin SR, Janzen J, Kjaer S, et al. IκB kinase-induced interaction of TPL-2 kinase with 14-3-3 is essential for Toll-like receptor activation of ERK-1 and -2 MAP kinases. *Proc Natl Acad Sci U S A*. 2014;111(23).
156. Gantke T, Sriskantharajah S, Sadowski M, Ley SC. IκB kinase regulation of the TPL-2/ERK MAPK pathway. *Immunol Rev*. 2012;246(1):168–82.
157. Lange-Carter CA, Pleiman CM, Gardner AM, Blumer KJ, Johnson GL. A divergence in the MAP kinase regulatory network defined by MEK kinase and Raf. *Science* (1979). 1993;260(5106):315–9.
158. von Kriegsheim A, Pitt A, Grindlay GJ, Kolch W, Dhillon AS. Regulation of the Raf-MEK-ERK pathway by protein phosphatase 5. *Nat Cell Biol*. 2006;8(9):1011–6.

159. Dougherty MK, Müller J, Ritt DA, Zhou M, Zhou XZ, Copeland TD, et al. Regulation of Raf-1 by direct feedback phosphorylation. *Mol Cell*. 2005;17(2):215–24.
160. Pritchard CA, Bolin L, Slattery R, Murray R, McMahon M. Post-natal lethality and neurological and gastrointestinal defects in mice with targeted disruption of the A-Raf protein kinase gene. *Current Biology*. 1996;6(5):614–7.
161. Wojnowski L, Zimmer AM, Beck TW, Hahn H, Bernal R, Rapp UR, et al. Endothelial apoptosis in braf-deficient mice. *Nat Genet*. 1997;16(3):293–7.
162. Wojnowski L, Stancato LF, Zimmer AM, Hahn H, Beck TW, Larner AC, et al. Craf-1 protein kinase is essential for mouse development. *Mech Dev*. 1998;76(1–2):141–9.
163. Galabova-Kovacs G, Matzen D, Piazzolla D, Meissl K, Plyushch T, Chen AP, et al. Essential role of B-Raf in ERK activation during extraembryonic development. *Proc Natl Acad Sci U S A*. 2006;103(5):1325–30.
164. Hüser M, Luckett J, Chiloeches A, Mercer K, Iwobi M, Giblett S, et al. MEK kinase activity is not necessary for Raf-1 function. *EMBO Journal*. 2001;20(8):1940–51.
165. Mikula M, Schreiber M, Husak Z, Kucerova L, Rütth J, Wieser R, et al. Embryonic lethality and fetal liver apoptosis in mice lacking the c-raf-1 gene. *EMBO Journal*. 2001;20(8):1952–62.
166. Allen LF, Sebolt-Leopold J, Meyer MB. CI-1040 (PD184352), a Targeted Signal Transduction Inhibitor of MEK (MAPKK). *Semin Oncol*. 2003;30(5 SUPPL. 16):105–16.
167. McCubrey JA, Steelman LS, Chappell WH, Abrams SL, Wong EWT, Chang F, et al. Roles of the Raf/MEK/ERK pathway in cell growth, malignant transformation and drug resistance. *Biochim Biophys Acta Mol Cell Res*. 2007;1773(8):1263–84.
168. Emuss V, Garnett M, Mason C, Marais R. Mutations of C-RAF are rare in human cancer because C-RAF has a low basal kinase activity compared with B-RAF. *Cancer Res*. 2005;65(21):9719–26.
169. Chesi M, Bergsagel PL. Molecular pathogenesis of multiple myeloma: Basic and clinical updates. *Int J Hematol*. 2013;97(3):313–23.
170. Wan PTC, Garnett MJ, Roe SM, Lee S, Niculescu-Duvaz D, Good VM, et al. Mechanism of activation of the RAF-ERK signaling pathway by oncogenic mutations of B-RAF. *Cell*. 2004;116(6):855–67.
171. Lito P, Rosen N, Solit DB. Tumor adaptation and resistance to RAF inhibitors. *Nat Med*. 2013;19(11):1401–9.
172. Peng S Bin, Henry JR, Kaufman MD, Lu WP, Smith BD, Vogeti S, et al. Inhibition of RAF Isoforms and Active Dimers by LY3009120 Leads to Anti-tumor Activities in RAS or BRAF Mutant Cancers. *Cancer Cell*. 2015;28(3):384–98.
173. Swamy SG, Kameshwar VH, Shubha PB, Looi CY, Shanmugam MK, Arfuso F, et al. Targeting multiple oncogenic pathways for the treatment of hepatocellular carcinoma. *Target Oncol [Internet]*. 2017;12(1):1–10. Available from: <http://dx.doi.org/10.1007/s11523-016-0452-7>
174. Holderfield M, Nagel TE, Stuart DD. Mechanism and consequences of RAF kinase activation by small-molecule inhibitors. *Br J Cancer*. 2014;111(4):640–5.

175. Lohmeyer J, Nerreter T, Dotterweich J, Einsele H, Seggewiss-Bernhardt R. Sorafenib paradoxically activates the RAS/RAF/ERK pathway in polyclonal human NK cells during expansion and thereby enhances effector functions in a dose- and time-dependent manner. *Clin Exp Immunol*. 2018;193(1):64–72.
176. Lai LP, Fer N, Burgan W, Wall VE, Xu B, Soppet D, et al. Classical RAS proteins are not essential for paradoxical ERK activation induced by RAF inhibitors. *Proc Natl Acad Sci U S A*. 2022;119(5):1–10.
177. Hatzivassiliou G, Song K, Yen I, Brandhuber BJ, Anderson DJ, Alvarado R, et al. RAF inhibitors prime wild-type RAF to activate the MAPK pathway and enhance growth. *Nature*. 2010;464(7287):431–5.
178. Brummer T, Shaw PE, Reth M, Misawa Y. Inducible gene deletion reveals different roles for B-Raf and Raf-1 in B-cell antigen receptor signalling. *EMBO Journal*. 2002;21(21):5611–22.
179. Iritani BM, Forbush KA, Farrar MA, Perlmutter RM. Control of B cell development by Ras-mediated activation of Raf. *EMBO Journal*. 1997;16(23):7019–31.
180. Iritani BM, Alberola-Lla J, Forbush KA, Perlmutter RM. Distinct signals mediate maturation and allelic exclusion in lymphocyte progenitors. *Immunity*. 1999;10(6):713–22.
181. Rowland SL, DePersis CL, Torres RM, Pelanda R. Ras activation of Erk restores impaired tonic BCR signaling and rescues immature B cell differentiation. *Journal of Experimental Medicine*. 2010;207(3):607–21.
182. Richards JD, Davé SH, Chou CHG, Mamchak AA, DeFranco AL. Inhibition of the MEK/ERK Signaling Pathway Blocks a Subset of B Cell Responses to Antigen. *The Journal of Immunology*. 2001;166(6):3855–64.
183. Lionetti M, Barbieri M, Todoerti K, Agnelli L, Marzorati S, Fabris S, et al. Molecular spectrum of BRAF, NRAS and KRAS gene mutations in plasma cell dyscrasias: Implication for MEK-ERK pathway activation. *Oncotarget*. 2015;6(27):24205–17.
184. Scheffler L, Feicht S, Babushku T, Kuhn LB, Ehrenberg S, Frankenberger S, et al. ERK phosphorylation is RAF independent in naïve and activated B cells but RAF dependent in plasma cell differentiation. *Sci Signal*. 2021 May 11;14(682).
185. Yasuda T, Sanjo H, Pagès G, Kawano Y, Karasuyama H, Pouyssegur J, et al. Erk kinases link pre-B cell receptor signaling to transcriptional events required for early B cell expansion. *Immunity*. 2008;28(4):499–508.
186. Jesenberger BV, Procyk KJ, Rùth J, Schreiber M, Theussl H christian, Wagner EF, et al. Protective Role of Raf-1 in Salmonella -induced Macrophage Apoptosis. *Journal of Experimental Medicine*. 2001;193((3)):353–64.
187. Chen AP, Ohno M, Giese KP, Kühn R, Chen RL, Silva AJ. Forebrain-specific knockout of B-raf kinase leads to deficits in hippocampal long-term potentiation, learning, and memory. *J Neurosci Res*. 2006 Jan 1;83(1):28–38.
188. Hobeika E, Thiemann S, Storch B, Jumaa H, Nielsen PJ, Pelanda R, et al. Testing gene function early in the B cell lineage in mb1-cre mice. *Proceedings of the National Academy of Sciences [Internet]*. 2006;103(37):13789–94. Available from: <http://www.pnas.org/cgi/doi/10.1073/pnas.0605944103>

189. Pelanda R, Braun U, Hobeika E, Nussenzweig MC, Reth M. B Cell Progenitors Are Arrested in Maturation but Have Intact VDJ Recombination in the Absence of Ig- α and Ig- β . *The Journal of Immunology*. 2002;169(2):865–72.
190. Rickert RC, Roes J, Rajewsky K. B lymphocyte-specific, Cre-mediated mutagenesis in mice. Vol. 25, *Nucleic Acids Research*. Oxford University Press; 1997.
191. Feicht S. Die Rolle der Raf - Kinasen bei der B - Zell - Entwicklung und - Aktivierung. Dissertation an der medizinischen Fakultät der LMU München, angefertigt am Helmholtz Zentrum München Deutsches Forschungszentrum für Gesundheit und Umwelt. 2011.
192. Rui L, Healy JI, Blasioli J, Goodnow CC. ERK Signaling Is a Molecular Switch Integrating Opposing Inputs from B Cell Receptor and T Cell Cytokines to Control TLR4-Driven Plasma Cell Differentiation. *The Journal of Immunology*. 2006;177(8):5337–46.
193. Kurosaki T, Johnson SA, Pao L, Sada K, Yamamura H, Cambier JC. Role of the syk autophosphorylation site and SH2 domains in B cell antigen receptor signaling. *Journal of Experimental Medicine*. 1995;182(6):1815–23.
194. Craxton A, Jiang A, Kurosaki T, Clark EA. Syk and Bruton's tyrosine kinase are required for B cell antigen receptor-mediated activation of the kinase Akt. *Journal of Biological Chemistry*. 1999;274(43):30644–50.
195. Kanarek N, London N, Schueler-Furman O, Ben-Neriah Y. Ubiquitination and degradation of the inhibitors of NF- κ B. *Cold Spring Harb Perspect Biol*. 2010;2(2):1–16.
196. Pontoriero M, Fiume G, Vecchio E, Laurentiis A De, Albano F, Iaccino E, et al. Activation of NF- κ B in B cell receptor signaling through Bruton's tyrosine kinase-dependent phosphorylation of I κ B- α . *Jornal of Molecular Medicine*. 2019;675–90.
197. Ari H, Okada H, Jiang A, Kurosaki M, Greenberg S, Clark E a, et al. Involvement of Guanosine Triphosphatases and Phospholipase C γ 2 in Extracellular Signal-regulated Kinase, c-Jun NH $_2$ -terminal Kinase, and p38 Mitogen-activated Protein Kinase Activation by the B Cell Antigen Receptor. *Journal of Experimental Medicine*. 1998;188(7):1287–95.
198. Allman DM, Cancro MP. pERKING up the BLIMP in plasma cell differentiation. *Sci Signal*. 2011;4(169):19–22.
199. Maik-Rachline G, Hacoheh-Lev-Ran A, Seger R. Nuclear erk: Mechanism of translocation, substrates, and role in cancer. *Int J Mol Sci*. 2019;20(5):1–18.
200. Andreadi C, Noble C, Patel B, Jin H, Aguilar Hernandez MM, Balmanno K, et al. Regulation of MEK/ERK pathway output by subcellular localization of B-Raf. Vol. 40, *Biochemical Society Transactions*. 2012. p. 67–72.
201. Lee IH, Sohn M, Lim HJ, Yoon S, Oh H, Shin S, et al. Ahnak functions as a tumor suppressor via modulation of TGF β /Smad signaling pathway. *Oncogene*. 2014 Sep 18;33(38):4675–84.
202. Bello-Fernandez C, Packham G, Cleveland JL. The ornithine decarboxylase gene is a transcriptional target of c-Myc. Vol. 90, *Proc. Natl. Acad. Sci. USA*. 1993.

203. Deng M, Gui X, Kim J, Xie L, Chen W, Li Z, et al. LILRB4 signalling in leukaemia cells mediates T cell suppression and tumour infiltration. *Nature*. 2018 Oct 25;562(7728):605–9.
204. Higuchi T, Nakayama T, Arao T, Nishio K, Yoshie O. SOX4 is a direct target gene of FRA-2 and induces expression of HDAC8 in adult T-cell leukemia/lymphoma. *Blood* [Internet]. 2013;121(18):3640–9. Available from: <http://ashpublications.org/blood/article-pdf/121/18/3640/1363108/3640.pdf>
205. Gonzalez-Nieves R, Desantis AI, Cutler ML. Rsu1 contributes to regulation of cell adhesion and spreading by PINCH1-dependent and -Independent mechanisms. *J Cell Commun Signal*. 2013 Dec;7(4):279–93.
206. Natrajan R, Little SE, Reis-Filho JS, Hing L, Messahel B, Grundy PE, et al. Amplification and overexpression of CACNA1E correlates with relapse in favorable histology Wilms' tumors. *Clinical Cancer Research*. 2006 Dec 15;12(24):7284–93.
207. Dong Y, Kang H, Liu H, Wang J, Guo Q, Song C, et al. Myoferlin, a Membrane Protein with Emerging Oncogenic Roles. Vol. 2019, *BioMed Research International*. Hindawi Limited; 2019.
208. Benz AH, Renné C, Maronde E, Koch M, Grabiec U, Kallendrusch S, et al. Expression and functional relevance of cannabinoid receptor 1 in hodgkin lymphoma. *PLoS One*. 2013 Dec 9;8(12).
209. Kholodnyuk I, Rudevica Z, Leonciks A, Ehlin-Henriksson B, Kashuba E. Expression of the chemokine receptors CCR1 and CCR2B is up-regulated in peripheral blood B cells upon EBV infection and in established lymphoblastoid cell lines. *Virology*. 2017 Dec 1;512:1–7.
210. Garcia-Areas R, Libreros S, Iragavarapu-Charyulu V. Semaphorin7A: Branching beyond axonal guidance and into immunity. *Immunol Res*. 2013;57(1–3):81–5.
211. Zhang P, Zhao Y, Sun XH. Notch-Regulated Periphery B Cell Differentiation Involves Suppression of E Protein Function. *The Journal of Immunology*. 2013 Jul 15;191(2):726–36.
212. Nie L, Zhao Y, Wu W, Yang YZ, Wang HC, Sun XH. Notch-induced Asb2 expression promotes protein ubiquitination by forming non-canonical E3 ligase complexes. *Cell Res*. 2011 May;21(5):754–69.
213. Chen D, Qin Y, Dai M, Li L, Liu H, Zhou Y, et al. BGN and COL11A1 regulatory network analysis in colorectal cancer (CRC) reveals that BGN influences CRC cell biological functions and interacts with miR-6828-5p. *Cancer Manag Res*. 2020;12:13051–69.
214. Camponeschi A, Todi L, Cristofolletti C, Lazzeri C, Carbonari M, Mitrevski M, et al. DEC1/STRA13 is a key negative regulator of activation-induced proliferation of human B cells highly expressed in anergic cells. *Immunol Lett*. 2018 Jun 1;198:7–11.
215. Carroll MC. CD21/CD35 in B cell activation. Vol. 10, *Seminars in Cell and Developmental Biology*. 1998.

216. Ng HL, Taylor RL, Cheng J, Abraham LJ, Quail E, Cruickshank MN, et al. Notch signaling induces a transcriptionally permissive state at the Complement C3d Receptor 2 (CR2) promoter in a pre-B cell model. *Mol Immunol*. 2020 Dec 1;128:150–64.
217. Moens L, Tangye SG. Cytokine-mediated regulation of plasma cell generation: IL-21 takes center stage. Vol. 5, *Frontiers in Immunology*. Frontiers Research Foundation; 2014.
218. Agosti V, Corbacioglu S, Ehlers I, Waskow C, Sommer G, Berrozpe G, et al. Critical Role for Kit-mediated Src Kinase but Not PI 3-Kinase Signaling in Pro T and Pro B Cell Development. *Journal of Experimental Medicine*. 2004 Mar 15;199(6):867–78.
219. Costantini JL, Cheung SMS, Hou S, Li H, Kung SK, Johnston JB, et al. TAPP2 links phosphoinositide 3-kinase signaling to B-cell adhesion through interaction with the cytoskeletal protein utrophin: Expression of a novel cell adhesion-promoting complex in B-cell leukemia. *Blood*. 2009;114(21):4703–12.
220. Hill L, Schwickert TA. NR4As apply brakes on the B cell response. Vol. 21, *Nature Immunology*. Nature Research; 2020. p. 1137–9.
221. Dondi E, Sibarita JB, Varin-Blank N, Velazquez L. The adaptor protein APS modulates BCR signalling in mature B cells. *Cell Signal*. 2020 Sep 1;73.
222. Iseki M, Kubo C, Kwon SM, Yamaguchi A, Kataoka Y, Yoshida N, et al. Increased Numbers of B-1 Cells and Enhanced Responses against TI-2 Antigen in Mice Lacking APS, an Adaptor Molecule Containing PH and SH2 Domains. *Mol Cell Biol*. 2004 Mar 15;24(6):2243–50.
223. Naito Y, Takematsu H, Koyama S, Miyake S, Yamamoto H, Fujinawa R, et al. Germinal Center Marker GL7 Probes Activation-Dependent Repression of N-Glycolylneuraminic Acid, a Sialic Acid Species Involved in the Negative Modulation of B-Cell Activation. *Mol Cell Biol*. 2007;27(8):3008–22.
224. Fan Y, Han Q, Li J, Ye G, Zhang X, Xu T, et al. Revealing potential diagnostic gene biomarkers of septic shock based on machine learning analysis. *BMC Infect Dis*. 2022 Dec 1;22(1).
225. Mi H, Muruganujan A, Ebert D, Huang X, Thomas PD. PANTHER version 14: More genomes, a new PANTHER GO-slim and improvements in enrichment analysis tools. *Nucleic Acids Res*. 2019;47(D1):D419–26.
226. Heng TSP, Painter MW, Immunological T, Project G. The Immunological Genome Project: networks of gene expression in immune cells. *Nat Immunol*. 2008;9(10):1091–4.
227. Strobl LJ, Höfelmayr H, Marschall G, Brielmeier M, Bornkamm GW, Zimmer-Strobl U. Activated Notch1 Modulates Gene Expression in B Cells Similarly to Epstein-Barr Viral Nuclear Antigen 2 [Internet]. Vol. 74, *JOURNAL OF VIROLOGY*. 2000. Available from: <https://journals.asm.org/journal/jvi>
228. Hu H, Wu X, Jin W, Chang M, Cheng X, Sun SC. Noncanonical NF- κ B regulates inducible costimulator (ICOS) ligand expression and T follicular helper cell development. *Proc Natl Acad Sci U S A*. 2011 Aug 2;108(31):12827–32.

229. Yasuda S, Zhou Y, Wang Y, Yamamura M, Wang JY. A model integrating tonic and antigen-triggered BCR signals to predict the survival of primary B cells. *Sci Rep* [Internet]. 2017;7(1):1–12. Available from: <http://dx.doi.org/10.1038/s41598-017-13993-x>
230. Houde N, Beuret L, Bonaud A, Fortier-Beaulieu SP, Truchon-Landry K, Aoidi R, et al. Fine-tuning of MEK signaling is pivotal for limiting B and T cell activation. *Cell Rep*. 2022;38(2).
231. Kidger AM, Keyse SM. The regulation of oncogenic Ras/ERK signalling by dual-specificity mitogen activated protein kinase phosphatases (MKPs). *Semin Cell Dev Biol*. 2016;50:125–32.
232. Kidger AM, Rushworth LK, Stellzig J, Davidson J, Bryant CJ, Bayley C, et al. Dual-specificity phosphatase 5 controls the localized inhibition, propagation, and transforming potential of ERK signaling. *Proc Natl Acad Sci U S A*. 2017;114(3):E317–26.
233. Ito T, Young MJ, Li R, Jain S, Wernitznig A, Krill-Burger JM, et al. Paralog knock-out profiling identifies DUSP4 and DUSP6 as a digenic dependence in MAPK pathway-driven cancers. *Nat Genet*. 2021;53(12):1664–72.
234. Jiang K, Zhong B, Gilvary DL, Corliss BC, Hong-Geller E, Wei S, et al. Pivotal role of phosphoinositide-3 kinase in regulation of cytotoxicity in natural killer cells. *Nat Immunol*. 2000;1(5):419–25.
235. Ebi H, Costa C, Faber AC, Nishtala M, Kotani H, Juric D, et al. PI3K regulates MEK/ERK signaling in breast cancer via the Rac-GEF, P-Rex1. *Proc Natl Acad Sci U S A*. 2013;110(52):21124–9.
236. Djeu JY, Jiang K, Wei S. A view to a kill: Signals triggering cytotoxicity. *Clinical Cancer Research*. 2002;8(3):636–40.
237. Eblen ST, Slack JK, Weber MJ, Catling AD. Rac-PAK Signaling Stimulates Extracellular Signal-Regulated Kinase (ERK) Activation by Regulating Formation of MEK1-ERK Complexes. *Mol Cell Biol*. 2002;22(17):6023–33.
238. Jacob A, Cooney D, Pradhan M, Mark Coggeshall K. Convergence of signaling pathways on the activation of ERK in B cells. *Journal of Biological Chemistry*. 2002;277(26):23420–6.
239. Guo B, Kato RM, Garcia-Lloret M, Wahl MI, Rawlings DJ. Engagement of the human pre-B cell receptor generates a lipid raft-dependent calcium signaling complex. *Immunity*. 2000;13(2):243–53.
240. Chung JB, Silverman M, Monroe JG. Transitional B cells: Step by step towards immune competence. Vol. 24, *Trends in Immunology*. Elsevier Ltd; 2003. p. 342–8.
241. Chung JB, Baumeister MA, Monroe JG. Cutting Edge: Differential Sequestration of Plasma Membrane-Associated B Cell Antigen Receptor in Mature and Immature B Cells into Glycosphingolipid-Enriched Domains. *The Journal of Immunology*. 2001;166(2):736–40.
242. Cheng PC, Dykstra ML, Mitchell RN, Pierce SK. A Role for Lipid Rafts in B Cell Antigen Receptor Signaling and Antigen Targeting. Vol. 190, *J. Exp. Med*. 1999.

243. Yang J, Reth M. The dissociation activation model of B cell antigen receptor triggering. *FEBS Lett.* 2010;584(24):4872–7.
244. Dawson G, Fuller M, Helmsley KM, Hopwood JJ. Abnormal Gangliosides are Localized in Lipid Rafts in Sanfilippo (MPS3a) Mouse Brain. *Neurochem Res.* 2012;37(6):1372–80.
245. Moreno-Altamirano MMB, Aguilar-Carmona I, Sánchez-García FJ. Expression of GM1, a marker of lipid rafts, defines two subsets of human monocytes with differential endocytic capacity and lipopolysaccharide responsiveness. *Immunology.* 2007;120(4):536–43.
246. Barteneva NS, Vorobjev Editors IA. *Imaging Flow Cytometry Methods and Protocols Methods in Molecular Biology.* 2016. 311 p.
247. Hostager BS, Catlett IM, Bishop GA. Recruitment of CD40 and tumor necrosis factor receptor-associated factors 2 and 3 to membrane microdomains during CD40 signaling. *Journal of Biological Chemistry.* 2000;275(20):15392–8.
248. Scharer CD, Barwick BG, Guo M, Bally APR, Boss JM. Plasma cell differentiation is controlled by multiple cell division-coupled epigenetic programs. *Nat Commun.* 2018;9(1).
249. Pouysségur J, Lenormand P. Fidelity and spatio-temporal control in MAP kinase (ERKs) signalling: Delivered on 24 October 2002 at the 28th FEBS Meeting in Istanbul. In: *European Journal of Biochemistry.* 2003. p. 3291–9.
250. Fey D, Matallanas D, Rauch J, Rukhlenko OS, Kholodenko BN. The complexities and versatility of the RAS-to-ERK signalling system in normal and cancer cells. *Semin Cell Dev Biol.* 2016;58:96–107.
251. Kao SC, Jaiswal RK, Kolch W, Landreth GE. Identification of the Mechanisms Regulating the Differential Activation of the MAPK Cascade by Epidermal Growth Factor and Nerve Growth Factor in PC12 Cells. *Journal of Biological Chemistry.* 2001;276(21):18169–77.
252. Marshall CJ. Specificity of Receptor Tyrosine Kinase Signaling: Transient versus Sustained Extracellular Signal-Regulated Kinase Activation. *Cell.* 1995;80:179–85.
253. Yaka R, Gamliel A, Gurwitz D, Stein R. NGF induces transient but not sustained activation of ERK in PC12 mutant cells incapable of differentiating. *J Cell Biochem.* 1998;70(3):425–32.
254. Rui L, Vinuesa CG, Blasioli J, Goodnow CC. Resistance to CpG DNA-induced autoimmunity through tolerogenic B cell antigen receptor ERK signaling. *Nat Immunol.* 2003;4(6):594–600.
255. Lee SR, Rutan JA, Monteith AJ, Jones SZ, Kang SA, Krum KN, et al. Receptor cross-talk spatially restricts pERK during TLR4 stimulation of autoreactive B cells. *Journal of immunology.* 2012;189(8):3859–68.
256. Eliopoulos AG, Wang CC, Dumitru CD, Tschlis PN. Tpl2 transduces CD40 and TNF signals that activate ERK and regulates IgE induction by CD40. *EMBO Journal.* 2003;22(15):3855–64.

257. Parolini I, Sargiacomo M, Lisanti MP, Peschle C. Signal transduction and glyco-phosphatidylinositol-linked proteins (LYN, LCK, CD4, CD45, G proteins, and CD55) selectively localize in triton-insoluble plasma membrane domains of human leukemic cell lines and normal granulocytes. *Blood*. 1996;87(9):3783–94.
258. Geisberger R, Cramer R, Achatz G. Models of signal transduction through the B-cell antigen receptor. Vol. 110, *Immunology*. 2003. p. 401–10.
259. Ren BCL, Morio T, Fu SM, Geha RS, Virginia C. Signal Transduction via CD40 Involves Activation of lyn kinase and Phosphatidylinositol-3-kinase, and Phosphorylation of Phospholipase Cgamma2. *J Exp Med*. 1994;179(February):673–80.
260. Mebratu Y, Yohannes Tesfaigzi. How ERK1/2 Activation Controls Cell Proliferation and Cell Death. Is Subcellular Localization the Answer? *Cell Cycle*. 2009;8(8):1168–75.
261. Formstecher E, Ramos JW, Fauquet M, Calderwood DA, Hsieh JC, Canton B, et al. PEA-15 Mediates Cytoplasmic Sequestration of ERK MAP Kinase. *Dev Cell*. 2001;1(2):239–50.
262. Torii S, Nakayama K, Yamamoto T, Nishida E. Regulatory mechanisms and function of ERK MAP kinases. *J Biochem*. 2004;136(5):557–61.
263. Makar KW, Ulgiati D, Hagman J, Holers VM. A site in the complement receptor 2 (CR2/CD21) silencer is necessary for lineage specific transcriptional regulation. *Int Immunol*. 2001;13(5):657–64.
264. Thomas M, Calamito M, Srivastava B, Maillard I, Pear WS, Allman D. Notch activity synergizes with B-cell-receptor and CD40 signaling to enhance B-cell activation. *Blood*. 2007;109(8):3342–50.
265. Zapf S. Die Rolle des nicht-kanonischen NF- κ B Transkriptionsfaktor RelB in murinen B-Zellen und B- Zellymphomen Angefertigt am Helmholtz Zentrum München Deutsches Forschungszentrum für Gesundheit und Umwelt. Dissertation an der medizinischen Fakultät der LMU München. 2017.
266. Wang J, Shan Y, Jiang Z, Feng J, Li C, Ma L, et al. High frequencies of activated B cells and T follicular helper cells are correlated with disease activity in patients with new-onset rheumatoid arthritis. *Clin Exp Immunol*. 2013;174(2):212–20.
267. Kischkel FC, Hellbardt S, Behrmann I, Germer M, Pawlita M, Krammer PH, et al. Cytotoxicity-dependent APO-1 (Fas/CD95)-associated proteins form a death-inducing signaling complex (DISC) with the receptor. *EMBO Journal*. 1995;14(22):5579–88.
268. Koncz G, Hueber AO. The Fas/CD95 receptor regulates the death of autoreactive B cells and the selection of antigen-specific B cells. *Front Immunol*. 2012;3(JUL):1–12.
269. Le Gallo M, Poissonnier A, Blanco P, Legembre P. CD95/Fas, non-apoptotic signaling pathways, and kinases. *Front Immunol*. 2017;8(SEP).
270. Levoine N, Jean M, Legembre P. CD95 Structure, Aggregation and Cell Signaling. *Front Cell Dev Biol*. 2020;8(May):1–13.

271. Hoogwater FJH, Nijkamp MW, Smakman N, Steller EJA, Emmink BL, Westendorp BF, et al. Oncogenic K-Ras Turns Death Receptors Into Metastasis-Promoting Receptors in Human and Mouse Colorectal Cancer Cells. *Gastroenterology*. 2010;138(7):2357–67.
272. Homann D, Tishon A, Berger DP, Weigle WO, von Herrath MG, Oldstone MBA. Evidence for an Underlying CD4 Helper and CD8 T-Cell Defect in B-Cell-Deficient Mice: Failure To Clear Persistent Virus Infection after Adoptive Immunotherapy with Virus-Specific Memory Cells from μ MT/ μ MT Mice. *J Virol*. 1998;72(11):9208–16.
273. Shen H, Whitmire JK, Fan X, Shedlock DJ, Kaech SM, Ahmed R. A Specific Role for B Cells in the Generation of CD8 T Cell Memory by Recombinant *Listeria monocytogenes*. *The Journal of Immunology*. 2003;170(3):1443–51.
274. Lund FE, Randall TD. Effector and regulatory B cells: Modulators of CD4+ T cell immunity. *Nat Rev Immunol*. 2010;10(4):236–47.
275. Weinstein JS, Bertino SA, Hernandez SG, Poholek AC, Teplitzky TB, Nowyhed HN, et al. B Cells in T Follicular Helper Cell Development and Function: Separable Roles in Delivery of ICOS Ligand and Antigen. *The Journal of Immunology*. 2014;192(7):3166–79.
276. Ou X, Xu S, Lam KP. Deficiency in TNFRSF13B (TACI) expands T-follicular helper and germinal center B cells via increased ICOS-ligand expression but impairs plasma cell survival. *Proc Natl Acad Sci U S A*. 2012;109(38):15401–6.
277. Koschella M, Voehringer D, Pircher H. CD40 Ligation In Vivo Induces Bystander Proliferation of Memory Phenotype CD8 T Cells. *The Journal of Immunology*. 2004;172(8):4804–11.
278. Tay C, Kanellakis P, Hosseini H, Cao A, Toh BH, Bobik A, et al. B Cell and CD4 T Cell Interactions Promote Development of Atherosclerosis. *Front Immunol*. 2020;10(January):1–15.
279. O'Neill SK, Cao Y, Hamel KM, Doodles PD, Hutas G, Finnegan A. Expression of CD80/86 on B Cells Is Essential for Autoreactive T Cell Activation and the Development of Arthritis. *The Journal of Immunology*. 2007;179(8):5109–16.
280. Nakayama T, Higuchi T, Oiso N, Kawada A, Yoshie O. Expression and function of FRA2/JUND in cutaneous T-cell lymphomas. *Anticancer Res*. 2012;32(4):1367–73.
281. Shtivelman E, Cohent FE, Bishop JM. A human gene (AHNAK) encoding an unusually large protein with a 1.2- μ m polyionic rod structure. *Proceedings of the National Academy of Sciences*. 1993;90(9):4328–4328.
282. Dang C V., O'Donnell KA, Zeller KI, Nguyen T, Osthus RC, Li F. The c-Myc target gene network. *Semin Cancer Biol*. 2006;16(4):253–64.
283. Nguyen L, Papenhausen P, Shao H. The Role of c-MYC in B-Cell Lymphomas: Diagnostic and molecular aspects. *Genes (Basel)*. 2017;8(4):2–22.
284. Adhikary S, Eilers M. Transcriptional regulation and transformation by Myc proteins. *Nat Rev Mol Cell Biol*. 2005;6(8):635–45.

285. Kerkhoff E, Houben R, Löffler S, Troppmair J, Lee J eun, Rapp UR. Regulation of c -myc expression by Ras / Raf signalling. *Oncogene*. 1998;16:211–6.
286. Cleveland JL, Jansen HW, Bister K, Fredrickson TN, Morse HC 3rd, Ihle JN, et al. Interaction between Raf and Myc oncogenes in transformation in vivo and in vitro. *J Cell Biochem*. 1986;30(3):195–218.
287. Poe JC, Minard-Colin V, Kountikov EI, Haas KM, Tedder TF. A c-Myc and Surface CD19 Signaling Amplification Loop Promotes B Cell Lymphoma Development and Progression in Mice. *Journal of immunology*. 2012;189(5):2318–25.
288. Kolch W, Kotwaliwale A, Vass K, Janosch P. The role of Raf kinases in malignant transformation. *Expert Rev Mol Med*. 2002;4(8):1–18.
289. Bello-Fernandez C, Cleveland JL. c-myc transactivates the ornithine decarboxylase gene. *Curr Top Microbiol Immunol*. 1992;182:445–52.
290. Nilsson JA, Keller UB, Baudino TA, Yang C, Norton S, Old JA, et al. Targeting ornithine decarboxylase in Myc-induced lymphomagenesis prevents tumor formation. *Cancer Cell*. 2005;7(5):433–44.
291. Auvinen M, Paasinen A, Andersson LC, Hölttä E. Ornithine decarboxylase activity is critical for cell transformation. *Nature*. 1992;360(6402):355–8.
292. Hogarty MD, Norris MD, Davis K, Liu X, Evageliou NF, Hayes CS, et al. ODC1 is a critical determinant of MYCN oncogenesis and a therapeutic target in neuroblastoma. *Cancer Res*. 2008;68(23):9735–45.
293. Bettuzzi S, Davalli P, Astancolle S, Pinna C, Roncaglia R, Boraldi F, et al. Coordinate changes of polyamine metabolism regulatory proteins during the cell cycle of normal human dermal fibroblasts. *FEBS Lett*. 1999;446(1):18–22.
294. Gerner EW, Meyskens FL. Polyamines and cancer: Old molecules, new understanding. *Nat Rev Cancer*. 2004;4(10):781–92.
295. Bachmann AS, Geerts D. Polyamine synthesis as a target of MYC oncogenes. *Journal of Biological Chemistry*. 2018;293(48):18757–69.
296. Crawford JM, Watanabe K. Cell adhesion molecules in inflammation and immunity: Relevance to periodontal diseases. *Critical Reviews in Oral Biology and Medicine*. 1994;5(2):91–123.
297. Westerberg L, Larsson M, Hardy SJ, Fernández C, Thrasher AJ, Severinson E. Wiskott-Aldrich syndrome protein deficiency leads to reduced B-cell adhesion, migration, and homing, and a delayed humoral immune response. *Blood*. 2005;105(3):1144–52.
298. Xiao Y, Hendriks J, Langerak P, Jacobs H, Borst J. CD27 is acquired by primed B cells at the centroblast stage and promotes germinal center formation. *J Immunol*. 2004;172(12):7432–41.
299. Raman VS, Akondy RS, Rath S, Bal V, George A. Ligation of CD27 on B Cells In Vivo during Primary Immunization Enhances Commitment to Memory B Cell Responses. *The Journal of Immunology*. 2003;171(11):5876–81.
300. Batten M, Groom J, Cachero TG, Qian F, Schneider P, Tschopp J, et al. BAFF Mediates Survival of Peripheral Immature B Lymphocytes. Vol. 192, *J. Exp. Med*. © The Rockefeller University Press; 2000.

301. Sasaki Y, Casola S, Kutok JL, Rajewsky K, Schmidt-Supprian M. TNF Family Member B Cell-Activating Factor (BAFF) Receptor-Dependent and -Independent Roles for BAFF in B Cell Physiology. *The Journal of Immunology*. 2004 Aug 15;173(4):2245–52.
302. Smulski CR, Eibel H. BAFF and BAFF-receptor in B cell selection and survival. Vol. 9, *Frontiers in Immunology*. Frontiers Media S.A.; 2018.
303. Kumanogoh A, Watanabe C, Lee I, Wang X, Shi W, Araki H, et al. Identification of CD72 as a lymphocyte receptor for the class IV semaphorin CD100: A novel mechanism for regulating B cell signaling. *Immunity*. 2000;13(5):621–31.
304. Kumanogoh A, Kikutani H. Immunological functions of the neuropilins and plexins as receptors for semaphorins. *Nat Rev Immunol*. 2013;13(11):802–14.
305. Suzuki K, Kumanogoh A, Kikutani H. Semaphorins and their receptors in immune cell interactions. Vol. 9, *Nature Immunology*. 2008. p. 17–23.
306. Takamatsu H, Kumanogoh A. Diverse roles for semaphorin-plexin signaling in the immune system. *Trends Immunol*. 2012;33(3):127–35.
307. Angelisová P, Drbal K, Cerný J, Hilgert I, Horejsí V. Characterization of the human leukocyte GPI-anchored glycoprotein CDw108 and its relation to other similar molecules. *Immunobiology*. 1999 Jun;200(2):234–45.
308. Holl EK, O'Connor BP, Holl TM, Roney KE, Zimmermann AG, Jha S, et al. Plexin-D1 Is a Novel Regulator of Germinal Centers and Humoral Immune Responses. *The Journal of Immunology*. 2011;186(10):5603–11.
309. Casazza A, Finisguerra V, Capparuccia L, Camperi A, Swiercz JM, Rizzolio S, et al. Sema3E-Plexin D1 signaling drives human cancer cell invasiveness and metastatic spreading in mice. *Journal of Clinical Investigation*. 2010;120(8):2684–98.
310. Capparuccia L, Tamagnone L. Semaphorin signaling in cancer cells and in cells of the tumor microenvironment - Two sides of a coin. *J Cell Sci*. 2009;122(11):1723–36.
311. Wei L, Li H, Tamagnone L, You H. Semaphorins and their receptors in hematological malignancies. *Front Oncol*. 2019;9(MAY):1–5.
312. Kopan R, Ilagan MXG. The Canonical Notch Signaling Pathway: Unfolding the Activation Mechanism. *Cell*. 2009;137(2):216–33.
313. Giaimo BD, Gagliani EK, Kovall RA, Borggreffe T. Transcription Factor RBPJ as a Molecular Switch in Regulating the Notch Response. In: Reichrath J, Reichrath S, editors. *Notch Signaling in Embryology and Cancer: Notch Signaling in Cancer* [Internet]. Cham: Springer International Publishing; 2021. p. 9–30. Available from: https://doi.org/10.1007/978-3-030-55031-8_2
314. Kim MY, Park JY, Park HS. Akt1-Mediated Phosphorylation of RBP-Jκ Controls Notch1 Signaling. *Biochemistry (Moscow)* [Internet]. 2019;84(12):1537–46. Available from: <https://doi.org/10.1134/S0006297919120137>
315. Hailfinger S, Nogai H, Pelzer C, Jaworski M, Cabalzar K, Charton JE, et al. Malt1-dependent RelB cleavage promotes canonical NF-κB activation in lymphocytes and lymphomacell lines. *Proc Natl Acad Sci U S A*. 2011 Aug 30;108(35):14596–601.

316. Osipo C, Golde TE, Osborne BA, Miele LA. Off the beaten pathway: The complex cross talk between Notch and NF- κ B. *Laboratory Investigation*. 2008;88(1):11–7.
317. Shin HM, Minter LM, Ok HC, Gottipati S, Fauq AH, Golde TE, et al. Notch1 augments NF- κ B activity by facilitating its nuclear retention. *EMBO Journal*. 2006;25(1):129–38.
318. Oswald F, Liptay S, Adler G, Schmid RM. NF- κ B2 Is a Putative Target Gene of Activated Notch-1 via RBP-J κ . *Mol Cell Biol*. 1998;18(4):2077–88.
319. Hess C, Winkler A, Lorenz AK, Holecska V, Blanchard V, Eiglmeier S, et al. T cell-independent B cell activation induces immunosuppressive sialylated IgG antibodies. *Journal of Clinical Investigation*. 2013;123(9):3788–96.

Supplementary data

Suppl. Table 1: Significantly differentially expressed genes of the biological process “positive regulation of cell adhesion”	141
Suppl. Table 2: Significantly differentially expressed genes of the biological process “immune system response”	142
Suppl. Table 3: Significantly differentially expressed genes of the biological process “semaphorin interaction”	143
Suppl. Table 4: Gene Set for genes upregulated in MZ B cells.	144
Suppl. Table 5: Gene Set for genes upregulated in Fo B cells.	145
Suppl. Table 6: Gene Set for genes upregulated by early Notch2 signaling in B cells.	146
Suppl. Table 7: Gene Set for genes downregulated by early Notch2 signaling in B cells.	146
Suppl. Table 8: Gene Set for genes upregulated by late Notch2 signaling in B cells.	147
Suppl. Table 9: Gene Set for genes downregulated by late Notch2 signaling in B cells.	148
Suppl. Table 10: Gene set for upregulated genes of BAFF-tg (BAFF) B cells.	149
Suppl. Table 11: Gene set for downregulated genes of BAFF-tg (BAFF) B cells.	149
Suppl. Table 12: Gene sets for upregulated genes of TRAF2KO B cells.	149
Suppl. Table 13: Gene sets for downregulated genes of TRAF2KO B cells.	150
Suppl. Table 14: Gene sets for upregulated genes of TRAF3KO B cells.	150
Suppl. Table 15: Gene sets for downregulated genes of TRAF3KO B cells.	151

Suppl. Table 1: Significantly differentially expressed genes of the biological process “positive regulation of cell adhesion” (positive log₂Fold Changes correspond to a lower expression in LC40 compared to RafDKO/LC40 B cells)

	gene symbol	log ₂ FoldChange	padj
ENSMUSG00000030336	Cd27	0,710422629	0,01905751
ENSMUSG00000027111	Itga6	0,639132307	0,00415178
ENSMUSG00000037820	Tgm2	0,658907337	0,00902526
ENSMUSG00000026532	Spta1	0,792865578	0,00585005
ENSMUSG00000051457	Spn	0,846195671	0,00141486
ENSMUSG00000020101	Vsir	0,768358287	4,21E-06
ENSMUSG00000068566	Myadm	1,164797755	9,56E-21
ENSMUSG00000018899	Irf1	0,598787389	3,15E-06
ENSMUSG00000037104	Socs5	0,635352905	3,27E-07
ENSMUSG00000044447	Dock5	0,628093251	0,02060951
ENSMUSG00000068105	Tnfrsf13c	0,769848777	4,73E-21
ENSMUSG00000035042	Ccl5	0,833227407	0,00052988
ENSMUSG00000041959	S100a10	0,685758607	6,71E-06
ENSMUSG00000068220	Lgals1	0,620382706	NA

Suppl. Table 2: Significantly differentially expressed genes of the biological process “immune system response” (positive log₂Fold Changes correspond to a lower expression in LC40 compared to RafDKO/LC40 B cells)

	gene symbol	log ₂ FoldChange	padj
ENSMUSG00000068105	Tnfrsf13c	0,769848777	4,73E-21
ENSMUSG00000057337	Chst3	0,758659431	2,02E-15
ENSMUSG00000041247	Lamp3	0,910342205	0,00075963
ENSMUSG00000004730	Adgre1	0,686339072	0,01858641
ENSMUSG00000030149	Klrk1	0,609906599	0,05745056
ENSMUSG00000096844	Igkv6-14	0,608735654	0,0254144
ENSMUSG00000003420	Fcgrt	0,987337984	8,96E-07
ENSMUSG00000069268	Hist1h2bf	0,609508019	0,0408481
ENSMUSG00000051910	Sox6	0,622472178	0,05275069
ENSMUSG00000035042	Ccl5	0,833227407	0,00052988
ENSMUSG00000039153	Runx2	0,628494695	0,04923132
ENSMUSG00000032690	Oas2	0,644043975	0,0014383
ENSMUSG00000094345	Igkv14-126	0,695822994	0,02299116
ENSMUSG00000031168	Ebp	0,206793715	0,58850472
ENSMUSG00000030336	Cd27	0,710422629	0,01905751
ENSMUSG00000034317	Trim59	0,888927171	2,70E-13
ENSMUSG00000025270	Alas2	1,083209533	4,36E-05
ENSMUSG00000027111	Itga6	0,639132307	0,00415178
ENSMUSG00000075297	H60b	0,81510364	0,00422313
ENSMUSG00000015217	Hmgb3	0,672283755	0,02958422
ENSMUSG00000026532	Spta1	0,792865578	0,00585005
ENSMUSG00000016283	H2-M2	1,030987714	6,33E-05
ENSMUSG00000018899	Irf1	0,598787389	3,15E-06
ENSMUSG00000040447	Spns2	1,190029667	2,22E-08
ENSMUSG00000045092	S1pr1	0,780780666	1,68E-20
ENSMUSG00000038058	Nod1	0,591001042	0,00269096
ENSMUSG00000096632	Igkv9-124	0,620068964	0,0231259
ENSMUSG00000021703	Serinc5	0,812555521	5,75E-05
ENSMUSG00000022636	Alcam	1,039088478	1,28E-08
ENSMUSG00000015766	Eps8	0,603149925	0,02755986
ENSMUSG00000029570	Lfng	0,60919517	0,01967516
ENSMUSG00000078922	Tgtp1	0,468142079	0,10021815
ENSMUSG00000051457	Spn	0,846195671	0,00141486
ENSMUSG00000026399	Cd55	0,675584577	1,93E-17
ENSMUSG00000005057	Sh2b2	2,502443232	4,71E-40
ENSMUSG00000029798	Herc6	0,986090148	3,11E-12
ENSMUSG00000104213	Ighd	0,72420651	8,14E-19

Suppl. Table 3: Significantly differentially expressed genes of the biological process “semaphorin interaction” (negative log₂Fold Changes correspond to a higher expression in LC40 compared to RafDKO/LC40 B cells)

		gene symbol	log ₂ FoldChange	padj
Biological process semaphorin interaction	ENSMUSG00000048895	Cdk5r1	-0,594764332	1,66E-07
	ENSMUSG00000030084	Plxna1	-0,72228126	0,007952449
	ENSMUSG00000030123	Plxnd1	-1,331236874	3,17E-08
	ENSMUSG00000059495	Arhgef12	-0,916105336	8,08E-15
	ENSMUSG00000038264	Sema7a	-0,939827064	3,51E-30
	ENSMUSG00000019843	Fyn	-0,594195823	8,32E-09
additional semapho- rins and plexins	ENSMUSG00000074785	Plxnc1	-0,430111224	5,70E-07
	ENSMUSG00000031398	Plxna3	-0,188051964	0,676086203
	ENSMUSG00000036606	Plxnb2	-0,152400951	0,690551897
	ENSMUSG00000022231	Sema5a	-0,995988131	1,30E-23
	ENSMUSG00000027200	Sema6d	-0,460065666	0,127020178
	ENSMUSG00000021451	Sema4d	-0,15193229	0,206257131
	ENSMUSG00000028064	Sema4a	-0,154963221	0,776256039

Suppl. Table 4: Gene Set for genes upregulated in MZ B cells designed by using the ImmGen Population Comparison Tool based on microarray data (<http://rstats.immgen.org/PopulationComparison/index.html>) (226).

MZ B cells upregulated

I830077J02RIK	SRGAP3	INPP4A	IKBKE	CEPT1	HES5	RALB
S1PR3	SIRPA	CTSB	REC8	PRDM1	GRHPR	UBE2E3
MYOF	PTPN22	BZW2	LY6A	MDFIC	H2-T22	MFSD10
CEACAM2	CD59A	ELL3	RNASEL	ARSB	UTRN	PLAC1L
FCRL5	GPR156	AMICA1	LOC641050	TOP2A	ELK3	TMEM231
CDH17	DUSP16	TET1	CD81	FUCA2	GMNN	CD80
TSGA13	HMG3	TMEM154	GBP6	CYBB	ST3GAL6	HECTD1
PLXND1	ADAM28	HBB-B1	CD1D2	COPG2	S1PR1	MCCC2
ZC3H12C	LILRB4	PLBD1	SLC35F2	CACNB4	PPFIBP2	CDC25A
CD9	KCNK5	BC028528	SH2D1B1	CAPN2	ABCG1	PGK1
PLA2G7	DSE	ABR	ENTPD1	SLC29A1	PVR	RGS3
MPEG1	1700048020RIK	CRIM1	CD274	GM4979	TNFRSF18	ATXN7L1
ASB2	TAF1D	UBE2R2	GM4956	GM7609	EDEM1	LMBR1
GM10786	GM6377	LYNX1	TRPS1	GM7609	GCOM1	CTS2
CD36	SNORA61	RAP1GAP	WDFY2	NTNG2	DTX3	B4GALT1
DNASE1L3	MS4A7	CDC42BPB	LYSMD2	GBP3	ZFP239	PGK1
ZC3H12C	PIK3R4	4930426L09RIK	KCNN4	DTX4	RPSA	Sep 09
CCBP2	CDON	GP49A	GRAMD1B	MYO10	2310044G17RIK	PKD1
ABCB1A	BHLHE41	PDE4A	TRAF1	LOC100046496	PACSIN2	SFXN5
TBC1D9	SLC9A9	MS4A14	IFT27	ST3GAL2	BTBD19	CEBPB
EMB	SCD2	ZFP532	MICAL3	ROGDI	CSPRS	PLAUR
NEBL	CXCR7	SMYD2	PTAFR	FAM49A	GSTO1	ABHD6
SEMA7A	PDIA4	TREM1	ADORA3	GYPC	RPLP1	GM5779
TSPAN15	MCOLN3	BC005685	FAM129C	RRBP1	PSAP	BDH1
CD1D1	CCDC79	GBP8	ABHD5	IL6ST	SCARNA17	D8ERTD82E
MARCKS	TM6SF1	CD86	5033430I15RIK	RPLP1	SLC39A4	SEMA6B
CSF2RB	LRRC16A	AKR1E1	CR2	GM6251	THYN1	ZAP70
NEDD4	HCK	SEMA4B	KLRB1F	GADD45B	ARSB	ENTPD4
RGS10	GM10858	PLSCR1	ITGB1	ARL5C	PDZD2	CBFA2T3
STOM	PLXNC1	ALPK2	RHBDF1	CLIC4	SLC28A2	SLC46A3
MFHAS1	IL9R	BC005685	SLC43A1	CHN2	TMEM26	CYFIP1
FFAR2	TRPM2	ABCG3	SNORA73A	PLEKHA5	PTPRJ	LAX1
TLR3	ENDOD1	SMAD3	SLC39A6	TMEM206	TMCC3	PDLIM2
CFP	VAULTRC5	TSPAN31	ITM2C	FAM108C	1700029I01RIK	BIVM
PLAC8	RBM47	DRD5	RNU3B1	GM13251	CUL9	FGD2
CD300LF	SLC25A4	LPCAT2	TFDP1	PTPRS	GM2A	DCLRE1A
GM7265	ALPL	DENND2D	FAM92A	PABPC4	H2-T10	ZFP248
SERPINE2	PDE4D	PPL	NUCB2	MIR703	PHPT1	CEACAM16
DPH5	NAIP6	IMPDH2	AMIGO2	5730408K05RIK	CBR4	CCDC28B
PTPN14	LGALS3BP	CDCA7L	FGL2	BLK	CDK5R1	RPSA
CCR1	TMEM18	PRF1	GM13139	YPEL2	CSPRS	SBF2
AHR	PQLC2	LRRC25	2810416G20RIK	WDR6	TMEM131	RPSA
ATXN1	RXFP1	MYC	PIP4K2A	RPS6KA1	EEF1B2	KIF13A
LY96	CREBL2	CACNA1E	SLC7A7	POLD4	2010012O05RIK	RPL3
CYP39A1	PLSCR1	PMEP1A1	SLC20A2	9330129D05RIK	RPSA	WDR11
VWA5A	PDE8A	RILPL2	TFDP1	NAB1	GM13051	PGM1
GRN	SLC29A3	GPR55	TYROBP	BC016495	IMPACT	RPL13
1700106N22RIK	HBB-B2	MXD4	MYO6	OOSP1	PIK3R3	ADCK3
ID2	CD80	DRAM2	GBP2	TMOD2	TLCD2	HHAT
RUNDC3B	5830416P10RIK	1500011K16RIK	ALOX5AP	SFXN1	GM5167	RPL13
2010001M09RIK	PPAP2B	AS3MT	TET1	AHCYL2	ABCB8	LY6K
TNFRSF21	TPST2	9030625A04RIK	TAF1D	PTPRJ	CREG1	PNPO
A1452195	TMTC4	5033414D02RIK	ANXA9	RPS13	DECR2	FAM125B
GM10673	MGST1	AKR7A5	DKKL1	MZT2	A930005H10RIK	FAM26F
LOC625360	UBE2E2	NDST1	RCN1	TRIM32	GUSB	PLCG1
DTX1	NEBL	BC005685	ZDHHC14	ASAP2	FBXW17	EHMT2
NRP2	PLD4	EDARADD	DENND2D	PABPC4	PDCD4	
RSU1	9030617O03RIK	GML	ARHGEF12	PABPC4	ACAD10	
SORBS2	NAIP5	BST1	NLRP1B	PABPC4	TLR9	
ADRBK2	SRGAP3	SLC36A4	NEBL	GNS	3830406C13RIK	
LDLRAD3	BID	DDX60	MGST2	4930572J05RIK	D10WSU102E	
LAIR1	ABCB1B	5830416P10RIK	PLA2G4A	LGMN	NLRC3	

Suppl. Table 5: Gene Set for genes upregulated in Fo B cells designed by using the ImmGen Population Comparison Tool based on microarray data (<http://rstats.immgen.org/PopulationComparison/index.html>) (226).

Fo B cells upregulated

ACOT9	2410066E13RIK	FMNL1	STXBP3A	B3GNT8	GM1077	RARA	TAGAP
TPM4	BRPF3	MEX3B	SMC5	SPRED2	CCDC50	SORL1	RNF144A
BEND5	ZFP143	CTPS2	PARP8	SMC3	CDC14B	OTUD1	ADAMTS6
TSC22D2	GAB3	CYP51	RAD21	GVIN1	GBE1	IDI1	MYO9A
FOXO1	PIRA11	H3F3A	GCH1	CCDC50	GPD2	GM10850	RGL1
HIP1R	IRAK3	POC1B	GM11428	PIRA1	CBX7	STGGAL1	EMP3
MAN1A	MSI2	BAIAP2	DCAF12	RFK	CCR6	ACSL3	ZFP608
PRKCB	DHX57	LRRC8C	ATP11C	FANCM	IL6RA	MYO9A	CRISP3
PICALM	JAK1	SMAP2	PLK2	TLE1	JHDM1D	MYO9A	OLFR164
KIF16B	CTNNA1	ANK	PHKA1	SPNS2	RHOH	SH3BP5	SSH2
PCMTD1	SMAD1	SPNB2	RDH12	EIF2C4	MAP4K3	LIFR	AIDA
RHEBL1	GMEB2	RFX7	CDK19	ORAI2	PPP3CA	ABCA1	PIP5K1B
CDK13	MIR342	PEL1	MTSS1	FCGRT	C1GALT1	KCTD14	GM8995
TRIM25	CAPRIN2	SMAD7	CEP120	PARP1	DGKA	RASA3	SFN
RRM2B	SLC38A2	SGK3	DNAJC21	A1467606	SERPINB1A	CD46	BCLP2
MAP3K1	BPTF	EML4	ETAA1	NUP210L	GM8979	CNN3	TSC22D3
GM14484	WASF2	SLC15A3	ICOSL	TEX9	HSPA4L	RAPGEF4	FAM102B
AVL9	GLCC1	FBXO11	RB1CC1	PGM2L1	RFC1	RASGRP3	ITGB7
IKZF5	MED13	PPP1R2	MIER1	SKIL	HMGCS1	LAMP3	A430078G23RIK
YWHAZ	ZFP821	USP53	SLC4A11	CARD6	MYO9A	GMFG	MYO9A
HERC4	CTDSP2	TDRD7	ARHGAP5	FF4	4930565B19RIK	DCLK2	ARHGFB18
GABBR1	NAP1L1	9130011E15RIK	ZFP652	ZBTB33	GM10388	FAM65B	FCHSD2
PBRM1	TLE4	PRSS12	993002J03RIK	ORAI2	ANTXR2	SLFN5	GIMAP3
WDR26	GPR52	NSMCE1	STK24	EEA1	SAMHD1	DNAHC8	CDK11
H2-OB	NAB2	SEPP1	DEK	TUFT1	MEF2C	ZBTB10	CMAH
PRKD3	LIN54	PDE4B	AGPAT2	RBL1	INTS4	FLNA	CD69
SRSF2IP	MLL5	KCNJ1	UBA6	S1PR4	NEURL3	DENND5B	CAR2
KDM3A	IL27RA	CCM2	GM5972	ZFP874B	LMBRD1	RPS6KA5	RASSF3
SIK2	KPNA4	6430601O08RIK	MAML3	TBC1D14	BTLA	TCTN1	A630033H20RIK
NCK2	MPP6	CDC425E1	Sep 11	TAGAP1	QSER1	SGK1	MYO9A
IQGAP1	ICAM2	GM9874	IRF2	N4BP2	IL21R	ANGPTL1	DUSP4
EPB4_1L2	MDC1	FGD3	MYO9A	PLCL2	BBS9	ADD3	ENPP1
GORASP2	H3F3A	CDKN2D	CHST3	SIKE1	TEC	CCDC88A	MYO9A
ESYT2	SH3BP2	TAX1BP1	PPP1R2	RYR2	MYO9A	MYO9A	JUND
SHANK1	CHST15	UBR1	PANK3	GIMAP4	AHNAK	TAGLN2	CPM
CRLF3	SP3	ANKRD44	USP28	SMCHD1	HHEX	SFN	PGAP1
CIITA	SPATA6	PPP4R2	CASC5	RAP1GDS1	GRAP2	FAM69A	FAM101B
KCTD10	DENND4A	CTDSP1	AP1M1	EPB4_1	CNN3	STAT4	CC2D2B
MYH9	TRAK2	RYBP	ST3GAL1	SNX2	SELL	ADAP1	CXCR4
SMAGP	RSF1	ANKRD11	ROCK2	VPREB3	SCML4	GM16489	ALCAM
RNF19B	ST8SIA4	GM9948	2610018G03RIK	PTMA	MAPK12	TCP11L2	HCTR2
ARL13B	DENND4A	TPM4	SCCPDH	ITSN2	TNIK	ADD1	ARHGFB3
A230046K03RIK	ZBTB37	9530009G21RIK	1110028C15RIK	CLCF1	E230008N13RIK	CYTIP	SLAMF1
TMF1	SMS	RIF1	RAD17	RAP1B	KLF3	ITIH5	TRIB2
NUP210L	ARID5B	LATS2	STK38	SNX29	SLC25A24	MYO9A	SSBP2
AMZ2	CSRP2	STXBP3A	FXYD5	POLD1	GM16848	AKT3	MYADM
HCF2	DNAJC9	GPATCH8	DGKD	RAPGEF6	FAM46A	IDI1	HVCN1
INSR	FGFR1OP	STGGAL1	EIF2C2	LBH	KLF6	FAM46A	CRYBG3
NF1	LRRC8A	HEXB	PITPNC1	LASP1	GLCC1	ADRB2	ATP1B1
IKBKB	CCDC88C	PPP1R2	RNF2	IL4RA	QSER1	GM10759	B3GNT5
GRK6	GPR183	EPC2	E230008N13RIK	JHDM1D	MYO9A	CCR7	BCL6
NFYA	NRF1	ATP2B1	GM10551	CSNK1G3	KIF21B	S100A10	FRY
MSN	TBC1D1	CECR2	DPYSL2	SFXN3	EHD4	A430084P05RIK	KLF2
RBM38	GM608	H3F3A	CD83	SQLE	LPP	RBPMS	CD200
STK17B	CEP350	PLEKHF2	FAM108B	NUP210L	SSH2	STAC2	DAF2
ATN1	PRKAB2	BMF	CDKL5	SNX9	FAM107B	LMO2	TRIM59
PHF3	RASGRP2	CHML	STAP1	1110038D17RIK	UBE2L6	SLC4A3	VIM
BPTF	CREB1	GPD1L	LASP1	DMXL1	LDLR	L1CAM	ZFP318
CEP350	PIK3CG	ZFP53	NUP210L	YSK4	XK	MS4A4C	ITGA6
JAK2	LSP1	SLC14A1	ITPKB	MARVELD2	CERK	SERINC5	CD55
2700049A03RIK	NUAK2	PLEC	HSD11B1	SMCHD1	FLI1	CDC25B	PDE2A
RNF122	TUBA1A	GPR155	EPS8	DUSP7	ATP6V0A1	DUSP3	BACH2
INPP1	DENND4A	AIM1	CAMKK2	BRWD1	FAM134B	DENND5B	MAPK11
PRKD2	PHACTR4	PDP1	LPP	AFF3	P2RY10	LFNG	PGAP1
GNA13	1700001K23RIK	RABGEF1	CD2	GADD45G	OLFR165	AY512938	CACNA1I
PPP2R3A	SP4	CARNS1	RASA2	TMEM64	ARHGAP31	SBK1	D130062J21RIK
TOP2B	SIRT1	CCDC41	PACS1	SLC4A7	1300014I06RIK	XYLT1	FCER2A
ELMO1	CITED2	SC4MOL	SLC16A4	PXK	DYRK2	GPR146	MLLT6
ZMYM2	LPP	RPS6KA3	XKRX	GM8979	DOCK11	ZFP36L2	
SELE	ZFP81	MAP4K4	MYLIP	DYRK2	SLFN8	GMFG	
OSBPL8	ITGB3	D19ERTD737E	RFTN2	SPRED2	GPR174	LILRA6	
IFNAR1	CALM2	MTAP	HDAC9	CCDC52	RICTOR	SATB1	

Suppl. Table 6: Gene Set for genes upregulated by early Notch2 signaling in B cells comparing the RNA expression pattern of normal with Notch2IC expressing cells after 3 days of Tamoxifen treatment using the RNA-Seq data of Lechner et al., 2021 (54) with a minimal normalized read count of 50, an p-value below 0.0001, and a fold change above 1.

early Notch2 upregulated

AW011738	CD274	FFAR2	LAX1	NOP56	RP24-255G1.8	TIMM23
ABCE1	CD38	FTSJ3	LRPPRC	NOP58	RASAL1	TMA16
ALPK2	CR2	GADD45A	MAP3K8	NPM1	S1PR1	TMEM18
APRT	DDX25	GNL2	MDN1	PDCD11	S1PR3	TRIM35
BAG4	DPH5	GNL3	MIF	PEX1	SLC44A2	UTP14A
BCL7A	DTX1	HEG1	MPHOSPH10	PPAN	SLF2	UTP20
BMP2K	EEF1KMT4	HES1	MYC	RP23-152G20.2	SSSCA1	UTP3
BZW2	EIF3A	HES5	NCL	RP23-184H3.5	ST13	WDR43
CAAA011948	ELL3	HSPA5	NEDD4	RP23-252O5.3	STARD5	
CCDC86	FAM129C	HSPA9	NIFK	RP23-334J9.1	SUCLG2	
CD22	FAM26F	IPO4	NOLC1	RP24-155C13.1	TAF1D	

Suppl. Table 7: Gene Set for genes downregulated by early Notch2 signaling in B cells comparing the RNA expression pattern of normal with Notch2IC expressing cells after 3 days of Tamoxifen treatment using the RNA-Seq data of Lechner et al., 2021 (54) with a minimal normalized read count of 50, an p-value below 0.0001, and a fold change below 1.

early Notch2 downregulated

AC123686.3	CDKL1	FCHSD2	IGLJ3	PHF13	S100A13	TBC1D8B
AAMDC	CDKN2D	FKBP11	IL18R1	PIK3IP1	S100A6	TCP11L2
ABCB1B	CHST3	FKBP2	IL2RB	PLD3	S1PR4	TMEM115
ACAA2	CIAO1	FLI1	ITGB7	PLEC	SAT1	TMEM160
ACBD4	CLDN10	FLNA	JCHAIN	PLSCR3	SBK1	TNFRSF18
ADD1	COA5	FMNL1	KCTD12	PPDPF	SCPEP1	TRAPPC10
AHNAK	COX6A2	FTL1	KCTD14	PRDX5	SDC4	TRBC2
ARHGAP45	CPM	FXYD5	KEAP1	PSEN2	SH3BP5	TSC2
ATP1B1	CST7	GIMAP4	KLF2	PTPRS	SIGLECH	TSC22D1
ATP6V1G1	CTLA2A	GM23262	KLHL26	RP23-113O9.4	SIK1	TSC22D3
BHLHE41	CTNNA1	GNAI2	KLK1	RP23-197C15.1	SIT1	TUBA1A
BORCS6	CTSH	GNAI3	KLK1B27	RP23-29H5.3	SLA2	TXNDC5
BST2	CTSL	GNB2	KLRB1A	RP23-301O12.1	SLC35B2	TYROBP
CAPG	CTSW	GSAP	KRT222	RP23-362B7.1	SMAP2	VIM
CARHSP1	CXCR3	GZMA	LAT2	RP23-365O6.1	SMIM5	VSIR
CCL5	CYP27A1	H3F3A	LCORL	RP23-431C5.1	SMPD3	WARS
CCM2	CYTH4	HBA-A1	LGALS1	RP24-159O13.1	SNRNP25	WFDC17
CCR7	DCAF12	HBA-A2	LGALS3	RP24-387G4.1	SNX8	ZFP746
CD209D	DCLK2	HBB-BS	LMO2	RP24-420A20.8	SPNS2	HEXB
CD247	DDHD2	HBB-BT	LPPOS	RAB11A	SREBF2	
CD3D	DNPEP	HSD17B11	LSP1	RAMP1	SRSF4	
CD3E	DOK2	HVCN1	LY6C2	RASA3	SSBP2	
CD6	DUSP4	IER2	MGST2	RASSF3	ST6GAL1	
CD7	ELK3	IFI27L2A	MKRN2	RDH12	STK35	
CD8B1	EMP3	IFNAR1	NCF1	REEP5	STX4A	
CDC25B	ETHE1	IGHG2B	NOD1	RFK	SUGP1	
CDC42EP3	EVA1B	IGHV5-17	PACS1	RNASET2A	SUMO3	
CDC42SE1	FAM214A	IGKV12-41	PAFAH1B3	RUNX2	SYNJ1	
CDC42SE2	FCER2A	IGLC1	PANK1	S100A10	TAGLN2	

Suppl. Table 8: Gene Set for genes upregulated by late Notch2 signaling in B cells comparing the RNA expression pattern of cells after 3 days of Tamoxifen treatment with cells after 14 days of Tamoxifen treatment using the RNA-Seq data of Lechner et al., 2021 (54) with a minimal normalized read count of 50, an p-value below 0.0001, and a fold change above 1.

late Notch2 upregulated

AC015800.4	CDH17	FGD2	LOCKD	PMF1	RILPL2	SNHG18
AC121847.1	CEACAM2	FKBP11	MANF	PPIB	RPL10A-PS1	SNORA57
AC123686.3	CENPE	FKBP2	MARCKS	PPL	RPL11	SNORD104
ABCB1B	CENPM	GAS5	MGST1	PRC1	RPL22	SNX20
ABHD5	CFP	GM10073	MIR5136	PRDM1	RPL32	SP140
ACBD4	CIB1	GPCPD1	MIRT1	PTGR1	RPL37A	SSR2
ACKR2	CMC2	GPR156	MKI67	RP23-179K7.3	RPL39	SSR4
AKR7A5	CNPY2	GRN	MRPL57	RP23-209M8.7	RPL39-PS	STOM
ALPL	COPS9	H13	MS4A1	RP23-216O10.2	RPL41	SUB1
AMICA1	CRELD2	H1F0	MS4A7	RP23-234K24.8	RPLP0	SVIL
APOE	CSF2RB	HIST1H1B	MZB1	RP23-235E15.1	RPLP1	TLR3
ASB2	CTSB	HIST1H2AE	NCAPD3	RP23-366E4.5	RPS14	TM6SF1
B2M	CTSZ	HMG3	NEB	RP23-396N8.2	RPS20	TMEM154
BCL7A	CYBB	HS3ST1	NEDD4	RP23-402I8.2	RPS26	TMEM256
BLK	DPH5	HSP90B1	NUSAP1	RP23-426M5.1	RPS3	TNFRSF13B
BLNK	DUSP16	IFI27L2A	OSGIN1	RP23-463F7.8	RPS9	TOP1
BST1	EDARADD	IGKC	PCLAF	RP23-71G16.6	RRBP1	TOP2A
BTG2	EDEM1	IGKV2-109	PDCD2L	RP23-71J17.1	RSU1	TPST2
BZW2	EDEM2	IGKV3-4	PIK3R4	RP23-82K1.6	S1PR1	TRAPPC6A
CD24A	EEF1B2	IGLC1	PIM1	RP24-155C13.1	S1PR3	TSGA13
CD36	ENTPD1	IGLC2	PINLYP	RP24-262G23.6	SCAND1	TXN1
CD38	ERO1LB	IGLV1	PIP4K2A	RP24-310D17.9	SDF2L1	UBE2E2
CD59A	ERP29	INPP5F	PLAC8	RP24-500I24.7	SEC11C	UBE2R2
CD81	FAM149A	JCHAIN	PLGRKT	RP24-554B1.10	SEC61B	UBL5
CD9	FCRL5	KCNJ16	PLPP5	RAP1GAP	SEMA7A	XBP1
CDC25A	FFAR2	KRT222	PLXND1	RGS10	SLC28A2	ZFAS1

Suppl. Table 9: Gene Set for genes downregulated by late Notch2 signaling in B cells comparing the RNA expression pattern of cells after 3 days of Tamoxifen treatment with cells after 14 days of Tamoxifen treatment using the RNA-Seq data of Lechner et al., 2021 (54) with a minimal normalized read count of 50, an p-value below 0.0001, and a fold change below 1.

late Notch2 downregulated

ACTB	CD55	EPB41	ICAM2	NFIC	RALGPS2	STK17B
ADD1	CD74	EPRS	ICOSL	NFKB2	RAPGEF6	SWAP70
ADD3	CD83	ETS1	IER2	NFKBIA	RASA2	SYPL
AFF3	CDC42EP3	EXOSC1	IL21R	NOP58	RASAL1	TAX1BP1
AHNAK	CDC42SE1	FAAP24	IL4RA	NSMCE1	RBM38	TCOF1
AKAP13	CDKN2D	FAM101B	IRF2	PARP1	REL	TEC
ALDOA	CHCHD10	FAM204A	ITGB7	PDE4B	RNASEH2C	TGFBR2
ANKRD11	CHD4	FAM65B	JAK1	PELI1	S1PR4	TMEM108
AP3S2	CHERP	FCER2A	KIF21B	PFN1	SAMD9L	TMSB10
ARAP1	CMAH	FCHSD2	KLF2	PGLYRP1	SATB1	TNFRSF13C
ARF6	CNN2	FCMR	KLF3	PHF1	SBK1	TNIK
ARHGAP15	CNN3	FLNA	KPNA1	PITPNA	SCAF11	TPM3-RS7
ARHGAP26	CNOT3	GRP18	LAMP1	PLEC	SDC4	TPM4
ARHGDIB	CNP	GGA2	LARP7	PLEKHA2	SELL	TRIB2
ARHGEF1	COTL1	GIMAP3	LASP1	POLD1	SERPINB1A	TRMT112
ARID1A	CPM	GIMAP4	LBH	POLE4	SF3B2	TRP53
ARPC2	CYTIP	GIMAP6	LCP1	POM121	SFN	TSC22D3
B3GNT5	DAZAP2	GIMAP7	LMBRD1	PPIE	SFPQ	VPREB3
B4GALNT1	DDX18	GIMAP9	LMO2	PPP1R9B	SFR1	WASF2
BACH2	DEK	GRK6	LRP10	PRDM2	SGK1	WBP11
BCL10	DGKA	GTF3C6	MAN1A	PRKAR1A	SH3BGL3	WDR43
BCL6	DIP2B	HAAO	MAP3K4	PSMD4	SH3BP5	YTHDF3
BFSP2	DNAH8	HBA-A1	MAPK11	PTMA	SHISA5	YWHAB
BPTF	DNAJC9	HBA-A2	MAPK12	PTPN6	SIPA1	ZDHHC18
BRIX1	DNMT1	HBB-BS	MED28	PTPRC	SLC52A2	ZFP318
BTAF1	DOCK11	HBB-BT	MEF2C	PXDC1	SMAGP	ZFP507
BTLA	DPF2	HERC4	MIF4GD	PXK	SNRPB	ZFP608
CALM1	DUSP2	HIVEP2	MSN	RP23-362A12.3	SORL1	
CAR2	EED	HNRNPDL	MTAP	RP23-412L13.1	SPIB	
CCDC9	EGR1	HSPA9	MTSS1	RP23-465M17.1	SRSF11	
CCM2	EMD	HSPBP1	NAB2	RAB14	STAG1	
CCR7	EML4	HVCN1	NCOR1	RABAC1	STAP1	
CD200	EMP3	HYPK	NDUFS7	RAD21	STAT4	

Suppl. Table 10: Gene set for upregulated genes of BAFF-tg (BAFF) B cells displaying a hyperactive non-canonical NFkB signal were generated using the micro-array data of Gardam et al., 2008 (48).

BAFF upregulated

Skiv2l2	Ffar2	Ighg3	Hspa4l	Dnaja1	Gpr171	Itgb3
Gpr34	Inpp4b	Serpina3g	Paip1	Stard4	Chka	ApoE
Prelid2	Ptpn14	Pisd-ps3	P4ha1	Oas1a	Chka	Socs3
Sh2b2	St3gal5	Spic	Oas2	Chst10	Ffar2	Lrrc16a
Hspa13	Pisd-ps3	Lyz1	Epcam	Ccdc69	Ahsa2	
Ccr1	Ap1s3	NdrG1	Tk1	Lilrb4a	Cfp	
Hsph1	Tmco6	Ehd3	Ackr3	Cd9	Adm	
Fam46c	Gbp6	Lyz1	Neb1	Ighg3	Socs3	

Suppl. Table 11: Gene set for downregulated genes of BAFF-tg (BAFF) B cells displaying a hyperactive non-canonical NFkB signal were generated using the micro-array data of Gardam et al., 2008 (48).

BAFF downregulated

Klrb1b	Lipo2	Pcdh19	2610020C07Rik	Hnrnp	Rfx1	Sh2b3
Pak1	Ptpn6	Spp12a	BC025920	Bdkrb2	Lym7	Bnc1
Cndp2	Sulf2	Airn	Nr2c2	Gm6793	Tbc1d14	Acot9
Ddx6	Vipr1	Obp2a	Slc8a1	Slc7a11	4921511C10Rik	Cyp4f15
Gal3st1	Idh3g	Rhobtb2	Rbm19	Flot1	Cecr6	

Suppl. Table 12: Gene sets for upregulated genes of TRAF2KO B cells displaying a hyperactive non-canonical NFkB signal were generated using the micro-array data of Gardam et al., 2008 (48).

TRAF2 KO upregulated

Gpr34	Cd9	LOC102635638	Atxn1	Fam167a	Tmbim1	Cyp4v3	Zmiz2
Pygl	Ksr1	Trps1	Mpg	Faah	Ttc28	Anxa4	Tpi1
Rhbdf1	Cdon	Nedd4	Ighg3	1500011K16Rik	Smad3	Notch1	4833444G19Rik
Il9r	Marcks	Abcc1	Kcnk5	D3Ert254e	Hcst	Serpib9	Lipo3
Cnr1	Itgb3	AI447881	Pou2af1	Phlpp1	Bcl2	Chd3os	Lcp1
Thsd7a	Reep3	Cyfp1	Ehd1	Rras2	Akap5	Rubcn	Tspyl3
Ptpn14	Specc1	Cbarp	Mpg	Lgalsl	Ctnna1	Eva1b	2210013O21Rik
Chka	Reep3	Trps1	Dkk1	Inadl	Mast4	Abhd14b	Manea
Adm	Nid1	Reep3	Ackr3	Ehd1	Cdc42bpb	Cyp39a1	Larp4
Lilrb4a	Ebi3	Marcks	Fam213a	Nfatc2	Smim101	Man2a1	Cds2
Vwf	St8sia6	Inf2	Prmt2	Arhgap5	Smim101	Reep3	Gramd1b
Krt222	Neb1	A630023P12Rik	Mpg	Arhgap5	P4htm	Zfp563	Specc1l
Adm	Kynu	Rasgef1b	Fhit	Lynx1	Tbc1d5	Snap47	BC017158
Ccr1	Cd59a	Reep3	Asb2	Kdelc1	Tcf4	Fdx1	Kdm2a
Chka	Krt222	Plcg1	Stx11	Hspb1	Rnf24	Senp8	Tpk1
Snrnp25	Glt28d2	Bcl2	Prmt2	Hs3st3b1	Abcb1a	Mgat4a	Tbxa2r
Ppfbp2	Ptpn22	Coprs	Ahcyl2	Zadh2	Prkar2a	Cr2	Cdk5rap2
St8sia6	Pbx3	Dnase1l3	St14	Oosp1	Slc29a3	Rasgrp3	Gramd3
Rsu1	Whrn	Brms1l	Ttc28	Ehd3	Mst1	Grpel2	Nmrk1
Gcm2	NdrG1	Wnt10a	Anxa4	Pik3r4	Dclre1a	Cand1	Pqlc1
Epcam	Pibid1	Ifit1bl2	Ffar2	Gm16619	Tgif2	Slc39a14	Aldoa
Neb1	Tshz1	Pard3b	Capn2	Klhl7	Tank	Grpel2	Col20a1
Cfp	Pde8a	Id2	Fam160a1	Dusp16	St3gal2	Mllt4	Gm33374
St8sia6	Pard3b	Abcb9	Rinl	Pdia4	Nfat5	Osmr	Tm7sf3
Chst10	Tk1	Gabbr1	Lta	Stxbp1	Trim7	Cdh17	Zfp937
Lrrc16a	Atxn1	Myl4	Nfat5	Zfp287	Degs1	Tes	4930588G05Rik
Anxa4	Sbf2	Morn1	Daam1	Ehd1	Fpgt	Slc25a4	Adam22
Akap5	Ptk2	Kif1b	Ttc8	Map3k5	Lpcat1	Rgmb	
Ahcyl2	Ift140	Traf1	Ptpn14	Serinc4	Fam57a	Ints2	
Ffar2	Traf1	Naip2	Tbc1d9	Plid2	Pea15a	Spata6	

Suppl. Table 13: Gene sets for downregulated genes of TRAF2KO B cells displaying a hyperactive non-canonical NFκB signal were generated using the micro-array data of Gardam et al., 2008 (48).

TRAF2 KO downregulated

Rhobtb2	Hjurp	Smc4	Txnrd3	Cd93	Gm7429	Jun	Wfdc17
Pcdhb11	Zeb2	Slc16a1	Rapgef4	Hist1h1c	Vps18	Eya1	Ptger4
Strbp	Zfp821	Aurkc	Man2a2	Gm11346	Fam129c	Ms4a4b	Hivep3
Ppp2r5c	Agpat5	Rbm25	AU014973	Eps8	Hist1h1c	Egr1	Kctd14
Asna1	Foxp1	Cox5b	Arhgef18	Ehd4	Sgk1	Csrp2	Tsc22d1
Tgfb1	Dhrs11	Piga	Alcam	Ostc	Snhg1	Il18	Lifr
9230104K21Rik	Slx1b	Strbp	Sdc1	Sys1	Epc1	Spns2	Tsc22d1
Rps6	Msl1	Ager	Serinc1	Evi5	Pabpc1	Cd93	Sdc1
4933427D14Rik	Fcgr2b	Phxr1	Plcx2	Trib2	Ezh2	Slc15a3	Klf4
Gm7367	Ankrd11	Alcam	Ankrd33b	Snx5	D8Erd82e	Maf	Sox4
Rheb1	Sepp1	Cpt1a	B3gnt5	Coro1a	Ubl5	Rapgef3	Fos
Abhd17b	Hmgn5	Apaf1	Alcam	Ahctf1	Smad1	Slco4a1	
Zfp825	Prpf31	Tnfrsf13c	Gng12	Serp1b1a	Myadm	Gpr155	
Zfx	Timm8a1	Saraf	Snord47	Slamf9	Pltp	Car2	
Zwilch	LOC102638110	Mgst1	Srsf7	Fam101b	Myadm	Pltp	
Gramd4	9430034N14Rik	Cdkn2c	Tfrc	Btf3	Akap12	Kctd14	
Slc1a5	Sec61a1	Cpt1a	Slc25a51	Cmah	Il5ra	Socs3	
Crybg3	Smim3	Rnpc3	Slamf1	Tmem176b	Gpr146	Socs3	

Suppl. Table 14: Gene sets for upregulated genes of TRAF3KO B cells displaying a hyperactive non-canonical NFκB signal were generated using the micro-array data of Gardam et al., 2008 (48).

TRAF3 KO upregulated

Gpr34	Anxa4	Cbarp	Atxn1	Trim7	Pld2	Chid1	Dnajc16
Rhbd1	Neb1	Pard3b	Kynu	Optn	Tgif2	Stxbp1	Tpi1
Il9r	Pde8a	Cyfp1	Ksr1	Cyp39a1	Hcst	Eva1b	Prkar1b
Pygl	Cd9	Morn1	Lta	Dusp16	LOC102642406	Pqlc1	Phlpp1
Ccr1	Thsd7a	Reep3	Rras2	Pard3b	Golim4	Ldlrad3	Pea15a
Ffar2	Chst10	Krt222	1500011K16Rik	Serinc4///E13	St6galnac3	Hck	Hpcal1
Lilrb4a	Lrrc16a	Mpg	Vwf	Kdelc1	Tpk1	Zbtb42	Sfmbt1
Chka	Plbd1	St8sia6	Rasgef1b	Reep3	Specc1	Kif3a	Nfkb2
Cfp	Cnr1	LOC102635638	Pik3r4	St3gal2	Pde3b	Pim2	Ptpn18
Chka	Gpm6a	Abcc1	Klhl7	Plcg1	Arrb2	Nubpl	Rpl13a
Ptpn14	Pbx3	Daam1	Ttc8	Hdac11	Aire	Tbxa2r	Pawr
Cacna1e	Itgb3	Myl4	Fam213a	Myo1b	Cdc42bpb	Prlr	Ttll12
Adm	Mpg	Naip2	Ptk2	Inadl	Meis3	Zfp763	Cds2
Ackr3	Cd59a	Trps1	Marcks	Rras2	Fdx1	Afg3l2	Dcbl1d1
Neb1	Traf1	Ptpn14	Sbf2	Trim7	Nfatc2	Naprt	Ankrd36
Serpina3g	A1447881	Cd300lf	Nr2f6	Capn2	Pmepa1	Tes	Gpi1
Ighg3	Ubash3b	Tbc1d9	Lgalsl	Whrn	Slc29a3	Tmbim1	Chd3os
Snrnp25	Cdon	Coprs	Traf1	Lgalsl	Prmt2	Map3k5	H1f0
Ffar2	Trps1	Fam92a	Tmem18	Ttc28	Zscan12	Nr2c1	5430416N02Rik
Adm	Ighg3	Oosp1	Fam160a1	Ccr1	Odc1	Acs13	Itgam
Rsu1	St8sia6	Pglyrp1	Gramd3	Slc25a4	P4htm	Rps6	
Epcam	Ptpn22	Reep3	Zadh2	St8sia6	Ccdc163	Anxa4	
Tk1	Marcks	Pou2af1	A630023P12Rik	Nedd4	2210013021Rik	Cdca7l	
Ppfbp2	Ebi3	Ift140	Wnt10a	Abhd14b	2210016L21Rik	Htra2	
Mpeg1	Ahcy12	Ubash3b	Faah	Glit28d2	Kif3a	Cenpp	
Trps1	Smpd5	Ehd1	Rgmb	Lmntd2	Grpel2	Spib	
Krt222	Tshz1	St14	Reep3	Cdh17	Slc12a2	Snrnp70	

Suppl. Table 15: Gene sets for downregulated genes of TRAF3KO B cells displaying a hyperactive non-canonical NFκB signal were generated using the micro-array data of Gardam et al., 2008 (48).

TRAF3 KO downregulated

Stk4	Rps6kb1	Sept11	Arih1	Crybg3	5830415B17Rik	Slc15a3	Lifr
Mef2c	Nol8	Cytip	Knop1	Klf3	Tbl1x	D8Erttd82e	Ptger4
Cbx4	Abhd17b	Phxr1	Cpsf2	Vsir	Akap12	Pde2a	Eya1
Strbp	Vps11	Arl5b	Cited2	Vcpkmt	Cd93	Hist1h1c	Maf
Timm8a1	Sepp1	Sdc1	Hmgn5	Lrrc8a	Spns2	Cd93	Cxcr4
Gramd4	Ceacam2	Smpd4	Saraf	Tmem176b	Hist1h1c	Fam129c	Kctd14
Kdm3a	Cmss1	Fam65b	Egr1	Ube2h	Ppm1e	Myadm	Sdc1
Tor1aip2	Chic2	Dync1li2	Gpr155	Dennd5b	Slc2a4rg-ps	Hivep3	Kctd14
Mapre1	Plaur	Socs3	Fyn	Agpat9	Myadm	Smad1	Sox4
Yy1	B4galt1	Hdac9	Cmah	Alcam	Ii18	Sgk1	
Sept2	Cpt1a	Coro1a	Slamf1	Ppp1r8	Gpr146	Rapgef3	
LOC102641500	Gm11346	Wfdc18	Papola	Slco4a1	Fam101b	Tsc22d1	

Danksagung

Diese Doktorarbeit wäre ohne die Unterstützung einiger nicht möglich gewesen. Auf diesem Weg möchte ich diesen Menschen nachfolgend einen großen Dank aussprechen:

Meine Doktormutter, PD Dr. Ursula Zimmer-Strobl, gab mir die Möglichkeit an der Rolle der Raf-Kinasen in B-Zellen zu forschen. Hierbei legte Sie mit Ihrer Idee des Projektes nicht nur den Grundstein dieser Arbeit, sondern Sie prägte mich durch eine intensive Zusammenarbeit, sehr anregende Diskussionen und die Förderung zur eigenständigen Entwicklung von Hypothesen und Experimenten als Wissenschaftler. Vielen Dank, liebe Ulla!

Außerdem gilt mein Dank den weiteren Gutachtern, die sich die Zeit nehmen, meine Dissertation zu prüfen.

Ich möchte mich auch bei Prof. Dr. Daniel Krappmann und Prof. Dr. Vigo Heissmeyer bedanken. Sie standen mir als Mitglieder in meinem Thesis Advisory Committee mit Ihrer Expertise und zusätzlichen Blickwinkeln auf die Forschungsergebnisse mit Rat und Tat zur Seite.




Besonders herzlich möchte ich mich bei meinen Kollegen und Kolleginnen Lothar, Alex, Steffi V., Markus, Kris, Laura, Tea, Ursula und Yana bedanken. Auch ihr habt durch die gute Zusammenarbeit, die wissenschaftlichen Diskussionen und die sehr angenehme Arbeitsatmosphäre maßgeblich zur Vervollständigung dieser Doktorarbeit beigetragen. Außerdem habt ihr mich während meiner Schwangerschaften emotional und auch im Labor tatkräftig unterstützt. Durch eure Unterstützung konnte ich die Doktorarbeit fortsetzen und die Publikation abschließen. In diesem Zusammenhang sei vor allem auch Dr. Lothar Strobl zu erwähnen. Er unterstützte mich in vielen Bereichen, vor allem aber bei der Interpretation und Auswertung der RNA-Sequenzierung und bei der Erstellung der Publikation. Ein besonderer Dank geht an dieser Stelle auch an Alex, Steffi V. und Markus. Ihr habt mich nicht nur als Arbeitskolleg*innen, sondern auch als Freunde immer unterstützt. Vielen Dank auch an Kris, die uns als technische Assistentin nicht nur bei der Genotypisierung half, sondern auch bei methodischen und persönlichen Fragen immer eine Antwort parat hatte. Danke, euch allen!

Die Mitarbeiter*innen des Tierstalles, besonders Michael, Martina, Franz L. und Franz W., haben mich durch die Betreuung meiner Mäuse enorm unterstützt. Die Zusammenarbeit war mehr als perfekt. Danke schön!

Außerdem möchte ich mich bei Dr. Helmut Blum und bei Dr. Sonja Grath für die enge Kollaboration bei der Durchführung und Auswertung der RNA-Sequenzierung bedanken.

Zu guter Letzt möchte ich mich aus tiefsten Herzen bei meinen Eltern, meinen Schwestern, meinen Schwiegereltern, aber vor allem auch bei meinem Mann und meinen Kindern bedanken. Ihr habt mich bei allen Berg- und Talfahrten dieser Doktorarbeit und der Publikation immer unterstützt, mir so oft unter die Arme gegriffen und mir den emotionalen Rückhalt gegeben, den ich zur Fertigstellung dieser Doktorarbeit gebraucht habe. Vielen vielen lieben Dank, euch allen!

Affidavit

	LUDWIG- MAXIMILIANS- UNIVERSITÄT MÜNCHEN	Promotionsbüro Medizinische Fakultät		
Eidesstattliche Versicherung				

Scheffler, Laura

Name, Vorname

Ich erkläre hiermit an Eides statt, dass ich die vorliegende Dissertation mit dem Titel:

The Role of Raf-1 and B-Raf in B cell activation, differentiation,
and tumorigenesis in mice.

selbständig verfasst, mich außer der angegebenen keiner weiteren Hilfsmittel bedient und alle Erkenntnisse, die aus dem Schrifttum ganz oder annähernd übernommen sind, als solche kenntlich gemacht und nach ihrer Herkunft unter Bezeichnung der Fundstelle einzeln nachgewiesen habe.

Ich erkläre des Weiteren, dass die hier vorgelegte Dissertation nicht in gleicher oder in ähnlicher Form bei einer anderen Stelle zur Erlangung eines akademischen Grades eingereicht wurde.

Planegg, 20.11.2023

Ort, Datum

Laura Scheffler

Unterschrift Doktorandin bzw. Doktorand